Higher Order Immersed Finite Element Methods for Interface Problems

Haroun Meghaichi

Dissertation submitted to the Faculty of the
Virginia Polytechnic Institute and State University
in partial fulfillment of the requirements for the degree of

Doctor of Philosophy
in
Mathematics

Slimane Adjerid, Chair
Tao Lin, Co-chair
Timothy Warburton
Pengtao Yue

April 23, 2024
Blacksburg, Virginia

Keywords: Immersed finite element, interface problems, error analysis, unfitted methods

Higher Order Immersed Finite Element Methods for Interface Problems

Haroun Meghaichi

(ABSTRACT)

In this dissertation, we provide a unified framework for analyzing immersed finite element methods in one spatial dimension, and we design a new geometry conforming IFE space in two dimensions with optimal approximation capabilities, alongside with applications to the elliptic interface problem and the hyperbolic interface problem.

In the first part, we discuss a general m-th degree IFE space for one dimensional interface problems with many polynomial-like properties, then we develop a general framework for obtaining error estimates for the IFE spaces developed for solving a variety of interface problems, including but not limited to, the elliptic interface problem, the Euler-Bernoulli beam interface problem, the parabolic interface problem, the transport interface problem, and the acoustic interface problem.

In the second part, we develop a new m-th degree finite element space based on the differential geometry of the interface to solve interface problems in two spatial dimensions. The proposed IFE space has optimal approximation capabilities, easy to construct, and the IFE functions satisfy the interface conditions exactly. We provide several numerical examples to demonstrate that the IFE space yields optimally converging solutions when applied to the elliptic interface problem and the hyperbolic interface problem with a symmetric interior penalty discontinuous Galerkin formulation.

Higher Order Immersed Finite Element Methods for Interface Problems

Haroun Meghaichi

(GENERAL AUDIENCE ABSTRACT)

Interface problems appear naturally in many physics and Engineering applications where a physical quantity is considered across materials of different physical properties, such as heat transfer or sound propagation through different materials. Typically, these physical phenomena are modelled by partial differential equations with discontinuous coefficients representing the material properties.

The main topics of this dissertation are about the development and analysis of immersed finite element methods for interface problems. The IFE method can use interface independent meshes, and employs approximating functions that capture the features of the solution at the interface.

Specifically, we provide a unified framework for analyzing one-dimensional IFE problems, and we design a new framework to construct geometry conforming IFE spaces in two dimensions, with applications to the elliptic interface problem and the hyperbolic interface problem.

Dedication

To my parents, Noureddine and Salima.

Acknowledgments

First and foremost, I would like to take this opportunity to thank my advisor, Dr. Slimane Adjerid for his continuous support, guidance and encouragement during my Masters and Ph.D. study and for motivating me to explore the beautiful world of numerical analysis and sharing his wisdom. I am fairly certain that this dissertation would not have been possible without his help. For that, I am forever grateful.

I would like to thank my co-advisor Dr. Tao Lin for the constant advice and unwavering support. I have learned greatly from our meetings and discussions. Both Dr. Adjerid and Dr. Lin have inspired me to strive and improve, which I plan to take with me on my next journey.

I would also like to sincerely thank my PhD. committee, Dr. Timothy Warburton and Dr. Pengtao Yue for their insightful comments and valuable feedback. Their guidance helped me improve my thesis greatly, and enriched my knowledge on the subject.

Contents

List of Figures

List of Tables

Chapter 1

Introduction

Many physical phenomena occur over different media separated by interfaces, which are typically points, curves or surfaces depending on the dimension of the ambient space, leading to an interface problem. We start this chapter with an overview of interface problems, and we provide a review of the previously developed immersed finite element and dG methods for interface problems. After that, we describe the topics of this dissertation. At the end, we outline the structure of the dissertation.

1.1 An Overview of Numerical Methods for Interface Problems

Interface problems are ubiquitous in science and engineering where a physical quantity, such as temperature or pressure, is considered across two or more mediums with different physical properties, such as conductivity or density. In many instances, the physics is modeled by ordinary or partial differential equations, where the material properties are coefficients in the equations. In the presence of multiple materials, these coefficients can be discontinuous across the interface between two different materials, which could introduce a challenge to the numerical methods used to solve the differential equations.

There are two major approaches for solving interface problems using a finite element or a

dG method: Fitted methods [21, 28, 102, 105], where the mesh is constructed according to the interface such that each element is on one side of the interface, and unfitted methods where the mesh is independent of the interface. See Figure 1.1 for an illustration of a fitted mesh and a Cartesian unfitted mesh.

Typically, unfitted methods offer numerous advantages over interface-fitted meshes. For instance, an unfitted mesh is easy to construct, whereas a fitted mesh can be expensive when the geometry of the interface is complex, or when the problem requires successive re-meshing, such as topology optimization problems [2, 68, 89] and moving interface problems [93, 96]. Unfortunately, using the traditional finite element with an unfitted mesh usually leads to suboptimally convergent approximations [20]. For this reason, researchers explored alternative approaches to develop optimally converging unfitted methods. Among those methods, we mention the extended finite element method (XFEM) [24, 31, 103], the CutFEM method [38, 59, 60, 74], the generalized finite element method (GFEM) [109, 110], and the immersed finite element method discussed in this dissertation.

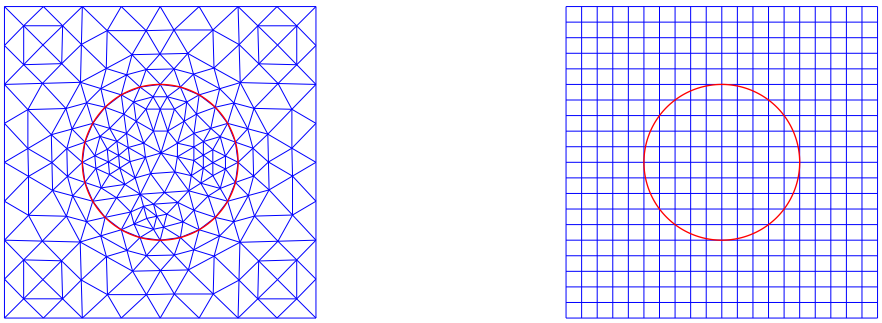

(a) An interface fitted mesh (b) An unfitted mesh

Figure 1.1: An interface-fitted mesh (left) and an unfitted mesh (right). The interface is shown in red.

The immersed finite element method is an unfitted method. Thus, the interface is allowed to intersect the interior of some elements, called interface elements. On non-interface elements, The IFE method employs the traditional finite element polynomial spaces to approximate

the solution, whereas, on the interface elements, the IFE method uses a Hsieh-Clough-Tocher type macro element [39], where each shape function is a piecewise polynomial constructed according to the interface conditions satisfied by the solution.

The immersed finite element was first used to solve the elliptic interface problem using piecewise linear shape functions in one dimension [76]. Since then, the IFE method evolved in many directions and was applied to multiple interface problems. In one spatial dimension, higher order finite element methods were introduced and analyzed for the elliptic interface problem [7] and optimal interpolation estimates were derived. Cubic Hermite IFE methods for the fourth order Euler-Beam equation were discussed in [81, 101] and analyzed in [78]. A fully discrete IFE scheme was proposed for the parabolic interface problem [70] and a method of lines was devised for the parabolic interface problem with a moving interface [82]. Lastly, vector IFE functions of degree $1 \leq m \leq 4$ were used to solve the acoustic interface with a discontinuous Galerkin formulation in [8, 88].

In two dimensions, linear and bilinear IFE spaces were discussed for the elliptic interface problem [36, 50, 61, 62, 63, 67, 77, 112] where the interface conditions are enforced at a selected number of points on the interface. To reduce the L^∞ error of the method around the interface, partial penalization techniques were introduced and analyzed in [84, 111], where a penalty term, borrowed from the interior penalty dG method, is added to the discrete formulation. However, the penalization here is only applied on the edges cut by the interface. Multiple IFE methods were proposed for the elasticity interface problem using linear and bilinear IFE functions [53, 57, 79] and using the so-called rotated Q^1 IFE functions [83] for its desirable locking-free feature. Partially penalized methods were applied to the parabolic interface problem with a static interface [80, 85], and with a moving interface [64] without the need to regenerate the mesh at every time step [49]. The Stokes interface problem was studied extensively and discontinuous immersed DG methods were developed in

[11, 14, 33] as well as partially penalized IFE methods based on the P^2-P^1 pair [35]. Recently, bilinear and biquadratic immersed dG methods were introduced for the acoustic interface problem [9, 88] and discrete stability results were derived. In addition to single-physics interface problems, the immersed dG method was applied recently to the acoustic-elastic wave propagation problem [17] where the acoustic wave is modeled by a system of three PDEs, whereas the elastic wave is modeled by a system of five PDEs. Also, higher order methods were developed in [5, 12, 13, 16, 25, 48, 51, 113] using different approaches for the construction and the analysis of the IFE space, and three-dimensional IFE methods were explored in [34, 52, 58, 71, 99].

The main feature of the IFE method is the IFE space. Typically, the IFE method employs polynomials to approximate the solution on elements away from the interface, and uses a special space, called the IFE space, on the interface elements. The IFE space consists of piecewise polynomial functions that satisfy the interface conditions exactly (in one dimension) or approximately (in two or three dimensions). As for the formulation, the IFE method usually uses the standard FE or dG discrete formulation, with minor changes if any. Therefore, the bulk of the research conducted in the IFE method revolves around studying IFE spaces.

We can classify the trends of the recent developments of the IFE method over the last decade into four major categories:

- Higher order IFE methods: Higher order methods typically outperform low order methods, with the same number of degrees of freedom, significantly. Furthermore, higher order methods allow us to use coarse meshes while retaining the desired accuracy, the cost of the construction of the IFE spaces reduces greatly.
- Higher dimensional problems: In higher dimensions, generating interface fitted meshes is expensive. Thus, unfitted methods are highly desirable.

- Analysis of the current methods: Several proposed IFE methods lack rigorous error analysis. Recently, many new techniques to analyze IFE methods have appeared [16, 18, 55] and motivated researchers in this direction.
- Applications: After the success of the IFE method to solve interface problems, there is ongoing research to use the IFE method for multi-physics simulations [17], plasma simulation [58] and inverse problems [48, 54, 56].

One of the main issues in the IFE method is the lack of a unifying framework. In general, the IFE space constructed for a specific interface problem cannot be used for a different interface problem. Furthermore, there are multiple methods to construct an IFE space for the same problem. In some methods, the interface conditions are imposed on a set of points [5, 79, 112], whereas in other methods, the interface conditions are imposed weakly [12, 16, 51]. Each approach requires a different set of techniques to obtain an error estimate, which ultimately slows the progress of research.

Another concern revolves around higher order IFE methods. In one spatial dimension, it is relatively easy to construct higher order spaces. The same is not true in two and three dimensions, where the construction is significantly more demanding.

1.2 Topics of the Dissertation

The contributions reported in this dissertation are twofold. Firstly, we focus on IFE spaces constructed for some one-dimensional interface problems, where we revisit multiple IFE and IDG methods that were proposed in the past to solve different interface problems, and we provide a set of mathematical tools that can be employed to analyze IFE methods for a set of interface problems.

Secondly, we develop a new approach to construct IFE functions for two-dimensional interface problems based on a local curvilinear coordinate system using the differential geometry of the interface. In this coordinate system, the interface is a vertical line segment.

1.3 Analysis of IFE Methods in One Dimension

In one spatial dimension, we can observe that the IFE methods such as those in [8, 70, 76, 81] are based on an IFE space of piecewise polynomial functions satisfying a condition of the form

$$\varphi^{(k)}(\alpha^+) = r_k \varphi^{(k)}(\alpha^-), \qquad k = 0, 1, \ldots, m, \tag{1.1}$$

where $(r_k)_k$ is a positive sequence that depends on the pertinent problem, and $\varphi^{(k)}$ is the k-th derivative of φ. For example, the IFE space for the elliptic interface problem

$$\begin{cases} \beta u'' = f, \quad \text{in } (a,\alpha) \cup (\alpha, b) \\ u(\alpha^+) - u(\alpha^-) = 0, \\ \beta^+ u'(\alpha^+) - \beta^- u'(\alpha^-) = 0, \end{cases} \qquad \beta(x) = \begin{cases} \beta^+, & x > \alpha, \\ \beta^-, & x < \alpha, \end{cases} \tag{1.2}$$

consists of piecewise polynomial functions that satisfy (1.1) with $r_0 = 1$ and $r_k = \frac{\beta^-}{\beta^+}$ for $k \geq 1$, assuming that f is a smooth function. We also subject u to appropriate boundary conditions.

The general form (1.1) allows us to understand the IFE spaces more abstractly, and to develop a rich theory around them. Furthermore, this approach has other advantages:

- By considering the general form, we can prove the existence of a Lagrange basis of any degree relatively easily. Previously, the research in this topic focused on constructing

a Lagrange basis for a specific interface problem at a time. For instance, in the case of the elliptic interface problem, the sequence $(r_k)_k$ is constant starting from $k = 1$, which was used extensively in [7] to prove the existence of a Lagrange basis of degree m by showing that a certain matrix is invertible. A similar approach for a more complicated sequence $(r_k)_k$ proved to be extremely difficult as reported in [88]. Instead, the author was only able to symbolically check the existence of the Lagrange basis for degrees $1 \leq m \leq 4$. In our framework, we show that functions in the m-th degree IFE space have at most m roots, which immediately implies the existence of the Lagrange basis.

- Similarly to the idea above, by considering the general case, we are able to derive several important results about IFE spaces, such as the inverse inequality and the trace inequality.
- A general theory allows us to consider a variety of projection operators for the analysis of IFE and IDG methods. Moreover, it allows us to re-purpose the classical projections used for non-interface problem, such as the Radau projection and the Lobatto projection, to analyze IFE and IDG methods.
- This framework allows us to extend the classical scaling argument to the analysis of immersed methods, whereas the previous analysis techniques relied on the multipoint Taylor expansion [7, 78], which leads to cumbersome and lengthy calculations, even for the simplest interface problem.

The last point is crucial and highly non-trivial. In the traditional finite element and dG methods, each element in the mesh is mapped to the same reference element, where the reference FE space is constructed. On the other hand, in the IFE method, when an interface element is mapped to the reference element $[0, 1]$, the interface point α is then mapped to a point $\breve{\alpha} \in (0, 1)$, which, under mesh refinement, $\breve{\alpha}$ changes position in $(0, 1)$. For this reason, we need to guarantee that the inequalities employed in the scaling argument, such as the

operator norm of the projection and the inverse inequality, hold independently of $\check{\alpha}$.

To achieve this, we start by considering the reference element $\check{I} = [0, 1]$ with an interface point $\check{\alpha} \in (0, 1)$. Now, let $\mathcal{V}^m_{\check{\alpha},r}(\check{I})$ be the space of all piecewise polynomial function $\check{\varphi}$ such that $\check{\varphi}|_{[0,\check{\alpha})}$ and $\check{\varphi}|_{(\check{\alpha},1]}$ are polynomials of degree not exceeding m, and

$$\check{\varphi}^{(k)}(\check{\alpha}^+) = r_k \check{\varphi}^{(k)}(\check{\alpha}^-), \qquad k = 0, 1, \ldots, m, \tag{1.3}$$

where $r_0, r_1, \ldots, r_m$ are positive constants. We show that $\mathcal{V}^m_{\check{\alpha},r}(\check{I})$ shares many properties with the polynomial space $\mathcal{P}^m(\check{I})$, such as

- The dimension of $\mathcal{V}^m_{\check{\alpha},r}(\check{I})$ is $m + 1$. Furthermore, there is a bounded invertible map from $\mathcal{V}^m_{\check{\alpha},r}(\check{I})$ to $\mathcal{P}^m([0, \check{\alpha}))$.
- The inverse inequality: Given $\check{\varphi} \in \mathcal{V}^m_{\check{\alpha},r}(\check{I})$, we have $\left\|\check{\varphi}^{(1)}\right\|_{0,\check{I}} \leq C \left\|\check{\varphi}\right\|_{0,\check{I}}$, where C is independent of $\check{\alpha}$, $\check{\varphi}^{(1)}$ is the piecewise derivative of $\check{\varphi}$, and $\|\cdot\|_{0,\check{I}}$ is the L^2 norm.
- If $\check{\varphi} \in \mathcal{V}^m_{\check{\alpha},r}(\check{I})$, then $\check{\varphi}$ has at most m roots, counting multiplicities. Consequently, given any $\xi_0, \xi_1, \ldots, \xi_m$, there is a *Lagrange basis* $\{L_i\}_{i=0}^m$ of $\mathcal{V}^m_{\check{\alpha},r}(\check{I})$ such that $L_i(\xi_j) = \delta_{i,j}$.
- If $\check{\varphi} \in \mathcal{V}^m_{\check{\alpha},r}(\check{I})$ is orthogonal to $\mathcal{V}^{m-1}_{\check{\alpha},r}(\check{I})$, then $\|\check{\varphi}\|_{0,\check{I}} \leq C(|\check{\varphi}(0)| + |\check{\varphi}(1)|)$. Again, C here is independent of $\check{\alpha}$.

Next, we shift our attention to the interface element $I_{k_0} = [x_{k_0-1}, x_{k_0-1} + h]$ which contains the interface point α. Then, the local interface element space $\mathcal{V}^m_{\alpha,r}(I_{k_0})$ is constructed directly from the reference element space $\mathcal{V}^m_{\check{\alpha},r}(\check{I})$ using the standard affine transformation. We consider the immersed Sobolev space $\mathcal{H}^{m+1}_{\alpha,r}(I_{k_0})$, the space of piecewise functions u that satisfy the interface conditions $u^{(k)}(\alpha^+) = r_k u^{(k)}(\alpha^-)$ for $0 \leq k \leq m$, and we consider a projection $P^m_{\alpha,r} : \mathcal{H}^{m+1}_{\alpha,r}(I_{k_0}) \to \mathcal{V}^m_{\alpha,r}(I_{k_0})$. Then, we show that if $P^m_{\alpha,r}$ is uniformly bounded

(see Definition 2.7), then

$$\left\|u - P_{\alpha,r}^{m} u\right\|_{0,I_{k_0}} \leq C h^{m+1} |u|_{m+1,I_{k_0}}, \tag{1.4}$$

where C is independent of α, and $|u|_{m+1,I_{k_0}}$ denotes the $m+1$ broken Sobolev semi-norm of u on I_{k_0}. At this point, we are ready to apply our theory to analyze IFE and IDG methods. For each method, we construct a suitable projection, we prove that it is well-defined and uniformly bounded, then we use the classical finite element and dG techniques to obtain an error estimate.

Below, we list the interface problems discussed in Chapter 2 with a brief description of our contributions.

- The elliptic interface problem $\beta u'' = f$: An IFE method for this problem was fully analyzed in [7] using a multipoint expansion technique. Nevertheless, we provide a simpler approach based on the immersed Lobatto projection.
- The parabolic interface problem $u_t = \beta u_{xx}$: Low order IFE methods for this problem were discussed in [70] but no error analysis appeared. Even though the interface conditions here are more complicated than those for the elliptic interface problem (see (2.52)), we are able to use the immersed Lobatto projection to produce an optimal error estimate.
- The Euler-Bernoulli beam interface problem $\beta u^{(4)} = f$: In the literature, only cubic IFE spaces were constructed and studied [78, 81], we expand those results to any degree m using the immersed Hermite projection.
- The transport interface problem $u_t + c u_x = 0$: Since this problem has not appeared in the IFE/IDG literature, we presented a full analysis using an immersed Radau projection with numerical examples to showcase the accuracy and robustness of the

IDG scheme.

- The acoustic interface problem $\mathbf{u}_t + A\mathbf{u}_x = 0$: Here A is a discontinuous matrix function. An IDG method was proposed for this problem in [8, 88] without error estimates. Here, we provide a full analysis of the method based on the vector Radau projection.

Here, we acknowledge that the success of our theory is due in part to the simplicity of the geometry in one dimension, where the interface is a point. Nevertheless, our theory presents a different approach for the construction and analysis of IFE spaces, where the structure of the IFE space is of utmost importance. Generally speaking, one can view the IFE space as a direct consequence of imposing the interface conditions on a finite dimensional space of piecewise functions, independently of the finite element or dG scheme used. This is similar to the history of the finite element method, where polynomials were studied extensively for centuries before they were employed in the FE method. In result, the finite element community benefited from the rich theory of polynomial functions, such as the interpolation capabilities, the well-studied orthogonal families, the inverse and trace inequalities, among other properties that we consider elementary today.

Yet, another reason for the success of the error analysis can be attributed to the local conformity of the IFE space, meaning that the IFE functions satisfy the interface conditions exactly, which eliminates the necessity of penalty terms on the interface in the numerical scheme, and simplifies the analysis of said scheme greatly.

The two observations given above led us to consider a new approach to construct IFE spaces in two dimensions, where the geometry is simplified through a coordinate transformation based on the differential geometry of the interface and the IFE space is locally conforming, which we discuss next.

1.4 The Frenet IFE Method in Two Dimensions

In order to illustrate the situation in two dimensions, we consider a domain Ω split by an interface Γ into Ω^- and Ω^+ such that $\Gamma = \partial\Omega^- \cap \partial\Omega^+$, and we consider the following elliptic interface problem

$$\begin{cases} -\nabla \cdot (\beta \nabla u) = f, & \text{in } \Omega^- \cup \Omega^+, \\ u|_{\partial\Omega} = g, \end{cases} \tag{1.5}$$

where the diffusion coefficient β is a piecewise constant positive function

$$\beta(\mathbf{x}) = \begin{cases} \beta^+, & \mathbf{x} \in \Omega^+, \\ \beta^-, & \mathbf{x} \in \Omega^-. \end{cases} \tag{1.6}$$

Then, the solution u is the piecewise function

$$u(\mathbf{x}) = \begin{cases} u^+(\mathbf{x}), & \mathbf{x} \in \Omega^+, \\ u^-(\mathbf{x}), & \mathbf{x} \in \Omega^-, \end{cases} \tag{1.7}$$

where, the functions $u^\pm$ satisfy the following elliptic partial differential equation

$$\begin{cases} \beta^\pm \Delta u^\pm = f|_{\Omega^\pm}, & \text{in } \Omega^\pm, \\ u^\pm = g, & \text{on } \partial\Omega \cap \partial\Omega^\pm. \end{cases} \tag{1.8}$$

Here, note that the boundary conditions given above do not cover the interface $\Gamma = \partial\Omega^- \cap \partial\Omega^+$. In an interface problem, the values of u^+ and u^-, and possibly their derivatives, are related on the interface via the so-called *interface conditions*, also known in the literature as jump conditions, or transmission conditions. In this dissertation, we restrict ourselves to

studying the homogeneous interface conditions [21, 28, 77]

$$u^+|_\Gamma - u^-|_\Gamma = 0, \qquad \text{(Continuity condition)} \tag{1.9a}$$

$$\left(\beta^+\nabla u^+ \cdot \mathbf{n}\right)|_\Gamma - \left(\beta^-\nabla u^- \cdot \mathbf{n}\right)|_\Gamma = 0, \qquad \text{(Flux continuity condition)} \tag{1.9b}$$

where $\mathbf{n}$ is the unit normal vector on Γ. Now, consider a rectangular element K split by the interface Γ into $K^- \subset \Omega^-$ and $K^+ \subset \Omega^+$, as shown in Figure 1.2. Naturally, we would seek to find a piecewise polynomial function $\varphi : K \to \mathbb{R}$ such that

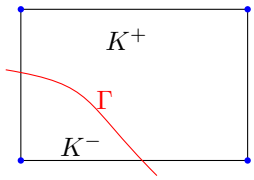

Figure 1.2: An illustration of an element K split by the interface Γ into K^- and K^+.

$$\varphi(\mathbf{x}) = \begin{cases} \varphi^+(\mathbf{x}), & \mathbf{x} \in K^+, \\ \varphi^-(\mathbf{x}), & \mathbf{x} \in K^-, \end{cases} \tag{1.10}$$

where φ^- and φ^+ are polynomial functions that satisfy the interface conditions (1.9) on $\Gamma \cap K$, that is,

$$\varphi^+|_{\Gamma\cap K} - \varphi^-|_{\Gamma\cap K} = 0, \tag{1.11a}$$

$$\left(\beta^+\nabla\varphi^+ \cdot \mathbf{n}\right)|_{\Gamma\cap K} - \left(\beta^-\nabla\varphi^- \cdot \mathbf{n}\right)|_{\Gamma\cap K} = 0. \tag{1.11b}$$

However, finding two polynomials φ^- and φ^+ such that (1.11) holds is not always possible, even for simple interfaces Γ. For example, consider the case where $\varphi^\pm$ are picewise linear functions, and the Interface Γ is a circle. Then, the continuity conditions (1.11a) implies that $\varphi^+ = \varphi^-$. Hence, the flux continuity condition(1.11b) becomes $(\beta^+ - \beta^-)\nabla\varphi^+ \cdot \mathbf{n} = 0$,

which eventually leads to $\varphi^+ = \varphi^- = 0$. This observation led researchers to consider other ways to enforce the interface conditions (1.9) as discussed in Section 1.1.

Another issue, that is not emphasized often, is the hidden complexity in (1.11b), which, when expanded is equivalent to

$$\beta^+ \left(\varphi_x^+ n_1 + \varphi_y^+ n_2\right)|_{\Gamma\cap K} - \beta^- \left(\varphi_x^- n_1 + \varphi_y^- n_2\right)|_{\Gamma\cap K} = 0, \tag{1.12}$$

where $(n_1, n_2) = \mathbf{n}$ are the components of the normal vector, which complicates the construction procedure of the IFE space [10, 17, 25], and add additional challenges when discussing the dimension of the IFE space [12].

We note that these two issues were not present in one dimensional case, since interface conditions (1.1) are simple and can be satisfied exactly by a piecewise polynomial function φ. Similarly, in two dimensions, we do not observe these issues when the interface is trivial, such as when the interface is a vertical line. At first, this might suggest approximating the interface locally with a line segment, as done in [62, 77]. However, this approximation is not suitable for higher order IFE methods since it introduces a discretization error of order $O(h^2)$. Instead, we propose a different approach which yields IFE functions that satisfy the interface conditions (1.11) exactly, and simplifies (1.12) considerably. Additionally, this new approach is capable of constructing IFE spaces of any degree efficiently and reliably, without the need for any user chosen parameters.

The key idea here lies in the differential geometry properties of the interface: If we consider a parametrization $\mathbf{g} : I \subset \mathbb{R} \to \mathbb{R}^2$ of Γ, then every point $\mathbf{x} \in \Gamma$ is of the form $\mathbf{x} = \mathbf{g}(\xi)$ for some $\xi \in I$. However, if $\mathbf{x} \notin \Gamma$, then there is no ξ such that $\mathbf{g}(\xi) = \mathbf{x}$. Instead, we can search

for the closest point to $\mathbf{x}$ on the curve Γ, which leads to the following minimization problem

$$\text{Find } \xi_{\mathbf{x}} \in I, \qquad \|\mathbf{x} - \mathbf{g}(\xi_{\mathbf{x}})\|^2 = \min_{\xi \in I} \|\mathbf{x} - \mathbf{g}(\xi)\|^2, \tag{1.13}$$

where $\|\cdot\|$ denotes the Euclidean norm. Then, by considering derivative of the distance function $d(\xi) = \|\mathbf{x} - \mathbf{g}(\xi)\|^2$ at $\xi_{\mathbf{x}}$, we obtain

$$\mathbf{g}'(\xi_{\mathbf{x}}) \cdot (\mathbf{x} - \mathbf{g}(\xi_{\mathbf{x}})) = 0,$$

which suggests that $\mathbf{x} - \mathbf{g}(\xi_{\mathbf{x}}) = \eta_{\mathbf{x}}\mathbf{n}(\xi_{\mathbf{x}})$, where $\mathbf{n}(\xi_x)$ is the unit normal vector on Γ at $\mathbf{g}(\xi_{\mathbf{x}})$, and $\eta_{\mathbf{x}}$ is a real number. Therefore, we observe that $\mathbf{x} = \mathbf{g}(\xi_{\mathbf{x}}) + \eta_{\mathbf{x}}\mathbf{n}(\xi_{\mathbf{x}})$, i.e. $\mathbf{x}$ is characterized by the ξ-value of the closest point on the curve, and its (signed) distance from the curve. Here, note that we are assuming that $\mathbf{g}$ is differentiable and that $\mathbf{g}'$ is never zero, these conditions (and more) will be discussed in details in Chapter 3.

Now, we observe that we have two transformations P and R, where $P : (\eta, \xi) \mapsto \mathbf{g}(\xi) + \eta\mathbf{n}(\xi)$, and $R : \mathbf{x} \to\!\!\!\mapsto (\eta_{\mathbf{x}}, \xi_{\mathbf{x}})$. It is easy to see that P is well-defined on $\mathbb{R} \times I$. However, it is not clear whether R is well-defined since the minimization problem (1.13) might have multiple solutions. As we will see later in Section 5.1, the map R is well-defined in a neighborhood of Γ by the tubular neighborhood theorem [1]. Furthermore, the maps P and R are inverses of each other.

Next, consider the map R and a point $\mathbf{x} \in \Gamma$, since the distance from $\mathbf{x}$ to Γ is zero, then $R(\mathbf{x}) = (0, \xi_{\mathbf{x}})$ for some $\xi_{\mathbf{x}} \in I$. Hence, R maps points on the interface to points on the vertical axis in the (η, ξ) frame. Furthermore, when the transformation R is applied to an element cut by the interface, such as the one shown in Figure 1.2, we obtain a curvilinear element, which we denote $\hat{K} = R(K)$, such that $\hat{K}$ is split by the vertical line segment $\hat{\Gamma} = R(\Gamma)$ into $\hat{K}^-$ and $\hat{K}^+$, as illustrated in Figure 1.3. More importantly, if $u : K \to \mathbb{R}$

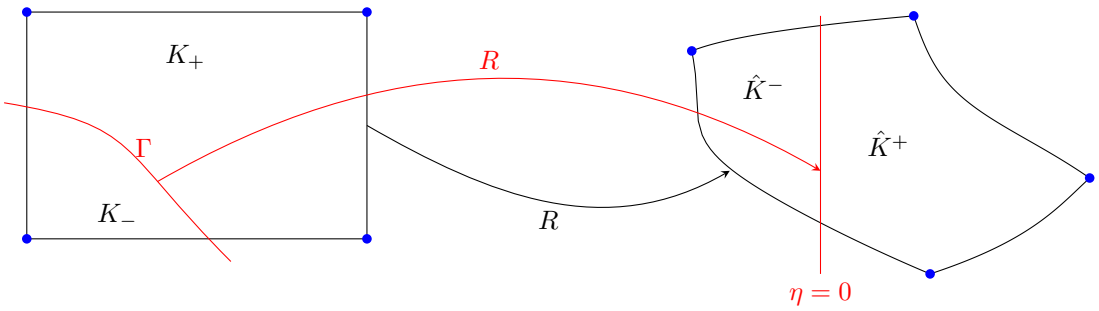

Figure 1.3: The curved interface Γ (left) mapped to the vertical line $\eta = 0$ (right) by the transformation R.

satisfies the interface conditions (1.9), then $\hat{u} = u \circ P : \hat{K} \to \mathbb{R}$ satisfies

$$\hat{u}^+(0,\xi) = \hat{u}^-(0,\xi), \tag{1.14a}$$

$$\beta^+ \hat{u}_\eta^+(0,\xi) = \beta^- \hat{u}_\eta^-(0,\xi), \tag{1.14b}$$

for all $\xi \in R(\Gamma \cap K)$, where $\hat{u}^\pm = \hat{u}|_{\hat{K}^\pm}$. Note here that the new interface conditions (1.14) are extremely similar to the one dimensional interface conditions (1.1) with $\alpha = 0$. Furthermore, these new interface conditions are much simpler than (1.9) since the normal derivative is now a derivative with respect to η, and the interface is merely a segment on the line $\eta = 0$. Additionally, we note that it is relatively easy to construct a piecewise polynomial function $\hat{\varphi} : \hat{K} \to \mathbb{R}$ that satisfies (1.14) exactly, that is

$$\hat{\varphi}^+(0,\xi) = \hat{\varphi}^-(0,\xi), \tag{1.15a}$$

$$\beta^+ \hat{\varphi}_\eta^+(0,\xi) = \beta^- \hat{\varphi}_\eta^-(0,\xi). \tag{1.15b}$$

For instance, the functions $\hat{\varphi}_0, \hat{\varphi}_1$ and $\hat{\varphi}_2$ shown below satisfy (1.15) exactly.

$$\hat{\varphi}_0(\eta,\xi) = 1, \quad \hat{\varphi}_1(\eta,\xi) = \xi, \quad \hat{\varphi}_2(\eta,\xi) = \begin{cases} \frac{\eta}{\beta^+}, & (\eta,\xi) \in \hat{K}^+, \\ \frac{\eta}{\beta^-}, & (\eta,\xi) \in \hat{K}^-. \end{cases} \tag{1.16}$$

Higher order basis functions can be obtained easily by adding the Laplacian interface conditions (3.1d) to (1.11), yielding a Frenet IFE space $\hat{\mathcal{V}}_\beta^m(\hat{K})$ of dimension $(m+1)^2$. Next, a local Frenet IFE space $\mathcal{V}_\beta^m(K)$ is formed using the transformation R, that is, the local IFE space consists of functions of the form $\varphi = \hat{\varphi} \circ R$ where $\hat{\varphi} \in \hat{\mathcal{V}}_\beta^m(\hat{K})$.

Again, we recall that, unlike the traditional IFE functions, the functions in the local Frenet IFE space are continuous since they satisfy (1.11) exactly. To see this more clearly, we present in Figure 1.4 a bilinear IFE function constructed using [61, 62] on the left. On the right, we present the newly introduced $\varphi_2 = \hat{\varphi}_2 \circ R$, where $\hat{\varphi}_2$ is defined in (1.16). The former is only continuous at two points on the interface, whereas the latter is continuous everywhere on the element.

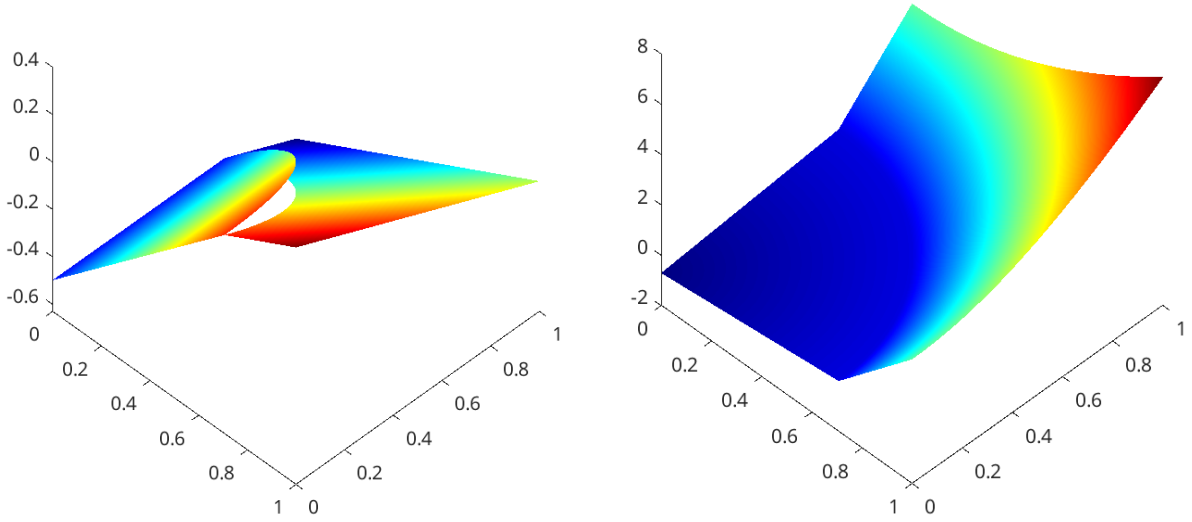

(a) A traditional IFE function [77]. (b) The function $\hat{\varphi}_2$ from (1.16).

Figure 1.4: An illustration of a traditional IFE function (left) and a Frenet IFE function (right).

Another advantage of the Frenet IFE method is the simplicity of the construction. In fact, out of the $(m+1)^2$ basis functions for $\hat{\mathcal{V}}_\beta^m(\hat{K})$, $m(m+1)$ of them are given explicitly by the

following formula

$$\hat{\varphi}_{i,j}(\eta,\xi)=\begin{cases}\frac{1}{\beta^+}\xi^i\eta^j, & (\eta,\xi)\in\hat{K}^+,\\ \frac{1}{\beta^-}\xi^i\eta^j, & (\eta,\xi)\in\hat{K}^-,\end{cases}\qquad 0\le i\le m,\ 1\le j\le m.$$

Thus, it remains to construct the remaining $m+1$ basis functions by solving a linear system, which is described thoroughly in Chapter 3.

In addition to its simplicity, the Frenet IFE space has optimal approximation capabilities: If $\hat{u}:\hat{K}\to\mathbb{R}$ is smooth and satisfies the interface conditions on the flattened interface $\eta=0$, then

$$\left\|\hat{u}-\hat{P}_h\hat{u}\right\|_{0,\hat{K}}\le Ch^{m+1}|\hat{u}|_{m+1,\hat{K}},$$

where $\hat{P}_h\hat{u}$ is the L^2 projection of $\hat{u}$ onto $\hat{\mathcal{V}}_\beta^m(\hat{K})$, and C is independent of the relative position of the interface, the mesh size h, and the diffusion coefficients $\beta^\pm$. Consequently, if $u:K\to\mathbb{R}$ satisfies the interface conditions on the physical interface Γ, then

$$\|u-P_hu\|_{0,K}\le Ch^{m+1}\|u\|_{m+1,K},$$

where, P_h is the L^2 projection onto $\mathcal{V}_\beta^m(K)$. Again, the constant C in the previous error estimate is independent of the relative position of the interface, the mesh size h, and the diffusion coefficients $\beta^\pm$. We note here that the last inequality involves the $(m+1)$ norm of u, instead of the semi-norm.

Finally, we employ the Frenet IFE space to solve the elliptic interface problem and the hyperbolic interface problem using a symmetric interior penalty discontinuous Galerkin (SIPDG) formulation. For both problems, the numerical scheme produces optimally converging solutions. Furthermore, for the elliptic interface problem, the Frenet IFE method can be

employed on extremely coarse meshes and produces highly accurate solutions when higher order element are used. This leads to a significant cost reduction over the existing low order IFE methods. For example, see the errors associated with the Frenet SIPDG method applied to two interface problems on a 5×5 mesh in Example 5.3.

1.5 Outline of the Dissertation

The dissertation is organized as follows.

In Chapter 2, we provide a unified framework to analyze one-dimensional IFE methods for a variety of interface problems based on the immersed Bramble-Hilbert lemma developed in Section 2.3. For each problem, we show that the IFE method converges optimally to the solution by following the same three steps:

1. First, we construct a suitable projection operator for the IFE space associated with the interface problem.

2. Second, we show that the projection operator is well-defined, and its norm is not affected by the relative position of the interface.

3. Lastly, we use the immersed Bramble-Hilbert lemma and the classical finite element arguments to derive an optimal error bound for the IFE method.

In Chapter 3, we present a new framework for constructing higher order IFE methods based on the Frenet transformation. We begin the chapter by discussing the local curvilinear coordinates system associated with the interface, and the relevant differential geometry and calculus identities. Then, we describe the construction of the Frenet IFE space in detail.

In Chapter 4, we investigate the approximation capabilities of the Frenet IFE space, and we provide numerical examples at the end.

In Chapter 5, we introduce an interior penalty dG method based on the Frenet IFE space to solve the elliptic and the hyperbolic interface problem, and provide numerical examples that show the optimal convergence of the IFE method.

In Chapter 6, we summarize the contributions of this dissertation, and we propose some future research directions pertaining to the Frenet IFE framework.

Chapter 2

Unified Analysis for One Dimensional IFE Methods

In this chapter, we develop a framework for analyzing various IFE spaces for one-dimensional interface problems. We start this chapter by describing multiple interface problems that we are interested in studying. Next, we develop a general IFE space and an immersed Bramble-Hilbert lemma for a general class of IFE projections, then we use this result to analyze the IFE/IDG scheme for each interface problem.

The results in this chapter are partially reported in [18].

2.1 Motivation and Notation

In this chapter, we intend to investigate a few representative interface problems, which we will list shortly. In all the problems below, let $I = (a, b)$ be a bounded interval and let $\alpha \in I$ be the interface point, splitting I into two subdomains $I^- = (a, \alpha)$ and $I^+ = (\alpha, b)$. We note that although we are restricting our attention here to interface problems with one interface point, the analysis extends naturally to interface problems with multiple interfaces.

Let $\beta : I \to \mathbb{R}^+$ be a piecewise constant function such that $\beta|_{I^s} = \beta^s > 0$, where $s \in \{+, -\}$. To simplify the presentation, we use $[\![f]\!]_a$ to denote the jump of a function f at a point z,

that is,

$$[\![f]\!]_z = f(z^+) - f(z^-), \qquad \text{where} \quad f(z^\pm) = \lim_{x \to z^\pm} f(x).$$

Next, we briefly describe the interface problem discussed in this chapter below:

- The elliptic interface problem seeks to find a solution to

$$\begin{cases} -\beta(x)u''(x) = f(x), & x \in I^- \cup I^+, \\ u(a) = u(b) = 0, \end{cases} \tag{2.1a}$$

  subject to the interface conditions $[\![u]\!]_\alpha = [\![\beta u']\!]_\alpha = 0$.

- The Euler-Bernoulli beam interface problem is the fourth order analog of (2.1a), that is

$$\begin{cases} \beta(x)u^{(4)}(x) = f(x), & x \in I^- \cup I^+, \\ u(a) = u'(a) = u(b) = u'(b) = 0, \end{cases} \tag{2.1b}$$

  subject to the interface conditions

$$[\![u]\!]_\alpha = [\![u']\!]_\alpha = [\![\beta u^{(2)}]\!]_\alpha = [\![\beta u^{(3)}]\!]_\alpha = 0.$$

- The parabolic interface problem

$$\begin{cases} u_t(x,t) = \beta(x)u_{xx}(x,t), & x \in I^- \cup I^+,\ t > 0, \\ u(a,t) = u(b,t) = 0, & t > 0, \\ u(x,0) = g(x), & x \in (a,b), \end{cases} \tag{2.1c}$$

  subject to the interface conditions $[\![u(\cdot,t)]\!]_\alpha = [\![\beta u_x(\cdot,t)]\!] = 0$.

- The transport interface problem

$$\begin{cases} u_t(x,t) + \beta(x)u_x(x,t) = 0, & x \in I^- \cup I^+,\ t > 0, \\ u(a,t) = u_a(t), & t > 0, \\ u(x,0) = u_0(x), & x \in (a,b), \end{cases} \tag{2.1d}$$

  subject to the interface condition $[\![u(\cdot,t)]\!]_\alpha = 0$

- The acoustic interface problem: Let $\rho, c : I \to \mathbb{R}_+$ be two positive piecewise constant functions such that $\rho|_{I^s} = \rho^s$ and $c|_{I^s} = c^s$ for $s \in \{-,+\}$. We seek $u, p : I \times [0,\infty)$ such that

$$\begin{cases} p_t(x,t) = \rho(x)c(x)^2 u_x(x,t), & x \in I^- \cup I^+,\ t > 0, \\ \rho(x)u_t(x,t) = p_x(x,t), & x \in I^- \cup I^+,\ t > 0 \\ p(x,0) = p_0(x),\ u(x,0) = u_0(x), & x \in (a,b), \end{cases} \tag{2.1e}$$

  subject to the interface conditions $[\![p]\!]_\alpha = [\![u]\!]_\alpha = 0$ and suitable boundary conditions that will be discussed later.

IFE methods for most of the interface problems listed above have appeared in the literature before. For instance, the first appearance of the IFE method in the literature can be traced back to [76] where linear IFE spaces were introduced and analyzed for the elliptic interface problem. Later, higher order methods were studied in [7] using some problem-specific techniques. The Euler-Bernoulli beam interface problem received considerable attention [78, 81, 101] from the IFE community for its many applications in mechanics. However, only cubic immersed finite element space were developed and studied. On the other hand, only low order IFE methods were developed for the parabolic and the acoustic interface problems [8, 70, 88] and no IFE methods were developed for the transport interface problems to our

knowledge.

In addition to the interface conditions listed above, one can derive extended interface conditions that relate the k-th derivative of the solution on the two sides of the interface. In general, the solutions to the interface problems described above can be shown to satisfy

$$u^{(k)}(\alpha^+) = r_k u^{(k)}(\alpha^-), \qquad k = 0, 1, \ldots. \tag{2.2}$$

under suitable smoothness assumptions, where (r_k) is a positive sequence that depends on the interface problem. In general, we only need to consider finite sequences $(r_k)_{k=0}^{\tilde{m}}$ for some $\tilde{m} \geq 1$. However, to simplify the presentation, we will treat (r_k) as an infinite sequence $(r_k)_{k=0}^{\infty}$, while we use only a finite subsequence. Typically, we only need the subsequence $(r_k)_{k=0}^{m}$, where m the degree of the polynomials used in the construction of the m-th degree IFE space.

The general form of the extended jump conditions (2.2) motivates us to define an immersed Sobolev space, which we will use later to describe the solutions to the interface problems and analyze the IFE solutions

Definition 2.1. Let $m \geq 0$ be an integer, let (r_k) be a positive sequence. Consider an interval $B \subset \mathbb{R}$ that contains a point α, we use $\mathcal{H}_{\alpha,r}^{m+1}(B)$ to denote the immersed Sobolev space defined as

$$\mathcal{H}_{\alpha,r}^{m+1}(B) = \left\{ u \mid u|_{B^\pm} \in H^{m+1}(B^\pm) \text{ and } u^{(k)}(\alpha^+) = r_k u^{(k)}(\alpha^-),\ \forall k = 0, 1, \ldots, m \right\}$$

We note here that in the definition above, the traces of $u^{(k)}|_{B^\pm}$ at α are well-defined for $k \leq m$ since $u^{(k)}|_{B^\pm} \in H^{m+1}(I^\pm)$ by the Sobolev trace theorem [4].

Now, we move to describing some notation that will be used in this chapter. For ease of

presentation, we will use ∂_x and ∂_t to denote the differential operator with respect to x and t, respectively. Additionally, we will use $s \in \{+, -\}$ to denote a sign choice and s' to denote the dual of s, that is, if $s = +$, then $s' = -$, and if $s = -$, then $s' = +$.

When stating inequalities, we will use $\lesssim$ and $\gtrsim$ to denote an inequality with a generic hidden constant. That is $a \lesssim b$ if there is a generic constant C such that $a \leq Cb$, and we use $a \simeq b$ to denote the equivalence $a \lesssim b$ and $b \lesssim a$.

If the inequality involves the degree m, the sequence $r = (r_k)$, the interface location, the physical parameters or other quantities, we will include them as subscript in the inequality or equivalence notation. For example, we will use $a \lesssim_\beta b$ (resp. $a \gtrsim_\beta b$) if $a \leq Cb$ (resp. $a \geq Cb$) and C depends on β.

Throughout this chapter, we will consider a bounded open interval $I = (a, b)$, and let $\alpha \in I$ be the interface point dividing I into two open intervals $I^- = (a, \alpha), I^+ = (\alpha, b)$. This convention extends to any other open interval $B \subseteq \mathbb{R}$ with $B^- = B \cap (-\infty, \alpha)$ and $B^+ = B \cap (\alpha, \infty)$. For every bounded open interval B not containing α, let $H^m(B)$ be the usual Sobolev space $W^{m,2}(B)$ on B equipped with the norm $\|\cdot\|_{m,B}$ and the semi-norm $|\cdot|_{m,B}$. We will use $(\cdot,\cdot)_B$ and $(\cdot,\cdot)_{w,B}$ to denote the classical and the weighted L^2 inner product defined as

$$(f, g)_B = \int_B f(x)g(x)\, dx, \qquad (f, g)_{w,B} = \int_B w(x)f(x)g(x)\, dx, \qquad w(x) > 0,\ \forall\ x \in B.$$

Moreover, we use $H_0^1(B) \subset H^1(B)$ to denote the Sobolev space of functions with zero trace on the boundary of B. Similarly, $H_0^2(B) \subset H^2(B)$ is the Sobolev space of functions u such that $u|_{\partial B} = u'|_{\partial B} = 0$.

Given a positive sequence $r = (r_k)$. We define

$$\mathcal{V}^m_{\alpha,r}(B) = \left\{p \in \mathcal{H}^{m+1}_{\alpha,r}(B) \mid p|_{B^\pm} \in \mathcal{P}^m(B^\pm)\right\} \tag{2.3}$$

to be the local immersed finite element space on B. Additionally, we use $\|\cdot\|_{m,B}$ and $|\cdot|_{m,B}$ to denote the broken Sobolev norms on B, that is

$$\|\cdot\|^2_{m,B} = \|\cdot\|^2_{m,B^+} + \|\cdot\|^2_{m,B^-}, \qquad |\cdot|^2_{m,B} = |\cdot|^2_{m,B^+} + |\cdot|^2_{m,B^-}.$$

We will use u' to denote the piecewise derivative of u, i.e., given $u \in \mathcal{H}^m_{\alpha,r}(B)$, $u|'_{B^\pm}$ is the classical derivative of $u|_{B^\pm}$, and it should not be confused with the distributional or the weak derivative of u. This is important because the immersed Sobolev space $\mathcal{H}^{m+1}_{\alpha,r}(B)$ is not necessarily a subspace of $H^1(B)$.

By dividing I into N sub-intervals, we obtain the following mesh on I:

$$I_k = [x_{k-1}, x_k], \quad \mathcal{T}_h = \{I_k\}_{k=1}^N, \quad a = x_0 < x_1 < \cdots < x_N = b, \qquad h = \max_{1\le k\le N}(x_k - x_{k-1}).$$

We will assume that there is $k_0 \in \{1, 2, \ldots, N\}$ such that $x_{k_0-1} < \alpha < x_{k_0}$, which is equivalent to $\alpha \in \overset{\circ}{I}_{k_0}$. We define the discontinuous immersed finite element space $\mathcal{V}^m_{\alpha,r}(\mathcal{T}_h)$ as

$$\mathcal{V}^m_{\alpha,r}(\mathcal{T}_h) = \left\{\varphi \mid \varphi|_{I_k} \in \mathcal{P}^m(I_k) \text{ for } k \in \{1, \ldots, N\}\backslash\{k_0\} \text{ and } \varphi|_{I_{k_0}} \in \mathcal{V}^m_{\alpha,r}(I_{k_0})\right\}, \tag{2.4}$$

where $\mathcal{P}^m(I_k)$ is the space of polynomials of degree at most m on I_k and $\mathcal{V}^m_{\alpha,r}(I_{k_0})$ is the local immersed finite element (*LIFE*) space defined in (2.3).

2.2 The Reference IFE Space

In the remainder of this chapter, let $(r_k)_{k\geq 0}$ be a positive sequence and let $\check{I} = [0,1]$ be the reference element containing a reference interface point $\check{\alpha} \in \check{I}$. The interface point $\check{\alpha}$ splits the element $\check{I}$ into two sub-elements $\check{I}^- = [0,\check{\alpha})$ and $\check{I}^+ = (\check{\alpha},1]$. We use $\mathcal{V}^m_{\check{\alpha},r}(\check{I})$ to denote the reference IFE space defined as

$$\mathcal{V}^m_{\check{\alpha},r}(\check{I}) = \left\{\check{\varphi} : \check{I} \to \mathbb{R} \mid \check{\varphi}|_{\check{I}^s} \in \mathcal{P}^m(\check{I}^s),\ \check{\varphi}^{(k)}(\check{\alpha}^+) = r_k\check{\varphi}^{(k)}(\check{\alpha}^-),\ k = 0,1,\ldots,m\right\}. \tag{2.5}$$

For a function $\check{\varphi} \in \mathcal{V}^m_{\check{\alpha},r}(\check{I})$, we write $\check{\varphi} = (\check{\varphi}_-, \check{\varphi}_+)$ where $\check{\varphi}_\pm = \check{\varphi}|_{\check{I}^\pm}$. Additionally, we will use $\check{\varphi}^{(k)}_\pm(\check{\alpha})$ to denote the trace of $\check{\varphi}^{(k)}_\pm$ at $\check{\alpha}$. More precisely,

$$\check{\varphi}^{(k)}_\pm(\check{\alpha}) = \lim_{\epsilon\to 0^\pm} \check{\varphi}^{(k)}(\check{\alpha}+\epsilon).$$

Then, we can re-write the definition of $\mathcal{V}^m_{\check{\alpha},r}(\check{I})$ in terms of $\check{\varphi}_-$ and $\check{\varphi}_+$ as

$$(\check{\varphi}_-,\check{\varphi}_+) \in \mathcal{V}^m_{\check{\alpha},r}(\check{I}) \text{ iff } \check{\varphi}_\pm \in \mathcal{P}^m(\check{I}^\pm) \text{ and } \check{\varphi}^{(k)}_+(\check{\alpha}) = r_k\check{\varphi}^{(k)}_-(\check{\alpha}),\ k = 0,1,\ldots,m. \tag{2.6}$$

The reference IFE space (2.5) arises naturally when studying the local IFE space (2.3). Typically, in the finite element method, we study the basis functions on a reference element, then we map our results to the physical element. However, in the presence of an interface, one has to account for the relative position of the interface in the interface element. That is, even if the interface is fixed, the relative position of the interface inside the interface element changes when the mesh is refined as illustrated in Figure 2.1. Therefore, we need to ensure that the inequalities derived here are independent of $\check{\alpha}$ since we cannot control its value.

Lemma 2.1. *Let (r_k) be a positive sequence, $\check{\alpha} \in \check{I}$ and $s \in \{-,+\}$. Then,*

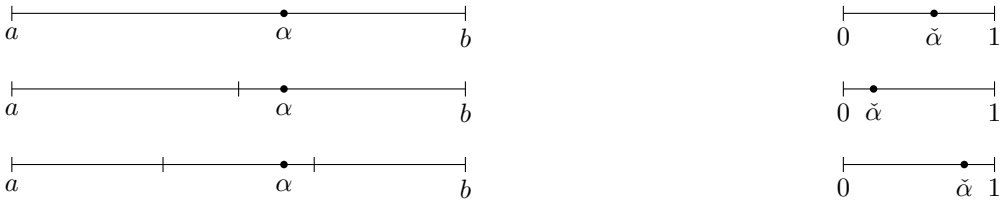

Figure 2.1: Illustration of three meshes (left) and the associated reference interface elements $\check{I}$ (right).

1. *Given $\check{\varphi}_s \in \mathcal{P}^m(\check{I}^s)$, there is a unique $\check{\varphi}_{s'} \in \mathcal{P}^m(\check{I}^{s'})$ such that $(\check{\varphi}_-, \check{\varphi}_+) \in \mathcal{V}^m_{\check{\alpha},r}(\check{I})$.*

2. $\dim \mathcal{V}^m_{\check{\alpha},r}(\check{I}) = m + 1$.

3. *The set $\{\mathcal{N}^k_{\check{\alpha},r}\}_{k=0}^m$ of functions*

$$\mathcal{N}^k_{\check{\alpha},r} = \begin{cases} (x-\check{\alpha})^k, & x \in \check{I}^-, \\ r_k(x-\check{\alpha})^k, & x \in \check{I}^+ \end{cases} \tag{2.7}$$

   is basis of $\mathcal{V}^m_{\check{\alpha},r}(\check{I})$ that we will refer to as the canonical basis.

4. *If $r_k = 1$ for all $0 \le k \le m$, then $\mathcal{V}^m_{\check{\alpha},r}(\check{I}) = \mathcal{P}^m(\check{I})$.*

5. *Let $\check{\varphi} \in \mathcal{V}^m_{\check{\alpha},r}(\check{I})$, then $\check{\varphi}' \in \mathcal{V}^{m-1}_{\check{\alpha},\tau(r)}(\check{I})$, where τ is the left shift operator defined as $\tau : (r_0, r_1, \dots) \mapsto (r_1, r_2, \dots)$.*

Proof. We will prove the statements in order:

1. Without loss of generality, consider $\check{\varphi}_- \in \mathcal{P}^m(\check{I}^-)$, then

$$\check{\varphi}_-(x) = \sum_{k=0}^m \frac{c_k}{k!}(x-\check{\alpha})^k.$$

   Now, consider the problem of finding $\check{\varphi}_+ \in \mathcal{P}^m(\check{I}^+)$ such that $(\check{\varphi}_-, \check{\varphi}_+) \in \mathcal{V}^m_{\check{\alpha},r}(\check{I})$.

First, we express $\check{\varphi}_+$ as

$$\check{\varphi}_+(x) = \sum_{k=0}^{m} \frac{d_k}{k!}(x-\check{\alpha})^k,$$

for some coefficients $\{d_k\}_{k=0}^m$. Then by the definition (2.6), we have

$$d_k = \check{\varphi}_+^{(k)}(\check{\alpha}) = r_k \check{\varphi}_-^{(k)}(\check{\alpha}) = r_k c_k,$$

which uniquely determines $\check{\varphi}_+$ in terms of $\check{\varphi}_-$.

2. Since every polynomial $\check{\varphi}_- \in \mathcal{P}^m(\check{I}^-)$ can be *extended* to $(\check{\varphi}_-, \check{\varphi}_+) \in \mathcal{V}_{\check{\alpha},r}^m(\check{I})$. Then,

$$\dim(\mathcal{V}_{\check{\alpha},r}^m(\check{I})) = \dim(\mathcal{P}^m(\check{I}^-)) = m+1.$$

3. The set $\{\mathcal{N}_{\check{\alpha},r}^k\}_{k=0}^m$ is linearly independent since the set of restrictions $\{(\mathcal{N}_{\check{\alpha},r}^k)|_{\check{I}^-}\}_{k=0}^m$ is a basis of $\mathcal{P}^m(\check{I}^-)$. Additionally, the cardinality of $\{\mathcal{N}_{\check{\alpha},r}^k\}_{k=0}^m$ matches the dimension of the space $\mathcal{V}_{\check{\alpha},r}^m(\check{I})$. Therefore, it forms a basis.

4. If $r_k = 1$ for all $0 \le k \le m$, then the set $\{\mathcal{N}_{\check{\alpha},r}^k\}_{k=0}^m$ forms a basis of $\mathcal{P}^m(\check{I})$. Hence, we have $\mathcal{V}_{\check{\alpha},r}^m(\check{I}) = \mathcal{P}^m(\check{I})$.

5. Let $\psi = \check{\varphi}'$ and let $\rho = \tau(r)$, then by definition of $\mathcal{V}_{\check{\alpha},r}^m(\check{I})$, we have

$$\psi_+^{(k)}(\check{\alpha}) = \check{\varphi}_+^{(k+1)}(\check{\alpha}) = r_{k+1}\check{\varphi}_-^{(k+1)}(\check{\alpha}) = \rho_k \psi_-^{(k)}(\check{\alpha}), \qquad 0 \le k \le m.$$

Thus, $\psi \in \mathcal{V}_{\check{\alpha},\rho}^{m-1}(\check{I})$, which is the desired result. □

Remark 2.1. By definition, the canonical basis functions $\mathcal{N}_{\check{\alpha},r}^k$ with $k \ge 1$ are continuous. However, the first basis function $\mathcal{N}_{\check{\alpha},r}^0$ can be discontinuous if $r_0 \ne 1$ as Figure 2.2 shows.

In light of Lemma 2.1, we introduce an *extension* operator that pairs a polynomial $\check{\varphi}_s \in$

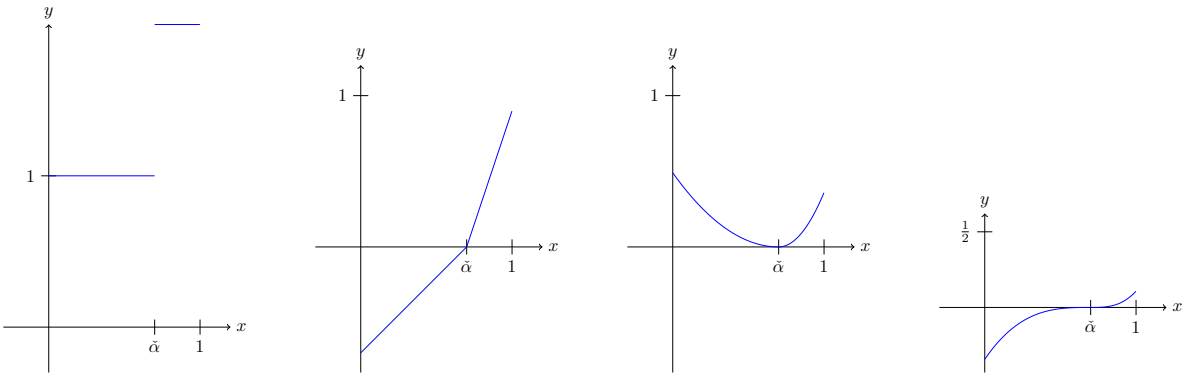

(a) $\mathcal{N}^0_{\check{\alpha},r}$ (b) $\mathcal{N}^1_{\check{\alpha},r}$ (c) $\mathcal{N}^2_{\check{\alpha},r}$ (d) $\mathcal{N}^3_{\check{\alpha},r}$

Figure 2.2: An example of the first four canonical basis functions with $r_k = k + 1$.

$\mathcal{P}^m(\check{I}^s)$ with a polynomial $\check{\varphi}_{s'} \in \mathcal{P}^m(\check{I}^{s'})$, where $s \in \{-,+\}$, such that $\check{\varphi} = (\check{\varphi}_-, \check{\varphi}_+) \in \mathcal{V}^m_{\check{\alpha},r}(\check{I})$. We note here that, since the intervals $\check{I}^{\pm}$ are disjoint, our use of the term *extension* here is different from the standard one.

Definition 2.2. Let (r_k) be a positive sequence, $\check{\alpha} \in \check{I}$ and $s \in \{-,+\}$. We use $\mathcal{E}^{m,s'}_{\check{\alpha},r}$ to denote the extension operator

$$\mathcal{E}^{m,s'}_{\check{\alpha},r} : \mathcal{P}^m(\check{I}^s) \to \mathcal{P}^m(\check{I}^{s'})$$

defined as the unique $\check{\varphi}_{s'} = \mathcal{E}^{m,s'}_{\check{\alpha},r}(\check{\varphi}_s)$ such that $(\check{\varphi}_-, \check{\varphi}_+) \in \mathcal{V}^m_{\check{\alpha},r}(\check{I})$.

It follows immediately from Lemma 2.1 that the extension operator is well-defined and bijective. Furthermore, it is easy to show that

$$\mathcal{E}^{m,+}_{\check{\alpha},r} \circ \mathcal{E}^{m,-}_{\check{\alpha},r} = \mathcal{E}^{m,-}_{\check{\alpha},r} \circ \mathcal{E}^{m,+}_{\check{\alpha},r} = \mathrm{id},$$

where id is the identity operator. Next, we are interested in the operator norm of $\mathcal{E}^{m,s}_{\check{\alpha},r}$ since it will be useful later to derive an inverse inequality on $\mathcal{V}^m_{\check{\alpha},r}(\check{I})$, that is, given $\check{\varphi}_s \in \mathcal{P}^m(\check{I}^s)$, we want to bound $\left\|\mathcal{E}^{m,s'}_{\check{\alpha},r}\check{\varphi}_s\right\|_{0,\check{I}^{s'}}$ in terms of $\|\check{\varphi}_s\|_{0,\check{I}^s}$, for $s \in \{-,+\}$. First, we state a useful

fact about polynomials.

Lemma 2.2. *Let $m \geq 0$ be an integer. Then,*

$$\|p\|_{0,[0,1]} \underset{m}{\gtrsim} \max_{0\leq k\leq m} \left|p^{(k)}(1)\right|,$$

for any polynomial $p \in \mathcal{P}^m([0,1])$.

Proof. Let $E : \mathcal{P}^m([0,1]) \to [0,\infty)$ be the map such that $E(p) = \max_{0\leq k\leq m} \left|p^{(k)}(1)\right|$ for all $p \in \mathcal{P}^m([0,1])$, then E is a norm on $\mathcal{P}^m([0,1])$. By the norm equivalency property in finite dimensional spaces [47], we have

$$E(p) \underset{m}{\lesssim} \|p\|_{0,[0,1]}, \qquad \forall p \in \mathcal{P}^m([0,1]),$$

which is the desired result. □

For ease of presentation, we use $\check{h}_- = \check{\alpha}$ and $\check{h}_+ = 1 - \check{\alpha}$ to denote the size of $\check{I}^-$ and $\check{I}^+$, respectively. Now, we are ready to state an estimate on the norm of the extension operator $\mathcal{E}^{m,s'}_{\check{\alpha},r}$.

Lemma 2.3. *Let $s \in \{-,+\}$ and let (r_k) be a positive sequence. Then, the following inequality holds*

$$\left\|\mathcal{E}^{m,s'}_{\check{\alpha},r}\check{\varphi}_s\right\|_{0,\check{I}^{s'}} \underset{m}{\lesssim} \sqrt{\frac{\check{h}_{s'}}{\check{h}_s}} \left(\max_{0\leq i\leq m} r_i^{s1}\right) \max\left(1, \left(\frac{\check{h}_{s'}}{\check{h}_s}\right)^m\right) \|\check{\varphi}_s\|_{0,\check{I}^s}, \tag{2.8}$$

where $s1$ is 1 if $s = +$ and is -1 if $s = -$.

Proof. Without loss of generality, we will assume that $s = -$. Since $\check{\varphi} = (\check{\varphi}_-, \check{\varphi}_+) \in \mathcal{V}^m_{\check{\alpha},r}(\check{I})$, then we can write $\check{\varphi}$ as $\check{\varphi} = c_0\mathcal{N}^0 + c_1\mathcal{N}^1 + \ldots c_m\mathcal{N}^m$ for some coefficients c_k. Consequently,

we have

$$\check{\varphi}_-(x) = \sum_{k=0}^{m} c_k (x-\check{\alpha})^k, \qquad \check{\varphi}_+(x) = \sum_{k=0}^{m} r_k c_k (x-\check{\alpha})^k. \tag{2.9}$$

Now, we estimate the L^2 norm of $\check{\varphi}_+$

$$\begin{aligned} \|\check{\varphi}_+\|^2_{0,\check{I}^-} &= \int_{\check{\alpha}}^{1} \left(\sum_{k=0}^{m} r_k c_k (x-\check{\alpha})^k \right)^2 dx = \int_0^{\check{h}_+} \left(\sum_{k=0}^{m} r_k c_k z^k \right)^2 dz \\ &\le 2 \sum_{k=0}^{m} \int_0^{\check{h}_+} r_k^2 c_k^2 z^{2k} dz \le 2h_+ \sum_{k=0}^{m} r_k^2 c_k^2 \check{h}_+^{2k} \\ &\le 2\check{h}_+ \left(\max_{0\le k\le m} r_k \right)^2 \sum_{k=0}^{m} c_k^2 \check{h}_+^{2k}. \end{aligned} \tag{2.10}$$

On the other hand, by matching the Taylor series coefficients of $\check{\varphi}_-$ with (2.9), we obtain $k! c_k = \check{\varphi}_-^{(k)}(\check{\alpha})$. Therefore,

$$c_k = \frac{1}{k!} \check{\varphi}_-^k (\check{\alpha}) \tag{2.11}$$

Now, let $\hat{\varphi} \in \mathcal{P}^m([0,1])$ such that $\hat{\varphi}(z) = \check{\varphi}_-(\check{h}_- z)$ for all $z \in [0,1]$. Then, by the chain rule and a change of variables, we have

$$\|\hat{\varphi}\|_{0,[0,1]} = \check{h}_-^{-1} \|\check{\varphi}_-\|_{0,\check{I}^-}, \quad \text{and} \quad \hat{\varphi}^{(k)}(1) = \check{h}_-^k \check{\varphi}_-(\check{\alpha}), \quad k = 0,1,\dots,m. \tag{2.12}$$

Next, we apply Lemma 2.2 to $\hat{\varphi}$ and use the (2.12) to obtain

$$\begin{aligned} \|\check{\varphi}_-\|^2_{0,\check{I}} = \check{h}_- \|\hat{\varphi}\|^2_{0,[0,1]} &\underset{m}{\gtrsim} \check{h}_- \max_{0\le k\le m} |\hat{\varphi}^{(k)}(1)|^2, \\ &\underset{m}{\gtrsim} \check{h}_- \max_{0\le k\le m} \check{h}_-^{2k} |\check{\varphi}_-^{(k)}(\check{\alpha})|^2, \\ &\underset{m}{\gtrsim} \check{h}_- \max_{0\le k\le m} \check{h}_-^{2k} c_k^2, \end{aligned} \tag{2.13}$$

where the last line follows from (2.11). To finish the proof, we combine (2.10) and (2.13) to

obtain

$$\begin{aligned}\|\check{\varphi}_+\|^2_{0,\check{I}^+} &\lesssim_m \|\check{\varphi}_-\|^2_{0,\check{I}^-} \frac{\check{h}_+}{\check{h}_-}\left(\max_{0\le k\le m} r_k\right)^2 \sum_{k=0}^{m}\left(\frac{\check{h}_+}{\check{h}_-}\right)^{2k},\\ &\lesssim_m \|\check{\varphi}_-\|^2_{0,\check{I}^-} \frac{\check{h}_+}{\check{h}_-}\left(\max_{0\le k\le m} r_k\right)^2 \max\left(1,\left(\frac{\check{h}_+}{\check{h}_-}\right)^{2m}\right),\end{aligned}$$

which is equivalent to (2.8) with $s=-$. The other case $s=+$ can be obtained similarly. □

The lemma above shows that the operator norm of $\mathcal{E}^{m,s'}_{\check{\alpha},r}$ depends on the ratio of the sizes of the $\check{I}^-$ and $\check{I}^+$. In particular, if we extend a polynomial from the smaller sub-element to the larger sub-element, then the norm of the resulting polynomial might be significantly larger than the original polynomial, especially if $\min(\check{h}_-,\check{h}_+)\ll 1$. On the other hand, the extension from the larger sub-element to the smaller one will always be bounded regardless of $\check{h}_-,\check{h}_+$ as the following corollary shows.

Corollary 2.1. *Let (r_k) be a positive sequence and assume that $\check{h}_s \ge \check{h}_{s'}$, then*

$$\left\|\mathcal{E}^{m,s'}_{\check{\alpha},r}\check{\varphi}_s\right\|_{0,\check{I}^{s'}} \lesssim_{m,r} \sqrt{\check{h}_{s'}}\,\|\check{\varphi}_s\|_{0,\check{I}^s}, \qquad \forall \check{\varphi}_s\in\mathcal{P}^m(\check{I}^s). \tag{2.14}$$

Proof. Since $\check{h}_s+\check{h}_{s'}=1$ and $\check{h}_s>\check{h}_{s'}$, it follows that $\check{h}_s\ge\frac{1}{2}$. Therefore, the inequality (2.8) now reads

$$\left\|\mathcal{E}^{m,s'}_{\check{\alpha},r}\check{\varphi}_s\right\|_{0,\check{I}^{s'}} \lesssim_m (\max_{0\le k\le m} r_k^{s1})\sqrt{2\check{h}_{s'}}\,\|\check{\varphi}_s\|_{0,\check{I}^s} \lesssim_{m,r} \sqrt{\check{h}_{s'}}\,\|\check{\varphi}_s\|_{0,\check{I}^s}.$$ □

We note here that we are choosing to obfuscate the dependence on the interface jump coefficients (r_k) and the degree m, this allows us to present our inequalities in more compact form. Next, we proceed to obtain an inverse inequality for the IFE space $\mathcal{V}^m_{\check{\alpha},r}(\check{I})$. First, we recall the classical inverse inequality for polynomials.

Lemma 2.4. *Let $m \geq 0$ and $0 \leq i \leq m$ be integers, then*

$$|p|_{i,[a,b]} \lesssim_m (b-a)^{-i} \|p\|_{0,[a,b]}, \qquad \forall p \in \mathcal{P}^m([0,1]).$$

Proof. This is a special case of Lemma 4.5.3 in [29]. □

The next natural step is to extend Lemma 2.4 to the IFE space $\mathcal{V}_{\check{\alpha},r}^m(\check{I})$. However, the direct application of the classical inverse inequality leads to an inequality that depends on $\check{\alpha}$:

$$|\check{\varphi}|_{i,\check{I}} \lesssim |\check{\varphi}|_{i,[0,\check{\alpha}]} + |\check{\varphi}|_{i,[\check{\alpha},1]} \lesssim_m \left(\check{\alpha}^{-i} + (1-\check{\alpha})^{-i}\right) \|\check{\varphi}\|_{0,\check{I}}.$$

Here, the dependency on $\check{\alpha}$ is problematic since $\check{\alpha}^{-i} + (1-\check{\alpha})^{-i}$ grows unbdoundedly as $\check{\alpha} \to 0^+$ or $\check{\alpha} \to 1^-$. To avoid this issue, we will use the classical trace inequality on the largest sub-element of $\check{I}$, then we employ the stability of the extension operator derived in Lemma 2.3 to obtain an inverse inequality independent of $\check{\alpha}$.

Lemma 2.5. *Let (r_k) be a positive sequence and let $0 \leq i \leq m+1$ be a positive integer, then*

$$|\check{\varphi}|_{i,\check{I}} \lesssim_{m,r} \|\check{\varphi}\|_{0,\check{I}}, \tag{2.15}$$

for all $\check{\varphi} \in \mathcal{V}_{\check{\alpha},r}^m(\check{I})$.

Proof. Without loss of generality, we assume that $\check{h}_- \geq \check{h}_+$, and we will only consider the case $i = 1$. The other case $\check{h}_+ \geq \check{h}_-$ follows similarly, and the case $i \geq 2$ follows by induction.

Since $\check{h}_- \geq \check{h}_+$, we conclude that $\check{h}_- \geq \frac{1}{2}$. Therefore, Lemma 2.4 with $a = 0$ and $b = \check{h}_-$ yields

$$|\check{\varphi}_-|_{1,\check{I}^-} \lesssim_m \check{h}_-^{-1} \|\check{\varphi}_-\|_{0,\check{I}^-} \lesssim_m 2 \|\check{\varphi}_-\|_{0,\check{I}^-} \lesssim_m \|\check{\varphi}_-\|_{0,\check{I}^-}. \tag{2.16}$$

Now, we recall from Lemma 2.1 that $\check{\varphi}' \in \mathcal{V}_{\check{\alpha},\tau(r)}^{m-1}$. Then, by combining Lemma 2.3 and (2.16), we have

$$|\check{\varphi}_+|_{1,\check{I}^+} = \left\|\check{\varphi}_+'\right\|_{0,\check{I}^+} \underset{m,r}{\lesssim} \left\|\check{\varphi}_-'\right\|_{0,\check{I}^-} \underset{m,r}{\lesssim} \|\check{\varphi}_-\|_{0,\check{I}^-} \tag{2.17}$$

Finally, we conclude the proof by summing (2.16) and (2.17). □

Remark 2.2. The inequalities (2.16) and (2.17) lead to an inequality stronger than (2.15). More precisely, we have $|\check{\varphi}|_{i,\check{I}} \lesssim_{m,r} \|\check{\varphi}\|_{0,\check{I}^-}$ if $\check{h}_- \geq \check{h}_+$.

Since $\mathcal{V}_{\check{\alpha},r}^m(\check{I})$ will be used later to construct an IFE space, we are interested in whether $\mathcal{V}_{\check{\alpha},r}^m(\check{I})$ admits a Lagrange basis on the local (physical) element, that is, given a set of distinct points $\{x_i\}_{i=0}^m \subset \check{I}$, is there a basis $\{L_i\}_{i=0}^m$ of $\mathcal{V}_{\check{\alpha},r}^m(\check{I})$ such that $L_i(x_j) = \delta_{i,j}$ for all $0 \leq i, j \leq m$? This question is important since:

- It allows us to construct a C^0 IFE space for the elliptic and the parabolic interface problems.
- It will be used to construct a Radau projection in the analysis of immersed discontinuous Galerkin method for the acoustic interface problem.

In order to prove that $\mathcal{V}_{\check{\alpha},r}^m(\check{I})$ admits a Lagrange basis, we first show that any function $\check{\varphi} \in \mathcal{V}_{\check{\alpha},r}^m(\check{I})$ cannot have more than m roots (counting multiplicities). We note here that the notion of multiplicity extends to $\check{\alpha}$ since if $\check{\alpha}$ is a root of $\check{\varphi}_-$ with multiplicity k, then it is a root of $\check{\varphi}_+$ with multiplicity k as well, where $(\check{\varphi}_-, \check{\varphi}_+) \in \mathcal{V}_{\check{\alpha},r}^m(\check{I})$.

Lemma 2.6. *Let (r_k) be a positive sequence, and let $\check{\varphi} \in \mathcal{V}_{\check{\alpha},r}^m(\check{I})$ be a non-zero function, then $\check{\varphi}$ has at most m zeros in $\check{I}$, counting multiplicities.*

Proof. For the sake of conciseness, we will assume that the roots are always counted with multiplicity in this proof. We will prove the statement by induction over $m \in \mathbb{N} \cup \{0\}$. First, we consider the case $\check{\varphi} \in \mathcal{V}_{\check{\alpha},r}^0(\check{I})$. In this case, there is a constant $c \neq 0$ such as $\check{\varphi}(x) = c$ for

all $c \in \check{I}^-$. Therefore, by the interface conditions, we have $\check{\varphi}(x) = r_0 c \neq 0$ for all $x \in \check{I}^+$. Hence, $\check{\varphi}$ has no zeros.

Now, let $m \geq 1$, and we assume that all non-zero functions $\check{\psi} \in \mathcal{V}_{\check{\alpha},\tilde{r}}^{m-1}(\check{I})$ have at most $m-1$ in $\check{I}$ (counting multiplicities), for all positive sequences $(\tilde{r}_k)$, and let $\check{\varphi} \in \mathcal{V}_{\check{\alpha},r}^{m}(\check{I})$.

To show that $\check{\varphi}$ has at most m roots (counting multiplicities), we argue by contradiction: We assume that $\check{\varphi}$ has $m+1$ roots, then we show that this contradicts the induction hypothesis.

Let $\check{\varphi} = (\check{\varphi}_-, \check{\varphi}_+) \in \mathcal{V}_{\check{\alpha},r}^{m}(\check{I})$ be a function with k distinct roots $\{z_i\}_{i=1}^k$. Let m_i be the multiplicity of the root z_i for $1 \leq i \leq m+1$. To argue by contradiction, we assume that $M = m_1 + m_2 + \cdots + m_k > m$.

Without loss of generality, we assume that $z_1 < z_2 < \cdots < z_k$. Therefore, there is $1 \leq i_0 \leq k$ such that $z_{i_0} \leq \check{\alpha} < z_{i_0+1}$. We define M_- and M_+ as the sum of multiplicities of the roots of $\check{\varphi}_-$ in $[0, \check{\alpha}]$, and the roots of $\check{\varphi}_+$ in z_{i_0+1}, respectively, that is

$$M_- = \sum_{i=1}^{i_0} m_i, \qquad M_+ = \sum_{i=i_0+1}^{k} m_i, \qquad M_- + M_+ = M \geq m.$$

Since $\check{\varphi}_-$ and $\check{\varphi}_+$ are polynomials, we know that $\check{\varphi}_-'$ has $M_- - 1$ roots in $[0, \check{\alpha}]$ and $\check{\varphi}_+$ has $M_+ - 1$ roots in $[z_{i_0+1}, 1]$. Hence, we have shown so far that $\check{\varphi}'$ has $M-2$ roots. In our next step, we will show that $\check{\varphi}'$ has an additional root in the interval (z_{i_0}, z_{i_0+1}).

If $z_{i_0} = \check{\alpha}$, then $\check{\varphi}$ is continuous at $\check{\alpha}$. Then, by the mean value theorem, $\check{\varphi}'$ has a root in (z_{i_0}, z_{i_0+1}). On the other hand, if $\check{\alpha} \in (z_{i_0}, z_{i_0+1})$. Then

$$0 = \check{\varphi}(z_{i_0+1}) - r_0 \check{\varphi}(z_{i_0}) = \int_{z_{i_0}}^{z_{i_0+1}} w(x) \check{\varphi}'(x)\, dx = 0, \qquad \text{where } w(x) = \begin{cases} r_0, & x \in (z_{i_0}, \check{\alpha}), \\ 1, & x \in (\check{\alpha}, z_{i_0+1}). \end{cases}$$

Therefore, $\check{\varphi}' \in \mathcal{V}_{\check{\alpha},r}^{m-1}(\check{I})$ changes sign at some $z^* \in (z_{i_0}, z_{i_0+1})$. Since $\check{\varphi}'$ does not change sign

at $\check{\alpha}$, we conclude that $\check{\varphi}'(z^*) = 0$ since $\check{\varphi}'$ is continuous on $I\backslash\{\check{\alpha}\}$.

In conclusion, we have shown that $\check{\varphi}' \in \mathcal{V}_{\check{\alpha},r}^{m-1}(\check{I})$ has $M-1 > m-1$ roots, which contradicts our induction hypothesis. Hence, $\check{\varphi}$ has at most m roots, which is the claim of the lemma. □

Lemma 2.6 allows us to assert the existence of a Lagrange basis on $\check{I}$ easily.

Theorem 2.1. *Let (r_k) a positive sequence, and let $\xi_0, \xi_1, \ldots, \xi_m$ be distinct points in $\check{I}$. Then there exists a basis $\{L_i\}_{i=0}^m$ of $\mathcal{V}_{\check{\alpha},r}^m(\check{I})$ that satisfies*

$$L_i(\xi_j) = \delta_{i,j} = \begin{cases} 1, & i = j \\ 0, & i \neq j \end{cases}, \qquad 0 \leq i, j \leq m.$$

Proof. Let $\{\mathcal{N}_{\check{\alpha},r}^i\}_{i=0}^m$ be the canonical basis defined by (2.7), and let $A = (a_{i,j})$ be the $(m+1) \times (m+1)$ matrix defined as

$$a_{i+1,j+1} = \mathcal{N}_{\check{\alpha},r}^i(\xi_j), \qquad 0 \leq i, j \leq m+1.$$

To prove the lemma, it is sufficient to show that A is invertible. Now, let $\mathbf{c} = (c_i)$ be a solution to the equation $A\mathbf{c} = \mathbf{0}$, and let

$$p = \sum_{i=0}^{m} c_{i+1} \mathcal{N}_{\check{\alpha},r}^i \in \mathcal{V}_{\check{\alpha},r}^m(\check{I}).$$

Since $A\mathbf{c} = \mathbf{0}$, we have $p(\xi_i) = 0$ for all $0 \leq i \leq m$. Therefore, by Lemma 2.6, we conclude that $p = 0$. Consequently, $\mathbf{c} = \mathbf{0}$ and A is invertible. □

It is worth here to mention that a restricted version of Theorem 2.1 was proved previously in [7, 8] by using specific properties of the sequence (r_k) or by employing symbolic techniques

to check the invertibility of the matrix A in the proof above for low values of m. However, our construction here is general and accommodates all positive sequence (r_k).

In addition to the Lagrange basis detailed in the previous theorem, we are also interested in constructing and studying orthogonal bases on $\mathcal{V}_{\check{\alpha},r}^{m}(\check{I})$. Generally speaking, an orthogonal basis leads to a diagonal mass matrix in the discontinuous Galerkin method, which is a desired property when using an explicit time integrator. Furthermore, the analysis of the immersed dG method in the later sections will require the use of an immersed Radau IFE projection which employs orthogonal IFE functions, similar to the traditional approach for the analysis of dG methods [107].

First, let $\check{w} : \check{I} \to \mathbb{R}_+$ be a piecewise constant function such that $\check{w}|_{\check{I}^\pm}$ is constant. For simplicity, we will use $\check{w}^\pm$ to denote $\check{w}|_{\check{I}^\pm}$, and we will use $(\cdot,\cdot)_{\check{w},\check{I}}$ to denote the weighted L^2 inner product

$$(f,g)_{\check{w},\check{I}} = \int_{\check{I}} \check{w}(x) f(x) g(x)\, dx, \qquad f,g \in L^2(\check{I}).$$

Additionally, let

$$\mathcal{V}_{\check{\alpha},r}^{\check{w},m}(\check{I}) = \left\{ \check{\varphi} \in \mathcal{V}_{\check{\alpha},r}^{m}(\check{I}) \mid (\check{\varphi},\check{\psi})_{\check{w},\check{I}} = 0, \forall \check{\psi} \in \mathcal{V}_{\check{\alpha},r}^{m-1}(\check{I}) \right\}, \qquad m \geq 1. \tag{2.18}$$

That is, $\mathcal{V}_{\check{\alpha},r}^{\check{w},m}(\check{I})$ is spanned an m-th degree IFE function $\check{\varphi}$ that is orthogonal to $\mathcal{V}_{\check{\alpha},r}^{m-1}(\check{I})$ with respect to the weighted L^2 inner product $(\cdot,\cdot)_{\check{w},\check{I}}$. It is worth noting here that in the special case $\check{w} = 1$ and $r = 1$, the space $\mathcal{V}_{\check{\alpha},r}^{\check{w},m}(\check{I})$ is the span of the m-th Legendre polynomial [3] on $[0,1]$. It is well known that the m-th orthogonal polynomial has m simple roots in the interior of the domain. Below, we extend this result to orthogonal IFE functions, which will be an important ingredient in the construction of the Radau and Lobatto projections later.

Lemma 2.7. *Let (r_k) be a positive sequence and let $\check{\varphi} \in \mathcal{V}_{\check{\alpha},r}^{\check{w},m}(\check{I})$ be a non-zero function, where $m \geq 1$, then $\check{\varphi}$ has exactly m distinct roots in $(0,1)$.*

Proof. Let $\check{\varphi} \in \mathcal{V}_{\check{\alpha},r}^{\check{w},m}(\check{I})$ be non-zero, and assume that $\check{\varphi}$ has $k < m$ distinct roots $Z = \{z_1, z_2, \ldots, z_k\} \subset (0,1)$. From Theorem 2.1, there is a function $\check{\psi} \in \mathcal{V}_{\check{\alpha},r}^{k}(\check{I})$ such that Z is the set of roots of $\check{\psi}$. Therefore, the function $\check{\varphi}\check{\psi}$ does not change sign on $\check{I}$. However, $(\check{\varphi}, \check{\psi})_{\check{w},\check{I}} = 0$. Therefore, $\check{\varphi} = 0$, which contradicts our assumption. Hence, $\check{\varphi}$ has m distinct roots in $(0,1)$. □

To illustrate the lemma above, we consider the case where $r_k = k + 1$ and plot an element of $\mathcal{V}_{\check{\alpha},r}^{\check{w},i}(\check{I})$ for $0 \le i \le 4$ with $\check{w}|_{\check{I}^{\pm}} = \check{w}^{\pm}$ in Figure 2.3. We observe that p_i has exactly i roots in $(0,1)$ for $(\check{w}^-, \check{w}^+) = (1,1)$ and $(\check{w}^-, \check{w}^+) = (1,10)$. The findings of Lemma 2.7 show

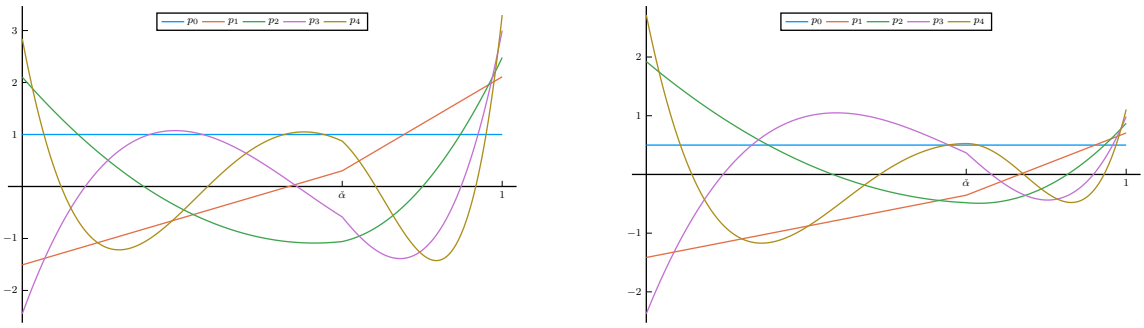

(a) $(\check{w}^-, \check{w}^+) = (1,1)$. (b) $(\check{w}^-, \check{w}^+) = (1,10)$.

Figure 2.3: An illustration of an orthogonal basis $p_i \in \mathcal{V}_{\check{\alpha},r}^{\check{w},i}(\check{I})$ with $\check{\alpha} = 2/3$ and $r_k = k + 1$ for $(\check{w}^-, \check{w}^+) = (1,1)$ (left) and $(\check{w}^-, \check{w}^+) = (1,10)$ (right).

that $\check{\varphi} \mapsto |\check{\varphi}(0)| + |\check{\varphi}(1)|$ is indeed a norm on $\mathcal{V}_{\check{\alpha},r}^{\check{w},m}(\check{I})$. Therefore, since $\mathcal{V}_{\check{\alpha},r}^{\check{w},m}(\check{I})$ is finite dimensional, it follows that

$$|\check{\varphi}(0)| + |\check{\varphi}(1)| \underset{\check{\alpha},\check{w},m,r}{\gtrsim} \|\check{\varphi}\|_{0,\check{I}}, \qquad \forall \check{\varphi} \in \mathcal{V}_{\check{\alpha},r}^{\check{w},m}(\check{I}). \tag{2.19}$$

However, in our analysis later, we will need (2.19) to hold independently of $\check{\alpha}$, which is described in the theorem below.

Theorem 2.2. *Let (r_k) be a positive sequence and let $m \geq 0$, then*

$$|\check{\varphi}(0)| + |\check{\varphi}(1)| \underset{\check{w},m,r}{\gtrsim} \|\check{\varphi}\|_{0,\check{I}}, \qquad \forall \check{\varphi} \in \mathcal{V}_{\check{\alpha},r}^{\check{w},i}(\check{I}). \tag{2.20}$$

Proof. Let $(h_-, h_+) = (\check{\alpha}, 1-\check{\alpha})$ be the length of the sub-intervals $\check{I}^{\pm}$ and let $\check{\varphi} = (\check{\varphi}_-, \check{\varphi}_+) \in \check{\varphi} \in \mathcal{V}_{\check{\alpha},r}^{\check{w},i}(\check{I})$ be a non-zero function. Without loss of generality, we assume that $\check{h}_- \geq \check{h}_+$ in the remainder of this proof. The other case $\check{h}_- < \check{h}_+$ can be done similarly. For the ease of the reader, we will split this proof into three steps:

Step 1: Let $p \in \mathcal{P}^m(\check{I}^+)$, then by the orthogonality of $\check{\varphi}$, we have

$$0 = \check{w}^-(\check{\varphi}_-, p)_{\check{I}^-} + \check{w}^+ \left(\mathcal{E}_{\check{\alpha},r}^{m,+}(\check{\varphi}_-), \mathcal{E}_{\check{\alpha},r}^{m,+}(p)\right)_{\check{I}^+}$$

We rearrange the terms, and use Cauchy-Schwarz inequality and Lemma 2.3 to obtain

$$|(\check{\varphi}_-, p)_{\check{I}^-}| \underset{\check{w}}{\lesssim} \left\|\mathcal{E}_{\check{\alpha},r}^{m,+}(\check{\varphi}_-, p)\right\|_{\check{I}^-} \left\|\mathcal{E}_{\check{\alpha},r}^{m,+}(p)\right\|_{\check{I}^-} \underset{\check{w},m,r}{\lesssim} \check{h}_+ \|\check{\varphi}\|_{\check{I}^-} \|p\|_{\check{I}^-}. \tag{2.21}$$

Step 2: Let $q_i(x) = x^i$ for $0 \leq i \leq m-1$, and we define $\hat{\varphi}_- \in \mathcal{P}^m(\check{I}^-)$ as $\hat{\varphi}_-(\xi) = \check{\varphi}_-(\check{h}_-\xi)$, then

$$|(\check{\varphi}_-, q_i)_{\check{I}^-}| = h_-^{i+1} \left|(\hat{\varphi}_-, q_i)_{[0,1]}\right| \geq 2^{-m-1} \left|(\hat{\varphi}_-, q_i)_{[0,1]}\right|.$$

Therefore, by summing over all $0 \leq i \leq m-1$ and adding $\check{\varphi}(0)$, we obtain

$$|\check{\varphi}(0)| + \sum_{i=0}^{m-1} |(\check{\varphi}_-, q_i)_{\check{I}^-}| \underset{m}{\gtrsim} |\hat{\varphi}_-(0)| + \sum_{i=0}^{m-1} \left|(\hat{\varphi}_-, q_i)_{[0,1]}\right|. \tag{2.22}$$

Now, consider the right-hand side of (2.22) as a map $N : \mathcal{P}^m([0,1]) \to [0,\infty)$:

$$N(p) = |p(0)| + \sum_{i=0}^{m-1} \left|(p, q_i)_{[0,1]}\right|,$$

then N is a norm on $\mathcal{P}^m([0,1])$. By the equivalence of norms in finite dimensional spaces, we have $N(p) \gtrsim_m \|p\|_{0,[0,1]}$. We substitute this inequality back into (2.22) and use Lemma 2.3 to obtain

$$|\check{\varphi}(0)| + \sum_{i=0}^{m-1} |(\check{\varphi}_-, q_i)_{\check{I}^-}| \underset{m}{\gtrsim} \|\hat{\varphi}_-\|_{0,[0,1]} \underset{m}{\gtrsim} \|\check{\varphi}_-\|_{0,\check{I}^-} \underset{m,r}{\gtrsim} \|\check{\varphi}\|_{0,\check{I}}.$$

Using (2.21), we can bound the left-hand side from above

$$|\check{\varphi}(0)| + \check{h}_+ \|\check{\varphi}\|_{0,\check{I}} \underset{\check{w},m,r}{\gtrsim} \|\check{\varphi}\|_{0,\check{I}}.$$

Equivalently, we have

$$\frac{|\check{\varphi}(0)|^2}{\|\check{\varphi}\|_{0,\check{I}}^2} + \check{h}_+^2 \underset{\check{w},m,r}{\gtrsim} 1. \tag{2.23}$$

In the next step, w will show that the inequality (2.23) holds without the need for the $\check{h}_+$ term.

Step 3: Note that the quantity $\frac{|\check{\varphi}(0)|^2}{\|\check{\varphi}\|_{0,\check{I}}^2}$ does not depend on the choice of $\check{\varphi}$ in $\mathcal{V}_{\check{\alpha},r}^{\check{w},m}(\check{I})$ since this space is one-dimensional. Therefore, we can consider a sequence $\{\check{\psi}_{\check{\alpha},r}^i\}_{i=0}^m$ generated via the Gram-Schmidt process:

$$\check{\psi}_{\check{\alpha},r}^0 = 1, \qquad \check{\psi}_{\check{\alpha},r}^i = \mathcal{N}_{\check{\alpha},r}^i - \sum_{j=0}^{i-1} \frac{\left(\mathcal{N}_{\check{\alpha},r}^i, \check{\psi}_{\check{\alpha},r}^j\right)_{\check{w},\check{I}}}{\left(\check{\psi}_{\check{\alpha},r}^j, \check{\psi}_{\check{\alpha},r}^j\right)_{\check{w},\check{I}}} \check{\psi}_{\check{\alpha},r}^j, \ 1 \le i \le m,$$

then, by construction, each term $\check{\varphi}_i$ is in $\mathcal{V}_{\check{\alpha},r}^{\check{w},i}(\check{I})$. Then, by fixing m and r, we see that $\check{\psi}_{\check{\alpha},r}^m(0)^2$ and $\left\|\check{\psi}_{\check{\alpha},r}^m\right\|_{0,\check{I}}^2$ are rational functions in $\check{\alpha}$. Therefore, the quotient $\frac{\check{\psi}_{\check{\alpha},r}^m(0)^2}{\left\|\check{\psi}_{\check{\alpha},r}^m\right\|_{0,\check{I}}^2}$ is also a rational function, that we denote

$$\mathcal{J}(\check{\alpha}) = \frac{\check{\psi}_{\check{\alpha},r}^m(0)^2}{\left\|\check{\psi}_{\check{\alpha},r}^m\right\|_{0,\check{I}}^2}.$$

By taking $h_+ \to 0^+$ (Equivalently $\check{\alpha} \to 1^-$) in (2.23) with $\hat{\varphi} = \check{\psi}^m_{\check{\alpha},r}$, we obtain

$$\lim_{z \to 1^-} \mathcal{J}(z) \underset{\check{w},m,r}{\gtrsim} 1.$$

Therefore, since $\mathcal{J}$ is rational function, we conclude that

$$\mathcal{J}(\check{\alpha}) \underset{\check{w},m,r}{\gtrsim} 1, \qquad \forall \check{\alpha} \in \left[\frac{1}{2}, 1\right),$$

which is the desired result.

At the end, we note that we have shown that $|\check{\varphi}(0)| \gtrsim_{\check{w},m,r} \|\check{\varphi}\|_{\check{I}}$ when $\check{h}_- \geq \check{h}_+$. Similarly, if $\check{h}_- \leq \check{h}_+$, we obtain

$$|\check{\varphi}(1)| \underset{\check{w},m,r}{\gtrsim} \|\check{\varphi}\|_{\check{I}}.$$

Therefore, when combining the two cases, we obtain (2.20). □

2.2.1 Summary

In summary, we have shown that the reference IFE (RIFE) space $\mathcal{V}^m_{\check{\alpha},r}(\check{I})$ has several properties analogous to those of the polynomial space $\mathcal{P}^m(\check{I})$. These similarities will allow us to borrow the theoretical machinery of the traditional finite element method to analyze immersed finite element methods in the remainder of this chapter. For this reason, it is useful to summarize our finding in Table 2.1, where $p \in \mathcal{P}^m(\check{I})$ and $\check{\varphi} \in \mathcal{V}^m_{\check{\alpha},r}(\check{I})$.

Additionally, given a piecewise constant weight function, the behavior of the orthogonal IFE functions is closely related to that of Legendre polynomials as summarized in Table 2.2, where p_m is the m-th Legendre polynomial on $[0, 1]$. Again, it is worth emphasizing that all of our estimates in this summary are independent of the position of the interface point $\check{\alpha}$.

Property	The polynomial space $\mathcal{P}^m(\check{I})$	The RIFE space $\mathcal{V}_{\check{\alpha},r}^m(\check{I})$
Dimension	$m+1$	$m+1$
Derivative	$p' \in \mathcal{P}^{m-1}(\check{I})$	$\check{\varphi}' \in \mathcal{V}_{\check{\alpha},\tau(r)}^{m-1}(\check{I})$
Inverse inequality	$\|p'\|_{0,\check{I}} \lesssim_m \|p\|_{0,\check{I}}$	$\|\check{\varphi}'\|_{0,\check{I}} \lesssim_{m,r} \|\check{\varphi}\|_{0,\check{I}}$
Maximum number of roots	m if $p \neq 0$	m if $\check{\varphi} \neq 0$
Admits an interpolatory basis	✓ (The Lagrange basis)	✓

Table 2.1: The similarities between the polynomial space and the RIFE space.

However, they may depend on the positive sequence (r_k), the degree m and the weight $\check{w}$.

Property	p_m	$\check{\varphi}_m \in \mathcal{V}_{\check{\alpha},r}^{\check{w},m}(\check{I})$
Number of interior roots	m	m
Trace inequality	$\|p_m(0)\| + \|p_m(1)\| \gtrsim_m \|p_m\|_{0,\check{I}}$	$\|\check{\varphi}_m(0)\| + \|\check{\varphi}_m(1)\| \gtrsim_{\check{w},m,r} \|\check{\varphi}_m\|_{0,\check{I}}$

Table 2.2: Similarities between the m-th degree Legendre polynomial and m-th degree orthogonal IFE functions.

2.3 An Immersed Bramble Hilbert Lemma and Bounded Projections

In this section, we introduce a generalization of Bramble-Hilbert lemma [27, 37] in one spatial dimension that covers, in addition to polynomial-preserving operators, the projection operators onto the reference IFE space. In the classical theory of the finite element method and polynomial approximation [37, 43, 46], the Bramble-Hilbert lemma plays a crucial role in deriving optimal residual estimates for various projection operators, such as Lagrange interpolation, Hermite interpolation, L^2 projection, Radau projection, among other maps from a suitable Sobolev space to the space of polynomials. However, the Bramble-Hilbert lemma does not apply directly to projections onto the IFE space discussed earlier since the

function that we are interested in are not smooth around the interface, and the IFE space is composed of piecewise polynomials, which introduces another hurdle. Nevertheless, we are able to replicate the success of Bramble-Hilbert lemma in the context of IFE spaces.

First, we consider the reference interval $\check{I}$, a reference interface point $\check{\alpha} \in \check{I}$ and a positive sequence (r_k). We recall that the immersed Sobolev $\mathcal{H}^{m+1}_{\check{\alpha},r}(\check{I})$ consists of functions u that are not necessarily smooth at $\check{\alpha}$. In general, we do not expect the classical Poincaré inequality [4] to hold for the function u. For this reason, we develop a new immersed Poincaré inequality for immersed Sobolev space $\mathcal{H}^{m+1}_{\check{\alpha},r}(\check{I})$, which will be used later to derive the immersed Bramble Hilbert lemma.

Definition 2.3. Let $\check{\alpha} \in \check{I}$, let (r_k) be a positive sequence, and let i be a non-negative integer. We use $\omega^i_{\check{\alpha},r}$ to denote the function

$$\omega^i_{\check{\alpha},r}(x) = \begin{cases} r_i, & x \in \check{I}^-, \\ 1, & x \in \check{I}^+. \end{cases} \tag{2.24}$$

By construction, if $u \in \mathcal{H}^{m+1}_{\check{\alpha},r}(\check{I})$, then by multiplying it by the smoother function $\omega^i_{\check{\alpha},r}$, we obtain $u^{(i)}\omega^i_{\check{\alpha},r} \in H^1(\check{I})$, which will allow us to obtain the following immersed Poincaré inequality.

Theorem 2.3. *Let (r_k) be a positive sequence, and let $v \in \mathcal{H}^{m+1}_{\check{\alpha},r}(\check{I})$. If*

$$\left(\omega^i_{\check{\alpha},r}, v^{(i)}\right)_{\check{I}} = 0, \qquad \forall i = 0, 1 \ldots, m, \tag{2.25}$$

then

$$\|v\|_{j,\check{I}} \underset{m,r}{\lesssim} |v|_{m+1,\check{I}}, \qquad j = 0, 1, \ldots m. \tag{2.26}$$

Proof. Consider the function $z = \omega^0_{\check{\alpha},r} v$, then by construction of $\omega^0_{\check{\alpha},r}$ and the assumption

(2.25), we have

$$z \in H^1(\check{I}), \text{ and } \int_{\check{I}} z = 0,$$

which, by the Poincaré inequality [4], leads to $\|z\|_{0,\check{I}} \lesssim |z|_{1,\check{I}}$. Now, recall from (2.24) that $|\omega^i_{\check{\alpha},r}| \simeq_r 1$. Hence,

$$\|v\|_{0,\check{I}} \underset{r}{\lesssim} \|z\|_{0,\check{I}} \lesssim |z|_{1,\check{I}} \underset{r}{\lesssim} |v|_{1,\check{I}}. \tag{2.27}$$

That is, we have proven Theorem 2.3 for $j = 1$. Since $v' \in \mathcal{H}^m_{\check{\alpha},\tau(r)}(\check{I})$, the same approach yields

$$\|v'\|_{0,\check{I}} \underset{r}{\lesssim} |v|_{2,\check{I}}.$$

By using the same argument j times, we obtain (2.26). □

In order to use Theorem 2.3 in our analysis, we introduce the following immersed Poincaré projection.

Definition 2.4. Let (r_k) be a positive sequence, $\check{\alpha} \in \check{I}$ and $m \geq 0$. Given a function $v \in \mathcal{H}^{m+1}_{\check{\alpha},r}(\check{I})$, we define $\check{\pi}^m_{\check{\alpha},r} v \in \mathcal{V}^m_{\check{\alpha},r}(\check{I})$ as the solution to the system

$$\left(\omega^i_{\check{\alpha},r}, \frac{d^k}{dx^k}\check{\pi}^m_{\check{\alpha},r} v\right)_{\check{I}} = \left(\omega^i_{\check{\alpha},r}, \frac{d^k v}{dx^k}\right)_{\check{I}}, \quad \forall k = 0, 1, \ldots, m. \tag{2.28}$$

For the definition above to make sense, we show that the map $\check{\pi}^m_{\check{\alpha},r}$ is well-defined.

Lemma 2.8. *Let (r_k) be a positive sequence, $\check{\alpha} \in \check{I}$ and $m \geq 0$. Given a function $v \in \mathcal{H}^{m+1}_{\check{\alpha},r}(\check{I})$, then there is a unique $\check{\pi}^m_{\check{\alpha},r} v \in \mathcal{V}^m_{\check{\alpha},r}(\check{I})$ that satisfies Definition 2.4.*

That is, the projection $\check{\pi}^m_{\check{\alpha},r} : \mathcal{H}^{m+1}_{\check{\alpha},r}(\check{I}) \to \mathcal{V}^m_{\check{\alpha},r}(\check{I})$ is well-defined.

Proof. Let $v \in \mathcal{H}^{m+1}_{\check{\alpha},r}(\check{I})$. By definition, $\check{\pi}^m_{\check{\alpha},r} v$ is the solution to the system of $m+1$ equations

(2.28). By expressing $\check{\pi}^m_{\check{\alpha},r} v$ in terms of the canonical basis

$$\check{\pi}^m_{\check{\alpha},r} v = \sum_{i=0}^{m} c_i \mathcal{N}^i_{\check{\alpha},r},$$

the system (2.28) becomes

$$A \begin{bmatrix} c_0 \\ c_1 \\ \vdots \\ c_m \end{bmatrix} = \begin{bmatrix} (\omega^0_{\check{\alpha},r}, v)_{\check{I}} \\ (\omega^1_{\check{\alpha},r}, v')_{\check{I}} \\ \vdots \\ (\omega^m_{\check{\alpha},r}, v^{(m)})_{\check{I}} \end{bmatrix}, \qquad \text{where} \quad (A)_{i+1,j+1} = \left(\omega^i_{\check{\alpha},r}, \frac{d^i}{dx^i} \mathcal{N}^j_{\check{\alpha},r} \right)_{\check{I}}. \tag{2.29}$$

Since $\mathcal{N}^j_{\check{\alpha},r}$ is a piecewise j-th degree polynomial for $0 \le j \le m$, the matrix A is upper triangular, with diagonal entries

$$(A)_{i,i} = \left(\omega^{i-1}_{\check{\alpha},r}, \frac{d^{i-1}}{dx^{i-1}} \mathcal{N}^{i-1}_{\check{\alpha},r} \right)_{\check{I}} = (i-1)! r_{i-1} \neq 0, \qquad i = 1, 2, \dots, m+1.$$

Hence, the matrix A is invertible and the system (2.28) admits a unique solution. Since this result applies to all $v \in \mathcal{H}^{m+1}_{\check{\alpha},r}(\check{I})$, we conclude that $\check{\pi}^m_{\check{\alpha},r}$ is well-defined. □

The operator $\check{\pi}^m_{\check{\alpha},r}$ is a projection, that is $\check{\pi}^m_{\check{\alpha},r} v = v$ if and only if $v \in \mathcal{V}^m_{\check{\alpha},r}(\check{I})$. Furthermore, if v is not in the RIFE space, then $\check{\pi}^m_{\check{\alpha},r} v$ provides an *approximation* of v, where the error of the approximation can be estimated using Theorem 2.3

$$\left| v - \check{\pi}^m_{\check{\alpha},r} v \right|_{j,\check{I}} \lesssim_{m,r} |v|_{m+1,\check{I}}, \ j = 0, \dots, m, \quad \forall v \in \mathcal{H}^{m+1}_{\check{\alpha},r}(\check{I}). \tag{2.30}$$

It is crucial here that the error estimate above does not depend on the location of the interface $\check{\alpha}$. This is a key property that we want to extend to other projection operators. Our strategy here is very similar to the non-interface case [46], in the sense that we use

(2.30) and the triangle inequality to estimate the projection error. For example, consider a projection $\check{P}^m_{\check{\alpha},r} : \mathcal{H}^{m+1}_{\check{\alpha},r}(\check{I}) \to \mathcal{V}^m_{\check{\alpha},r}(\check{I})$, then

$$\left\|v - \check{P}^m_{\check{\alpha},r} v\right\|_{j,\check{I}} \leq \left\|v - \check{\pi}^m_{\check{\alpha},r} v\right\|_{j,\check{I}} + \left\|\check{P}^m_{\check{\alpha},r}\left(v - \check{\pi}^m_{\check{\alpha},r} v\right)\right\|_{j,\check{I}}.$$

The first term on the right side can be bounded directly using (2.30), whereas the second one will involve the operator norm of $\check{P}^m_{\check{\alpha},r}$, which we will define below.

Definition 2.5. Let $\check{P}^m_{\check{\alpha},r} : \mathcal{H}^{m+1}_{\check{\alpha},r}(\check{I}) \to \mathcal{V}^m_{\check{\alpha},r}(\check{I})$ be a linear map, we say that $\check{P}^m_{\check{\alpha},r}$ is j-bounded, if

$$\sup\left\{\left\|\check{P}^m_{\check{\alpha},r}(v)\right\|_{0,\check{I}} \mid v \in \mathcal{H}^{m+1}_{\check{\alpha},r}(\check{I}),\ \|v\|_{j,\check{I}} = 1\right\} < \infty, \tag{2.31}$$

where $0 \leq j \leq m+1$ is an integer.

If $\check{P}^m_{\check{\alpha},r}$ is j-bounded, then we use $\left\|\check{P}^m_{\check{\alpha},r}\right\|_{0,j,\check{I}}$ to denote the supremum in (2.31), that is

$$\left\|\check{P}^m_{\check{\alpha},r}\right\|_{0,j,\check{I}} = \sup\left\{\left\|\check{P}^m_{\check{\alpha},r}(v)\right\|_{0,\check{I}} \mid v \in \mathcal{H}^{m+1}_{\check{\alpha},r}(\check{I}),\ \|v\|_{j,\check{I}} = 1\right\}. \tag{2.32}$$

Additionally, if $\check{P}^m_{\check{\alpha},r}$ is j-bounded, then

$$\left\|\check{P}^m_{\check{\alpha},r} v\right\|_{i,\check{I}} \underset{m,r}{\lesssim} \left\|\check{P}^m_{\check{\alpha},r} v\right\|_{0,\check{I}} \leq \left\|\check{P}^m_{\check{\alpha},r}\right\|_{0,j,\check{I}} \|v\|_{j,\check{I}}, \qquad \forall v \in \mathcal{H}^{m+1}_{\check{\alpha},r}(\check{I}). \tag{2.33}$$

Therefore, the norm $\|\cdot\|_{i,j,\check{I}}$ defined below

$$\left\|\check{P}^m_{\check{\alpha},r}\right\|_{i,j,\check{I}} = \sup\left\{\left\|\check{P}^m_{\check{\alpha},r}(v)\right\|_{i,\check{I}} \mid v \in \mathcal{H}^{m+1}_{\check{\alpha},r}(\check{I}),\ \|v\|_{j,\check{I}} = 1\right\}, \tag{2.34}$$

is finite for all integers $0 \leq i \leq m+1$.

$$\left\|\check{P}^m_{\check{\alpha},r}\right\|_{i,j,\check{I}} = \sup\left\{\left\|\check{P}^m_{\check{\alpha},r}(v)\right\|_{i,\check{I}} \mid v \in \mathcal{H}^{m+1}_{\check{\alpha},r}(\check{I}),\ \|v\|_{j,\check{I}} = 1\right\},$$

Now, we are ready to state the Immersed Bramble-Hilbert lemma.

Lemma 2.9. *Let $\check{P}^m_{\check{\alpha},r} : \mathcal{H}^{m+1}_{\check{\alpha},r}(\check{I}) \to \mathcal{V}^m_{\check{\alpha},r}(\check{I})$ be a j-bounded projection, then*

$$\left\|v - \check{P}^m_{\check{\alpha},r} v\right\|_{i,\check{I}} \underset{m,r}{\lesssim} \left(1 + \left\|\check{P}^m_{\check{\alpha},r}\right\|_{i,j,\check{I}}\right) |v|_{m+1,\check{I}}, \qquad i = 0, 1, \ldots, m,$$

for all $v \in \mathcal{H}^{m+1}_{\check{\alpha},r}(\check{I})$, where $\left\|\check{P}^m_{\check{\alpha},r}\right\|_{i,j,\check{I}}$ is defined in (2.34)

Proof. Let $v \in \mathcal{H}^{m+1}_{\check{\alpha},r}(\check{I})$, then by the triangle inequality, we have

$$\left\|v - \check{P}^m_{\check{\alpha},r} v\right\|_{i,\check{I}} \leq \left\|v - \check{\pi}^m_{\check{\alpha},r} v\right\|_{i,\check{I}} + \left\|\check{P}^m_{\check{\alpha},r} v - \check{\pi}^m_{\check{\alpha},r} v\right\|_{i,\check{I}}.$$

Since $\check{P}^m_{\check{\alpha},r}$ is a projection, we have $\check{\pi}^m_{\check{\alpha},r} v = \check{P}^m_{\check{\alpha},r} \check{\pi}^m_{\check{\alpha},r} v$, which leads to

$$\begin{aligned}
\left\|v - \check{P}^m_{\check{\alpha},r} v\right\|_{i,\check{I}} &\leq \left\|v - \check{\pi}^m_{\check{\alpha},r} v\right\|_{i,\check{I}} + \left\|\check{P}^m_{\check{\alpha},r}\left(v - \check{\pi}^m_{\check{\alpha},r} v\right)\right\|_{i,\check{I}} \\
&\leq \left\|v - \check{\pi}^m_{\check{\alpha},r} v\right\|_{i,\check{I}} + \left\|\check{P}^m_{\check{\alpha},r}\right\|_{i,j,\check{I}} \left\|v - \check{\pi}^m_{\check{\alpha},r} v\right\|_{j,\check{I}} \\
&\underset{m,r}{\lesssim} (1 + \left\|\check{P}^m_{\check{\alpha},r}\right\|_{i,j,\check{I}}) |v|_{m+1,\check{I}}, \qquad \text{(Using (2.30))}
\end{aligned}$$

which is the desired result. □

The lemma above is a generalization of the classical Bramble-Hilbert lemma in one-dimension in the sense that if $r_k = 1$ for all $k = 0, 1 \ldots, m$, then the RIFE space $\mathcal{V}^m_{\check{\alpha},r}(\check{I})$ is exactly the polynomial space $\mathcal{P}^m(\check{I})$, and the immersed Sobolev space $\mathcal{H}^{m+1}_{\check{\alpha},r}(\check{I})$ is the Sobolev space $H^{m+1}(\check{I})$.

Next, we extend the results of Lemma 2.9 to the local (physical) interface element $I_{k_0} = [x_{k_0-1}, x_{k_0-1} + h]$, which contains the interface point α. To achieve this, we use $F : \check{I} \to I_{k_0}$

to denote the affine map given by

$$F(\xi) = x_{k_0-1} + h\xi, \qquad \forall \xi \in \check{I}, \tag{2.35}$$

and we use $\mathcal{M} : L^2(I_{k_0}) \to L^2(\check{I})$ to denote the change of variables $\mathcal{M}\varphi = \varphi \circ F$ for all functions in $L^2(I_{k_0})$. One key property of the map $\mathcal{M}$ is that it maps $\mathcal{H}^{m+1}_{\alpha,r}(I_{k_0})$ to $\mathcal{H}^{m+1}_{\check{\alpha},r}(\check{I})$ and $\mathcal{V}^m_{\alpha,r}(I_{k_0})$ to $\mathcal{V}^m_{\check{\alpha},r}(\check{I})$ as shown in the lemma below

Lemma 2.10. *Let $v \in \mathcal{H}^{m+1}_{\alpha,r}(I_{k_0})$, then $\mathcal{M}v \in \mathcal{H}^{m+1}_{\check{\alpha},r}(\check{I})$. In particular, if $v \in \mathcal{V}^m_{\alpha,r}(I_{k_0})$, then $\mathcal{M}v \in \mathcal{V}^m_{\check{\alpha},r}(\check{I})$.*

Proof. Let $v \in \mathcal{H}^{m+1}_{\alpha,r}(I_{k_0})$ and let $\check{v} = \mathcal{M}v = v \circ F$. Then, since $\check{v}|_{\check{I}^\pm} \in H^{m+1}(\check{I}^\pm)$, and by definition of the immersed Sobolev space, we have

$$\check{v}^{(k)}(\check{\alpha}^+) = h^k v^{(k)}(\alpha^+) = r_k h^k v^{(k)}(\alpha^-) = r_k \check{v}^{(k)}(\check{\alpha}^-), \qquad k = 0, 1, 2, \ldots, m.$$

Hence, $\check{v} \in \mathcal{H}^{m+1}_{\check{\alpha},r}(\check{I})$, which proves the first claim.

To prove the second claim, consider $v \in \mathcal{V}^m_{\alpha,r}(I_{k_0})$ and $\check{v} = \mathcal{M}v$, then $\check{v}|_{\check{I}^\pm} \in \mathcal{P}^m(\check{I}^\pm)$ since F is affine, and $\check{v}^{(k)}(\check{\alpha}^+) = r_k \check{v}^{(k)}(\check{\alpha}^-)$ for all $0 \le k \le m$ by our previous argument. Therefore, $\check{v} \in \mathcal{V}^m_{\check{\alpha},r}(\check{I})$. □

It is worth noting here that the sequence (r_k) associated with the local (physical) IFE space is the same sequence associated with the reference IFE space. Hence, the immersed Bramble-Hilbert lemma can be extended to the projections onto the local IFE space (LIFE) via the scaling argument. Again, this step is very similar to arguments used in the traditional finite element method. To be more precise, we are interested in projections $P^m_{\alpha,r}$ onto the LIFE space that are constructed from a projection $\check{P}^m_{\check{\alpha},r}$ onto the RIFE space, such that $\mathcal{M} \circ P^m_{\alpha,r} = \check{P}^m_{\check{\alpha},r} \circ \mathcal{M}$. However, we note here that under mesh refinement, the relative position

of the interface within the local element changes, which in turn, changes the location of $\check{\alpha}$ in $\check{I}$. Therefore, we need to consider the norm of all $\check{P}^m_{\check{\alpha},r}$ for all $\check{\alpha} \in \check{I}$.

Definition 2.6. Let $\{\check{P}^m_{\check{\alpha},r}\}_{\check{\alpha}\in\check{I}}$ be a family of projections from $\mathcal{H}^{m+1}_{\check{\alpha},r}(\check{I})$ onto $\mathcal{V}^m_{\check{\alpha},r}(\check{I})$. We say that $\{\check{P}^m_{\check{\alpha},r}\}_{\check{\alpha}\in\check{I}}$ is a uniformly bounded family of RIFE projections if

$$\left\|\check{P}^m_{\check{\alpha},r}\right\|_{0,j,\check{I}} \lesssim_{m,r} 1, \qquad \forall \check{\alpha} \in \check{I}, \tag{2.36}$$

for some integer $0 \le j \le m+1$.

That is, $\{\check{P}^m_{\check{\alpha},r}\}_{\check{\alpha}\in\check{I}}$ is a uniformly bounded family of RIFE projections consists of projections whose norms can be bounded independently of the interface location. This notion can be extended to the local (physical) IFE space as well.

Definition 2.7. Let I_{k_0} be an element and let $\{P^m_{\alpha,r}\}_{\alpha\in I_{k_0}}$ be a family of projections from $\mathcal{H}^{m+1}_{\alpha,r}(I_{k_0})$ onto $\mathcal{V}^m_{\alpha,r}(I_{k_0})$. We say that $\{P^m_{\alpha,r}\}_{\alpha\in I_{k_0}}$ is a uniformly bounded family of LIFE projections if $\{\check{P}^m_{\check{\alpha},r}\}_{\check{\alpha}\in\check{I}}$ is a uniformly bounded family of RIFE projections, where $\check{P}^m_{\check{\alpha},r} = \mathcal{M} \circ P^m_{\alpha,r} \circ \mathcal{M}^{-1}$ for all $\alpha \in I_{k_0}$.

In other words, S is a uniformly bounded family of LIFE projections if the *associated* family of RIFE projections is uniformly bounded. The main benefit of working with such projections is that we can derive the following estimate for the residual of the projection.

Theorem 2.4. *Let I_{k_0} be an element of size h and let $\{P^m_{\alpha,r}\}_{\alpha\in I_{k_0}}$ be a uniformly bounded family of LIFE projections, then*

$$|P^m_{\alpha,r}v - v|_{i,I_{k_0}} \lesssim_{m,r} h^{m+1-i}|v|_{m+1,I_{k_0}}, \qquad \forall v \in \mathcal{H}^{m+1}_{\alpha,r}(I_{k_0}),\ \forall \alpha \in I_{k_0},$$

for all integer $0 \le i \le m$.

Proof. Let $\check{P}^m_{\check{\alpha},r} = \mathcal{M} \circ P^m_{\alpha,r} \circ \mathcal{M}^{-1}$ and let $\check{v} = \mathcal{M}v$. Then $P^m_{\alpha,r} v = \mathcal{M}^{-1} \check{P}^m_{\check{\alpha},r} \check{v}$. Hence, by the change of variable $x \mapsto F(x)$

$$\begin{aligned} |P^m_{\alpha,r} v - v|_{i,I_{k_0}} &= h^{-i} |\mathcal{M}^{-1} \left(\check{P}^m_{\check{\alpha},r} \check{v} - \check{v} \right)|_{i,I_{k_0}} = h^{-i} |\left(\check{P}^m_{\check{\alpha},r} \check{v} - \check{v} \right) \circ F^{-1}|_{i,I_{k_0}} \\ &= h^{1-i} |\check{P}^m_{\check{\alpha},r} \check{v} - \check{v}|_{i,\check{I}}. \end{aligned} \tag{2.37}$$

Next, we use Lemma 2.9 and the uniform boundedness assumption to obtain

$$\begin{aligned} |P^m_{\alpha,r} v - v|_{i,I_{k_0}} &\underset{m,r}{\lesssim} h^{1-i} (1 + \left\| \check{P}^m_{\check{\alpha},r} \right\|_{i,j,\check{I}}) |\check{v}|_{m+1,\check{I}} \underset{m,r}{\lesssim} h^{1-i} |\check{v}|_{m+1,\check{I}} \\ &\underset{m,r}{\lesssim} h^{1-i} h^{m+1} h^{-1} |v|_{m+1,I_{k_0}} \qquad \text{(using the change of variables } x = F(\xi)) \\ &\underset{m,r}{\lesssim} h^{m+1-i} |v|_{m+1,I_{k_0}}, \end{aligned}$$

which is the desired result. □

The estimates derived above apply to many interesting and useful projections. In this dissertation we will focus on the following projections, which are relevant to our analysis later:

- The L^2 orthogonal projection $P^{m,\texttt{ort}}_{\alpha,r}$ maps a function v to the closest v_h in the LIFE space, in the sense of the L^2 norm. Although, we will not use this projection in our analysis, it will serve as a first example to illustrate the notion of uniformly bounded family of LIFE projections.
- The immersed Radau projection $P^{m,\texttt{Rad}}_{\alpha,r}$ interpolates a function v at one endpoint, plus some additional orthogonality conditions. This projection is similar to traditional Gauss-Radau projection used to analyze DG methods [40, 87, 95], and will be used to analyze the immersed discontinuous Galerkin method for the transport interface

problem (2.1d).

- The immersed Lobatto projection $P_{\alpha}^{m,\mathtt{Lob}}$ interpolates a function v at the two endpoints of the element, which will be used to establish a C^0-conforming IFE space for the elliptic interface problem (2.1a) and the parabolic interface problem (2.1c).
- The immersed Hermite projection $P_{\alpha,r}^{m,\mathtt{Her}}$ interpolates a function v and its derivative at the endpoints, which will be used to construct C^1-conforming IFE space for the Euler-Bernoulli beam interface problem (2.1b).

We note that we are not discussing the IFE spaces and projections for the acoustic interface problem here, and we will postpone that discussion since it will employ some problem-specific techniques. Nevertheless, our approach in that section will be inspired by the immersed Radau projection, and it will be similar to the analysis of the transport interface problem.

For each of the projections mentioned above, we will provide a precise definition, and we prove that it is well-defined, then we show that the collection of all said projections forms a uniformly bounded family of LIFE projection. Thus, they all provide an optimal approximation to functions v in the immersed Sobolev space $\mathcal{H}_{\alpha,r}^{m+1}(I_{k_0})$. To illustrate this idea, we study the L^2 projection below and derive an optimal approximation capability result.

Definition 2.8. Let $v \in L^2(I_{k_0})$, we use $P_{\alpha,r}^{m,\mathtt{ort}} v$ to denote the solution to the system

$$P_{\alpha,r}^{m,\mathtt{ort}} v \in \mathcal{V}_{\alpha,r}^{m}(I_{k_0}), \qquad \left(P_{\alpha,r}^{m,\mathtt{ort}} v, q\right)_{I_{k_0}} = (v,q)_{I_{k_0}}, \qquad \forall q \in \mathcal{V}_{\alpha,r}^{m}(I_{k_0}). \tag{2.38}$$

Lemma 2.11. *The L^2 projection $P_{\alpha,r}^{m,\mathtt{ort}}$ is a well-defined projection from $L^2(I_{k_0})$ onto $\mathcal{V}_{\alpha,r}^{m}(\check{I})$.*

Proof. The existence of The L^2 projection is a classical result of functional analysis [91]. □

Lemma 2.12. *The family $\{P_{\alpha,r}^{m,\mathtt{ort}}\}_{\alpha\in I_{k_0}}$ is a uniformly bounded family of LIFE projections.*

Proof. We only need to consider the associated RIFE projection $\check{P}_{\check{\alpha},r}^{m,\mathtt{ort}} : \mathcal{H}_{\check{\alpha},r}^{m+1}(\check{I}) \to \mathcal{V}_{\check{\alpha},r}^{m}(\check{I})$ defined as

$$\left(\check{P}_{\alpha,r}^{m,\mathtt{ort}} v, q\right)_{\check{I}} = (v, q)_{\check{I}}, \qquad \forall q \in \mathcal{V}_{\check{\alpha},r}^{m}(\check{I}).$$

By choosing $q = \check{P}_{\alpha,r}^{m,\mathtt{ort}} v$ and using the Cauchy-Schwarz inequality, we obtain

$$\left\|\check{P}_{\check{\alpha},r}^{m,\mathtt{ort}} v\right\|_{0,\check{I}}^2 = \left(v, \check{P}_{\check{\alpha},r}^{m,\mathtt{ort}} v\right)_{\check{I}} \leq \left\|\check{P}_{\check{\alpha},r}^{m,\mathtt{ort}} v\right\|_{0,\check{I}} \|v\|_{0,\check{I}}.$$

Therefore, $\left\|\check{P}_{\alpha,r}^{m,\mathtt{ort}} v\right\|_{0,\check{I}} \leq \|v\|_{0,\check{I}}$ for all $v \in \mathcal{H}_{\check{\alpha},r}^{m+1}(\check{I})$. Hence, the orthogonal L^2 projection is a uniformly bounded family of LIFE projections. □

Now, we can derive an estimate for the error of the L^2 projection onto the IFE space directly from the lemma above and Theorem 2.4.

Corollary 2.2. *Let $v \in \mathcal{H}_{\alpha,r}^{m+1}(I_{k_0})$, then*

$$\left|v - P_{\alpha,r}^{m,\mathtt{ort}} v\right|_{i,I_{k_0}} \underset{m,r}{\lesssim} h^{m+1-i} |v|_{m+1,I_{k_0}}, \qquad i = 0, 1, \ldots, m.$$

The corollary above shows that the local IFE space provides an optimal approximation to functions in the immersed Sobolev space, in the sense that the residual $v - P_{\alpha,r}^{m,\mathtt{ort}} v$ decays at rate of $O(h^{m+1-i})$ in the i-th Sobolev semi-norm, which is similar to the classical case of approximation functions with polynomials.

More importantly, the steps above illustrate a unified framework to study various IFE projections for different interface problems. More precisely, the steps that we will take for every problem in the next section will be the following:

1. We define a projection operator $P_{\alpha,r}^{m}$ from an immersed Sobolev space onto a local IFE space, which in turn, defines a family of projections $\{\check{P}_{\check{\alpha},r}^{m}\}_{\check{\alpha}\in\check{I}}$ from $\mathcal{H}_{\check{\alpha},r}^{m+1}(\check{I})$ onto

$\mathcal{V}^m_{\check{\alpha},r}(\check{I})$, where $\check{P}^m_{\check{\alpha},r} = \mathcal{M} \circ P^m_{\alpha,r} \circ \mathcal{M}^{-1}$.

2. We show that $\check{P}^m_{\check{\alpha},r}$ is well-defined. Typically, this involves proving that a square linear system admits a unique solution.

3. We prove that $\{\check{P}^m_{\check{\alpha},r}\}_{\check{\alpha}\in\check{I}}$ is a uniformly bounded family of RIFE projections.

After that, we can immediately derive an error estimate for the projection $P^m_{\alpha,r}$ that is independent of α, and use it in the study of the IFE method.

2.4 Analysis of IFE Methods for Interface Problems

In this section, we develop and analyze arbitrary-order IFE methods for the interface problems (2.1a)-(2.1e). For each interface problem, we will describe the extended jump conditions associated with the solution and the discrete weak formulation, then we will introduce a suitable projection to derive optimal convergence estimates for each method.

2.4.1 The Elliptic Interface Problem

Consider the following boundary value problem

$$\begin{cases} -\beta(x)u''(x) = f(x), & x \in I^- \cup I^+, \\ u(a) = u(b) = 0, \end{cases} \tag{2.39a}$$

where β is a piecewise constant function $\beta|_{I^\pm} = \beta^\pm > 0$. At the interface point, we assume that the solution satisfies the following interface conditions

$$[\![u]\!]_\alpha = [\![\beta u']\!]_\alpha = 0. \tag{2.39b}$$

The first IFE method for the interface problem (2.39) was presented in [76], where the IFE method was introduced. In that paper, the author only considered the first degree IFE space, where the shape functions are linear functions on non-interface elements and piecewise linear function on the interface element. Their construction was later extended to higher degree IFE space in [7], where the authors constructed an m-th order IFE space with a Lagrange basis. The key idea to construct higher order IFE spaces that the authors presented is to restrict our attention to the case where f, the right-hand side of (2.39a), is smooth around the interface. For instance, if f is continuous at α, we infer that $[\![\beta u'']\!]_\alpha = 0$. Similarly, if $f \in C^{m-2}(I)$, we obtain

$$[\![\beta u^{(k)}]\!]_\alpha = 0, \qquad k = 1, 2, \ldots, m,$$

which is, when combined with $u|_{I^\pm} \in H^{m-1}(I^\pm)$, yields $u \in \mathcal{H}^{m+1}_{\alpha,r^e}(I)$, where $r^e = (r^e_k)$ is the sequence

$$r^e_0 = 1, \ r^e_k = \frac{\beta^-}{\beta^+}, \qquad k = 1, 2, \ldots. \tag{2.40}$$

Therefore, it is suitable here to consider the following global continuous IFE space

$$\mathcal{V}^{m,\mathtt{cont}}_\alpha(\mathcal{T}_h) = \mathcal{V}^m_{\alpha,r^e}(\mathcal{T}_h) \cap H^1(I), \tag{2.41}$$

where r^e is defined in (2.40). Here, we are dropping the sequence r^e from the notation since it will remain unchanged in the remainder of this subsection. Now, the discrete weak formulation can be posed as follows: Find $u_h \in \mathcal{V}^{m,\mathtt{cont}}_\alpha(\mathcal{T}_h) \cap H^1_0(I)$ such that

$$(\beta u_h', v_h')_I = (f, v_h)_I, \quad \forall v_h \in \mathcal{V}^{m,\mathtt{cont}}_\alpha(\mathcal{T}_h) \cap H^1_0(I). \tag{2.42}$$

The discrete formulation (2.42) is the same as the one used in [7], where the authors used the special form of the sequence r^e to establish an estimate for the interpolation error,

and consequently, an estimate for the error of the method. Our goal here is to provide an alternative approach to analyzing the error $\|u-u_h\|_{0,I}$ based on the immersed Bramble-Hilbert lemma, which is simpler, and generalizable to other methods.

The main ingredient in the analysis is to construct an optimally convergent projection $P^{m,\texttt{cont}}$ from the immersed Sobolev space $\mathcal{H}^{m+1}_{\alpha,r^e}(I)$ onto the global continuous IFE space $\mathcal{V}^{m,\texttt{cont}}_{\alpha}(\mathcal{T}_h)$. Following the analysis of the classical finite element method, we choose $P^{m,\texttt{cont}}v|_{I_k}$ to be the Lagrange interpolant $P^{m,\texttt{Lag}}$ of v on a non-interface element I_k. On the interface element I_{k_0}, we propose the following immersed Lobatto projection for a function $v\in H^{m+1}_{\alpha,r^e}(I)$

$$\begin{cases} P^{m,\texttt{Lob}}_{\alpha}v(x_{k_0-1})=v(x_{k_0-1}),\\ P^{m,\texttt{Lob}}_{\alpha}v(x_{k_0})=v(x_{k_0}),\\ (P^{m,\texttt{Lob}}_{\alpha}v,q)_{w,I_{k_0}}=(v,q)_{w,I_{k_0}}\,, \quad \forall q\in\mathcal{V}^{m-2}_{\alpha,\tau^2(r^e)}(I_{k_0}), \end{cases} \qquad w(x)=\begin{cases} r_1^e, & x\in I^-_{k_0},\\ 1, & x\in I^+_{k_0}. \end{cases} \tag{2.43}$$

That is, the Lobatto projection $P^{m,\texttt{Lob}}_{\alpha}v$ interpolates the function v at the endpoints, and $P^{m,\texttt{Lob}}_{\alpha}v-v$ is orthogonal to the space $\mathcal{V}^{m-2}_{\alpha,\tau^2(r)}(I_{k_0})$ with respect to a weighted inner product. The interpolation property ensures that the global projection

$$P^{m,\texttt{cont}}: v\mapsto P^{m,\texttt{cont}}v, \qquad P^{m,\texttt{cont}}v|_{I_k}=\begin{cases} P^{m,\texttt{Lag}}(v|_{I_k}), & k\neq k_0\\ P^{m,\texttt{Lob}}_{\alpha}(v|_{I_k}), & k=k_0, \end{cases} \tag{2.44}$$

is indeed in the global continuous IFE space. The orthogonality condition is added to ensure the uniqueness of the projection and to prove that the immersed Lobatto projection is uniformly bounded.

First, recall that we only need to study the Lobatto projection on the reference element $\check{I}$,

denoted $\check{P}_{\check{\alpha}}^{m,\mathtt{Lob}}$, which maps a function $v \in \mathcal{H}_{\check{\alpha},r}^{m+1}(\check{I})$ into $v_h = \check{P}_{\check{\alpha}}^{m,\mathtt{Lob}} v$, where

$$\begin{cases} v_h(0) = v(0), \\ v_h(1) = v(1), \\ (v_h, q)_{\check{w},\check{I}} = (v, q)_{\check{w},\check{I}}, \quad \forall q \in \mathcal{V}_{\check{\alpha},\tau^2(r^e)}^{m-2}(\check{I}), \end{cases} \qquad \check{w}(x) = \begin{cases} r_1^e, & x \in \check{I}^-, \\ 1, & x \in \check{I}^+. \end{cases} \tag{2.45}$$

Lemma 2.13. *The projection $\check{P}_{\check{\alpha}}^{m,\mathtt{Lob}} : \mathcal{H}_{\check{\alpha},r^e}^{m+1}(\check{I}) \to \mathcal{V}_{\check{\alpha},r^e}^{m}(\check{I})$ is well-defined.*

Proof. Consider the system (2.45). By expressing $v_h = \check{P}_{\check{\alpha}}^{m,\mathtt{Lob}} v$ in terms of the canonical basis, we obtain a square linear system. Therefore, it is enough to show that if $v = 0$, then $v_h = 0$ to prove that $\check{P}_{\check{\alpha}}^{m,\mathtt{Lob}}$ is well-defined.

Now, suppose that $v = 0$ in (2.45), then $v_h(0) = v_h(1) = 0$, and $(v_h, \check{w}q)_{\check{I}} = 0$ for all $q \in \mathcal{V}_{\check{\alpha},\tau^2(r^e)}^{m-2}(\check{I})$. In particular, for $q = v_h''$, we have

$$(v_h, \check{w} v_h'')_{\check{I}} = 0.$$

By construction of $\mathcal{V}_{\check{\alpha},r^e}^{m}$, $\check{w}v_h''$ is continuous. Therefore, using integration by parts and $v_h(0) = v_h(1) = 0$, we obtain

$$0 = (v_h', \check{w} v_h')_{\check{I}} = \left\| \sqrt{\check{w}} v_h' \right\|_{0,\check{I}}.$$

Then, we have $v_h = 0$ since $v_h(0) = 0$. □

Lemma 2.14. *The family $\{P_{\alpha}^{m,\mathtt{Lob}}\}_{\alpha \in I_{k_0}}$ is a uniformly bounded family of LIFE projections.*

Proof. Here, it is enough to show that $\|v_h\|_{0,\check{I}} \lesssim_{m,\beta} \|v\|_{1,\check{I}}$, where $v_h = \check{P}_{\check{\alpha}}^{m,\mathtt{Lob}} v$ is given by (2.45).

Let $q_1 \in \mathcal{V}^1_{\check{\alpha},r^e}(\check{I})$ be the unique IFE function in $V^1_{\check{\alpha},r^e}(\check{I})$ such that $q_1(0) = v(0)$ and $q_1(1) = v(1)$. Then, it is easy [76] to check that

$$\|q_1\|_{0,\check{I}} \leq |v(0)| + |v(1)| \lesssim \|v\|_{1,\check{I}} \tag{2.46}$$

Now, let $q_2 = v_h - q_1$, then $q_2(0) = q_2(1) = 0$, and

$$(q_2, \check{w}q)_{\check{I}} = (v - q_1, \check{w}q)_{\check{I}}, \qquad \forall q \in \mathcal{V}^{m-2}_{\check{\alpha},\tau^2(r^e)}(\check{I}).$$

Next, we substitute q with q_2'', and integrate by parts

$$-(q_2', \check{w}q_2')_{\check{I}} = (v - q_1, q_2'')_{\check{I}}.$$

At this step, we recall that $\check{w} \simeq_\beta 1$. Then

$$\|q_2'\|^2_{0,\check{I}} \underset{\beta}{\lesssim} |(q_2', \check{w}q_2')_{\check{I}}| \underset{\beta}{\lesssim} \|v - q_1\|_{0,\check{I}} \, \|q_2''\|_{0,\check{I}} \, .$$

Next, we apply Friedrichs inequality to the left-hand side and the inverse inequality Lemma 2.5 to the right-hand side, and the Triangle inequality

$$\|q_2\|^2_{0,\check{I}} \underset{m,\beta}{\lesssim} \left(\|v\|_{0,\check{I}} + \|q_1\|_{0,\check{I}} \right) \|q_2\|_{0,\check{I}} \underset{m,\beta}{\lesssim} \|v\|_{1,\check{I}} \, \|q_2\|_{0,\check{I}} \, , \tag{2.47}$$

where the last inequality follows from (2.46). Finally, we combine (2.46) and (2.47) to obtain

$$\|v_h\|_{0,\check{I}} = \|q_1 + q_2\|_{0,\check{I}} \leq \|q_1\|_{0,\check{I}} + \|q_2\|_{0,\check{I}} \underset{m,\beta}{\lesssim} \|v\|_{1,\check{I}} \, .$$

Hence, $\{P^{m,\texttt{Lob}}_\alpha\}_{\alpha \in I_{k_0}}$ is a uniformly bounded family of LIFE projections. □

From the immersed Bramble-Hilbert, we obtain the following error estimate for immersed Lobatto projection.

Corollary 2.3. *Let $v \in \mathcal{H}^{m+1}_{\alpha,r^e}(I_{k_0})$, then*

$$\left|v - P^{m,\texttt{Lob}}_{\alpha} v\right|_{i,\check{I}} \underset{m,\beta}{\lesssim} h^{m+1-i}|v|_{m+1,I_{k_0}}, \qquad i = 0, 1, \ldots, m.$$

Now, we recall that $P^{m,\texttt{cont}}$ is defined piecewisely on each element. Then, by summing over all elements and using the traditional finite element estimates on non-interface elements, and Corollary 2.3 on the interface element, we have

$$|v - P^{m,\texttt{cont}} v|_{i,I} \underset{m,\beta}{\lesssim} h^{m+1-i}|v|_{m+1,I}, \qquad i = 0, 1. \tag{2.48}$$

Here, we are only considering the first two Sobolev norms. However, we can extend this result to higher-order norms easily by Theorem 2.4. Finally, we are ready to state the main result of this subsection.

Theorem 2.5. *Let $u \in \mathcal{H}^{m+1}_{\alpha,r^e}(I) \cap H^1_0(I)$ be the exact solution to (2.39), and let $u_h \in \mathcal{V}^{m,\texttt{cont}}_{\alpha}(\mathcal{T}_h) \cap H^1_0(I)$ be the solution to the discrete problem (2.42), then*

$$|u - u_h|_{1,I} \underset{m,\beta}{\lesssim} h^m |u|_{m+1,I}, \tag{2.49}$$

and

$$|u - u_h|_{0,I} \underset{m,\beta}{\lesssim} h^{m+1} |u|_{m+1,I}. \tag{2.50}$$

Proof. The first inequality (2.49) follows from Céa's lemma [29, 32, 69] and the approximation result (2.48), and the second inequality (2.50) follows from the duality argument [69], also known as the Aubin-Nitche trick. □

Remark 2.3. It is worth noting that the results of Theorem 2.5 appeared in [7], where the authors used a multipoint Taylor expansion technique to estimate the error of an immersed Lagrange interpolation on interface elements. Our approach, which relies on the immersed Lobatto projection, is much simpler and provides a similar approximation result.

Remark 2.4. We refer the reader to [7] for numerical examples illustrating the findings of Theorem 2.5 for $1 \leq m \leq 5$.

2.4.2 The Parabolic Interface Problem

Consider the following parabolic initial boundary value problem

$$\begin{cases} u_t(x,t) = \beta(x) u_{xx}(x,t), & x \in I^- \cup I^+,\ 0 < t \leq T, \\ u(a) = u(b) = 0, & \\ u(x,0) = u_0(x), & x \in I, \end{cases} \tag{2.51}$$

where $\beta|_{I^\pm} = \beta^\pm > 0$ is a piecewise constant function that represent the heat conductivity of a heterogeneous material, and u is assumed to satisfy the interface conditions $[\![u(\cdot,t)]\!]_\alpha = [\![\beta u_x(\cdot,t)]\!]_\alpha = 0$. An IFE method for this problem was briefly discussed in [64, 70], where the authors considered first order IFE methods based on the IFE space for the elliptic interface problem (2.41). However, higher order IFE methods were not developed and analyzed for this particular interface problem.

To derive the extended interface conditions for (2.51), we first restrict ourselves to the case where the solution is smooth enough, except (possibly) at the interface. Recall that the solution satisfies $[\![u(\cdot,t)]\!]_\alpha = 0$ for all $0 < t \leq T$, then if we differentiate with respect to t,

we obtain

$$[\![u_t(\cdot,t)]\!]_\alpha = [\![\beta u_{xx}(\cdot,t)]\!] = 0.$$

Similarly, if we differentiate the $[\![\beta u_x(\cdot,t)]\!]_\alpha = 0$ with respect to t, we obtain an additional interface condition

$$[\![\beta u_{tx}(\cdot,t)]\!]_\alpha = \left[\!\!\left[\beta^2 \frac{\partial^3 u}{\partial x^3}(\cdot,t)\right]\!\!\right]_\alpha = 0,$$

which is different from the extended interface conditions for the elliptic interface problem. Hence, we need to consider a slightly different immersed Sobolev space for the solution and consequently, a slightly different IFE space. By continuing this process of differentiating with respect to t, we obtain

$$\frac{\partial^k u}{\partial x^k}(\alpha^+,t) = r_k^d \frac{\partial^k u}{\partial x^k}(\alpha^-,t), \qquad r_k^d = \left(\frac{\beta^-}{\beta^+}\right)^{\lceil \frac{k}{2} \rceil}, \ k = 0,1,\ldots. \tag{2.52}$$

where $\lceil \cdot \rceil$ is the ceiling function. Now, we restrict our analysis to the case where the initial condition $u_0 \in \mathcal{H}^{m+1}_{\alpha,r^d}(I)$, and the solution $u(\cdot,t) \in \mathcal{H}^{m+1}_{\alpha,r^d}(I)$ for all $t \in (0,T)$, where the sequence $r^d = (r_k^d)$ is given by (2.52). In this case, the global continuous IFE space $\mathcal{V}_\alpha^{m,\mathtt{cont}}(\mathcal{T}_h)$ differs from the one described in the elliptic interface problem only in the choice of the sequence describing the interface conditions. Nevertheless, we use the same notation to describe both spaces to avoid complicating our notation. Similarly, when we use $P^{m,\mathtt{cont}}$ in this subsection, we are referring to the projection operator defined in (2.44), where the sequence r^e is now replaced by r^d from (2.52).

Remark 2.5. Note that the IFE space for the elliptic interface problem is identical to the IFE space for parabolic interface problem for $m \leq 2$, since the first three terms of r^d match those in r^e. Furthermore, the arguments used to derive Corollary 2.3 only use the first two

terms of r^e explicitly. Therefore, we have

$$|u(\cdot,t) - P^{m,\texttt{cont}}u(\cdot,t)|_{i,I} \underset{m,\beta}{\lesssim} h^{m+1-i} \max_{0\le t\le T} |u(\cdot,t)|_{m+1,I}, \qquad i = 0,1,\ldots,m.$$

Now, we are ready to state the discrete weak formulation to the problem (2.51): We are seeking $u_h : [0,T] \to \mathcal{V}_\alpha^{m,\texttt{cont}}(\mathcal{T}_h)$ such that

$$\begin{cases} (\partial_t u_h(t), v_h)_I = -\left(\partial_x u_h(t), \partial_x v_h\right)_{\beta,I}, \quad \forall v_h \in \mathcal{V}_\alpha^{m,\texttt{cont}}(\mathcal{T}_h), \quad 0 < t \le T, \\ u_h(0) = P^{m,\texttt{cont}} u_0, \end{cases} \tag{2.53}$$

which is equivalent to a system of differential equations $M\mathbf{c}'(t) = -S\mathbf{c}(t)$, where both M and S are symmetric positive definite matrices. The analysis of the method then follows the classical arguments for the traditional finite element method [97, pp. 5-10] to obtain

$$\|u_h(t) - u(\cdot,t)\|_{0,I} \underset{m,\beta}{\lesssim} h^{m+1} \left(\|u_0\|_{m+1,I} + \|u(\cdot,t)\|_{m+1,I} + \int_0^t \|u_t(\cdot,s)\|_{m+1,I}\, ds \right), \tag{2.54}$$

for $t \in [0,T]$. In the error estimate above, we are assuming that the time integration error is either negligible, or comparable to the spatial discretization error. It is worth mentioning here that an analysis of the fully discrete, higher order IFE method for the parabolic interface problem (2.51) is highly desirable. However, it would require a careful choice of a higher order time integration method that does not require excessively small time-steps. Such methods for low order, two-dimensional IFE methods were explored recently in [80] and remain a subject of active research. In the future, we will attempt to prove similar results for higher order IFE methods.

2.4.3 The Euler Bernoulli Beam Interface Problem

Consider the following interface problem

$$\begin{cases} \beta(x)u^{(4)}(x) = f(x), & x \in I^- \cup I^+, \\ u(a) = u'(a) = u(b) = u'(b) = 0, \end{cases} \tag{2.55a}$$

where the solution u satisfies the following jump conditions at α

$$[\![u]\!]_\alpha = [\![u']\!]_\alpha = [\![\beta u'']\!]_\alpha = [\![\beta u'']\!]_\alpha = 0. \tag{2.55b}$$

Cubic Hermite IFE methods were developed to solve the interface problem (2.55) in [81, 101] and analyzed in [78] using a multipoint Taylor expansion approach, which is cumbersome and hard to extend to higher order IFE methods. In this subsection, we will provide an alternative approach, based on the immersed Bramble-Hilbert lemma, to analyze m-th order IFE spaces for this problem. Our approach here is very similar to the one we used for the elliptic interface problem, in the sense that we only need to construct a suitable projection on the interface element, and prove that this projection is uniformly bounded. The rest follows from the immersed Bramble-Hilbert lemma and the classical finite element techniques.

First, we restrict our attention to the case where $f \in C^{m-3}$, where $m \geq 3$ is the degree of FE/IFE used. Then it follows from $\beta u^{(4)} = f$, and the interface jump conditions (2.55b) that $\left[\!\left[\beta u^{(k)}\right]\!\right]_\alpha = 0$ for $k = 2, \ldots, m$. Therefore, it is suitable to seek a solution to (2.55) in $\mathcal{H}^{m+1}_{\alpha,r^s}(I)$, where $r^s = (r^s_k)$ is the sequence

$$r^s_0 = r^s_1 = 1, \qquad r^s_k = \frac{\beta^-}{\beta^+}, \quad k = 2, \ldots, m. \tag{2.56}$$

Now, the discrete weak formulation can be stated as follows: Find $u_h \in \mathcal{V}^{m,\mathtt{Her}}_\alpha(\mathcal{T}_h) \cap H^2_0(I)$,

such that

$$(u_h'', v_h'')_I = (f, v_h)_I, \qquad \forall v_h \in \mathcal{V}_\alpha^{m,\mathtt{Her}}(\mathcal{T}_h) \cap H_0^2(I), \tag{2.57}$$

where $\mathcal{V}_\alpha^{m,\mathtt{Her}}(\mathcal{T}_h) = \mathcal{V}_{\alpha,r^s}^m(\mathcal{T}_h) \cap H^2(I)$ and r^s is given by (2.56). Next, we use $P^{m,\mathtt{Her}} : \mathcal{H}_{\alpha,r^s}^{m+1}(I) \to \mathcal{V}_\alpha^{m,\mathtt{Her}}(\mathcal{T}_h)$ to denote the global immersed Hermite projection constructed locally on each element: On non-interface elements, this projection is merely the classical C^1-conforming m-th degree Hermite interpolation, and on the interface element, it is the local immersed Hermite projection $P_\alpha^{m,\mathtt{Her}} = \mathcal{M}^{-1} \circ \check{P}_{\check{\alpha}}^{m,\mathtt{Her}} \circ \mathcal{M}$, where $\check{P}_{\check{\alpha}}^{m,\mathtt{Her}}$ will be presented shortly. To simplify the notation here, we use $\{\sigma_i\}_{i=0}^3$ to denote the four Hermite degrees of freedom on $\check{I}$, that is,

$$\sigma_0(v) = v(0), \quad \sigma_1(v) = v(1), \quad \sigma_2(v) = v'(0), \quad \sigma_3(v) = v'(1).$$

Using this notation, we can describe $\check{P}_{\check{\alpha}}^{m,\mathtt{Her}}$ as the map that associates with a function v, an IFE function $v_h \in \mathcal{V}_{\check{\alpha},r^s}^m(\check{I})$, such that

$$\begin{cases} \sigma_i(v_h) = \sigma_i(v), & 0 \le i \le 3, \\ (v_h, q)_{\check{w},\check{I}} = (v, q)_{\check{w},\check{I}}, & \forall q \in \mathcal{V}_{\check{\alpha},\tau^4(r^s)}^{m-4}(\check{I}), \end{cases} \qquad \check{w}(x) = \begin{cases} r_2^s, & x \in \check{I}^-, \\ 1, & x \in \check{I}^+. \end{cases} \tag{2.58}$$

Remark 2.6. In the case where $m = 3$, the immersed Hermite projection (2.58) reduces to the immersed cubic Hermite interpolation discussed in [81, 101], that is, our work here extends their IFE space to higher degrees m.

Remark 2.7. In (2.58), we can replace $\tau^4(r^s)$ with $\tau^2(r^s)$ since these two sequences are identical. We elected to use the former since, later in this subsection, we would substitute q with $v_h^{(4)}$ which is naturally in $\mathcal{V}_{\check{\alpha},\tau^4(r^s)}^{m-4}(\check{I})$.

Lemma 2.15. *The immersed Hermite projection $\check{P}_{\check{\alpha}}^{m,\mathtt{Her}}$ is well-defined.*

Proof. Let $v \in \mathcal{H}^{m+1}_{\check{\alpha},r^s}(\check{I})$. We recall that $\check{P}^{m,\texttt{Her}}_{\check{\alpha}} v$ is defined as v_h, the solution to (2.58), which is equivalent to a square linear system. Therefore, we only need to show that if $v = 0$, then $v_h = 0$.

Assume that $v = 0$, then

$$v_h(0) = v_h(1) = v_h'(0) = v_h'(1) = 0, \tag{2.59}$$

and

$$(v_h, \check{w} q)_{\check{I}} = 0, \qquad \forall q \in \mathcal{V}^{m-4}_{\check{\alpha},\tau^4(r^s)}(\check{I}).$$

In particular, for $q = v_h^{(4)}$, we have $\left(v_h, \check{w} v_h^{(4)}\right)_{\check{I}} = 0$. By construction, both v_h and $\check{w} v_h^{(4)}$ are in $C^1(\check{I})$. Then, by integrating by parts twice and using (2.59), we obtain

$$0 = (v_h'', \check{w} v_h'')_{\check{I}} \Longrightarrow v_h'' = 0,$$

which when combined with (2.59) yields $v_h = 0$ by Friedrichs inequality. □

Now, we recall the following result from [81] about the immersed cubic Hermite basis.

Lemma 2.16. *Let $\beta^{\pm} > 0$ and $\check{\alpha} \in \check{I}$, then there is basis $\{L^i_{\check{\alpha}}\}_{i=0}^3$ for $\mathcal{V}^3_{\check{\alpha},r^s}(\check{I})$ such that*

$$\sigma_i(L^j_{\check{\alpha}}) = \delta_{i,j}, \qquad 0 \le i, j \le 3.$$

Essentially, $\{L^i_{\check{\alpha}}\}_{i=0}^3$ are similar to the classical cubic Hermite basis since it provides a C^1 interpolation of a function $v \in H^2(\check{I})$ at the endpoints, as the Figure 2.4 shows. In fact, in the case where $\beta^- = \beta^+$, these two bases coincide.

Now, consider a function $v \in H^2(\check{I})$, let $v_h \in \mathcal{V}^3_{\check{\alpha},r^s}(\check{I})$ be its immersed Hermite projection,

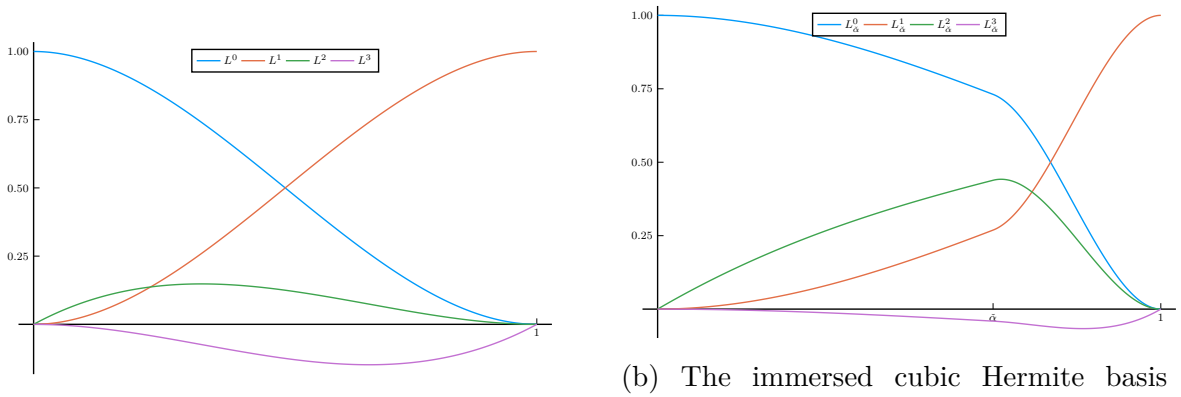

(a) The classical cubic Hermite basis

(b) The immersed cubic Hermite basis with $(\beta^-, \beta^+) = (100, 1)$

Figure 2.4: An illustration of the classical cubic Hermite basis (left) and the immersed cubic Hermite basis (right).

that is $\sigma_i(v) = \sigma_i(v_h)$ for $0 \leq i \leq 3$. Then, we have

$$\|v_h\|_{0,\check{I}} = \left\| \sum_{i=0}^{3} \sigma_i(v) L^i_{\check{\alpha}} \right\|_{0,\check{I}} \lesssim \|v\|_{2,\check{I}} \sum_{i=0}^{3} \left\| L^i_{\check{\alpha}} \right\|_{0,\check{I}}.$$

Then, to establish a bound on $\|v_h\|_{0,\check{I}}$ independently of $\check{\alpha}$, we need to show that the right-hand side of the inequality above is bounded independently of $\check{\alpha}$.

Lemma 2.17. *Let $\beta^{\pm} > 0$ and $\check{\alpha} \in \check{I}$, then*

$$-1 < L^i_{\check{\alpha}}(x) < 1, \qquad \forall\, x \in [0,1], \quad i = 0, 1, 2, 3, \tag{2.60}$$

where $\{L^i_{\check{\alpha}}\}_{i=0}^3$ is the immersed cubic Hermite basis described in Lemma 2.16.

Proof. This proof can be found in our paper [18], which we include here for the sake of completeness. Let us start with $p = L^0_{\check{\alpha}}$, we have

$$p(0) = 1, \quad p(1) = 0, \quad p'(0) = 0, \quad p'(1) = 0.$$

By Lemma 2.6, p' does not change sign in $(0,1)$ since $p' \in \mathcal{V}^2_{\check{\alpha},\tau(r^s)}(\check{I})$ and $p'(0) = p'(1) = 0$. Therefore, p is monotonically decreasing from $p(0) = 1$ to $p(1) = 0$. The same argument applies to $L^1_{\check{\alpha},r}$.

Next, we show that $q = L^2_{\check{\alpha}}$ is bounded between 0 and 1. We have

$$q(0) = 0, \quad q(1) = 0, \quad q'(0) = 1, \quad q'(1) = 0.$$

By Rolle's theorem, there is $c \in (0,1)$ such that $q'(c) = 0$. By Lemma 2.6, c the only root of q' in $(0,1)$. Now, by the generalized Rolle's theorem, there is $d \in (c,1)$ such that $q''(d^-)q''(d^+) \le 0$. If $d \neq \check{\alpha}$, then $q''(d^-) = q''(d^+) = q''(d)$ because q is a polynomial on either sides of $\check{\alpha}$. In this case we have $q''(d) = 0$. If $d = \check{\alpha}$, then $q''(d^-)q''(d^+) \le 0$ and jump condition implies

$$\frac{\beta^-}{\beta^+}\big(q''(\check{\alpha}^-)\big)^2 \le 0,$$

from which we have $q''(\check{\alpha}^-) = 0 = q''(\check{\alpha}^+)$. Hence, $q''(d) = 0$. Furthermore, by Lemma 2.6, d is the only root of q'' since $q'' \in \mathcal{V}^1_{\check{\alpha},\tau^2(r)}(\check{I})$. Since q'' is a linear polynomial on either sides of $\check{\alpha}$, the jump condition satisfied by q further implies that q'' does not change its sign $(0,d)$ and $(d,1)$. Because $q'(0) = 1$ and $q'(c) = 0$ and $0 < c < d$, we know that q' is decreasing on $(0,d)$ but increasing on $(d,1)$. These further imply that $q'(x) \in [0,1]$ for $x \in [0,c]$ and $q'(x) \le 0$ for $x \in [c,d]$; hence, $q(x) \le q(c)$ for all $x \in [0,d]$. Furthermore, since $q'(d) \le 0, q'(1) = 0$ and q' is monotonic on $[d,1]$, we know that $q'(x) \le 0$ for all $x \in [d,1]$. Hence, $0 = q(1) \le q(x) \le q(d) \le q(c)$ for all $x \in [d,1]$. Consequently, $q(c) \ge q(x)$ for $x \in [0,1]$. In addition, since q has no local minimum point on $(0,d)$, we have $q(x) \ge \min\{q(0), q(d)\} \ge 0$

for all $x \in [0, d]$. Thus, $q(x) \geq 0 \ \forall x \in [0, 1]$. On the other hand,

$$q(x) \leq q(c) = \int_0^c q'(x)dx \leq \int_0^c 1dx = c < 1 \quad \forall x \in [0, 1],$$

The last two estimates lead us to conclude that $0 \leq q(x) = L_{\check{\alpha}}^2(x) < 1$. Similarly, the proof of $-1 < L_{\check{\alpha}}^3 < 1$ follows similar steps. □

Now, we are ready to prove our main result about the immersed Hermite projection.

Lemma 2.18. *Let $\beta^{\pm} > 0$ and $m \geq 3$. Then*

$$\left\| \check{P}_{\check{\alpha}}^{m,\mathtt{Her}} v \right\|_{0,\check{I}} \underset{m,\beta}{\lesssim} \|v\|_{2,\check{I}},$$

for all $v \in \mathcal{H}_{\check{\alpha},r^s}^{m+1}(I)$.

Proof. Let $v \in \mathcal{H}_{\check{\alpha},r^s}^{m+1}(I)$, and let $q_1 \in \mathcal{V}_{\check{\alpha},r^s}^3(\check{I})$ be the immersed cubic Hermite interpolation of v, that is,

$$q_1 = \sum_{i=0}^{3} \sigma_i(v) L_{\check{\alpha}}^i.$$

By Lemma 2.17, we have

$$\|q_1\|_{0,\check{I}} \lesssim \sum_{i=0}^{3} |\sigma_i(v)| \lesssim \|v\|_{2,\check{I}}. \tag{2.61}$$

Now, let $v_h = \check{P}_{\check{\alpha}}^{m,\mathtt{Her}} v$, and consider $q_2 = v_h - q_1 \in \mathcal{V}_{\check{\alpha},r^s}^m(\check{I})$. By definition of v_h and q_1, we have

$$\begin{cases} \sigma_i(q_2) = 0, & 0 \leq i \leq 3, \\ (q_2, \check{w}q)_{\check{I}} = (v - q_1, \check{w}q)_{\check{I}}, & \forall q \in \mathcal{V}_{\check{\alpha},\tau^4(r^s)}^{m-4}(\check{I}). \end{cases} \tag{2.62}$$

In particular, if we choose $q = q_2^{(4)}$ and integrate by parts twice, we obtain the following

$$\left\| \sqrt{\check{w}} q_2'' \right\|_{0,\check{I}}^2 = (v - q_1, \check{w} q_2^{(4)})_{\check{I}}.$$

Then by Cauchy-Schwarz, the inverse inequality Lemma 2.5, and the definition of $\check{w}$, we have

$$\|q_2''\|_{0,\check{I}}^2 \underset{\beta}{\lesssim} \left(\|v\|_{0,\check{I}} + \|q_1\|_{0,\check{I}} \right) \left\| q_2^{(4)} \right\|_{0,\check{I}} \underset{m,\beta}{\lesssim} \left(\|v\|_{0,\check{I}} + \|q_1\|_{0,\check{I}} \right) \|q_2''\|_{0,\check{I}},$$

which, when combined with the inequality (2.61), and Friedrichs inequality, yields

$$\|q_2\|_{0,\check{I}} \lesssim \|q_2''\|_{0,\check{I}}^2 \underset{m,\beta}{\lesssim} \|v\|_{2,\check{I}}. \tag{2.63}$$

To finish the proof, we recall that $v_h = q_1 + q_2$. Therefore, by the (2.61), (2.63) and the triangle inequality, we have

$$\|v_h\|_{0,\check{I}} \underset{m,\beta}{\lesssim} \|v\|_{2,\check{I}}. \qquad \square$$

Again, the error estimate for the immersed Hermite projection follows immediately from Theorem 2.4.

Corollary 2.4. *Let $v \in \mathcal{H}^{m+1}_{\alpha,r^s}(I_{k_0})$, then*

$$\left| v - P_\alpha^{m,\mathtt{Her}} v \right|_{i,I_{k_0}} \underset{m,\beta}{\lesssim} h^{m+1-i} |v|_{m+1,I_{k_0}}, \qquad i = 0, 1, \ldots, m. \tag{2.64}$$

Therefore, by summing over all elements, using the classical interpolation results for polynomials on non-interface elements [37], and the error estimate (2.64) on interface elements, we obtain

$$\left| u - P_\alpha^{m,\mathtt{Her}} v \right|_{i,I} \underset{m,\beta}{\lesssim} h^{m+1-i} |v|_{m+1,I}, \qquad i = 0, 1, \ldots, m, \tag{2.65}$$

For all function $v \in \mathcal{H}^{m+1}_{\alpha,r^s}(I)$. Therefore, by using the classical finite element techniques, we

can derive the following estimate for the IFE solution to (2.55).

Theorem 2.6. *Let $u \in \mathcal{H}^{m+1}_{\alpha,r^s}(I)$ be the exact solution to (2.55), and let $u_h \in \mathcal{V}^{m,\mathtt{Her}}_{\alpha}(\mathcal{T}_h) \cap H^2_0(I)$ be the solution to the discrete problem (2.57), then*

$$\|u - u_h\|_{0,I} \underset{m,\beta}{\lesssim} h^{m+1}|u|_{m+1,I}.$$

Remark 2.8. We refer the reader to [81] for numerical examples illustrating the estimate in Theorem 2.6 for $m = 3$.

2.4.4 The Transport Interface Problem

Consider the following transport equation with a discontinuous coefficient

$$\begin{cases} u_t(x,t) + c(x)u_x(x,t) = 0, & x \in I^- \cup I^+,\ 0 < t \leq T, \\ u(a,t) = u_a(t), & 0 < t \leq T, \\ u(x,0) = u_0(x), & x \in I, \end{cases} \tag{2.66a}$$

where $c|_{I^\pm} = c^\pm > 0$ is a piecewise constant function, modeling the wave speeds in two different mediums. Additionally, we assume that the solution is continuous at the interface, that is $[\![u]\!]_\alpha = 0$. To our knowledge, no IFE methods were developed for this specific interface problem. Therefore, we will aim to provide a full overview of the discrete formulation, stability analysis, error analysis, and numerical examples in this subsection.

First, we restrict our attention to the case where u is smooth enough around the interface, except at the interface point itself, which allows us to derive additional interface conditions that we usually refer to as the extended interface conditions. More precisely, since $[\![u(\cdot,t)]\!]_\alpha = 0$ for all $0 < t \leq T$, we have $[\![u_t(\cdot,t)]\!]_\alpha = 0$, then by (2.66a) is equivalent to $[\![cu_x]\!]_\alpha = 0$. By

repeating this process m times, we obtain the following

$$\left[\!\left[c^k \frac{\partial^k u}{\partial x^k} \right]\!\right]_\alpha = 0, \qquad k = 0, 1, \ldots, m. \tag{2.66b}$$

Then, the solution u is in the time-dependent immersed Sobolev space $H^1([0,T], \mathcal{H}^{m+1}_{\alpha,r^h}(I))$, where $r^h = (r^h_k)$ is the sequence

$$r^h_k = \left(\frac{c^-}{c^+} \right)^k, \quad k = 0, 1, \ldots. \tag{2.67}$$

Additionally, we restrict our work to the case where $u_0 \in \mathcal{H}^{m+1}_{\alpha,r^h}(I)$, and to the case where the inflow boundary condition is zero, that is $u(a,t) = 0$ for simplicity. Later, in the numerical examples, we will describe briefly the case where u satisfies periodic boundaries conditions, in the case of two interfaces.

For this problem, we propose the following semi-discrete discontinuous Galerkin scheme, based on the upwind flux [65]: Find $u_h \in H^1([0,T], \mathcal{V}^m_{\alpha,r^h}(\mathcal{T}_h))$ such that

$$\begin{cases} M(\partial_t u_h(\cdot,t), v_h) = B(u_h(\cdot,t), v_h), & \forall v_h \in \mathcal{V}^m_{\alpha,r^h}(\mathcal{T}_h), \\ u_h(0,t) = 0, \\ u_h(\cdot,0) = P^{m,\mathtt{ort}} u_0, \end{cases} \tag{2.68}$$

where $P^{m,\mathtt{ort}}$ is the L^2 projection, and M and B are the bilinear forms defined below

$$M(w_h, v_h) = \left(\frac{1}{c} w_h, v_h \right)_I, \tag{2.69}$$

$$B(w_h, v_h) = \sum_{k=1}^{N} (w_h, v_h')_{I_k} + \sum_{k=1}^{N} [\![v_h]\!]_{x_k} w_h(x_k^-), \tag{2.70}$$

for all $w_h, v_h \in \mathcal{V}^m_{\alpha,r^h}(I)$. In the formula above, $[\![v_h]\!]_{x_k} = v(x_k^+) - v(x_k^-)$ for $k < n$ and $[\![v_h]\!]_{x_n} = -v_h(x_n^-)$. From the classical dG arguments [40, 65], it follows that

$$B(w_h, w_h) \leq 0, \qquad \forall w_h \in \mathcal{V}^m_{\alpha,r^h}(\mathcal{T}_h). \tag{2.71}$$

Therefore, the solution to the discrete problem (2.68) is stable in the energy norm, that is

$$\left\| \frac{1}{\sqrt{c}} u_h(\cdot, t) \right\|^2_{0,I} \leq \left\| \frac{1}{\sqrt{c}} u_h(\cdot, 0) \right\|^2_{0,I}, \qquad 0 < t \leq T. \tag{2.72}$$

Now, to analyze the L^2 error of this immersed dG scheme, we will follow a similar strategy to the one used for the standard dG method [6, 40, 108]: We introduce a projection operator, called the immersed Radau projection, which is a generalization of the classical right Radau projection, then we follow the classical technique to derive an optimal error estimate for the dG solution.

Definition 2.9. Let $v \in \mathcal{H}^{m+1}_{\alpha,r^h}(I)$, we define $P^{m,\texttt{Rad}} v \in \mathcal{V}^m_{\alpha,r^h}(\mathcal{T}_h)$ to be the solution to

$$\begin{cases} (P^{m,\texttt{Rad}} v, q')_{I_k} = (v, q')_{I_k}, & \forall q \in \mathcal{V}^{m-1}_{\alpha,\tau(r^h)}(\mathcal{T}_h), \quad \forall k \in \{1, 2, \ldots, N\}, \\ (P^{m,\texttt{Rad}} v)(x_k^-) = v(x_k^-), & \forall k \in \{1, 2, \ldots, N\}, \end{cases} \tag{2.73}$$

where $I_k = [x_{k-1}, x_k]$ is the k-th element. To unpack this definition, consider a non-interface element I_k with $k \neq k_0$, then the immersed Radau projection on this element $(P^{m,\texttt{Rad}} v)|_{I_k}$ is simply the classical Radau projection. On the interface element, the local Radau projection $P^{m,\texttt{Rad}}_\alpha = (P^{m,\texttt{Rad}} v)|_{I_{k_0}}$ is the solution to

$$\begin{cases} (P^{m,\texttt{Rad}}_\alpha v, q)_{I_{k_0}} = (v, q)_{I_{k_0}}, & \forall q \in \mathcal{V}^{m-1}_{\alpha,\tau(r^h)}(I_{k_0}), \\ (P^{m,\texttt{Rad}}_\alpha v)(x_{k_0}^-) = v(x_{k_0}^-). \end{cases} \tag{2.74}$$

As usual, we need to show that the immersed Radau projection is well-defined and uniformly bounded. In order to do so, we only need to show that $\check{P}_{\check{\alpha}}^{m,\mathtt{Rad}} = \mathcal{M} \circ P_{\alpha}^{m,\mathtt{Rad}} \circ \mathcal{M}^{-1}$ is well-defined and $\{\check{P}_{\check{\alpha}}^{m,\mathtt{Rad}}\}_{\check{\alpha}\in\check{I}}$ is a uniformly bounded family of RIFE projections.

By definition, the immersed Radau projection $\check{P}_{\check{\alpha}}^{m,\mathtt{Rad}} v$ of a function v is the solution $v_h \in \mathcal{V}_{\check{\alpha}}^{m}(\check{I})$ to the system

$$\begin{cases} (v_h, q)_{\check{I}} = (v, q)_{\check{I}}, & \forall q \in \mathcal{V}_{\check{\alpha},\tau(r^h)}^{m-1}(\check{I}), \\ v_h(1) = v(1). \end{cases} \tag{2.75}$$

Lemma 2.19. *The immersed Radau projection $\check{P}_{\check{\alpha},r^h}^{m,\mathtt{Rad}}$ is well-defined.*

Proof. Since the system (2.75) is a square linear system. It suffices to show that if $v = 0$, then $v_h = 0$.

First, recall that $r_k^h = \left(\frac{c^-}{c^+}\right)^k$. Therefore, $\tau(r^h) = \left(\frac{c^-}{c^+}\right) r^h$. In other words, if $q \in \mathcal{V}_{\check{\alpha},\tau(r^s)}^{m-1}(\check{I})$, then $q = \check{w}\tilde{q}$ for some $\tilde{q} \in \mathcal{V}_{\check{\alpha},r^h}^{m-1}(\check{I})$, where

$$\check{w}(x) = \begin{cases} 1 & x \in \check{I}^-, \\ r_1^h & x \in \check{I}^+. \end{cases} \tag{2.76}$$

We use this observation to rewrite (2.75) with $v = 0$ as

$$\begin{cases} (v_h, \tilde{q})_{\check{w},\check{I}} = 0, & \forall \tilde{q} \in \mathcal{V}_{\check{\alpha},r^h}^{m-1}(\check{I}), \\ v_h(1) = 0. \end{cases} \tag{2.77}$$

The first equation means that $v_h \in \mathcal{V}_{\check{\alpha},r}^{\check{w},m}(\check{I})$. By Lemma 2.7, it has exactly m interior roots in $\check{I}$, but $v_h(1) = 0$ which means that v_h has $m+1$ roots. Hence, $v_h = 0$ by Lemma 2.6. □

Lemma 2.20. *Let $c^{\pm} > 0$ and $m \geq 1$. Then*

$$\left\| \check{P}_{\check{\alpha}}^{m,\mathtt{Rad}} v \right\|_{0,\check{I}} \underset{m,c}{\lesssim} \|v\|_{1,\check{I}},$$

for all $v \in \mathcal{H}^{m+1}_{\check{\alpha},r^h}(\check{I})$.

Proof. Let $v \in \mathcal{H}^{m+1}_{\check{\alpha},r^h}(\check{I})$, $v_h = \check{P}_{\check{\alpha}}^{m,\mathtt{Rad}} v$, and let $q_1 \in \mathcal{V}^{m-1}_{\check{\alpha},r^h}(\check{I})$ be the solution to

$$(q_1, q)_{\check{I}} = (v, q)_{\check{I}} \qquad \forall q \in \mathcal{V}^{m-1}_{\check{\alpha},\tau(r^h)}(\check{I}),$$

which is equivalent to

$$(q_1, \tilde{q})_{\check{w},\check{I}} = (v, q)_{\check{I}} \qquad \forall q \in \mathcal{V}^{m-1}_{\check{\alpha},r^h}(\check{I}), \tag{2.78}$$

where $\check{w}$ is defined in (2.76). The system (2.78) admits a unique solution since it is equivalent to an $m \times m$ linear system with a symmetric positive definite matrix. Furthermore, by setting $q = q_1$ in (2.78), we obtain the following inequality

$$\|q_1\|^2_{0,\check{I}} \underset{c}{\lesssim} (q_1, q_1)_{\check{w},\check{I}} = (v, q_1)_{\check{I}} \leq \|v\|_{0,\check{I}} \|q_1\|_{0,\check{I}}. \tag{2.79}$$

Hence, $\|q_1\|^2_{0,\check{I}} \lesssim_c \|v\|_{0,\check{I}}$. Next, let $q_2 = v_h - q_1$, then

$$q_2 \in \mathcal{V}^{\check{w},m}_{\check{\alpha},r^h}(\check{I}), \text{ and } \quad q_2(1) = v(1) - q(1). \tag{2.80}$$

By the trace theorem (recall that $v, q_1 \in H^1(\check{I})$), the inverse inequality Lemma 2.5, and (2.79), we have

$$|q_2(1)| \lesssim |v(1)| + |q_1(1)| \lesssim \|v\|_{1,\check{I}} + \|q_1\|_{1,\check{I}} \underset{m,c}{\lesssim} \|v\|_{1,\check{I}}. \tag{2.81}$$

Next, to obtain a similar inequality for $|q_2(0)|$, we recall that

$$(q_2, q)_{\check{I}} = 0, \qquad \forall \mathcal{V}^{m-1}_{\check{\alpha},\tau(r^h)}(\check{I}).$$

In particular, for $q = q_2'$, we have

$$0 = (q_2, q')_{\check{I}} = \frac{1}{2}(q_2(1)^2 - q_2(0)^2).$$

Hence, $|q_2(0)| = |q_2(1)| \lesssim_{m,c} \|v\|_{1,\check{I}}$. Now, we can use Theorem 2.2 to conclude that

$$\|q_2\|_{0,\check{I}} \underset{m,c}{\lesssim} |q_2(0)| + |q_2(1)| \underset{m,c}{\lesssim} \|v\|_{1,\check{I}}. \tag{2.82}$$

Finally, the desired result $\|v_h\|_{0,\check{I}} \lesssim_{m,c} \|v\|_{0,\check{I}}$ follows immediately from (2.79) and (2.82) since $v_h = q_1 + q_2$. □

By definition, it follows from Lemma 2.20 that $\{P_\alpha^{m,\texttt{Rad}}\}_{\alpha\in I_{k_0}}$ is a uniformly bounded family of LIFE projections, which when combined with the error estimates for the classical Radau projection [107], yields the following estimate for the global immersed Radau projection

$$\left\|v - P^{m,\texttt{Rad}}v\right\|_{0,I} \underset{m,c}{\lesssim} h^{m+1}|v|_{m+1,I}, \qquad v \in H^{m+1}_{\alpha,r^h}(\check{I}). \tag{2.83}$$

Now, we are ready to state the main theorem of this subsection.

Theorem 2.7. *Let $u \in H^1([0,T], \mathcal{H}^{m+2}_{\alpha,r^h}(I))$ be the exact solution to (2.66) with $u_0 \in \mathcal{H}^{m+1}_{\alpha,r^h}(I)$, and let u_h be the solution to the semi-discrete problem (2.68), then*

$$\|u(\cdot,T) - u_h(\cdot,T)\|_{0,I} \underset{m,c}{\lesssim} h^{m+1}\left(|u_0|_{m+1,I} + |u(\cdot,T)|_{m+1,I} + T\max_{0\le t\le T}|u(\cdot,t)|_{m+2,I}\right).$$

Proof. Our proof here follows the standard techniques for non-interface problems [40]. Let

$$e = u_h - u, \quad z = u - P^{m,\mathtt{Rad}}u, \quad g = u_h - P^{m,\mathtt{Rad}}u.$$

Then by construction of $P^{m,\mathtt{Rad}}$, we have $B(z,g) = 0$. Hence,

$$B(g,g) = B(g-z,g) = B(e,g). \tag{2.84}$$

Next, by (2.68) and (2.84), we have

$$\begin{aligned} M(z_t(\cdot,t),g(\cdot,t)) &= M(g_t(\cdot,t),g(\cdot,t)) - M(e_t(\cdot,t),g(\cdot,t)) \\ &= \frac{1}{2}\frac{d}{dt}\left\|c^{-1/2}g(\cdot,t)\right\|_I^2 - B(e(\cdot,t),g(\cdot,t)) \\ &= \frac{1}{2}\frac{d}{dt}\left\|c^{-1/2}g(\cdot,t)\right\|_I^2 - B(g(\cdot,t),g(\cdot,t)) \\ &= \frac{1}{2}\frac{d}{dt}\left\|c^{-1/2}g(\cdot,t)\right\|_I^2 + \sigma(t), \end{aligned} \tag{2.85}$$

where $\sigma(t) \geq 0$ by (2.71). Let $\kappa(t) = \left\|c^{-1/2}g(\cdot,t)\right\|_I$, then by the Cauchy-Schwarz inequality, we have

$$|M\left(z_t(\cdot,t),g(\cdot,t)\right)| = \left|\left(z_t(\cdot,t),c^{-1}g(\cdot,t)\right)_I\right| \underset{c}{\lesssim} \|z_t(\cdot,t)\|_{0,I}\,\kappa(t). \tag{2.86}$$

Following the ideas in the proof of Lemma 2.19, we can prove easily that $u_t = -cu_x \in \mathcal{H}^{m+1}_{\alpha,r^h}(I)$ since $u_x \in \mathcal{H}^{m+1}_{\alpha,\tau(r^h)}(I)$. Therefore, by (2.83), we have

$$\|z_t(\cdot,t)\|_{0,I} \underset{m,c}{\lesssim} h^{m+1}|u(\cdot,t)|_{m+1,I}. \tag{2.87}$$

Now, we integrate (2.85) on $[0,T]$, and use the inequalities (2.86) and (2.87) to obtain

$$\frac{1}{2}\kappa(T)^2 - \frac{1}{2}\kappa(0)^2 \underset{m,c}{\lesssim} h^{m+1}\int_0^T \kappa(s)|u(\cdot,s)|_{m+2,I}\,ds. \tag{2.88}$$

Using a generalized version of Gronwall's inequality (see [22, p. 24]), we get the following bound on $\kappa(T)$

$$\begin{aligned}\kappa(T) &\underset{m,c}{\lesssim} \kappa(0) + h^{m+1}\int_0^T |u(\cdot,s)|_{m+2,I}\, ds,\\ &\underset{m,c}{\lesssim} \kappa(0) + h^{m+1} T \max_{0\le t\le T} |u(\cdot,t)|_{m+2,I}. \end{aligned} \tag{2.89}$$

From (2.83), we have

$$\kappa(0) \underset{c}{\lesssim} \left\| u_0 - P^{m,\mathtt{Rad}} u_0 \right\| \underset{m,c}{\lesssim} h^{m+1}|u_0|_{0,I}. \tag{2.90}$$

Now, the inequality (2.89) combined with (2.90) yields

$$\|\mathbf{g}(\cdot,T)\|_{0,I} \underset{c}{\lesssim} \kappa(T) \underset{m,c}{\lesssim} h^{m+1}\left(|u_0|_{0,I} + T\max_{0\le t\le T} |u(\cdot,t)|_{m+2,I}\right). \tag{2.91}$$

On the other hand, the error estimate (2.83) tells us that

$$\|z(\cdot,T)\|_{0,I} \underset{m,c}{\lesssim} h^{m+1}|u(\cdot,T)|_{m+1,I}. \tag{2.92}$$

Finally, we combine (2.91) and (2.92) to obtain

$$\|e(\cdot,T)\|_{0,I} \le \|z(\cdot,T)\|_{0,I} + \|g(\cdot,T)\|_{0,I} \underset{m,c}{\lesssim} h^{m+1}\left(|u_0|_{m+1,I} + |u(\cdot,T)|_{m+1,I} + T\max_{0\le t\le T} |u(\cdot,t)|_{m+2,I}\right),$$

which is the desired result. □

Since this particular immersed dG method has not appeared in the literature, we will finish this subsection by including two numerical examples to illustrate multiple features of this immersed dG method. Namely,

- The numerical solution converges to the true solution at a rate of h^{m+1} as shown in

Theorem 2.7.

- By writing the discrete form (2.68) as a system of ordinary equations $\mathbf{c}'(t) = K\mathbf{c}(t)$. We observe numerically that the spectral radius of K (i.e. the largest magnitude of eigenvalues) grows at a rate of h^{-1} regardless of the degree m, which is comparable to the standard dG method for non-interface problems [65]. This means that an explicit time integrator will be stable if the time step $\Delta t \leq Ch$ for some fixed constant $C > 0$ independent of h.
- The immersed dG (IDG) scheme is robust with respect to the relative position of α in the interface element, that is, if we fix the mesh and vary $\alpha \in I_{k_0}$, we do not observe a noticeable difference in the error, nor in the spectral radius of the global matrix K.
- The IDG scheme can be applied to problems with multiple interfaces and different boundary conditions, such as periodic boundary conditions.
- Our proposed scheme preserves the energy of the system remarkably well, especially for degree $m \geq 2$. This is observed when simulating a traveling wave through two interfaces, subject to periodic boundary conditions for an extended period of time.

Example 1: Let us consider the interface problem (2.66) with $I = (0, 4)$ and $u_a = 0$.

For our first experiment, we choose $\alpha = \frac{\pi}{3}$, $(c_-, c_+) = (1, 2)$ and $u_0(x) = f(3x - \frac{1}{2})$, where $f(x) = x(1 - x^2)^5$ if $|x| \leq 1$, zero otherwise. The exact solution to this problem is:

$$u(x,t) = \begin{cases} u_0(x - c_- t), & x \leq \alpha, \\ u_0\left(\dfrac{c_-}{c_+}(x - c_+ t) + \alpha\left(1 - \dfrac{c_-}{c_+}\right)\right), & x > \alpha. \end{cases}$$

For an illustration of the solution at $t = 0$ and $t = 1$, see Figure 2.5. We use our proposed IDG method for space discretization with degree $m = 1, 2, 3$ and adaptive RK45 for time integration on the time interval $[0, 1]$. In Figure 2.6, we see that the L^2 error decays at an

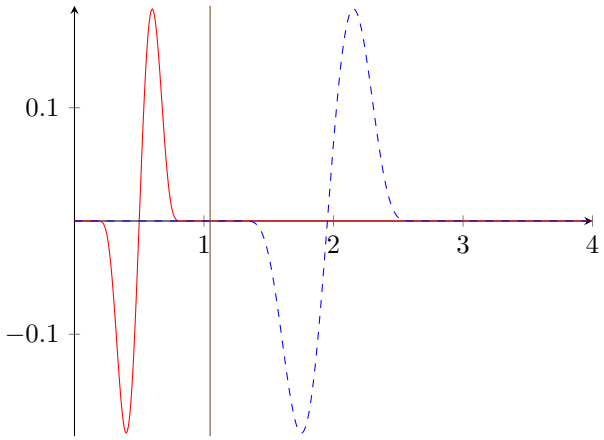

Figure 2.5: A plot of $u(x,0)$ (solid, red) and $u(x,1)$ (dashed, blue).

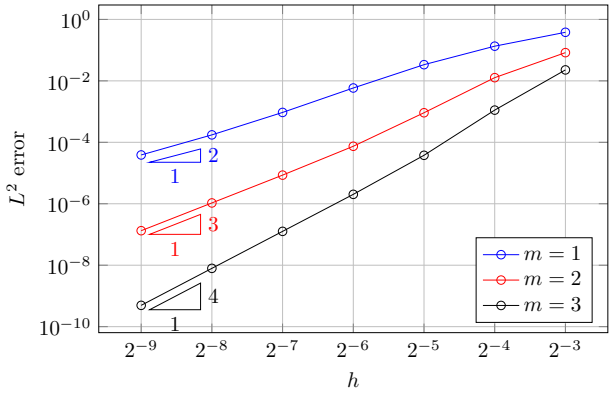

Figure 2.6: A plot of the L^2 error $\|u - u_h\|_{0,[0,4]}$ at $t = 1$ for $m = 1, 2, 3$ under mesh refinement.

optimal rate of $O(h^{m+1})$. We also observe in Figure 2.7 that the spectral radius of the global matrix K grows at a rate of $O(h^{-1})$ regardless of the degree m.

We note that throughout this experiment, the relative position of α within the interface element denoted $\check{\alpha} \in (0,1)$ changes with h, but it did not affect the convergence rate. In the previous example, we have $0.02 \leq \check{\alpha} \leq .75$ for $h = 2^{-i}, i = 3, \ldots, 9$. To show this more clearly, we fix $h = 2^{-6}$, then the previously mentioned value of $\alpha = \frac{\pi}{3}$ is in $I_{68} = [\frac{68}{2^6}, \frac{69}{2^6}]$. Instead of keeping α fixed, we vary $\alpha \in I_{68}$ (Hence, we vary $\check{\alpha}$ in $[0,1]$), then we compute the L^2 error at $t = 1$ and the spectral radius of the global matrix K. In Figure 2.8, we can

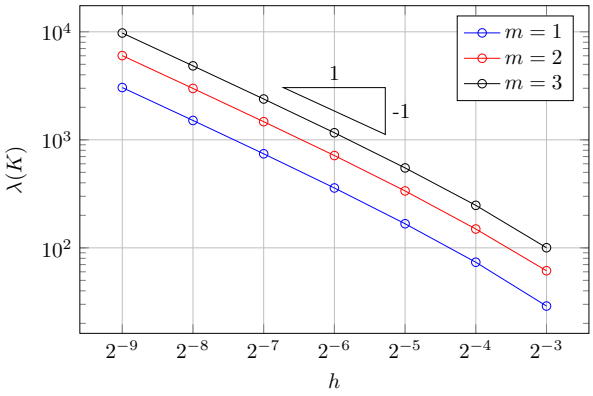

Figure 2.7: The spectral radius of the global matrix K for $m = 1, 2, 3$ under mesh refinement.

observe that the relative position of the interface does not affect the L^2 error nor the spectral radius of K.

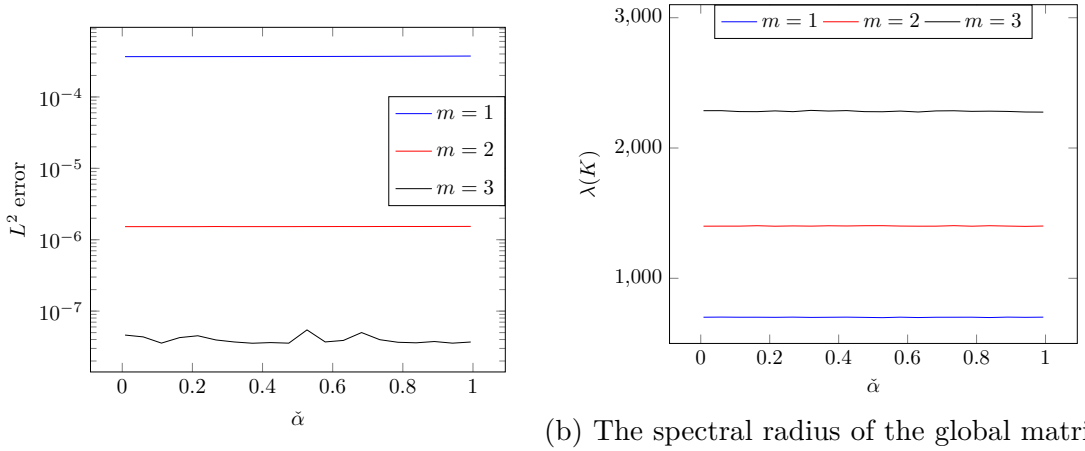

(a) $\|u - u_h\|_{0,[0,4]}$ at $t = 1$.

(b) The spectral radius of the global matrix K.

Figure 2.8: The L^2 error (left) and the spectral radius of K (right) versus the relative position of the interface $\check{\alpha}$.

Example 2: Consider the following transport equation with two interfaces $\alpha_1 < \alpha_2$ and

periodic boundary conditions

$$\begin{cases} u_t(x,t) + c(x)u_x(x,t) = 0, & t > 0,\ x \in (0,4)\backslash\{\alpha_1,\alpha_2\}, \\ u(0,t) = u(4,t), & t \geq 0, \\ u(x,0) = u_0(x), & x \in [0,4], \end{cases} \qquad c(x) = \begin{cases} 1, & x \leq \alpha_1, \\ 4, & \alpha_1 < x \leq \alpha_2, \\ 1, & x > \alpha_2, \end{cases}$$

where $(\alpha_1, \alpha_2) = \left(\frac{\pi}{3}, \frac{2\pi}{3}\right)$. Since $u(4,t) = u(0,t)$, the energy of the exact solution $\mathtt{E}(t) = \left\|c^{-1/2}\mathbf{u}(\cdot,t)\right\|_{0,[0,4]}$ is constant and u is periodic in time with period $\gamma = 4 - \frac{\pi}{6} \approx 3.48$. To analyze the dissipation of our numerical scheme, we fix $h = 2^{-6}$ and plot the relative energy $\tilde{\mathtt{E}}_h(t) = \frac{\mathtt{E}_h(t)}{\mathtt{E}_h(0)}$ for $0 \leq t \leq 10\gamma$, where $\mathtt{E}_h(t) = \left\|c^{-1/2}\mathbf{u}_h(\cdot,t)\right\|_{0,[0,4]}$ in Figure 2.9. We observe that our IDG method is dissipative when piecewise linear polynomials are used and highly conservative when higher order polynomials are used. For instance, for $m = 2$, we have $1 - \tilde{\mathtt{E}}_h(10\gamma) \leq 2 \cdot 10^{-4}$, and for $m = 3$, we have $1 - \tilde{\mathtt{E}}_h(10\gamma) \leq 10^{-8}$.

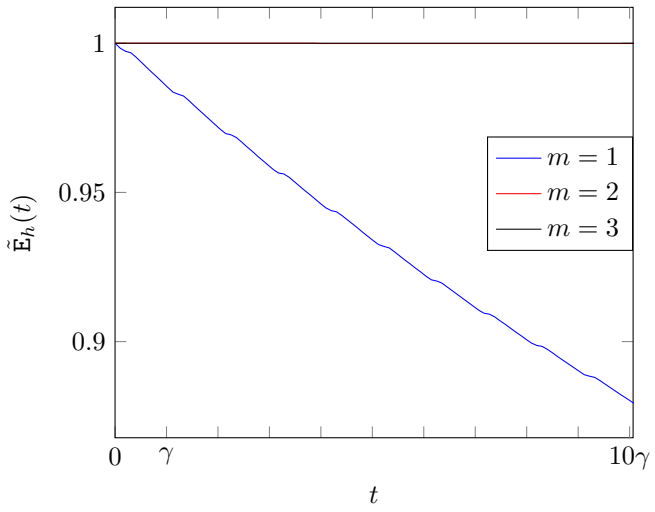

Figure 2.9: The relative dissipation $\tilde{\mathtt{E}}_h(t)$ for $0 \leq t \leq 10\gamma$ and $m = 1, 2, 3$.

2.4.5 The Acoustic Interface Problem

Consider the following acoustic interface problem

$$\begin{cases} p_t(x,t) = \rho(x)c(x)^2 u_x(x,t), \\ \rho(x)u_t(x,t) = p_x(x,t), \\ u(x,0) = u_0(x), \\ p(x,0) = p_0(x), \end{cases} \qquad x \in I^- \cup I^+, \qquad 0 < t < T, \tag{2.93a}$$

where $\rho|_{I^\pm} = \rho_\pm > 0$ and $c|_{I^\pm} = c_\pm > 0$ are piecewise constant functions representing the density and sound speed in a heterogeneous medium, respectively, and u, p represent the velocity and the pressure. We consider the case where the velocity and the pressure are continuous at the interface α, that is

$$[\![u]\!]_\alpha = [\![p]\!]_\alpha = 0. \tag{2.93b}$$

Multiple immersed dG methods were designed for the interface problem (2.93) in [8, 88], and the numerical experiments suggested that all of those immersed dG methods converge optimally to the solution. In this subsection, we will provide a rigorous analysis of the L^2 error of the immersed dG formulation using the immersed-Bramble Hilbert lemma.

First, we write the system (2.93a) in vector form by introducing $\mathbf{u} = (p, u)^T$ and the matrix

$$A(x) = \begin{pmatrix} 0 & \rho(x)c(x)^2 \\ \frac{1}{\rho(x)} & 0 \end{pmatrix}.$$

Then,

$$\begin{cases} \mathbf{u}_t(x,t) + A(x)\mathbf{u}_x(x,t) = 0, & x \in I^- \cup I^+, \quad 0 < t < T, \\ \mathbf{u}(x,0) = \mathbf{u}_0(x), \end{cases} \tag{2.94a}$$

where $\mathbf{u}_0 = (p_0, u_0)$. Additionally, the interface conditions (2.93b) can be written more compactly as

$$[\![\mathbf{u}]\!]_\alpha = 0. \tag{2.94b}$$

Now, to derive the extended interface conditions, we recall that (2.94b) holds for all $t \in (0,T)$, therefore by differentiating with respect to t and using (2.94a), we obtain

$$\left[\!\!\left[A^k \frac{\partial^k}{\partial x^k}\mathbf{u} \right]\!\!\right]_\alpha = 0, \qquad k = 0, 1, \ldots. \tag{2.94c}$$

Finally, to describe the boundary conditions, we use $A_\pm = A|_{I^\pm}$ to denote the restrictions of A to $I^\pm$. We recall that A_- and A_+ are constant matrices, more precisely:

$$A_- = \begin{pmatrix} 0 & \rho_- c_-^2 \\ \rho_-^{-1} & 0 \end{pmatrix}, \qquad A_+ = \begin{pmatrix} 0 & \rho_+ c_+^2 \\ \rho_+^{-1} & 0 \end{pmatrix}. \tag{2.94d}$$

The matrices $A_\pm$ can be decomposed as $A_\pm = P_\pm \Lambda_\pm P_\pm^{-1}$, where $\Lambda_\pm = \operatorname{diag}(-c_\pm, c_\pm)$. Using this eigendecomposition, we define $A_\pm^+ = P_\pm \operatorname{diag}(0, c_\pm) P_\pm^{-1}$, $A_\pm^- = P_\pm \operatorname{diag}(-c_\pm, 0) P_\pm^{-1}$, and $|A_\pm| = P_\pm \operatorname{diag}(c_\pm, c_\pm) P_\pm^{-1}$ to be the positive part, the negative part, and the absolute value of $A_\pm$, respectively. The acoustic interface problem that we are considering here is subject to the following homogeneous inflow boundary conditions

$$A_-^+ \mathbf{u}(a,t) = A_+^- \mathbf{u}(b,t) = 0, \qquad t \geq 0. \tag{2.94e}$$

In [88, 90], it was shown that the interface conditions (2.94c) can be decoupled into interface

jump conditions on p and u separately

$$\frac{\partial^k}{\partial x^k}p(\alpha^+,t)=r_k^p\frac{\partial^k}{\partial x^k}p(\alpha^-,t),\qquad \frac{\partial^k}{\partial x^k}u(\alpha^+,t)=r_k^u\frac{\partial^k}{\partial x^k}u(\alpha^-,t), \tag{2.95}$$

where the sequences (r_k^p) and (r_k^u) are given by the following formulas

$$r_{2k}^p=r_{2k}^v=\left(\frac{c_-}{c_+}\right)^{2k},\quad r_{2k+1}^p=\frac{\rho_+}{\rho_-}\left(\frac{c_-}{c_+}\right)^{2k},\quad r_{2k+1}^v=\frac{\rho_-}{\rho_+}\left(\frac{c_-}{c_+}\right)^{2k+2}. \tag{2.96}$$

For $k=0,1,\ldots,$ then it is suitable to consider solutions $\mathbf{u}$ in the immersed vector Sobolev space $H^1([0,T],\mathbb{H}^{m+1}_{\alpha,\mathbf{r}}(I))$, where $\mathbf{r}=(r^p,r^u)$ and

$$\mathbb{H}^{m+1}_{\alpha,\mathbf{r}}(I)=\mathcal{H}^{m+1}_{\alpha,r^p}(I)\times\mathcal{H}^{m+1}_{\alpha,r^u}(I). \tag{2.97}$$

Consequently, we define the local global IFE space as a product

$$\mathbb{V}^m_{\alpha,\mathbf{r}}(I_{k_0})=\mathcal{V}^m_{\alpha,r^p}(I_{k_0})\times\mathcal{V}^m_{\alpha,r^u}(I_{k_0}),\qquad \mathbb{V}^m_{\alpha,\mathbf{r}}(\mathcal{T}_h)=\mathcal{V}^m_{\alpha,r^p}(\mathcal{T}_h)\times\mathcal{V}^m_{\alpha,r^u}(\mathcal{T}_h). \tag{2.98}$$

Next, We use S to denote piecewise constant matrix function

$$S|_{I^\pm}=S_\pm,\qquad S_\pm=\begin{pmatrix}\rho_\pm^{-1}c_\pm^{-2} & 0\\ 0 & \rho_\pm\end{pmatrix}, \tag{2.99}$$

and we use $\tilde{A}$ to denote SA. Hence, we can rewrite $\mathbf{u}_t+A\mathbf{u}_x=0$ as

$$S(x)\mathbf{u}_t(x,t)+\tilde{A}\mathbf{u}_x(x,t)=0,\qquad x\in I^-\cup I^+,\qquad 0<t<T.$$

Here the matrix $\tilde{A}$ is independent of x, and is given by

$$\tilde{A} = \begin{pmatrix} 0 & 1 \\ 1 & 0 \end{pmatrix}.$$

We define the following bilinear forms

$$M(\mathbf{w}, \mathbf{v}) = \sum_{k=1}^{N} (S\mathbf{v}, \mathbf{w})_{I_k}, \tag{2.100a}$$

$$B(\mathbf{w}, \mathbf{v}) = \sum_{k=1}^{N} \left(\mathbf{v}', \tilde{A}\mathbf{w}\right)_{I_k} + \sum_{k=0}^{N} [\![\mathbf{v}]\!]_{x_k}^T S(x_k)\hat{\mathbf{w}}(x_k), \tag{2.100b}$$

where the numerical flux $\hat{\mathbf{w}}(x_k) = A(x_k)^+\mathbf{w}(x_k^-) + A(x_k)^-\mathbf{w}(x_k^+)$ at the interior nodes, and the jump at the interior nodes $[\![\mathbf{v}]\!]_{x_k} = \mathbf{w}(x_k^+) - \mathbf{w}(x_k^-)$. At the boundary, we have $\hat{\mathbf{w}}(x_N) = A(x_N)^+\mathbf{w}(x_N^-)$, $\hat{\mathbf{w}}(x_0) = A(x_0)^-\mathbf{w}(x_0^+)$, $[\![\mathbf{w}]\!]_{x_N} = -\mathbf{w}(x_N^-)$ and $[\![\mathbf{w}]\!]_{x_0} = \mathbf{w}(x_0^+)$.

Now we are ready to state the semi-discrete immersed DG formulation as: Find $\mathbf{u}_h \in H^1\left([0,T], \mathbb{V}_{\alpha,\mathbf{r}}^m(\mathcal{T}_h)\right)$ such that

$$M(\mathbf{u}_{h,t}(\cdot,t), \mathbf{v}_h) = B(\mathbf{u}_h(\cdot,t), \mathbf{v}_h), \qquad \forall \mathbf{v}_h \in \mathbb{V}_{\alpha,\mathbf{r}}^m(\mathcal{T}_h), \quad 0 < t < T, \tag{2.101a}$$

and

$$(\mathbf{u}_h(\cdot,0), \mathbf{v}_h)_I = (\mathbf{u}_0, \mathbf{v}_h)_I, \qquad \forall \mathbf{v}_h \in \mathbb{V}_{\alpha,\mathbf{r}}^m(\mathcal{T}_h), \tag{2.101b}$$

that is $\mathbf{u}_h(\cdot,0)$ is the L^2 projection of $\mathbf{u}_0$ onto the global IFE space $\mathbf{v}_h \in \mathbb{V}_{\alpha,\mathbf{r}}^m(\mathcal{T}_h)$. Therefore, it follows from Corollary 2.2 that

$$\|\mathbf{u}_h(\cdot,0) - \mathbf{u}_0\|_{0,I} \underset{m,c,\rho}{\lesssim} h^{m+1}|\mathbf{u}_0|_{m+1,I}. \tag{2.102}$$

Additionally, it follows from the traditional dG techniques and our choice of the flux that $\mathbf{u}_h$ is stable in the energy norm. In other words

$$M(\mathbf{u}_h(\cdot,t),\mathbf{u}_h(\cdot,t)) = \left\|\sqrt{S}\mathbf{u}_h(\cdot,t)\right\|_{0,I}^2 \leq \left\|\sqrt{S}\mathbf{u}_h(\cdot,0)\right\|_{0,I}^2. \tag{2.103}$$

Remark 2.9. The discrete weak formulation (2.101) is equivalent to the IDPGFE scheme described in [88], where the proof of (2.103) is discussed in detail.

The interface conditions (2.96) are quite complicated to work with directly as shown in the calculations done in [88]. In fact, the nature of these coefficients is what drove us to study the general form of the IFE space (2.5). Hence, we will avoid referring to them directly as much as possible in the remainder of this subsection. Instead, we derive some interesting facts about the matrices $A_\pm$ and $S_\pm$ from our paper [18] that we will use later. These facts allow us to study the vector Radau projection, without the need for the explicit formula (2.96). For the sake of completeness, we included the proof from [18].

Lemma 2.21. *Let $A_\pm$ be the matrices defined in (2.94d) and let $S_\pm = \operatorname{diag}(\rho_\pm^{-1}c_\pm^{-1}, \rho_\pm)$, then*

(a) For any integer $k \geq 0$, the matrix $A_+^{-k}A_-^k$ is diagonal with positive entries.

(b) Let $s \in \{+,-\}$, then there is an invertible matrix P_s such that $A_s = P_s \operatorname{diag}(-c_s, c_s)P_s^{-1}$ and $S_s = P_s^{-T}P_s^{-1}$.

(c) Let $s \in \{+,-\}$, then the matrices $S_sA_s^+$, $S_sA_s^-$ and $S_s|A_s|$ are symmetric. Furthermore, $S_sA_s^+$ is positive semi-definite, $S_sA_s^-$ is negative semi-definite and $S_s|A_s|$ is positive definite.

(d) Let $s, \tilde{s} \in \{+,-\}$, and let $\mathbf{w} \in \mathbb{R}^2$, then

$$\left(\left\|A_s^{\tilde{s}}\mathbf{w}\right\|^2 + \left|\mathbf{w}^T S_s A_s^{\tilde{s}'}\mathbf{w}\right| = 0\right) \Longrightarrow \mathbf{w} = 0. \tag{2.104}$$

where $\|\cdot\|$ *is Euclidean norm.*

(e) Let $s \in \{+,-\}$*. Then, there is a constant* $C(\rho_s, c_s) > 0$ *such that*

$$\mathbf{w}^T S_s A_s^+ \mathbf{w} - \mathbf{w}^T S_s A_s^- \mathbf{w} \underset{\rho,c}{\gtrsim} \|\mathbf{w}\|^2, \qquad \forall \mathbf{w} \in \mathbb{R}^2. \tag{2.105}$$

Proof. (a) We have $A_\pm^2 = c_\pm^2 \mathrm{Id}_2$, where Id_2 is the 2×2 identity matrix. Therefore,

$$A_\pm^{2k} = c_\pm^{2k}\mathrm{Id}_2, \qquad A_\pm^{2k+1} = c_\pm^{2k} A_\pm, \qquad k = 0, 1, \ldots. \tag{2.106}$$

Using (2.106), we immediately obtain $A_+^{-2k}A_-^{2k} = \left(\frac{c_-}{c_+}\right)^{2k}\mathrm{Id}_2$ and $A_+^{-2k-1}A_-^{2k+1} = \left(\frac{c_-}{c_+}\right)^{2k} A_+^{-1}A_-$. Finally, by direct computation, we have $A_+^{-1}A_- = \mathrm{diag}\left(\frac{\rho_+}{\rho_-}, \frac{\rho_- c_-^2}{\rho_+ c_+^2}\right)$. Hence, $A_+^{-k}A_-^k = \mathrm{diag}(r_k^p, r_k^u)$, where r_k^p and $r_k^u$are defined in (2.96).

(b) Let

$$P_s = \frac{1}{\sqrt{2\rho_s}}\begin{pmatrix} -c_s\rho_s & c_s\rho_s \\ 1 & 1 \end{pmatrix}, \tag{2.107}$$

then, by a simple computation, we can show that $S_s = P_s^{-T}P_s^{-1}$ and $A_s = P_s\,\mathrm{diag}(-c_s, c_s)P_s^{-1}$.

(c) We have $S_sA_s^+ = P_s^{-T}\,\mathrm{diag}(0, c_s)P_s^{-1}$, where P_s is defined in (2.107). Therefore, $S_sA_s^+$ is a symmetric semi-positive definite matrix. The other two claims can be proven similarly.

(d) We will only consider the case $\tilde{s} = +$ here, the other case can be proven similarly. Consider a vector $\mathbf{w} \in \mathbb{R}^2$ that satisfies

$$\left\|A_s^+\mathbf{w}\right\|^2 + \left|\mathbf{w}^T S_s A_s^-\mathbf{w}\right| = 0. \tag{2.108}$$

Now, let $\tilde{\mathbf{w}} = P_s\mathbf{w}$ where P_s is defined in (2.107), then (2.108) can be written as

$$\|P_s \operatorname{diag}(0, c_s)\tilde{\mathbf{w}}\|^2 + \|\operatorname{diag}(-c_s, 0)\tilde{\mathbf{w}}\|^2 = 0,$$

Since both norms are non-negative, we have $\operatorname{diag}(-c_s, 0)\tilde{\mathbf{w}} = 0$ and $P_s \operatorname{diag}(0, c_s)\tilde{\mathbf{w}} = 0$. P_s being invertible, we get $\tilde{\mathbf{w}} = 0$. Consequently, $\mathbf{w} = P_s^{-1}\tilde{\mathbf{w}} = 0$.

(e) We have by direct computation

$$\mathbf{w}^T S_s(A_s^+ - A_s^-)\mathbf{w} = \mathbf{w}^T \begin{pmatrix} \rho_s^{-1}c_s^{-1} & 0 \\ 0 & \rho_s c_s \end{pmatrix} \mathbf{w} \underset{\rho,c}{\gtrsim} \|\mathbf{w}\|. \qquad \square$$

Now, it is time to introduce the global immersed vector Radau projection $P^{m,\mathsf{vec}} : \mathbb{H}^{m+1}_{\alpha,\mathbf{r}}(I) \to \mathbb{V}^m_{\alpha,\mathbf{r}}(\mathcal{T}_h)$. Following the lines of Definition 2.9 and the definition of B in (2.100b), we use $P^{m,\mathsf{vec}}\mathbf{v}$ to denote the solution $\mathbf{v}_h$ to

$$\begin{cases} (\mathbf{v}_h, \tilde{A}\mathbf{q}')_{I_k} = (\mathbf{v}, \tilde{A}\mathbf{q}')_{I_k}, & \forall \mathbf{q} \in \mathbb{V}^m_{\alpha,\mathbf{r}}(\mathcal{T}_h), \\ A(x_{k-1})^- \mathbf{v}_h(x_{k-1}^+) = A(x_{k-1})^- \mathbf{v}(x_{k-1}^+) & \forall k \in \{1, 2, \ldots, N\}. \\ A(x_k)^+ \mathbf{v}_h(x_k^-) = A(x_k)^+ \mathbf{v}(x_k^-), \end{cases}$$

Again, $\mathbf{v}_h$ is chosen such that $B(\mathbf{v} - \mathbf{v}_h, \mathbf{q}) = 0$ for all $\mathbf{q} \in \mathbb{V}^m_{\alpha,\mathbf{r}}(\mathcal{T}_h)$, and it can be constructed locally on each element. On non-interface elements, it reduces to two Radau projections, which are well known. Therefore, we will focus on the construction of the reference immersed Radau projection on $\check{I}$ denoted $\check{P}^{m,\mathsf{vec}}_{\check{\alpha}} : \mathbf{v} \mapsto \mathbf{v}_h$, where $\mathbf{v}_h$ is the solution $\mathbf{v}_h \in \mathbb{V}^m_{\check{\alpha},\mathbf{r}}(\check{I})$ to

the system

$$\begin{cases} (\mathbf{v}_h, \tilde{A}\mathbf{q}')_{\check{I}} = (\mathbf{v}, \tilde{A}\mathbf{q}')_{\check{I}}, & \forall \mathbf{q} \in \mathbb{V}^m_{\check{\alpha},\mathbf{r}}(\check{I}), \\ A^-_- \mathbf{v}_h(0) = A^-_- \mathbf{v}(0), \\ A^+_+ \mathbf{v}_h(1) = A^+_+ \mathbf{v}(1). \end{cases} \tag{2.109}$$

Lemma 2.22. *The immersed vector Radau projection* $\check{P}^{m,\mathtt{vec}}_{\check{\alpha}} : \mathbb{H}^{m+1}_{\check{\alpha},\mathbf{r}}(\check{I}) \to \mathbb{V}^m_{\check{\alpha},\mathbf{r}}(\check{I})$ *is well-defined.*

Proof. First, note that the system (2.109) is a square linear system since the first condition is equivalent to

$$(\mathbf{v}_h, \tilde{A}\mathbf{q})_{\check{I}} = (\mathbf{v}, \tilde{A}\mathbf{q})_{\check{I}}, \qquad \forall \mathbf{q} \in \mathbb{V}^{m-1}_{\check{\alpha},\tau(\mathbf{r})}(\check{I}),$$

where $\tau(\mathbf{r}) = (\tau(r^p), \tau(r^u))$. Hence, it is enough to show that if $\mathbf{v} = 0$, then $\mathbf{v}_h = 0$. If $\mathbf{v} = 0$, then

$$(\mathbf{v}_h, \tilde{A}\mathbf{v}_h')_{\check{I}} = 0 \Longrightarrow \mathbf{v}_h(1)^T \tilde{A} \mathbf{v}_h(1) - \mathbf{v}_h(0)^T \tilde{A} \mathbf{v}_h(0) = 0, \tag{2.110}$$

Now, we recall that $\tilde{A} = S_\pm A_\pm$ and use

$$A^-_- \mathbf{v}_h(0) = A^+_+ \mathbf{v}_h(1) = 0, \tag{2.111}$$

to obtain

$$\begin{aligned} 0 &= \mathbf{v}_h(1)^T \tilde{A} \mathbf{v}_h(1) - \mathbf{v}_h(0)^T \tilde{A} \mathbf{v}_h(0) && (2.112) \\ &= \mathbf{v}_h(1)^T S_+ A_+ \mathbf{v}_h(1) - \mathbf{v}_h(0)^T S_- A_- \mathbf{v}_h(0) && (2.113) \\ &= \mathbf{v}_h(1)^T S_+ A^-_+ \mathbf{v}_h(1) - \mathbf{v}_h(0)^T S_- A^+_- \mathbf{v}_h(0). && (2.114) \end{aligned}$$

But $S_+A_+^-$ and $-S_-A_-^+$ are both negative semi-definite by Lemma 2.21 (part c), then

$$0 = \mathbf{v}_h(1)^T S_+ A_+^- \mathbf{v}_h(1) = \mathbf{v}_h(0)^T S_- A_-^+ \mathbf{v}_h(0), \tag{2.115}$$

which when combined with (2.111) and Lemma 2.21 (part d), yields

$$\mathbf{v}_h(0) = \mathbf{v}_h(1) = 0. \tag{2.116}$$

Now, Let us recall that

$$(\mathbf{v}_h, SA\mathbf{q}')_{\check{I}} = 0, \qquad \forall \mathbf{q} \in \mathbb{V}_{\check{\alpha},\mathbf{r}}^m(\check{I}),$$

which is, by (2.94c), equivalent to

$$(\mathbf{v}_h, S\mathbf{q})_{\check{I}} = 0, \qquad \forall \mathbf{q} \in \mathbb{V}_{\check{\alpha},\mathbf{r}}^{m-1}(\check{I}). \tag{2.117}$$

Since S is a diagonal matrix, the equation above is equivalent to $\mathbf{v}_h \in \mathcal{V}_{\check{\alpha},r^p}^{\check{w}^p,m}(\check{I}) \times \mathcal{V}_{\check{\alpha},r^u}^{\check{w}^u,m}(\check{I})$, where

$$\check{w}^p = \frac{1}{\rho c^2}, \qquad \check{w}^u = \rho.$$

Hence, each component of $\mathbf{v}_h$ has m interior roots (by Lemma 2.7), but $\mathbf{v}_h(1) = \mathbf{v}_h(0) = 0$. Therefore, $\mathbf{v}_h = 0$ by Lemma 2.6, which finishes the proof. □

Lemma 2.23. *The immersed vector Radau projection* $\left\{\check{P}_{\check{\alpha}}^{m,\mathtt{vec}}\right\}_{\check{\alpha}\in\check{I}}$ *is a uniformly bounded family of RIFE projections.*

Proof. Let $\mathbf{v} \in \mathbb{H}_{\check{\alpha},\mathbf{r}}^{m+1}(\check{I})$ and let $\mathbf{v}_h = \check{P}_{\check{\alpha}}^{m,\mathtt{vec}}\mathbf{v}$. Recall from the previous proof, that we have

$$(\mathbf{v}_h, S\mathbf{q})_{\check{I}} = (\mathbf{v}, S\mathbf{q}), \qquad \forall \mathbf{q} \in \mathbb{V}_{\check{\alpha},\mathbf{r}}^{m-1}(\check{I}).$$

Now, let $\mathbf{q}_1 \in \mathbb{V}_{\check{\alpha},\mathbf{r}}^{m-1}(\check{I})$ such that

$$(\mathbf{q}_1, S\mathbf{q})_{\check{I}} = (\mathbf{v}, S\mathbf{q}), \qquad \forall \mathbf{q} \in \mathbb{V}_{\check{\alpha},\mathbf{r}}^{m-1}(\check{I}).$$

Then, by choosing $\mathbf{q} = \mathbf{q}_1$ and Cauchy-Schwarz inequality. We obtain

$$\|\mathbf{q}_1\|_{0,\check{I}} \underset{\rho,c}{\lesssim} \|\mathbf{v}\|_{0,\check{I}}\,. \tag{2.118}$$

Now, let $\mathbf{q}_2 = \mathbf{v}_h - \mathbf{q}_1$, then

$$(\mathbf{q}_2, S\mathbf{q})_{\check{I}} = 0, \qquad \forall \mathbf{q} \in \mathbb{V}_{\check{\alpha},\mathbf{r}}^{m-1}(\check{I}) \tag{2.119}$$

$$A_+^+\mathbf{q}_2(1) = A_+^+(\mathbf{v}(1) - \mathbf{q}_1(1)), \tag{2.120}$$

$$A_-^-\mathbf{q}_2(0) = A_-^-(\mathbf{v}(0) - \mathbf{q}_1(0)), \tag{2.121}$$

Therefore, by Theorem 2.2, we have

$$\|\mathbf{q}_2\|_{0,\check{I}} \le |\mathbf{q}_2(0)| + |\mathbf{q}_2(1)|. \tag{2.122}$$

On the other hand, from (2.121), we have

$$\left|\mathbf{q}_2(0)^T A_-^-\mathbf{q}_2(0)\right| \le \|\mathbf{q}_2(0)\| \left(\|\mathbf{q}_1\|_{1,\check{I}} + \|\mathbf{v}\|_{1,\check{I}}\right) \underset{\rho,c}{\lesssim} \|\mathbf{q}_2(0)\|\,\|\mathbf{v}\|_{1,\check{I}}\,. \tag{2.123}$$

Similarly, (2.120) leads to

$$\left|\mathbf{q}_2(1)^T A_+^+\mathbf{q}_2(1)\right| \underset{\rho,c}{\lesssim} \|\mathbf{q}_2(1)\|\,\|\mathbf{v}\|_{1,\check{I}}\,. \tag{2.124}$$

Now, by choosing $\mathbf{q} = A\mathbf{q}_2'$ in (2.119) and integrating, we obtain

$$\mathbf{q}_2(1)S_+A_+\mathbf{q}_2(1) - \mathbf{q}_2(0)S_-A_-\mathbf{q}_2(0) = 0,$$

which can be rearranged as

$$\mathbf{q}_2(1)S_+A_+^+\mathbf{q}_2(1) - \mathbf{q}_2(0)S_-A_-^-\mathbf{q}_2(0) = \mathbf{q}_2(0)S_-A_-^+\mathbf{q}_2(0) - \mathbf{q}_2(1)S_+A_+^-\mathbf{q}_2(1).$$

$$\mathbf{q}_2(1)^TS_+A_+^+\mathbf{q}_2(1)+\mathbf{q}_2(1)^TS_+A_+^-\mathbf{q}_2(1)-\mathbf{q}_2(0)^TS_-A_-^+\mathbf{q}_2(0)-\mathbf{q}_2(0)^TS_-A_-^-\mathbf{q}_2(0) = 0. \quad (2.125)$$

Now, from (2.105), we have

$$\mathbf{q}_2(0)^TS_-A_-^+\mathbf{q}_2(0) - \mathbf{q}_2(0)^TS_-A_-^-\mathbf{q}_2(0) \underset{\rho,c}{\gtrsim} \|\mathbf{q}_2(0)\|^2, \quad (2.126a)$$

$$\mathbf{q}_2(1)^TS_+A_+^+\mathbf{q}_2(1) - \mathbf{q}_2(1)^TS_+A_+^-\mathbf{q}_2(1) \underset{\rho,c}{\gtrsim} \|\mathbf{q}_2(1)\|^2. \quad (2.126b)$$

Next, we sum (2.125), (2.126a) and (2.126b) to obtain

$$\mathbf{q}_2(1)S_+A_+^+\mathbf{q}_2(1) - \mathbf{q}_2(0)S_-A_-^-\mathbf{q}_2(0) \underset{\rho,c}{\gtrsim} \left(\|\mathbf{q}_2(0)\|^2 + \|\mathbf{q}_2(1)\|^2\right). \quad (2.127)$$

The left-hand side is bounded by (2.123) and (2.124)

$$\|v\|_{1,\check{I}} \left(\|\mathbf{q}_2(0)\| + \|\mathbf{q}_2(1)\|\right) \underset{\rho,c}{\gtrsim} \|\mathbf{q}_2(0)\|^2 + \|\mathbf{q}_2(1)\|^2. \quad (2.128)$$

So, by Theorem 2.2, we have

$$\|\mathbf{q}_2\|_{0,\check{I}} \underset{m,\rho,c}{\lesssim} \|\mathbf{q}_2(0)\| + \|\mathbf{q}_2(1)\| \underset{\rho,c}{\lesssim} \|\mathbf{v}\|_{1,\check{I}}.$$

Finally, we recall that $\mathbf{v}_h = \mathbf{q}_1 + \mathbf{q}_2$, then

$$\|\mathbf{v}_h\|_{0,\check{I}} \leq \|\mathbf{q}_1\|_{0,\check{I}} + \|\mathbf{q}_2\|_{0,\check{I}} \underset{m,\rho,c}{\lesssim} \|\mathbf{v}\|_{1,\check{I}}.$$

Which proves the lemma. □

It follows then, from Theorem 2.4 that

$$\|\mathbf{u} - P^{m,\mathsf{vec}}\mathbf{u}\|_{0,\check{I}} \underset{m,\rho,c}{\lesssim} h^{m+1}|\mathbf{u}|_{m+1,I}, \tag{2.129}$$

for all $\mathbf{u} \in \mathbb{H}^{m+1}_{\alpha,\mathbf{r}}(I)$. Here we note that the immersed Poincaré projection defined in Definition 2.4 and the immersed Bramble-Hilbert lemma extend naturally to the product space $\mathcal{V}^m_{\alpha,r^p}(\mathcal{T}_h) \times \mathcal{V}^m_{\alpha,r^u}(\mathcal{T}_h)$ to give (2.129).

Finally, the global error estimate for the immersed DG solution for this problem follows from the standard dG techniques used in Theorem 2.7.

Theorem 2.8. *Let* $\mathbf{u}$ *be the solution of problem* (2.94) *and let* $\mathbf{u}_h \in H^1([0,T], \mathbb{V}^m_{\alpha,\mathbf{r}}(\mathcal{T}_h))$ *be the solution of* (2.101). *If* $\mathbf{u} \in H^1([0,T]; \mathbb{H}^{m+2}_{\alpha,\mathbf{r}}(I))$ *and* $\mathbf{u}_0 \in \mathbb{H}^{m+1}_{\alpha,\mathbf{r}}(I)$, *then*

$$\|\mathbf{u}(\cdot,T) - \mathbf{u}_h(\cdot,T)\|_{0,I} \underset{m,\rho,c}{\lesssim} h^{m+1}\left(|\mathbf{u}_0|_{m+1,I} + |\mathbf{u}(\cdot,T)|_{m+1,I} + T\max_{0\leq t\leq T}|\mathbf{u}(\cdot,t)|_{m+2,I}\right).$$

This theorem validates the results of the numerical experiments in [88].

2.5 Conclusion

In this chapter, we have developed a unified framework for studying immersed finite element and immersed discontinuous Galerkin methods for a group of one dimensional problems.

This framework is based on an immersed Bramble-Hilbert lemma, which allowed us to use the traditional scaling argument to analyze IFE methods for scalar and for vector interface problems.

Chapter 3

The Frenet Immersed Finite Element Space

In this chapter, we introduce a new approach for constructing high-order, locally conforming IFE functions for two-dimensional interface problems. In this approach, the interface is mapped via a nonlinear coordinate transformation into a straight line, then the IFE functions are constructed in this new coordinate system, called the Frenet coordinates, then the IFE functions are mapped back to the interface element. At the end, we provide a discussion of the implementation of the Frenet transformation, as well as the construction of the Frenet IFE basis.

The results in this chapter are partially reported in [19].

3.1 Introduction and Motivation

Let $\Omega \subset \mathbb{R}^2$ be a domain split by an interface Γ into $\Omega^+ \cup \Omega^- \cup \Gamma$, we consider the following elliptic interface problem

$$\begin{cases} -\nabla \cdot (\beta \nabla u) = f, \quad \text{on } \Omega^+ \cup \Omega^-, \\ u|_{\partial\Omega} = g, \end{cases} \tag{3.1a}$$

where β is a positive piecewise constant function

$$\beta(\mathbf{x}) = \begin{cases} \beta^+, & \mathbf{x} \in \Omega^+ \\ \beta^-, & \mathbf{x} \in \Omega^-. \end{cases} \tag{3.1b}$$

Additionally, we assume that u satisfies the following interface conditions on Γ

$$[\![u]\!]_\Gamma = [\![\beta \nabla u \cdot \mathbf{n}]\!]_\Gamma = 0, \tag{3.1c}$$

where $[\![\cdot]\!]_\Gamma$ denotes the jump across the interface Γ, that is, if $v^\pm = v|_{\Omega^\pm}$ for some function v, then

$$[\![v]\!]_\Gamma = v^+|_\Gamma - v^-|_\Gamma,$$

and $\mathbf{n}$ is a normal vector on Γ. Furthermore, we assume that f is smooth around the interface, which allows us to restrict our work to the case where u satisfies the following extended interface conditions [12, 13, 51]

$$\left[\!\!\left[\beta \frac{\partial^k}{\partial \mathbf{n}^k} \Delta u \right]\!\!\right]_\Gamma = 0, \qquad k = 0, 1, \ldots, m-2, \tag{3.1d}$$

for some integer m.

The interface problem (3.1) can be considered as the two-dimensional analogue to the one-dimensional interface problem (2.39). However, unlike the one-dimensional case, where the interface is a single point, the space of possible interfaces Γ is extremely rich in two dimensions, which introduces multiple challenges for unfitted methods. Having said that, unfitted methods are extremely attractive since they tend to be computationally efficient, while maintaining an optimal convergence rate. For instance, one can use a simple Cartesian mesh, where the elements are merely a translation of each other. Thus, reducing the cost of

meshing and assembly greatly. For a comparison between an interface-fitted mesh and an unfitted mesh, see Figure 3.1.

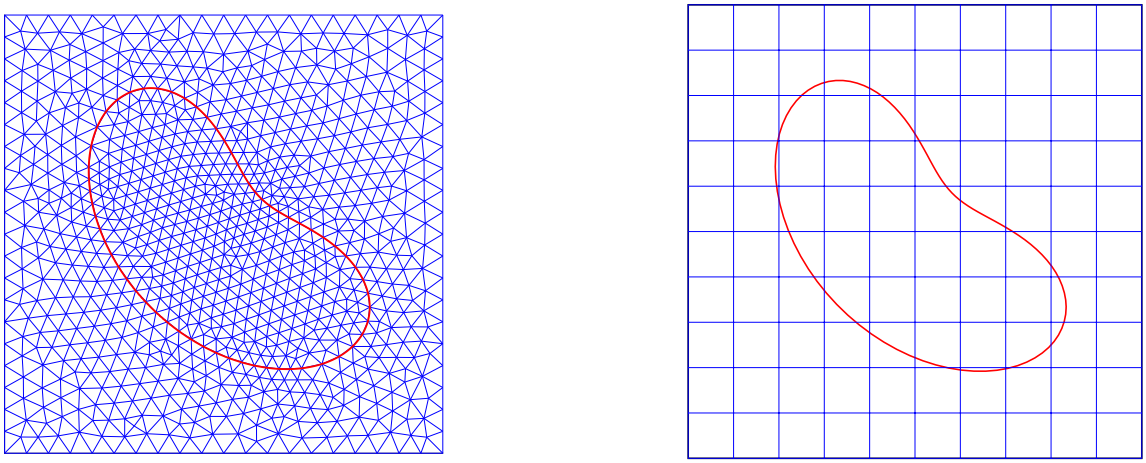

(a) An example of an interface-fitted mesh (b) An example of an unfitted mesh

Figure 3.1: An illustration of an interface-fitted mesh (left), and an unfitted Cartesian mesh (right). The interface Γ is shown in red.

Because of the previously mentioned advantages, numerous unfitted methods were developed for this problem in the last thirty years. Unfitted finite difference methods, were developed and analyzed in [45, 75, 104] amongst other papers. On the other hand, in the finite element community, there are a few approaches to implementing an unfitted method. We mention here the CutFEM method [30, 74], the extended finite element method (XFEM) [103], and the immersed finite element method [13, 16, 51, 62, 76, 77, 84].

In the immersed finite element method, we consider an unfitted mesh, such as the one shown in Figure 3.1b, and we distinguish two types of elements:

- Elements that are not cut by the interface, called non-interface elements.
- Elements that are cut by the interface, called interface elements.

On non-interface elements, polynomials are used to approximate the solution. Whereas, on interface elements, a finite dimensional space called the local IFE space is constructed.

Typically, the local IFE space consists of piecewise polynomials that satisfy the interface conditions (3.1c) and (3.1d) in a certain weak sense.

Consider, for example, an interface element K, such as the ones shown in Figure 3.2 split by the interface Γ into K^- and K^+, where $\partial K^- \cap \partial K^+ \subset \Gamma$.

(a) Example I (b) Example II

Figure 3.2: Two examples of interface elements K.

In general, it is impossible to find two polynomials $p^{\pm}$ such that $p^+ = p^-$ and $\beta^+ \nabla p^+ \cdot \mathbf{n} = \beta^- \nabla p^- \cdot \mathbf{n}$ on the interface Γ, unless the curve Γ is an algebraic curve (e.g. a line, a conic, ...). For this reason, the immersed finite element spaces in the literature focused on creating spaces of piecewise polynomials

$$\varphi(\mathbf{x}) = \begin{cases} p^-(\mathbf{x}), & \mathbf{x} \in K^-, \\ p^+(\mathbf{x}), & \mathbf{x} \in K^+, \end{cases}$$

where φ satisfies a weaker version of (3.1c). For illustration, we mention a few approaches

- In [77], the authors proposed a space of functions of piecewise linear functions φ, such that

$$p^+(D) = p^-(D), \qquad p^+(E) = p^-(E), \qquad \beta^+ \nabla p^+(M) \cdot \overline{\mathbf{n}} = \beta^- \nabla p^-(M) \cdot \overline{\mathbf{n}},$$

  where D and E are the intersections of Γ with ∂K, M is the midpoint of D and E, and $\overline{\mathbf{n}}$ is a normal vector to the line $\overline{DE}$. This construction was later extended to

bilinear IFE functions [61, 62]. This idea of enforcing the interface conditions at a finite number of points was later extended to higher degree IFE methods in [5] by considering points $D_0, D_1, \ldots, D_m$ on $\Gamma \cap K$.

- In [13], the authors explored a weak formulation of the IFE conditions. That is, p^+ and p^- are chosen such that

$$\int_{\Gamma\cap K} p^+ q = \int_{\Gamma\cap K} p^- q, \quad \text{and} \quad \int_{\Gamma\cap K} (\beta^+ \nabla p^+ \cdot \mathbf{n}) q = \int_{\Gamma\cap K} (\beta^- \nabla p^- \cdot \mathbf{n}) q, , \quad \forall q \in \mathcal{P}^m(\Gamma \cap K).$$

  Similarly, the extended interface conditions (3.1d) are enforced weakly. This approach is interesting since it considers the jump of φ on the entirety of $\Gamma \cap K$, and it generalizes naturally to all polynomial degrees. However, it was observed that this approach leads to an ill conditioned system when $\Gamma \cap K$ is very small.

- In [12], the authors proposed to state the interface conditions (3.1c) and (3.1d) as minimization problem, that is, given a polynomial p^- on K^-, a polynomial p^+ is constructed such that it minimizes a positive definite quadratic form. One of the major benefit of this approach is that the resulting local system is guaranteed to be consistent. However, it was observed that this system suffers from a similar ill conditioning issue to the one described in the previous approach. This issue was circumvented later by enforcing the interface conditions on a larger element, called the fictitious element [55, 114].

In each of the methods described above, and other methods in the literature, the immersed finite element functions do not satisfy the interface conditions exactly, even the condition $[\![u]\!]_\Gamma = 0$, which may necessitate the use of extra penalties on the interface [51] or on the edges cut by the interface [84] in the discrete weak formulation, unless the interface is a line, where the methods above produce IFE functions that satisfy $[\![u]\!]_\Gamma = 0$ exactly.

Here, we make two observations regarding the IFE methods described above

- The IFE methods in the literature do not use all the properties of the curve, such as the curvature, tangent vector and normal vector. These quantities are trivial in the case of a linear interface, which explains why constructing higher order IFE functions on linear interfaces is much easier than for general curved interfaces [25].
- To construct a finite dimensional space of functions that satisfy the interface conditions (3.1c) exactly, one needs to consider non-polynomial functions.

With these two observations, we are motivated to introduce a coordinate transformation that maps the interface locally onto a line segment, which will simplify the geometry greatly and allow us to construct a locally conforming space of piecewise polynomials in these new coordinates, then finally we map the newly constructed space back to the interface element. Since this transformation is not necessarily affine, the resulting local IFE space is no longer a space of piecewise polynomial functions as our second observation suggested.

To illustrate this idea, consider a curve Γ parametrized by a function $\mathbf{g} : I \subset \mathbb{R} \to \Gamma$, and let $\mathbf{n}(\xi)$ be the unit normal vector at $\mathbf{g}(\xi)$ for $\xi \in I$. Then, notice that a point $\mathbf{x}$ on the interface can be associated with $\xi \in I$, such as $\mathbf{g}(\xi) = \mathbf{x}$. On the other hand, if $\mathbf{x} \notin \Gamma$, one can consider finding a representation of $\mathbf{x}$ of the form $\mathbf{g}(\xi) + \eta\mathbf{n}(\xi)$, that is, (η, ξ) are the coordinates of $\mathbf{x}$ in a curvilinear coordinate system. For instance, consider the unit circle parametrized by $\mathbf{g}(\xi) = (\cos(\xi), \sin(\xi))$, and consider $\mathbf{x} = (1, 1)$ which is not on the circle, then $\mathbf{x} = \mathbf{g}(\xi)+\eta\mathbf{n}(\xi)$ for $\xi = \frac{\pi}{4}$ and $\eta = \sqrt{2}-1$, as Figure 3.3 shows. Notice here that there is another solution to $\mathbf{g}(\xi)+\eta\mathbf{n}(\xi) = (1, 1)$, namely $\xi = \frac{5\pi}{4}$ and $\eta = -\sqrt{2}-1$. Therefore, we need to be careful when discussing the invertibility of the map $(\eta, \xi) \mapsto \mathbf{g}(\xi) + \eta\mathbf{n}(\xi)$. Generally speaking, this map will be invertible in a tubular neighborhood around the interface, which we will discuss later. For now, we can think of the map $\mathbf{x} = (x, y) \mapsto (\eta, \xi)$ as a local change of variables, where points on the interface are mapped into points on the vertical axis $\eta = 0$.

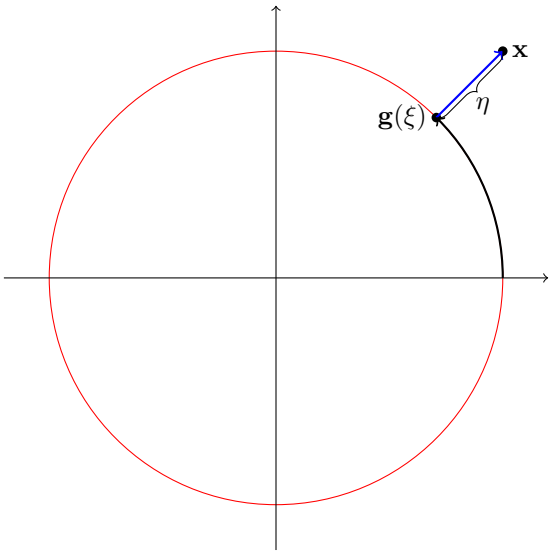

Figure 3.3: The point $\mathbf{x}$ is represented as $\mathbf{g}(\xi) + \eta\mathbf{n}(\xi)$. Here, $\eta\mathbf{n}(\xi)$ is shown in blue.

The last point is crucial in our construction since it transforms (3.1c) and (3.1d) into interface conditions on a vertical line segment instead of a curve. To describe this construction in detail, we first introduce the notation used in this chapter in Section 3.2, then we define and analyze the Frenet transformation in Section 3.3. After that, we define the Frenet IFE space in Section 3.4. Finally, we provide an overview of the computational aspects associated with creating a basis for the Frenet IFE space in Section 3.5.

3.2 Notation and Assumptions

Without loss of generality, we assume that $\Omega \subset \mathbb{R}^2$ is a rectangular domain, split by the interface Γ into Ω^- and Ω^+. Given a subset $B \subset \Omega$, we define $B^\pm = \Omega^\pm \cap B$. Additionally, we use $H^s(B)$ to denote the classical Sobolev space $W^{s,2}(B)$ equipped with the norm $\|\cdot\|_{m,B}$, the semi-norm $|\cdot|_{m,B}$ and the L^2 inner product $(\cdot,\cdot)_B$, and we use $PH^s(B)$ to denote the broken Sobolev space consisting of functions u such that $u|_{B^\pm} \in H^s(B^\pm)$. The broken Sobolev space

is then equipped with the broken Sobolev norm and the broken Sobolev semi-norm

$$\|\cdot\|_{s,B}^2 = \|\cdot\|_{s,B^+}^2 + \|\cdot\|_{s,B^-}^2 , \qquad |\cdot|_{s,B}^2 = |\cdot|_{s,B^+}^2 + \|\cdot\|_{s,B^-}^2 .$$

Additionally, we use $\langle\cdot,\cdot\rangle_{\partial B}$ to denote the L^2 inner product on ∂B.

Given two vectors $\mathbf{u} = (u_1, u_2)$ and $\mathbf{v} = (v_1, v_2)$ in $\mathbb{R}^2$, we use $\|\mathbf{u}\|$ and $\mathbf{u}\cdot\mathbf{v}$ to denote the Euclidean norm of $\mathbf{u}$ and the Euclidean dot product, respectively. In addition, we use $\mathbf{u}\wedge\mathbf{v}$ to denote the wedge product $\mathbf{u}\wedge\mathbf{v} = u_1v_2 - u_2v_1$.

We partition the domain Ω into a uniform Cartesian mesh $\mathcal{T}_h$ independent of the interface Γ, where h is the diameter of each element. Given an element $K \in \mathcal{T}_h$, we say that K is a non-interface element if $\mathring{K}\cap\Gamma = \varnothing$, where $\mathring{K} = K\backslash\partial K$ is the interior of K. Else, we call K an interface element. We use $\mathcal{T}_h^i$ to denote the set of all interface elements and $\mathcal{T}_h^n$ to denote the set of all non-interface elements. Additionally, we use $\mathcal{E}_h, \mathcal{E}_h^\circ$ and $\mathcal{E}_h^b$ to denote the set of edges, the set of interior edges and the set of boundary edges, respectively.

We assume that the interface Γ is parametrized by $\mathbf{g} : [\xi_s, \xi_e] \to \mathbb{R}^2$, where $\mathbf{g} = (g_1, g_2)$ and $g_1, g_2 \in C^3([\xi_s, \xi_e])$. Furthermore, we restrict our work to the case where Γ is a simple Jordan curve [1, 41, 98], that is

$$\mathbf{g}(\xi_s) = \mathbf{g}(\xi_e), \text{ and} \qquad \mathbf{g}|_{[\xi_s,\xi_e)} \text{ is injective.} \tag{3.2}$$

However, as we will show later in the numerical examples, our methods applies to non Jordan curves as well. In addition, we assume that the parametrization $\mathbf{g}$ is regular, meaning $\mathbf{g}'(\xi) \neq \mathbf{0}$ for any $\xi \in [\xi_s, \xi_e]$, which allows us to define the unit tangent vector and the unit

normal vectors at each point $\mathbf{g}(\xi) \in \Gamma$

$$\boldsymbol{\tau}(\xi) = \frac{1}{\|\mathbf{g}'(\xi)\|}\mathbf{g}'(\xi), \quad \mathbf{n}(\xi) = \mathcal{Q}\boldsymbol{\tau}(\xi), \quad \xi \in [\xi_s, \xi_e], \quad \text{where } \mathcal{Q} = \begin{bmatrix} 0 & 1 \\ -1 & 0 \end{bmatrix}. \tag{3.3}$$

We use κ to denote the curvature at the point $\mathbf{g}(\xi) \in \Gamma$

$$\kappa(\xi) = \frac{\mathbf{g}'(\xi) \wedge \mathbf{g}''(\xi)}{\|\mathbf{g}'(\xi)\|^3} = \frac{g_1'(\xi)g_2''(\xi) - g_2'(\xi)g_1''(\xi)}{(g_1'(\xi)^2 + g_2'(\xi)^2)^{\frac{3}{2}}}, \qquad \xi \in [\xi_s, \xi_e]. \tag{3.4}$$

3.3 The Frenet Transform

Let $P : [\xi_s, \xi_e] \times \mathbb{R} \to \mathbb{R}^2$ be the transformation given by

$$P(\eta, \xi) = \mathbf{g}(\xi) + \eta\mathbf{n}(\xi), \qquad (\eta, \xi) \in \mathbb{R} \times [\xi_s, \xi_e], \tag{3.5}$$

which we will refer to as the Frenet transformation. Then, P maps the vertical segment $\{0\} \times [\xi_s, \xi_e]$ onto the interface Γ. Furthermore, for a fixed η_0, $\{P(\eta_0, \xi)\}_{\xi \in [\xi_s, \xi_e]}$ is a parallel curve to Γ in the sense that $\|P(\eta_0, \xi) - \mathbf{g}(\xi)\|$ remains constant. On the other hand, for a fixed ξ_0, $\{P(\eta, \xi_0)\}_{\eta \in \mathbb{R}}$ is a line orthogonal to $\mathbf{g}'(\xi_0)$. Hence, one can view P, at least locally, as a change of coordinates. However, one needs to be careful about the invertibility of P since, as we have observed in the previous section, it may not be injective.

The transformation P appeared in differential geometry in the context of parallel curves [98] and in the context of tubular neighborhoods [1, 66]. Also, a simplified version of P was considered in [25] and in [67] for constructing IFE functions. Additionally, a different version of this transformation, based on the Cartesian equation of the interface was discussed recently for high-order CutFEM methods [74].

First, we recall the following theorem about the invertibility of P, also known as the tubular neighborhood theorem for Jordan curves.

Theorem 3.1. *Let P be the Frenet transformation defined in (3.5). Then, there is $\epsilon > 0$ such that*

$$P|_{(-\epsilon,\epsilon)\times[\xi_s,\xi_e)}$$

is invertible.

Proof. See [1, p. 77] for a detailed proof. □

In the theorem above, we note that we excluded ξ_e from the domain since we assumed that Γ is Jordan curve (3.2). Hence, $\mathbf{g}(\xi_e) = \mathbf{g}(\xi_s)$.

Remark 3.1. The theorem above is a special case of the tubular neighborhood theorem for smooth manifolds [66].

Geometrically, Theorem 3.1 states that if the distance between a point $\mathbf{x}$ and the curve Γ is less than ϵ, then $\mathbf{x}$ can be represented uniquely as $P(\eta, \xi)$. Now, if you consider all points $\mathbf{x}$ whose distance from Γ is at most ϵ, you obtain a *tube* containing Γ. Hence, the name of the theorem. For a visual illustration, see Figure 3.4 and observe that the normal vectors do not intersect each other within the tube, as expected from the tubular neighborhood theorem.

In the remainder of this chapter, we will use $N(\delta)$ to denote $P((-\delta, \delta) \times [\xi_s, \xi_e))$ for all $\delta > 0$, and use ϵ to denote the constant described in Theorem 3.1, which we will call the radius of the tubular neighborhood. Thus, there is a mapping $R : N(\epsilon) \to (-\epsilon, \epsilon) \times [\xi_s, \xi_e)$ such that

$$P(R(\mathbf{x})) = \mathbf{x}, \qquad \forall \mathbf{x} \in N(\epsilon). \tag{3.6}$$

Next, we derive some useful calculus formulas for the derivatives of $\boldsymbol{\tau}$ and $\mathbf{n}$, also known

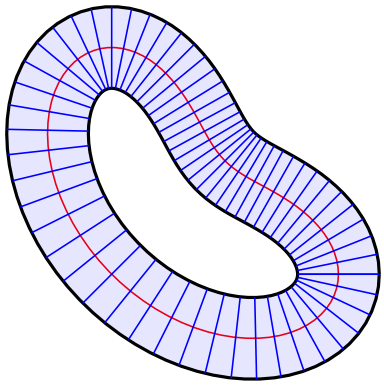

Figure 3.4: An illustration of a Jordan curve Γ (red), its tubular neighborhood (light blue), and normal vectors on Γ (blue).

as the Frenet-Serret formulas (in two dimensions). Even though the proof of these formulas can be found in many differential geometry textbooks, we will include a proof here for the sake of completion.

Lemma 3.1. *Let $\boldsymbol{\tau}$ and $\mathbf{n}$ be the unit tangent vector and unit normal vector defined in (3.3), respectively, then*

$$\boldsymbol{\tau}'(\xi) = -\kappa(\xi)\,\|\mathbf{g}'(\xi)\|\,\mathbf{n}(\xi), \qquad \mathbf{n}'(\xi) = \kappa(\xi)\,\|\mathbf{g}'(\xi)\|\,\boldsymbol{\tau}(\xi). \tag{3.7}$$

Proof. By definition of $\boldsymbol{\tau}$, we have

$$\begin{aligned}\boldsymbol{\tau}'(\xi) &= \frac{d}{d\xi}\left(\frac{1}{\sqrt{\mathbf{g}'(\xi)\cdot\mathbf{g}'(\xi)}}\mathbf{g}'(\xi)\right)\\ &= \frac{\mathbf{g}'(\xi)\cdot\mathbf{g}''(\xi)}{\|\mathbf{g}'(\xi)\|^3}\mathbf{g}'(\xi) - \frac{1}{\|\mathbf{g}'(\xi)\|}\mathbf{g}''(\xi),\end{aligned} \tag{3.8}$$

On the other hand, $\boldsymbol{\tau}(\xi)$ and $\mathbf{n}(\xi)$ form an orthonormal basis of $\mathbb{R}^2$, so

$$\begin{aligned}\mathbf{g}''(\xi) &= (\boldsymbol{\tau}(\xi)\cdot\mathbf{g}''(\xi))\boldsymbol{\tau}(\xi) + (\mathbf{n}(\xi)\cdot\mathbf{g}''(\xi))\mathbf{n}\\ &= \|\mathbf{g}'(\xi)\|^{-2}\left((\mathbf{g}'(\xi)\cdot\mathbf{g}''(\xi))\mathbf{g}' - (\mathbf{g}'(\xi)\wedge\mathbf{g}''(\xi))\mathcal{Q}\mathbf{g}'(\xi)\right)\\ &= \|\mathbf{g}'(\xi)\|^{-2}\left((\mathbf{g}'(\xi)\cdot\mathbf{g}''(\xi))\mathbf{g}'(\xi) - \kappa\|\mathbf{g}'(\xi)\|^3\mathcal{Q}\mathbf{g}'(\xi)\right).\end{aligned} \tag{3.9}$$

Hence, by substituting (3.9) back into (3.8), we obtain

$$\boldsymbol{\tau}'(\xi) = -\kappa(\xi)\mathcal{Q}\mathbf{g}'(\xi) = -\kappa(\xi)\|\mathbf{g}'(\xi)\|\,\mathbf{n}(\xi),$$

which proves the first formula of (3.7). To prove the second formula, we recall that $\mathbf{n}(\xi) = \mathcal{Q}\boldsymbol{\tau}(\xi)$, and use $\mathcal{Q}^2 = -I_2$ to conclude that

$$\mathbf{n}'(\xi) = \mathcal{Q}\boldsymbol{\tau}'(\xi) = -\kappa(\xi)\|\mathbf{g}'(\xi)\|\,\mathcal{Q}^2\boldsymbol{\tau}(\xi) = \kappa(\xi)\|\mathbf{g}'(\xi)\|\,\boldsymbol{\tau}(\xi).$$

□

Before deriving some other important calculus formulas, we note that we will be considering derivatives with respect to x, y, as well as derivatives with respect to η and ξ. Therefore, it is important for us to use different notations for the differential operators. As usual, we will use $\nabla, \nabla\cdot, J$ and Δ to denote the gradient, divergence, Jacobian matrix and Laplacian, respectively, with respect to the variables x, y. On the other hand, we use $\widehat{\nabla}, \widehat{\nabla}\cdot, \hat{J}$ and $\hat{\Delta}$ to denote their counterparts with respect to η, ξ.

Lemma 3.2. *Let P be the Frenet transformation defined in (3.5), then*

$$\hat{J}_P(\eta,\xi) = \left[\mathbf{n}(\xi) \mid \mathbf{g}'(\xi) + \eta\mathbf{n}'(\xi)\right], \tag{3.10a}$$

and

$$\det\left(\hat{J}_P(\eta,\xi)\right) = \|\mathbf{g}'(\xi)\|\,(1+\eta\kappa(\xi))\,. \tag{3.10b}$$

Proof. The formula for $\hat{J}_P(\eta,\xi)$ follows by a direct computation. Hence, we will focus on the second formula

$$\begin{aligned}
\det\left(\hat{J}_P(\eta,\xi)\right) &= \det[\mathbf{n}(\xi) \mid \mathbf{g}'(\xi) + \eta\mathbf{n}'(\xi)] \\
&= \mathbf{n}(\xi) \wedge \mathbf{g}'(\xi) + \eta\mathbf{n}(\xi) \wedge \mathbf{n}'(\xi) && \text{(By the definition of } \wedge) \\
&= \|\mathbf{g}'(\xi)\| + \eta\mathbf{n}(\xi) \wedge \mathbf{n}'(\xi) && \text{(Using } \mathbf{n} = \|\mathbf{g}'(\xi)\|^{-1}\,\mathcal{Q}\mathbf{g}'(\xi)) \\
&= \|\mathbf{g}'(\xi)\| + \eta\mathbf{n}(\xi) \wedge (\kappa(\xi)\,\|\mathbf{g}'(\xi)\|\,\boldsymbol{\tau}(\xi)) && \text{(Using (3.7))} \\
&= \|\mathbf{g}'(\xi)\|\,(1+\eta\kappa(\xi)\mathbf{n}(\xi) \wedge \boldsymbol{\tau}(\xi)) \\
&= \|\mathbf{g}'(\xi)\|\,(1+\eta\kappa(\xi))\,.
\end{aligned}$$

The last equality follows from $\mathbf{n}(\xi) \wedge \boldsymbol{\tau}(\xi) = (\mathcal{Q}\boldsymbol{\tau}(\xi))^T\mathcal{Q}\boldsymbol{\tau}(\xi) = 1$. □

Next, we will derive a formula for the Jacobian of R. For the sake of conciseness, we will treat η and ξ as functions of $\mathbf{x}$, that is, $R(\mathbf{x}) = (\eta(\mathbf{x}), \xi(\mathbf{x}))$ or simply $R = (\eta, \xi)$, which will allows us to describe R in terms of its components η and ξ.

Lemma 3.3. *Let $R = (\eta, \xi)$ be the inverse Frenet transformation (3.6), then*

$$J_R = \begin{bmatrix} \mathbf{n}(\xi)^T \\ \|\mathbf{g}'(\xi)\|^{-1}\,(1+\eta\kappa(\xi))^{-1}\,\boldsymbol{\tau}(\xi)^T \end{bmatrix}, \tag{3.11}$$

and

$$\det(J_R) = \|\mathbf{g}'(\xi)\|^{-1}\,(1+\eta\kappa(\xi))^{-1}\,. \tag{3.12}$$

Proof. The formula for the determinant (3.12) follows immediately from Lemma 3.2. To

prove (3.12), we only need to show that $J_R \hat{J}_P = I_2$. Since $\boldsymbol{\tau} \cdot \mathbf{n} = 0 = \mathbf{n} \cdot \mathbf{n}' = 0$, then

$$\begin{bmatrix} \mathbf{n}(\xi)^T \\ \boldsymbol{\tau}(\xi)^T \end{bmatrix} \begin{bmatrix} \mathbf{n}(\xi) \mid \mathbf{g}'(\xi) + \eta \mathbf{n}'(\xi) \end{bmatrix} = \begin{bmatrix} 1 & 0 \\ 0 & \|\mathbf{g}'(\xi)\| + \eta \boldsymbol{\tau}(\xi) \cdot \mathbf{n}'(\xi) \end{bmatrix}.$$

Next, we use the Frenet-Serret formulas Lemma 3.1 to obtain

$$\|\mathbf{g}'(\xi)\| + \eta \boldsymbol{\tau}(\xi) \cdot \mathbf{n}'(\xi) = \|\mathbf{g}'(\xi)\| \, (1 + \eta \kappa(\xi)).$$

Hence, the formula (3.11) holds. □

The quantity $(1 + \eta\kappa(\xi))^{-1}$ is of great importance to us since it will appear repeatedly in the formulas to follow. For conciseness, we will use $\psi(\eta, \xi)$ to denote it. Hence, the Jacobian of R can be written compactly as

$$\det(J_R) = \|\mathbf{g}'(\xi)\|^{-1} \psi(\eta, \xi). \tag{3.13}$$

In order to guarantee that $\psi(\eta, \xi)$ is bounded, we will assume that $1 + \eta\kappa(\xi) \geq \frac{1}{2}$ for all $\xi \in [\xi_s, \xi_e]$, or simply,

$$|\eta| \leq \frac{1}{2\kappa_0}, \qquad \kappa_0 = \max_{\xi_s \leq \xi \leq \xi_e} |\kappa(\xi)|. \tag{3.14}$$

The condition (3.14) is a purely geometric condition, meaning that it is independent of the choice of parametrization $\mathbf{g}$ since the maximum curvature κ_0 is a property of the curve Γ, and it is independent of $\mathbf{g}$ [1].

At this point, we recall that the inverse Frenet map is defined on the tubular neighborhood $N(\epsilon)$. However, the condition (3.14) suggests considering a potentially smaller tubular

neighborhood N_0 where

$$N_0 = N(\epsilon_0), \qquad \epsilon_0 = \min\left(\epsilon, \frac{1}{2\kappa_0}\right). \tag{3.15}$$

Thus, $R|_{N_0}$ is well-defined and $|\det(J_R(\mathbf{x}))| \geq \frac{1}{2}\|\mathbf{g}'(\xi(\mathbf{x}))\|$ for all $\mathbf{x} \in N_0$.

Remark 3.2. The choice of $\frac{1}{2}$ in (3.14) can be replaced by any other $c \in (0, 1)$.

Example 3.1. Consider the circle $\Gamma = \{(x, y) \in \mathbb{R}^2 \mid x^2 + y^2 = r\}$ for some $r > 0$, then $\mathbf{g}(\xi) = (r\cos(\xi), r\sin(\xi))$ for $\xi \in [0, 2\pi]$ is a regular parametrization of Γ. Then, by direct computation, we have $\kappa(\xi) = r^{-1}$. In this case, we can take $\epsilon_0 = \frac{r}{2}$ to obtain the tubular neighborhood shown in Figure 3.5. In this special case, we can calculate $\xi(\mathbf{x})$ and $\eta(\mathbf{x})$ explicitly: $\xi(\mathbf{x})$ is the angle of $\mathbf{x}$ in polar coordinates, then $\mathbf{g}(\xi(\mathbf{x})) = \frac{r\mathbf{x}}{\|\mathbf{x}\|}$, and $\eta(\mathbf{x})$ is the (signed) distance between $\mathbf{x}$ and $\frac{r\mathbf{x}}{\|\mathbf{x}\|} \in \Gamma$. To find an explicit formula for $\eta(\mathbf{x})$, we recall that $\mathbf{n}$ is defined by (3.3), then

$$\mathbf{n}(\xi(\mathbf{x})) = \begin{bmatrix} 0 & 1 \\ -1 & 0 \end{bmatrix} \begin{bmatrix} -\sin(\xi(\mathbf{x})) \\ \cos(\xi(\mathbf{x})) \end{bmatrix} = \frac{1}{r}\mathbf{g}(\xi(\mathbf{x})) = \frac{\mathbf{x}}{\|\mathbf{x}\|}.$$

Now, we substitute $\mathbf{n}(\xi(\mathbf{x}))$ and $\mathbf{g}(\xi(\mathbf{x}))$ back in the definition of P to obtain

$$\mathbf{x} = \mathbf{g}(\xi(\mathbf{x})) + \eta(\mathbf{x})\mathbf{n}(\xi(\mathbf{x})) = (r + \eta(\mathbf{x}))\frac{\mathbf{x}}{\|\mathbf{x}\|}.$$

Hence, $\eta(\mathbf{x}) = \|\mathbf{x}\| - r$.

Remark 3.3. In Example 3.1, we are able to find an explicit formula for $\eta(\mathbf{x})$ and $\xi(\mathbf{x})$. In general, such explicit formulae are hard to obtain. Nevertheless, we will describe later an efficient numerical method to calculate η and ξ.

In the remainder of this section, we focus our attention on functions defined on subsets of

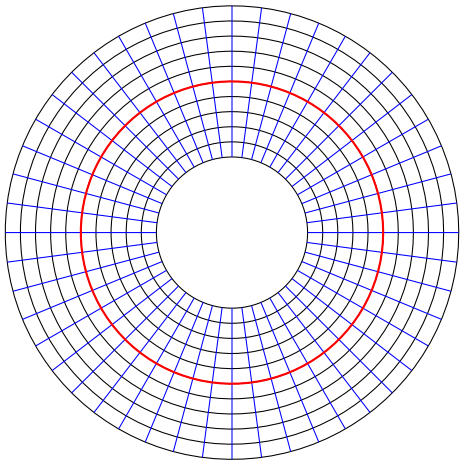

Figure 3.5: A tubular neighborhood of Γ (red) with non-intersecting normal lines (blue) and parallel curves (black).

N_0, where $R = (\eta, \xi)$ is well-defined and differentiable. For every domain $D \subset N_0$, we will use $\hat{D}$ to denote $R(D)$, and for every function $u : D \subset N_0 \to \mathbb{R}$, we will use $\hat{u}$ to denote $u \circ P : \hat{D} \to \mathbb{R}$. Similarly, if $\mathbf{u} : D \subset N_0 \to \mathbb{R}^d$ is a vector function, we use $\hat{\mathbf{u}}$ to denote $\mathbf{u} \circ P$.

From Lemma 3.3, it follows that the gradients of η and ξ on N_0 are given by

$$\nabla \eta = \mathbf{n}(\xi), \qquad \nabla \xi = \|\mathbf{g}'(\xi)\|^{-1} \psi(\eta, \xi) \boldsymbol{\tau}(\xi). \tag{3.16}$$

Here we are dropping the variable $\mathbf{x}$ from the equation to avoid lengthy formulas. However, it is important to remember that we are treating η and ξ as functions of $\mathbf{x}$ in this context.

Lemma 3.4. *On N_0, we have*

$$\nabla \cdot \mathbf{n}(\xi) = \kappa(\xi)\psi(\xi), \qquad \nabla \cdot \boldsymbol{\tau}(\xi) = 0. \tag{3.17}$$

Proof. Let us start with $\nabla \cdot \mathbf{n}(\xi)$. From (3.16), we have

$$\nabla \cdot \mathbf{n}(\xi) = \nabla \xi \cdot \mathbf{n}'(\xi) = \psi(\eta, \xi) \|\mathbf{g}'(\xi)\|^{-1} \boldsymbol{\tau}(\xi) \cdot \mathbf{n}'(\xi).$$

Next, we recall that $\mathbf{n}'(\xi) = \kappa(\xi)\,\|\mathbf{g}'(\xi)\|\,\boldsymbol{\tau}(\xi)$, then

$$\nabla \cdot \mathbf{n}(\xi) = \kappa(\xi)\psi(\eta,\xi).$$

The second formula $\nabla \cdot \boldsymbol{\tau}(\xi) = 0$ follows from a similar argument

$$\begin{aligned}
\nabla \cdot \boldsymbol{\tau}(\xi) &= \nabla\xi \cdot \boldsymbol{\tau}'(\xi) \\
&= \psi(\eta,\xi)\,\|\mathbf{g}'(\xi)\|^{-1}\,\boldsymbol{\tau}(\xi)\cdot\boldsymbol{\tau}'(\xi) \\
&= -\psi(\eta,\xi)\kappa(\xi)\boldsymbol{\tau}(\xi)\cdot\mathbf{n}(\xi) \\
&= 0,
\end{aligned}$$

which concludes the proof. □

Our next step is to derive some elementary calculus formulas for the gradient and Laplacian of functions on N_0 in terms of the Frenet coordinates η, ξ.

Lemma 3.5. *Let $u : N_0 \to \mathbb{R}$ be differentiable, then $\hat{u} = u \circ P$ is differentiable and*

$$\nabla u = \hat{u}_\eta(\eta,\xi)\mathbf{n}(\xi) + \|\mathbf{g}'(\xi)\|^{-1}\,\psi(\eta,\xi)\hat{u}_\xi(\eta,\xi)\boldsymbol{\tau}(\xi). \tag{3.18}$$

In particular

$$\nabla u \cdot \mathbf{n}(\xi) = \hat{u}_\eta(\eta,\xi), \;\; \textit{and} \;\; \nabla u \cdot \boldsymbol{\tau}(\xi) = \|\mathbf{g}'(\xi)\|^{-1}\,\psi(\eta,\xi)\hat{u}_\xi(\eta,\xi). \tag{3.19}$$

Proof. This follows immediately from (3.16) since $u = \hat{u} \circ R = \hat{u}(\eta,\xi)$. □

Lemma 3.6. *Let $a, b : N_0 \to \mathbb{R}$ be differentiable functions, and let $\hat{a} = a \circ P$, $\hat{b} = b \circ P$ and $\mathbf{u} = a\mathbf{n}(\xi) + b\boldsymbol{\tau}(\xi)$, then*

$$\nabla \cdot \mathbf{u} = \hat{a}_\eta(\eta,\xi) + \kappa(\xi)\psi(\eta,\xi)\hat{a}(\eta,\xi) + \psi(\eta,\xi)\left\|\mathbf{g}'(\xi)\right\|^{-1}\hat{b}_\xi(\eta,\xi). \tag{3.20}$$

Proof. We start first with $\nabla \cdot (a\mathbf{n}(\xi))$, we have

$$\begin{aligned}\nabla \cdot (a\mathbf{n}(\xi)) &= \nabla a \cdot \mathbf{n}(\xi) + a\nabla \cdot \mathbf{n}(\xi)\\ &= \hat{a}_\eta(\eta,\xi) + \hat{a}(\eta,\xi)\kappa(\xi)\psi(\eta,\xi),\end{aligned} \tag{3.21a}$$

where the last equality follows from (3.19) and (3.17). Similarly,

$$\begin{aligned}\nabla \cdot (b\boldsymbol{\tau}(\xi)) &= \nabla b \cdot \boldsymbol{\tau}(\xi) + b\nabla \cdot \boldsymbol{\tau}(\xi)\\ &= \hat{b}_\xi(\eta,\xi)\left\|g'(\xi)\right\|^{-1}\psi(\eta,\xi) + 0.\end{aligned} \tag{3.21b}$$

Finally, by summing (3.21a) and (3.21b), we obtain (3.20). □

Lemma 3.7. *Let $u : N_0 \to \mathbb{R}$ be twice differentiable, and let $\hat{u} = u \circ P$, then*

$$\Delta u = \mathscr{L}(\hat{u})(\eta,\xi), \tag{3.22a}$$

where

$$\mathscr{L}(\hat{u})(\eta,\xi) = \hat{u}_{\eta\eta}(\eta,\xi) + \rho_0(\eta,\xi)\hat{u}_{\xi\xi}(\eta,\xi) + \rho_1(\eta,\xi)\hat{u}_\eta(\eta,\xi) + \rho_2(\eta,\xi)\hat{u}_\xi(\eta,\xi), \tag{3.22b}$$

and

$$\begin{aligned}\rho_0(\eta,\xi) &= \left(\frac{\psi(\eta,\xi)}{\|\mathbf{g}'(\xi)\|}\right)^2, \qquad \rho_1(\eta,\xi) = \kappa(\xi)\psi(\eta,\xi),\\ \rho_2(\eta,\xi) &= -\left(\frac{\psi(\eta,\xi)}{\|\mathbf{g}'(\xi)\|}\right)^2\left(\eta\kappa'(\xi)\psi(\eta,\xi) + \frac{\mathbf{g}'(\xi)\cdot\mathbf{g}''(\xi)}{\|\mathbf{g}'(\xi)\|^2}\right).\end{aligned} \tag{3.22c}$$

Proof. From (3.5), we have

$$\Delta u = \nabla \cdot \left(\hat{u}_\eta(\eta,\xi)\mathbf{n}(\xi) + \frac{\psi(\eta,\xi)}{\|\mathbf{g}'(\xi)\|}\hat{u}_\xi(\eta,\xi)\boldsymbol{\tau}(\xi) \right).$$

By applying Lemma 3.6 and Lemma 3.4, we obtain

$$\Delta u = \hat{u}_{\eta\eta}(\eta,\xi) + \kappa(\xi)\psi(\eta,\xi)\hat{u}_\eta(\eta,\xi) + \frac{\psi(\eta,\xi)}{\|\mathbf{g}'(\xi)\|}\frac{\partial}{\partial\xi}\left(\frac{\psi(\eta,\xi)}{\|\mathbf{g}'(\xi)\|}\hat{u}_\xi(\eta,\xi) \right), \tag{3.23a}$$

Next, we use $\psi_\xi(\eta,\xi) = -\eta\kappa'(\xi)\psi(\eta,\xi)^2$ to obtain

$$\frac{\partial}{\partial\xi}\left(\frac{\psi(\eta,\xi)}{|\mathbf{g}'(\xi)|} \right) = -\eta\kappa'(\xi)\psi(\eta,\xi)^2 \|\mathbf{g}'(\xi)\|^{-1} - \psi(\eta,\xi)(\mathbf{g}'(\xi)\cdot\mathbf{g}''(\xi))\|\mathbf{g}'(\xi)\|^{-3}. \tag{3.23b}$$

Thus, the desired formula (3.22) is obtained by substituting (3.23b) back into (3.23a). □

3.4 The Frenet IFE Space

In this section, we proceed to construct an m-th degree Frenet immersed finite element space using the Frenet transformation introduced in the previous section. First, we assume that mesh size $h < \epsilon_0$ where ϵ_0 is defined in (3.15). Hence, for each interface element K, the inverse Frenet transformation R is well-defined and differentiable on K. For example, see Figure 3.6, where every interface element is contained in the tubular neighborhood N_0.

Now, consider an interface element K, then K is contained in a section of the tubular neighborhood N_0 of the form $K_F = P([\xi_0,\xi_1]\times[-h,h])$, which we will call the local fictitious Frenet element as shown in Figure 3.7. Additionally, we will call $\mathbf{g}([\xi_0,\xi_1]) = K_F \cap \Gamma$ fictitious local interface and denote it by Γ_{K_F}.

In accordance with the notation in the previous section, we will use $\hat{K}, \hat{K}^+$ and $\hat{K}^-$ to

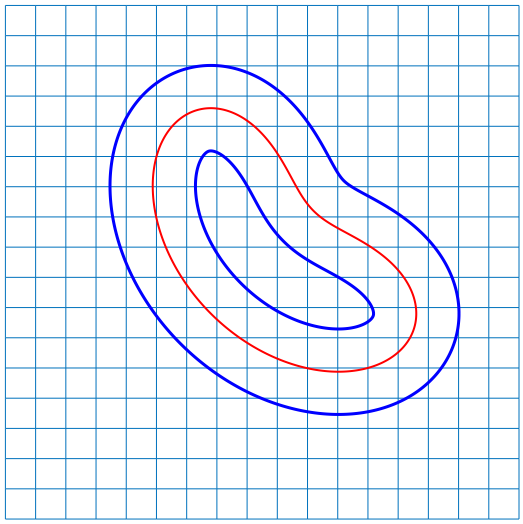

Figure 3.6: A uniform mesh $\mathcal{T}_h$ such that each interface element is in N_0, where the boundary of N_0 is in dark blue.

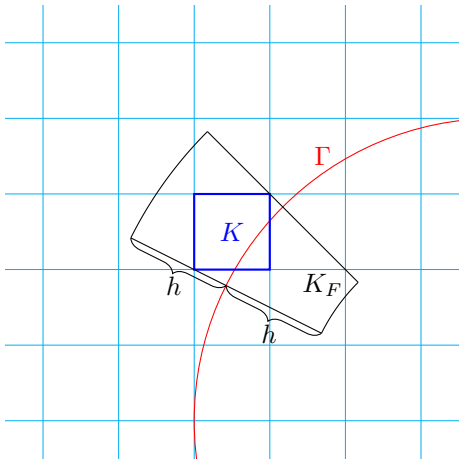

Figure 3.7: An illustration of an interface element K and its associated fictitious Frenet element K_F.

denote $R(K), R(K^+)$ and $R(K^-)$, respectively. Similarly, we will use $\hat{K}_F, \hat{\Gamma}_{K_F}, \hat{K}_F^+$ and $\hat{K}_F^-$ to denote $R(K_F), R(\Gamma_{K_F}), R(K_F^+)$ and $R(K_F^-)$ as shown in Figure 3.8. Then, $\hat{K}^\pm$ is contained in the rectangle $\hat{K}_F^\pm$, and more importantly, $\hat{\Gamma}_{K_F}$ is a vertical line segment. This last property is a key ingredient in the construction of the Frenet IFE functions. To illustrate these observations, we consider the previously shown interface element in Figure 3.7, and we apply the transformation R to K and K_F to obtain $\hat{K}$ and $\hat{K}_F$. Notice here that $\hat{K}$ is not a polygon since R is non-linear.

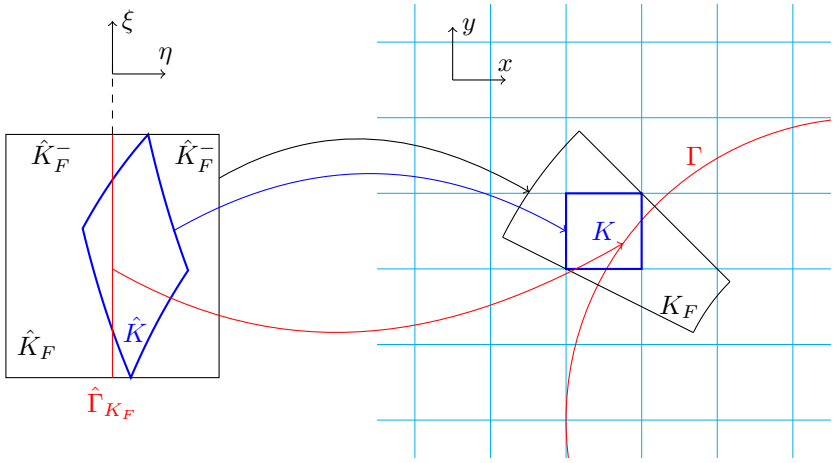

Figure 3.8: The plot on the right shows an example of an interface K and its associated local fictitious element K_F. The plot on the right shows their images under the inverse Frenet transformation R.

Now, consider a function $u : K_F \to \mathbb{R}$ that satisfies the interface conditions (3.1c) and (3.1d) on Γ_{K_F} and let $\hat{u} = u \circ P$ and $\hat{\beta} = \beta \circ P$, then by Lemma 3.5 and Lemma 3.7, we have

$$[\![\hat{u}]\!]_{\hat{\Gamma}_{K_F}} = 0, \qquad \left[\!\!\left[\hat{\beta}\hat{u}_\eta\right]\!\!\right]_{\hat{\Gamma}_{K_F}} = 0, \tag{3.24a}$$

and

$$\left[\!\!\left[\hat{\beta}\frac{\partial^j}{\partial \eta^j}\mathscr{L}(\hat{u})\right]\!\!\right]_{\hat{\Gamma}_{K_F}} = 0, \qquad j = 0, 1, \ldots, m-2. \tag{3.24b}$$

Here, we note that the *flattened* interface conditions (3.24a) are simpler than the original

interface conditions (3.1c) since Γ_{K_F} is merely a line segment.

Next, we proceed to the construction of the Frenet IFE space on $\hat{K}_F$, which consists of piecewise polynomial functions that satisfy (3.24a) exactly and (3.24b) weakly. To make our presentation clear, we will use $Q^m(B)$ to denote the space of tensor-product polynomials of degree at most m on B, that is,

$$Q^m(B) = \left\{ p : B \to \mathbb{R} \mid p(\eta, \xi) = \sum_{i=0}^{m} \sum_{j=0}^{m} c_{i,j} \eta^j \xi^i \text{ for some } \{c_{i,j}\}_{i,j=0}^{m} \right\}.$$

Additionally, given a line segment I, we use $\mathcal{P}^m(I)$ to denote the space of univariate polynomials of degree at most m on I.

We define the Frenet IFE space on $\hat{K}_F$ as the space of piecewise polynomials $\hat{\varphi} : \hat{K}_F \to \mathbb{R}$ such that $\hat{\varphi}^{\pm} = \hat{\varphi}|_{K_F^{\pm}} \in Q^m(\hat{K}_F^{\pm})$ such that

$$[\![\hat{\varphi}]\!]_{\hat{\Gamma}_{K_F}} = 0, \qquad \left[\!\!\left[\hat{\beta}\hat{\varphi}_\eta\right]\!\!\right]_{\hat{\Gamma}_{K_F}} = 0, \tag{3.25a}$$

$$\int_{\hat{\Gamma}_{K_F}} \left[\!\!\left[\frac{\partial^j}{\partial \eta^j} \mathscr{L}(\hat{\varphi})\right]\!\!\right]_{\hat{\Gamma}_{K_F}} v = 0, \qquad \forall v \in \mathcal{P}^m(\hat{\Gamma}_{K_F}), \qquad j = 0, 1, \ldots, m-2. \tag{3.25b}$$

Then, $\hat{\varphi}$ satisfies the interface conditions (3.24a) exactly, and the extended interface conditions (3.24b) in a weak sense. This is because we cannot enforce the latter exactly since the terms in (3.22) may be non-linear unless Γ_{K_F} is a curve with a constant curvature, such as a circle or a line. In general, the curvature $\kappa(\xi)$ of Γ may be a non-polynomial function and so is $\mathscr{L}(\hat{\varphi})$. Fortunately, the extended interface conditions do not affect the weak formulation of the problem.

The following lemma shows that when $\hat{\varphi}^-$ is given, the system (3.25) is uniquely solvable for $\hat{\varphi}^+$, which is similar to the extension operator discussed in Chapter 2 for one-dimensional problems.

Lemma 3.8. *Given a polynomial $\hat{\varphi}^{\pm} \in Q^m(\hat{K}_F^{\pm})$, there is a unique polynomial $\hat{\varphi}^{\mp} \in Q^m(\hat{K}_F^{\mp})$ such that the piecewise polynomial function*

$$\hat{\varphi} = \begin{cases} \hat{\varphi}^- & \text{on } \hat{K}_F^-, \\ \hat{\varphi}^+ & \text{on } \hat{K}_F^+, \end{cases}$$

satisfies the interface conditions (3.25).

Proof. Without loss of generality, we assume that $\hat{\varphi}^- \in Q^m(\hat{K}_F^-)$ is given, and that $\hat{\beta}|_{\hat{K}_F^{\pm}} = \beta^{\pm}$. Then the conditions (3.25) can be formulated as a linear system in the following way

$$\int_{\hat{\Gamma}_{K_F}} \hat{\varphi}^+(0,\xi)\xi^i \, d\xi = \int_{\hat{\Gamma}_{K_F}} \hat{\varphi}^-(0,\xi)\xi^i \, d\xi, \qquad i = 0, 1, \ldots, m. \tag{3.26a}$$

$$\int_{\hat{\Gamma}_{K_F}} \beta^+ \hat{\varphi}_\eta^+(0,\xi)\xi^i \, d\xi = \int_{\hat{\Gamma}_{K_F}} \beta^- \hat{\varphi}_\eta^-(0,\xi)\xi^i \, d\xi, \qquad i = 0, 1, \ldots, m. \tag{3.26b}$$

$$\int_{\hat{\Gamma}_{K_F}} \beta^+ \frac{\partial^j \mathscr{L}(\hat{\varphi}^+)}{\partial \eta^j}(0,\xi)\xi^i \, d\xi = \int_{\hat{\Gamma}_{K_F}} \beta^- \frac{\partial^j \mathscr{L}(\hat{\varphi}^-)}{\partial \eta^j}(0,\xi)\xi^i \, d\xi, \quad i = 0, 1, \ldots, m, \ j = 0, 1, \ldots, m-2. \tag{3.26c}$$

Then, the system (3.26) (and consequently (3.25)) is a square $(m+1)^2 \times (m+1)^2$ linear system. Therefore, it is enough to show that if $\hat{\varphi}^- = 0$, then $\hat{\varphi}^+ = 0$.

Assume that $\hat{\varphi}^- = 0$. Since $\hat{\varphi}^+ \in Q^m(\hat{K}_F^+)$, it can be written as

$$\hat{\varphi}^+(\eta,\xi) = \sum_{j=0}^{m} \eta^j p_j(\xi),$$

for some polynomials $p_0, p_1, \ldots, p_m$. Our goal is to show that all of these polynomials are zero. First, it follows from (3.26a) and (3.26b) that $p_0 = 0$ and $p_1 = 0$. Next, we proceed by

strong induction. Assume that $p_j = 0$ for all $j = 0, 1, \ldots, j_0$ for some $1 \leq j_0 \leq m$. Therefore,

$$\frac{p^{i+j}}{\partial \eta^j \partial \xi^i} \hat{\varphi}^+(0, \cdot) = 0, \quad 0 \leq i \leq m, \ 0 \leq j \leq j_0. \tag{3.27}$$

From (3.22), we have

$$\begin{aligned} \frac{\partial^{j_0-1}}{\partial \eta^{j_0-1}} \mathscr{L}(\hat{\varphi}^+) &= \frac{\partial^{j_0+1}}{\partial \eta^{j_0+1}} \hat{\varphi}^+ + \frac{\partial^{j_0-1}}{\partial \eta^{j_0-1}} \left(\rho_0 \hat{\varphi}^+_{\xi\xi} + \rho_1 \hat{\varphi}^+_{\eta} + \rho_2 \hat{\varphi}^+_{\xi} \right), \\ &= \frac{\partial^{j_0+1} \hat{\varphi}^+}{\partial \eta^{j_0+1}} + \sum_{l=0}^{j_0-1} \binom{j_0-1}{l} \left(\frac{\partial^{j_0-1-l} \rho_0}{\partial \eta^{j_0-1-l}} \frac{\partial^l \hat{\varphi}^+_{\xi\xi}}{\partial \eta^l} + \frac{\partial^{j_0-1-l} \rho_1}{\partial \eta^{j_0-1-l}} \frac{\partial^{l+1} \hat{\varphi}^+}{\partial \eta^{l+1}} + \frac{\partial^{j_0-1-l} \rho_2}{\partial \eta^{j_0-1-l}} \frac{\partial^l \hat{\varphi}^+_{\xi}}{\partial \eta^l} \right). \end{aligned} \tag{3.28}$$

Now, we substitute (3.28) into (3.26c) and use (3.27) to obtain

$$\int_{\hat{\Gamma}_{K_F}} (j_0 + 1)! p_{j_0+1}(\xi) \xi^i \, d\xi = 0, \qquad \forall i = 0, 1, \ldots, m.$$

Therefore, $p_{j_0+1} = 0$. Consequently, by strong induction, $p_j = 0$ for all $0 \leq j \leq m$, which proves that $\hat{\varphi}^+ = 0$ and concludes this proof. □

The lemma above shows that every polynomial $\hat{\varphi}^- \in Q^m(\hat{K}_F^-)$ can be paired (uniquely) with a polynomial $\hat{\varphi}^+ \in Q^m(\hat{K}_F^+)$ such that the resulting piecewise polynomial $\hat{\varphi}$ satisfies the conditions (3.25). Hence, we introduce the Frenet IFE space as

$$\hat{\mathcal{V}}_{\hat{\beta}}^m(\hat{K}_F) = \left\{ \hat{\varphi} : \hat{K}_F \to \mathbb{R} \mid \hat{\varphi}|_{\hat{K}_F^\pm} \in Q^m(\hat{K}_F^\pm) \quad \text{and} \quad \hat{\varphi} \text{ satisfies (3.25)} \right\}. \tag{3.29}$$

From our arguments in the previous proof, we can deduce more information about the immersed Frenet IFE space, as stated in the following corollary.

Corollary 3.1. *Let $\hat{\mathcal{V}}_{\hat{\beta}}^m(\hat{K}_F)$ be the Frenet IFE space (3.29), then $\dim(\hat{\mathcal{V}}_{\hat{\beta}}^m(\hat{K}_F)) = (m+1)^2$. Additionally, if $\beta^+ = \beta^-$, then $\hat{\mathcal{V}}_{\hat{\beta}}^m(\hat{K}_F) = Q^m(\hat{K}_F)$.*

Finally, we define the local Frenet IFE space on the interface element K as

$$\mathcal{V}_\beta^m(K) = \left\{ \hat{\varphi} \circ R|_K \mid \hat{\varphi} \in \hat{\mathcal{V}}_{\hat{\beta}}^m(\hat{K}_F) \right\}. \tag{3.30}$$

Remark 3.4. Since R is non-linear (in general), the IFE functions in $\mathcal{V}_{\hat{\beta}}^m(K)$ are not piecewise polynomials. This is very closely related to the isoparametric finite element method [26, 37] where the basis functions are mapped from a reference element to a curved element via a non-linear transformation. The benefit is that all Frenet IFE functions satisfy the interface conditions (3.1c) exactly, a property not shared by any other IFE method. More precisely, for every function $\varphi \in \mathcal{V}_{\hat{\beta}}^m(K)$, both φ and $\beta \nabla \varphi \cdot \mathbf{n}$ are continuous.

3.5 Computational Aspects of the Construction of the Frenet IFE Space

A major part of every immersed finite element method is the construction of the local IFE space. Since the number of interface elements grows as the mesh is refined, it is important for us to design efficient numerical methods to obtain a basis of IFE functions on each interface element. In this section, we describe an efficient and robust method to build a basis of Frenet IFE functions. In fact, we show that, out of the $(m+1)^2$ basis functions of the local Frenet IFE space for each interface element, we are able to explicitly express $m(m+1)$ of them. Hence, it remains to construct the remaining $m+1$ functions by solving a linear system. This is already a major advantage of the Frenet IFE over the classical higher order IFE methods [5, 12, 13, 51]. Furthermore, we will numerically show that this linear system is well conditioned even for small cut elements without the need for user-chosen parameters [114].

Additionally, we describe an efficient method to implement the inverse Frenet transformation, as well as an overview of the quadrature rules on interface elements.

3.5.1 Constructing a Basis for the Frenet IFE Space

In this subsection, we will describe the construction of a basis for the local Frenet IFE space. Since a basis of the local Frenet IFE space $\mathcal{V}_\beta^m(K)$ can be constructed directly from a basis of $\hat{\mathcal{V}}_{\hat{\beta}}^m(\hat{K}_F)$, we will only discuss a basis for the latter. First, recall that $\dim(\hat{\mathcal{V}}_{\hat{\beta}}^m(\hat{K}_F)) = (m+1)^2$, then, we need to find a basis

$$\{\hat{\varphi}_{i,j}\}_{i,j=0}^m$$

for the Frenet IFE space. Fortunately, we can express $m(m+1)$ elements of this basis explicitly as the following lemma shows.

Lemma 3.9. *Let $0 \le i \le m$ and $1 \le j \le m$ be integers, and let*

$$\hat{\varphi}_{i,j}(\eta,\xi) = \frac{1}{\hat{\beta}(\eta,\xi)}\eta^j\xi^i, \qquad (\eta,\xi) \in \hat{K}_F.$$

Then, $\hat{\varphi}_{i,j} \in \hat{\mathcal{V}}_{\hat{\beta}}^m(\hat{K}_F)$.

Proof. Let $0 \le i \le m$ and $1 \le j \le m$, and let $\hat{\varphi}_{i,j}^{\pm} = \hat{\varphi}_{i,j}|_{\hat{K}_F^{\pm}} \in Q^m(\hat{K}_F^{\pm})$.

Since $j \ge 1$, we have $\hat{\varphi}_{i,j}^{+}(0,\xi) = \hat{\varphi}_{i,j}^{-}(0,\xi) = 0$ for all $\xi \in \hat{\Gamma}_{K_F}$. Therefore, $[\![\hat{\varphi}_{i,j}]\!]_{\hat{\Gamma}_{K_F}} = 0$.

Next, consider $q = \hat{\beta}\hat{\varphi}_{i,j}$, then $q \in Q^m(\hat{K}_F)$. Consequently, we have

$$\left[\!\!\left[\hat{\beta}\hat{\varphi}_{i,j}\right]\!\!\right]_{\hat{\Gamma}_{K_F}} = [\![q]\!]_{\hat{\Gamma}_{K_F}} = 0.$$

Then, $\hat{\varphi}_{i,j}$ satisfies the interface conditions (3.25a) Similarly,

$$\left[\!\left[\hat{\beta}\frac{\partial^j \mathscr{L}(\hat{\varphi}_{i,j})}{\partial \eta^j}\right]\!\right]_{\hat{\Gamma}_{K_F}} = \left[\!\left[\frac{\hat{\beta}\partial^j \mathscr{L}(\hat{\varphi}_{i,j})}{\partial \eta^j}\right]\!\right]_{\hat{\Gamma}_{K_F}} = \left[\!\left[\frac{\partial^j \mathscr{L}(q)}{\partial \eta^j}\right]\!\right]_{\hat{\Gamma}_{K_F}} = 0.$$

Hence, $\hat{\varphi}_{i,j}$ satisfies (3.25b). □

Remark 3.5. The functions $\hat{\varphi}_{i,j}$ described in the lemma above satisfy the interface conditions exactly, which is a stronger condition than (3.25). This is yet another advantage of the Frenet IFE method.

Here, we observe that the set $B_1 = \{\hat{\varphi}_{i,j}\}_{i=0,j=1}^{m}$ is a subset of $\hat{\mathcal{V}}_{\hat{\beta}}^m(\hat{K}_F)$. Furthermore, the set B_1 is linearly independent by construction. Then, it remains to find a set $B_0 \subset \hat{\mathcal{V}}_{\hat{\beta}}^m(\hat{K}_F)$ with $m+1$ elements such that $B = B_0 \cup B_1$ is a basis for the Frenet IFE space.

In our subsequent derivation, we assume, without loss of generality, that $\hat{\beta}|_{\hat{K}_F^{\pm}} = \beta^{\pm}$ to simplify our presentation.

The key observation here is that the functions in Lemma 3.9 all vanish on the interface since $j \geq 1$. Then, to complete the basis, we need to construct a set $\{\hat{\varphi}_{i,0}\}_{i=0}^{m}$ such that

$$\hat{\varphi}_{i,0}^{-}(0,\xi) = p_i(\xi), \quad \text{and} \quad \hat{\varphi}_{i,0} \in \hat{\mathcal{V}}_{\hat{\beta}}^m(\hat{K}_F),$$

where $\{p_i\}_{i=0}^{m}$ is a basis for $\mathcal{P}^m(\Gamma_{K_F})$. Consequently, according to (3.25), we seek $\hat{\varphi}^+ \in Q^m(\hat{K}_F^+)$ such that

$$\hat{\varphi}_{i,0}^{+}(0,\xi) = \hat{\varphi}_{i,0}^{-}(0,\xi) = p_i(\xi), \qquad \xi \in \hat{\Gamma}_{K_F}, \tag{3.31a}$$

$$\beta^{+}\frac{\partial \hat{\varphi}_{i,0}^{+}}{\partial \eta}(0,\xi) = \beta^{-}\frac{\partial \hat{\varphi}_{i,0}^{-}}{\partial \eta}(0,\xi) = 0, \qquad \xi \in \hat{\Gamma}_{K_F}, \tag{3.31b}$$

$$\int_{\hat{\Gamma}_{K_F}} \beta^{+}\frac{\partial^j}{\partial \eta^j}\mathscr{L}(\hat{\varphi}_{i,0}^{+})v = \int_{\hat{\Gamma}_{K_F}} \beta^{-}\frac{\partial^j}{\partial \eta^j}\mathscr{L}(\hat{\varphi}_{i,0}^{-})v, \qquad \forall v \in \mathcal{P}^m(\hat{\Gamma}_{K_F}), \qquad j = 0,1,\ldots,m-2. \tag{3.31c}$$

Therefore, from (3.31a) and (3.31b), the polynomial $\hat{\varphi}^+_{i,0}$ can be written as

$$\hat{\varphi}^+_{i,0}(\eta,\xi) = p_i(\xi) + \sum_{l=1}^{m^2-1} c_l^{(i)} \mathcal{N}_l(\eta,\xi), \tag{3.32}$$

where $\{\mathcal{N}_l\}_{l=1}^{m^2-1}$ is an enumeration of $\{\eta^j p_i(\xi)\}_{i=0,j=2}^{m}$. In accordance with our paper [19], we choose $\{\mathcal{N}_l\}$ to be the lexicographical ordering of $\{\eta^j p_i(\xi)\}$, that is,

$$\begin{array}{llll}
\mathcal{N}_1(\eta,\xi) = \eta^2 p_0(\xi), & \mathcal{N}_{m+2}(\eta,\xi) = \eta^3 p_0(\xi), & \cdots & \mathcal{N}_{m^2-m-1}(\eta,\xi) = \eta^m p_0(\xi) \\
\mathcal{N}_2(\eta,\xi) = \eta^2 p_1(\xi), & \mathcal{N}_{m+3}(\eta,\xi) = \eta^3 p_1(\xi), & \cdots & \mathcal{N}_{m^2-m}(\eta,\xi) = \eta^m p_1(\xi) \\
\mathcal{N}_3(\eta,\xi) = \eta^2 p_2(\xi), & \mathcal{N}_{m+3}(\eta,\xi) = \eta^3 p_2(\xi), & \cdots & \mathcal{N}_{m^2-m+1}(\eta,\xi) = \eta^m p_2(\xi) \\
\vdots & \vdots & \ddots & \vdots \\
\mathcal{N}_{m+1}(\eta,\xi) = \eta^2 p_m(\xi), & \mathcal{N}_{2(m+1)}(\eta,\xi) = \eta^3 p_m(\xi), & \cdots & \mathcal{N}_{m^2-1}(\eta,\xi) = \eta^m p_m(\xi)
\end{array} \tag{3.33}$$

Now, we use the interface condition (3.31c) with $v = p_0, p_1, \ldots, p_m$, to obtain the following system of equations

$$\sum_{l=1}^{m^2-1} c_l^{(i)} \int_{\hat{\Gamma}_{K_F}} \frac{\partial^j}{\partial \eta^j} \mathscr{L}(\mathcal{N}_l)(0,\xi) p_k(\xi) d\xi = \frac{\beta^- - \beta^+}{\beta^+} \int_{\hat{\Gamma}_{K_F}} \frac{\partial^j}{\partial \eta^j} \mathscr{L}(p_i(\xi))(0,\xi) p_k(\xi) d\xi, \tag{3.34}$$

for all $0 \le k \le m$ and $0 \le j \le m-2$. The system (3.34) can be written in matrix form as

$$\mathbf{A}\mathbf{c}^{(i)} = \frac{\beta^- - \beta^+}{\beta^+} \mathbf{b}(i), \tag{3.35}$$

where $\mathbf{c}^{(i)} = (c_1^{(i)}, c_2^{(i)}, \ldots, c_{m^2-1}^{(i)})$. The matrix $\mathbf{A}$ and the vector $\mathbf{b}^{(i)}$ can be constructed from

their row blocks

$$\mathbf{A} = \begin{bmatrix} \mathbf{A}^{(0)} \\ \mathbf{A}^{(1)} \\ \vdots \\ \mathbf{A}^{(m-2)} \end{bmatrix}, \qquad \mathbf{b}(i) = \begin{bmatrix} \mathbf{b}^{(0)}(i) \\ \mathbf{b}^{(1)}(i) \\ \vdots \\ \mathbf{b}^{(m-2)}(i) \end{bmatrix}. \tag{3.36}$$

Each block of the matrix $\mathbf{A}$ is given by [19]

$$\mathbf{A}_{k,l}^{(j)} = \int_{\hat{\Gamma}_{K_F}} \frac{\partial^j}{\partial \eta^j} \mathscr{L}(\mathcal{N}_l)(0,\xi) p_k(\xi) d\xi, \qquad 0 \le j \le m-2, \quad 1 \le l \le m^2 - 1, \quad 0 \le k \le m. \tag{3.37}$$

Similarly, each block of $\mathbf{b}$ is given by

$$\mathbf{b}_k^{(j)}(i) = \int_{\hat{\Gamma}_{K_F}} \frac{\partial^j}{\partial \eta^j} \mathscr{L}(p_i(\xi))(0,\xi) p_k(\xi) d\xi, \qquad 0 \le j \le m-2, \quad 0 \le k \le m. \tag{3.38}$$

We note here that the matrix $\mathbf{A}$ does not depend on i. Then, we can combine the systems (3.35) for $0 \le i \le m$ in one matrix system

$$\mathbf{A} \begin{bmatrix} \mathbf{c}^{(0)} & \mathbf{c}^{(1)} & \dots & \mathbf{c}^{(m)} \end{bmatrix} = \frac{\beta^- - \beta^+}{\beta^+} \begin{bmatrix} \mathbf{b}^{(0)} & \mathbf{b}^{(1)} & \dots & \mathbf{b}^{(m)} \end{bmatrix}. \tag{3.39}$$

Next, we need to construct the matrix $\mathbf{A}$ and the vectors $\mathbf{b}(i)$. In both situations, one needs to evaluate quantities of the form

$$\frac{\partial^j}{\partial \eta^j} \mathscr{L}(v)(0,\xi), \tag{3.40}$$

where v is a polynomial (either $\mathcal{N}_l$ or p_i). Similarly to (3.28), we can write (3.40) as [19]

$$\frac{\partial^j}{\partial\eta^j}\mathscr{L}(v)(0,\xi) = \frac{\partial^{j+2}v(0,\xi)}{\partial\eta^{j+2}} \tag{3.41}$$

$$+\sum_{l=0}^{j}\binom{j}{l}\left(\frac{\partial^l\rho_0(0,\xi)}{\partial\eta^l}\frac{\partial^{j-l}v_{\xi\xi}(0,\xi)}{\partial\eta^{j-l}} + \frac{\partial^l\rho_1(0,\xi)}{\partial\eta^l}\frac{\partial^{j-l+1}v(0,\xi)}{\partial\eta^{j-l+1}} + \frac{\partial^l\rho_2(0,\xi)}{\partial\eta^l}\frac{\partial^{j-l}v_{\xi}(0,\xi)}{\partial\eta^{j-l}}\right) \tag{3.42}$$

where ρ_0, ρ_1 and ρ_2 are given by (3.22). Since v is a polynomial in our calculations, it is relatively easy to evaluate

$$\frac{\partial^{j+2}v(0,\xi)}{\partial\eta^{j+2}},\ \frac{\partial^{j-l}v_{\xi\xi}(0,\xi)}{\partial\eta^{j-l}},\ \frac{\partial^{j-l+1}v(0,\xi)}{\partial\eta^{j-l+1}},\ \frac{\partial^{j-l}v_{\xi}(0,\xi)}{\partial\eta^{j-l}}.$$

Then, it remains to evaluate the l-th order derivatives of ρ_0, ρ_1 and ρ_3 with respect to η. First, by differentiating (3.22), we obtain

$$\frac{\partial^l\rho_0(\eta,\xi)}{\partial\eta^l} = \frac{1}{\|\mathbf{g}'(\xi)\|^2}\frac{\partial^l\psi^2(\eta,\xi)}{\partial\eta^l}, \tag{3.43a}$$

$$\frac{\partial^l\rho_1(\eta,\xi)}{\partial\eta^l} = \kappa(\xi)\frac{\partial^l\psi(\eta,\xi)}{\partial\eta^l}, \tag{3.43b}$$

$$\frac{\partial^l\rho_2(\eta,\xi)}{\partial\eta^l} = -\frac{\kappa'(\xi)}{\|\mathbf{g}'(\xi)\|^2}\left(\eta\frac{\partial^l\psi^3(\eta,\xi)}{\partial\eta^l} + l\frac{\partial^{l-1}\psi^3(\eta,\xi)}{\partial\eta^{l-1}}\right) - \frac{\mathbf{g}'(\xi)\cdot\mathbf{g}''(\xi)}{\|\mathbf{g}'(\xi)\|^4}\frac{\partial^l\psi^2(\eta,\xi)}{\partial\eta^l}. \tag{3.43c}$$

The next step is to evaluate the l-th order derivatives of ψ, ψ^2 and ψ^3. In order to so, we recall that $\psi(\eta,\xi) = (1+\eta\kappa(\xi))^{-1}$, then by using the geometric series and its derivatives, we obtain

$$\psi(\eta,\xi) = \sum_{j=0}^{\infty}(-1)^j\kappa(\xi)^j\eta^j, \tag{3.44a}$$

$$(\psi(\eta,\xi))^2 = \sum_{j=0}^{\infty}(-1)^j(j+1)\kappa(\xi)^j\eta^j, \tag{3.44b}$$

$$(\psi(\eta,\xi))^3 = \sum_{j=0}^{\infty}(-1)^j\frac{(j+1)(j+2)}{2}\kappa(\xi)^j\eta^j, \tag{3.44c}$$

Then, by considering the coefficients of the Taylor expansion of each function in (3.44), we obtain

$$\frac{\partial^l\psi(0,\xi)}{\partial\eta^l} = (-1)^l l!\kappa(\xi)^l, \tag{3.45a}$$

$$\frac{\partial^l\psi^2(0,\xi)}{\partial\eta^l} = (-1)^l(l+1)!\kappa(\xi)^l, \tag{3.45b}$$

$$\frac{\partial^{l-1}\psi^3(0,\xi)}{\partial\eta^{l-1}} = (-1)^{l-1}\frac{(l+1)!}{2}\kappa(\xi)^{l-1}, \tag{3.45c}$$

$$\frac{\partial^l\psi^3(0,\xi)}{\partial\eta^l} = (-1)^l\frac{(l+2)!}{2}\kappa(\xi)^l. \tag{3.45d}$$

Now, we substitute (3.45) back into (3.43) to obtain the following

$$\frac{\partial^l\rho_0(0,\xi)}{\partial\eta^l} = \frac{(-1)^l(l+1)!\kappa(\xi)^l}{\|\mathbf{g}'(\xi)\|^2}, \tag{3.46a}$$

$$\frac{\partial^l\rho_1(0,\xi)}{\partial\eta^l} = \kappa(\xi)(-1)^l l!\kappa(\xi)^l, \tag{3.46b}$$

$$\frac{\partial^l\rho_2(0,\xi)}{\partial\eta^l} = -\frac{\kappa'(\xi)}{\|\mathbf{g}'(\xi)\|^2}\left(l(-1)^{l-1}\frac{(l+1)!}{2}\kappa(\xi)^{l-1}\right) - \frac{\mathbf{g}'(\xi)\cdot\mathbf{g}''(\xi)}{\|\mathbf{g}'(\xi)\|^4}(-1)^l(l+1)!\kappa(\xi)^l. \tag{3.46c}$$

Note here that all the quantities in (3.46) are simple evaluations of $\mathbf{g}, \kappa$ and κ'. Therefore, the assembly of the matrix $\mathbf{A}$ and the vectors $\mathbf{b}^{(i)}$ can be done efficiently.

Since the construction of the Frenet IFE space relies on solving the linear system (3.35), it is important to study the condition number of the matrix $\mathbf{A}$. In the classical higher-order IFE methods, it was observed [13] that the linear system associated with the IFE space tend to be ill conditioned in cases where interface Γ is close to one of the edges or one of the vertices of the interface element K, which are referred to as s small-cut element in the literature. Possible solutions to this issue were explored in [114], where the authors explored imposing

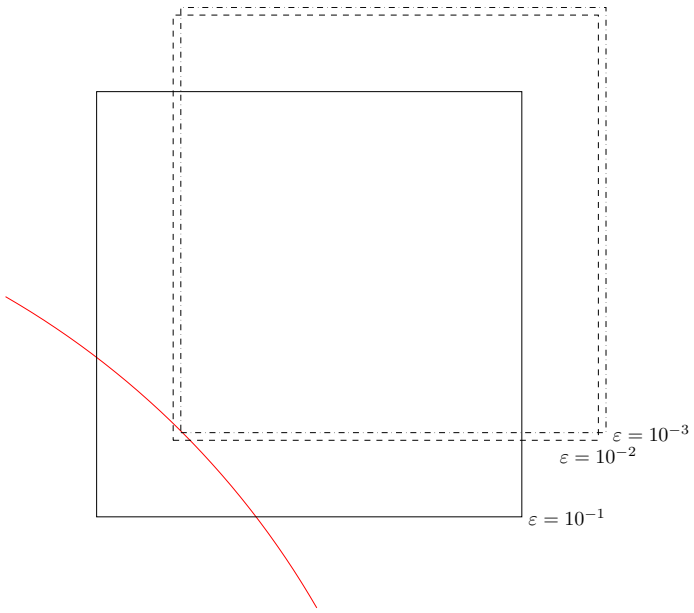

Figure 3.9: An illustration of the small cut element $K(\varepsilon)$ with $\varepsilon = 10^{-1}$ (solid), $\varepsilon = 10^{-2}$ (dashed) and $\varepsilon = 10^{-3}$ (dashed and dotted).

the interface conditions on a larger element, called the fictitious element. The fictitious element is typically a homothetic scaling λ of the interface element K. However, the best choice of the scaling factor λ remains a subject of ongoing research.

In our approach, the fictitious Frenet element $\hat{K}_F$ is defined naturally, with no user-chosen parameters. This has the added advantage that the condition number matrix $\mathbf{A}$ is not affected greatly by the position of the interface. To illustrate this observation, we consider the case where the interface Γ is a circle of radius 1 and the interface element is $K(\varepsilon) = \frac{1}{\sqrt{2}} - \varepsilon + [0, \frac{1}{2}]^2$ for some $\varepsilon > 0$. For an illustration, see Figure 3.9.

To investigate the condition number of IFE system, let $\mathbf{A}(m, \varepsilon)$ be the matrix described in (3.36) and (3.37) with the interface element $K(\varepsilon)$ described above. To construct the IFE basis functions on the element $K(\varepsilon)$, we use the basis $\{p_i(\xi)\}_{i=0}^m = \{L_i(\xi)\}_{i=0}^m$ in (3.33), where L_i is the i-th degree Legendre polynomial on $\hat{\Gamma}_{K_F}$, which makes the matrix $\mathbf{A}(m, \varepsilon)$

block lower triangular because

$$\left(\frac{\partial^k}{\partial \eta^k}\mathscr{L}(\eta^j \xi^i)\right)|_{\eta=0} = 0, \quad \text{if } k > j.$$

Since the terms in (3.46) grows with l, it is beneficial to apply the Jacobi preconditioner $\mathbf{J} = \text{diag}(\mathbf{A}(m,\varepsilon))$ to the matrix $\mathbf{A}(m,\varepsilon)$, and consider the condition number of the preconditioned matrix $\tilde{\mathbf{A}}(m,\varepsilon)$ as well as the original matrix $\mathbf{A}(m,\varepsilon)$ and observe their behaviors as $\varepsilon \to 0^+$ in Figure 3.10. We notice that the condition numbers of $\tilde{\mathbf{A}}(m,\varepsilon)$ is significantly smaller that those of $\mathbf{A}(m,\varepsilon)$, which supports our choice of the preconditioner. Furthermore, we observe that the condition number of both $\mathbf{A}(m,\varepsilon)$ and $\tilde{\mathbf{A}}(m,\varepsilon)$ remains relatively unchanged as the interface approaches the lower left vertex, i.e. as $\varepsilon \to 0^+$, which is an additional benefit of using the Frenet IFE method.

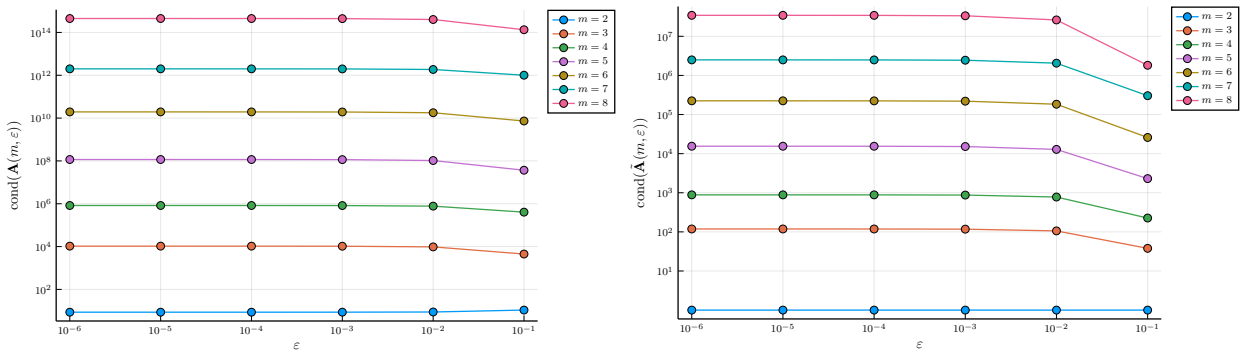

(a) The condition number of $\mathbf{A}(m,\varepsilon)$. (b) The condition number of $\tilde{\mathbf{A}}(m,\varepsilon)$.

Figure 3.10: Condition numbers of $\mathbf{A}(m,\varepsilon)$ and $\tilde{\mathbf{A}}(m,\varepsilon)$ for different degrees m versus ε.

Remark 3.6. The condition numbers reported in Figure 3.10 do not cover the case $m = 1$ because the matrix $\mathbf{A}$ is only needed to construct higher order Frenet IFE functions ($m \geq 2$). In the case of $m = 1$, a basis for $\hat{\mathcal{V}}^1_{\hat{\beta}}(\hat{K}_F)$ is obtained as

$$\hat{\mathcal{V}}^1_{\hat{\beta}}(\hat{K}_F) = \text{span}\left(\left\{1, \xi, \frac{1}{\hat{\beta}}\eta, \frac{1}{\hat{\beta}}\eta\xi\right\}\right). \tag{3.47}$$

To illustrate the idea in this section, we consider the element $K = [0,1]^2$, and the interface $\Gamma = \{(x,y) \in \mathbb{R}^2 \mid x^2 + y^2 = r_0^2\}$ parametrized by $\mathbf{g}(\xi) = (r_0\cos(\xi), r_0\sin(\xi))$, where $r_0 = \frac{1}{\sqrt{2}}$. The interface splits the element into $K^- = \{(x,y) \in \mathbb{R}^2 \mid x^2 + y^2 < r_0^2\}$ and $K^+ = \{(x,y) \in \mathbb{R}^2 \mid x^2 + y^2 > r_0^2\}$. Then, we construct a basis for the second order local Frenet IFE space $\mathcal{V}_\beta^2(K)$ according to Lemma 3.9, (3.31) and (3.30) with $(\beta^-, \beta^+) = (1, 10)$. We plot the resulting basis functions in Figure 3.11, where each sub-figure corresponds to one basis function and the interface is shown in red.

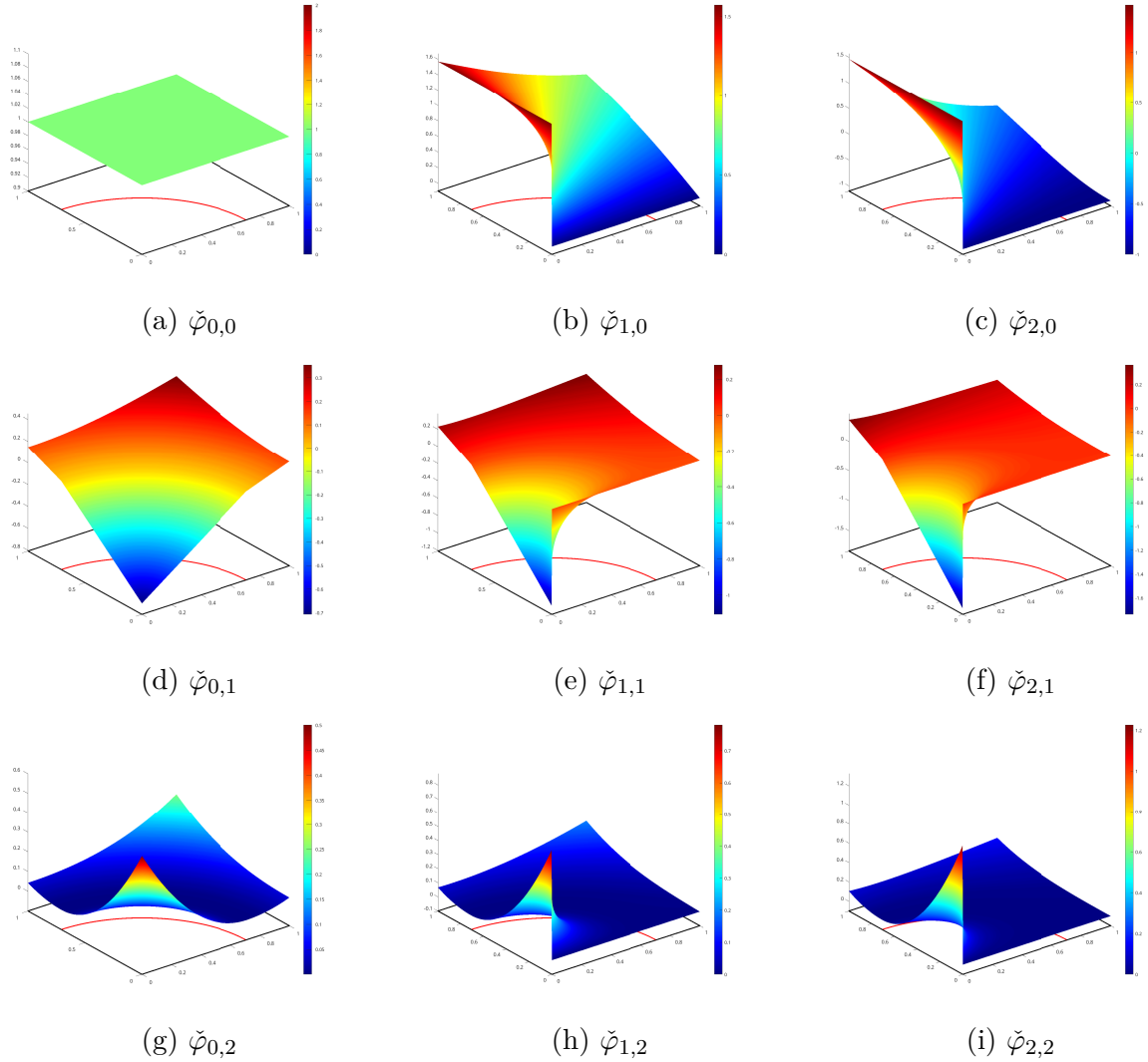

(a) $\check{\varphi}_{0,0}$ (b) $\check{\varphi}_{1,0}$ (c) $\check{\varphi}_{2,0}$

(d) $\check{\varphi}_{0,1}$ (e) $\check{\varphi}_{1,1}$ (f) $\check{\varphi}_{2,1}$

(g) $\check{\varphi}_{0,2}$ (h) $\check{\varphi}_{1,2}$ (i) $\check{\varphi}_{2,2}$

Figure 3.11: An instance of the basis functions for local Frenet IFE space $\mathcal{V}_\beta^2(K)$.

3.5.2 Implementation of the Inverse Frenet Transform

In this subsection, we describe an efficient algorithm to implement the inverse Frenet transformation R on a given interface element.

First, consider an interface element K and let D and E the intersection points of the interface with ∂K, and let $\mathbf{x} \in K$, as shown in Figure 3.12. Our goal is to find $\hat{\mathbf{x}} = (\eta, \xi) \in \hat{K}_F$ such that $P(\hat{\mathbf{x}}) = \mathbf{x}$. Equivalently, $\hat{\mathbf{x}} = R(\mathbf{x})$. To initiate Newton's iteration for solving $P(\hat{\mathbf{x}}) = \mathbf{x}$,

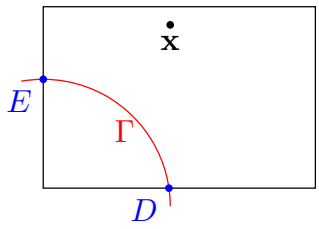

Figure 3.12: The intersections of the interface with ∂K (blue) and a point $\mathbf{x}$ in the interface element (black).

we need a good initial guess for $\hat{\mathbf{x}} = (\eta, \xi)$, namely $\hat{\mathbf{x}}_0 = (\xi_0, \eta_0)$. Naturally, we choose $\eta_0 = 0$ since $\mathbf{x}$ is close to the interface.

Next, consider the points D and E: Since they are on the interface Γ, there are $\xi_D, \xi_E \in [\xi_s, \xi_e]$, such that

$$\mathbf{g}(\xi_D) = D, \qquad \mathbf{g}(\xi_E) = E.$$

To find ξ_D and ξ_E, we perform a line search first. That is, given $\{z_i\}_{i=1}^{n_z} \subset [\xi_s, \xi_e]$, we find z_D such that

$$\|\mathbf{g}(z_D) - D\| = \min_{0 \le i \le n_z} \|\mathbf{g}(z_i) - D\|,$$

and similarly, we obtain z_E. At this point, z_D and z_E are relatively good approximations of ξ_E and ξ_D. To improve this approximation, we recall that ξ_D minimizes $\|\mathbf{g}(\cdot) - D\|^2$. Hence, we can accelerate the process greatly by using the gradient descent method with

Barzilai-Borwein step [23] to speed up the convergence

$$\begin{cases} \xi_D^0 = z_D, \\ \xi_D^1 = \xi_D^0 - \dfrac{\|\mathbf{g}(\xi_D^0) - D\|^2}{2\mathbf{g}'(\xi_D^0)\cdot(\mathbf{g}(\xi_D^0) - D)} \\ \xi_D^{n+1} = \xi_D^n - \gamma_n \dfrac{\|\mathbf{g}(\xi_D^n) - D\|^2}{2\mathbf{g}'(\xi_D^n)\cdot(\mathbf{g}(\xi_D^n) - D)}, \qquad n \geq 1, \end{cases} \tag{3.48a}$$

where γ_n is the Barzilai-Borwein step given by

$$\gamma_n = \left| \frac{\xi_D^{n+1} - \xi_D^n}{2\mathbf{g}'(\xi_D^n)\cdot(2\mathbf{g}'(\xi_D^n) - D) - 2\mathbf{g}'(\xi_D^{n-1})\cdot\left(2\mathbf{g}'(\xi_D^{n-1}) - D\right)} \right|. \tag{3.48b}$$

The iteration (3.48a) with the step (3.48b) converges typically in a few iterations, making it a good choice for our algorithm. Next, we apply a similar iteration to find ξ_E.

After finding ξ_D and ξ_E, we choose $\hat{\mathbf{x}}_0 = \left(0, \frac{1}{2}(\xi_D + \xi_E)\right)$ as an initial guess for $\hat{\mathbf{x}} = R(\mathbf{x})$ and use Newton's iteration to approximate $\hat{\mathbf{x}}$:

$$\hat{\mathbf{x}}_{n+1} = \hat{\mathbf{x}}_n + \hat{J}_P(\hat{\mathbf{x}})^{-1}(\hat{\mathbf{x}}_n - \mathbf{x}), \tag{3.49}$$

where $\hat{J}_P$ is the Jacobian matrix given in Lemma 3.2.

Remark 3.7. On each interface element, we save the initial guess $\left(0, \frac{1}{2}(\xi_D + \xi_E)\right)$ obtained from the iteration (3.48) to compute $R(\mathbf{x})$ for any point $\mathbf{x} \in K$ using (3.49). Thus, we can think of the gradient descent (3.48) as a way to obtain a good initial guess for the Newton iteration (3.49).

3.5.3 Comments about the Quadrature on Interface Elements

In this subsection, we explore the quadrature on both the interface element K and the Frenet element $\hat{K} = R(K)$. Typically, we are interested in evaluating integrals of the form

$$\int_{K^{\pm}} f(\mathbf{x})\, d\mathbf{x},$$

where f is either defined explicitly on $K^{\pm}$ or defined as $f = \hat{f} \circ P$ for some function $\hat{f}$ on $\hat{K}$. In either case, we need to construct a quadrature rule on $K^{\pm}$ then map the nodes to $\hat{K}^{\pm}$ if needed.

To generate a high order quadrature rule on $K^{\pm}$, we have explored two possible approaches:

- The ALGOIM method [94]: In essence, this method only requires access to a level-set function that describes the interface and its gradient. Using the Frenet coordinates, we can view $\mathbf{x} \mapsto \eta(\mathbf{x})$ as a level set function since $\eta|_{\Gamma_{K_F}} = 0$. After that, if needed, we map the quadrature nodes (and weights) to $\hat{K}$. For an illustatration of the quadrature nodes generated by this method, we present an example in Figure 3.13. One of the main benefits of this method is its adaptivity: The method splits the element into rectangles recursively until a certain flatness condition is met [94]. This results in dense set of nodes around the interface and a relatively sparse set of nodes away from the interface as shown in Figure 3.13a.
- The traditional approach: We can split the interface element K into triangles (with possibly curved edges), where each triangle lays in either K^{+} or K^{-}, then we use a high order quadrature method on each triangle. For instance, one can use the classical Gauss-Legendre quadrature nodes on $[0, 1]^2$, then map the nodes to a reference triangle, which are then mapped to a curved triangle as discussed in [88]. The approach carries multiple advantages. First, we can control the number of quadrature points exactly,

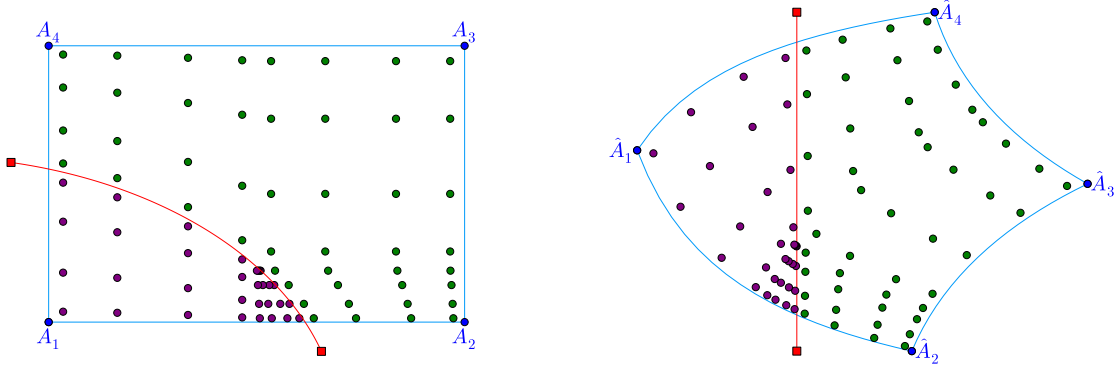

(a) Quadrature nodes on K (b) Quadrature nodes on $\hat{K}$

Figure 3.13: Quadrature nodes on the interface element (left) constructed using the Algoim method, and their images under the inverse Frenet transformation (right).

see for instance Figure 3.14a where each triangle (straight or curved) contains exactly 9 nodes. Additionally, this approach employs the parametrization $\mathbf{g}$ directly and does not require a level set function, and in our experience, this approach is slightly faster.

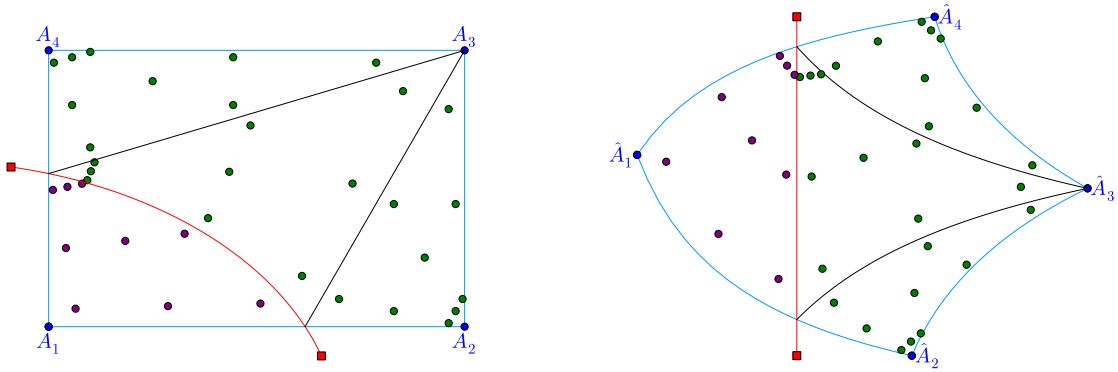

(a) Quadrature nodes on K (b) Quadrature nodes on $\hat{K}$

Figure 3.14: Quadrature nodes on the interface element (left) constructed using the traditional method, and their images under the inverse Frenet transformation (right).

Having said that, in our numerical experiments, we did not observe any noticeable difference between the two approaches. Although, we preferred using the second approach in our implementation, we recognize that the Algoim method might be more suitable for interface

problems in a higher spatial dimension since it can be implemented for any dimension.

Chapter 4

The Approximation Capabilities of the Frenet IFE Space

In this chapter, we investigate the approximation capabilities of the Frenet IFE space introduced in Chapter 3. In Section 4.1, we introduce additional notation for the relevant immersed Sobolev space, further assumptions about the regularity of the interface, and results about the geometry of Frenet elements that will be useful later. In Section 4.2, we present an analysis of the approximation capabilities of the Frenet IFE space. In Section 4.3, we provide numerical examples to illustrate our results.

The results in this chapter are reported partially in [19].

4.1 Notation and Preliminary Results

In addition to the notations used in Chapter 3, we will introduce more notations in this section to simplify our presentation.

First, consider $B \subset \Omega$ cut by the interface into B^+ and B^-. We use $\mathcal{H}^2_{\Gamma,\beta}(B)$ to denote the space of functions $u \in PH^2(B)$ that satisfy the interface conditions (3.1c). More precisely,

$$\mathcal{H}^2_{\Gamma,\beta}(B) = \left\{ u \in PH^2(B) \mid [\![u]\!]_{\Gamma\cap B} = [\![\beta\nabla u \cdot \mathbf{n}]\!]_{\Gamma\cap B} = 0 \right\}. \tag{4.1}$$

Additionally, for $m \geq 2$, we use $\mathcal{H}^{m+1}_{\Gamma,\beta}(B)$ to denote the space of functions $u \in \mathcal{H}^2_{\Gamma,\beta}(B)$ that satisfy the extended interface conditions (3.1d), that is,

$$\mathcal{H}^{m+1}_{\Gamma,\beta}(B) = \left\{ u \in \mathcal{H}^2_{\Gamma,\beta}(B) \cap PH^{m+1}(B) \mid \left[\!\!\left[\beta \frac{\partial^j \Delta u}{\partial \mathbf{n}^j} \right]\!\!\right]_{\Gamma \cap B} = 0,\ j = 0, 1, \dots m-2 \right\}. \quad (4.2)$$

We extend these spaces to piecewise functions on the mesh by defining

$$\mathcal{H}^2_{\Gamma,\beta}(\mathcal{T}_h) = \left\{ u : \Omega \to \mathbb{R} \mid u|_K \in H^2(K) \text{ if } K \in \mathcal{T}_h^n;\ \text{else } u|_K \in \mathcal{H}^2_{\Gamma,\beta}(K) \right\}, \quad (4.3a)$$

and

$$\mathcal{H}^{m+1}_{\Gamma,\beta}(\mathcal{T}_h) = \left\{ u : \Omega \to \mathbb{R} \mid u|_K \in H^{m+1}(K) \text{ if } K \in \mathcal{T}_h^n;\ \text{else } u|_K \in \mathcal{H}^{m+1}_{\Gamma,\beta}(K) \right\}. \quad (4.3b)$$

Now, using the Frenet transformation, we define the immersed Sobolev space on the fictitious Frenet element $\hat{K}_F$ as

$$\mathcal{H}^{m+1}_{\beta}(\hat{K}_F) = \left\{ u \circ P : \hat{K}_F \to \mathbb{R} \mid u \in \mathcal{H}^{m+1}_{\Gamma,\beta}(K_F) \right\}. \quad (4.4)$$

Here we note that we dropped the interface from the notation $\mathcal{H}^{m+1}_{\beta}(\hat{K}_F)$ since $\hat{\Gamma}_{\hat{K}_F}$ is merely the vertical line segment $\eta = 0$ in the middle of $\hat{K}_F$.

Next, we define the global Frenet IFE space as

$$\mathcal{V}^m_{\beta}(\mathcal{T}_h) = \left\{ u : \Omega \to \mathbb{R} \mid u|_K \in Q^m(K) \text{ if } K \in \mathcal{T}_h^n;\ \text{else } u|_K \in \mathcal{V}^m_{\beta}(K) \right\}. \quad (4.5)$$

Following the notation used in Chapter 2, we will use $\lesssim, \gtrsim$ and $\simeq$ to denote inequalities and equivalences with hidden constants. Typically, the hidden constant in this section depends solely on the degree m provided that the assumptions in the next paragraph hold.

In this chapter, we assume that the mesh size h is smaller than ϵ_0 where ϵ_0 is defined in (3.15). Thus,

- Every interface element is contained in the tubular neighborhood N_0 of the interface Γ.
- The inverse Frenet transformation is well-defined and differentiable on the local fictitious element K_F, and

$$|\psi(\eta,\xi)| \simeq 1, \quad \forall (\eta,\xi) \in \hat{K}_F, \quad \forall K \in \mathcal{T}_h^i. \tag{4.6a}$$

The last point is a direct consequence of $h < \frac{1}{2\kappa_0}$ where κ_0 is the maximum curvature of Γ.

Now, to analyze the approximation capabilities of the Frenet IFE space, we restrict ourselves to the case where Γ is a C^{m+2} curve and $\mathbf{g} \in C^{m+2}([\xi_s,\xi_e],\mathbb{R}^2)$ is a regular parametrization. Therefore,

$$\max_{\xi_s \le \xi \le \xi_e} \left\| \mathbf{g}^{(k)}(\xi) \right\| \lesssim 1, \qquad k = 0,\dots,m+2, \tag{4.6b}$$

and

$$\max_{\xi_s \le \xi \le \xi_e} \|\mathbf{g}'(\xi)\|^{-1} \lesssim 1. \tag{4.6c}$$

Then, it follows from (3.4) that $\kappa \in C^m([\xi_s,\xi_e],\mathbb{R})$ and $|\psi(\eta,\xi)| \lesssim 1$ for all $(\eta,\xi) \in \hat{K}_F$, for any interface element K.

Next, let K be an interface element and let $\hat{K}_F$ be its fictitious Frenet element. Then, by construction, $\hat{K}_F$ is a rectangle of the form $[-h,h] \times [\xi_0,\xi_1]$, where ξ_0, ξ_1 are the extrema of $\xi(K)$. In our analysis later, we will employ several inequalities, such as the trace inequality, that involve the size of $\hat{\Gamma}_{K_F}$, which is $\xi_1 - \xi_0$. In general, we are not able to derive a closed form expression for this quantity. Nevertheless, we can show that $\xi_1 - \xi_0$ is comparable to the mesh size h.

Lemma 4.1. *Let K be an interface element, and let $\hat{K}_F$ be the associated fictitious Frenet element, and let $\hat{\Gamma}_K = (\{0\} \times \mathbb{R}) \cap \hat{K}_F$. Then*

$$|\hat{\Gamma}_{K_F}| \simeq h.$$

Proof. First, we recall that h is the diameter of K, then

$$h^2 \simeq \int_K d\mathbf{x} = \int_{\hat{K}} |\hat{D}P(\eta,\xi)| d\eta d\xi \lesssim \int_{\hat{K}} d\eta d\xi \leq \int_{\hat{K}_F} d\eta d\xi = |\hat{\Gamma}_{K_F}| h. \tag{4.7}$$

Then, we divide both sides by h to obtain $h \lesssim |\hat{\Gamma}_{K_F}|$. Next, let $\mathbf{x}_1, \mathbf{x}_2 \in K$, then by the multivariate mean value theorem, we have

$$|\xi(\mathbf{x}_1) - \xi(\mathbf{x}_2)| \leq \left(\max_{\mathbf{x} \in K} \|\nabla \xi(\mathbf{x})\| \right) \|\mathbf{x}_1 - \mathbf{x}_2\| \leq h \left(\max_{\mathbf{x} \in K} \|\nabla \xi(\mathbf{x})\| \right).$$

We recall from (3.16) that $\|\nabla \xi\| = \|\mathbf{g}'(\xi)\|^{-1} |\psi(\eta,\xi)|$. By our assumptions (4.6), we have $\|\mathbf{g}'(\xi)\|^{-1} |\psi(\eta,\xi)| \lesssim 1$. Therefore,

$$|\hat{\Gamma}_{K_F}| = \max_{\mathbf{x}_1, \mathbf{x}_2 \in K} |\xi(\mathbf{x}_1) - \xi(\mathbf{x}_2)| \lesssim h. \tag{4.8}$$

Combining (4.7) and (4.8), we obtain $|\hat{\Gamma}_{K_F}| \simeq h$. □

Now, we show that the local fictitious element K_F intersect a (uniformly) finite number of elements.

Lemma 4.2. *Let K be an interface element and let K_F be its local fictitious element, then K_F intersects at most 7^2 elements in $\mathcal{T}_h$.*

Proof. Let $\mathbf{x} \in K_F$, then $\mathbf{x} = \mathbf{g}(\xi) + \eta \mathbf{n}(\xi)$ for some $\eta \in [-h, h]$ and $\xi \in [\xi_0, \xi_1]$. By construction of K_F, there is $\tilde{\eta} \in [-h, h]$ such that $\mathbf{y} = \mathbf{g}(\xi) + \tilde{\eta} \mathbf{n}(\xi) \in K$. Then, $\|\mathbf{x} - \mathbf{y}\| =$

$|\eta - \tilde{\eta}| \leq 2h$. In conclusion, we have $K_F \subset K + \overline{B}(\mathbf{0}, 2h)$.

Next, let ω_K be the union of the 7^2 elements surrounding K (including K) as shown in Figure 4.1. Then $K + \overline{B}(\mathbf{0}, 2h) \subset \omega_K$. Consequently, K_F intersects at most 7^2 elements.

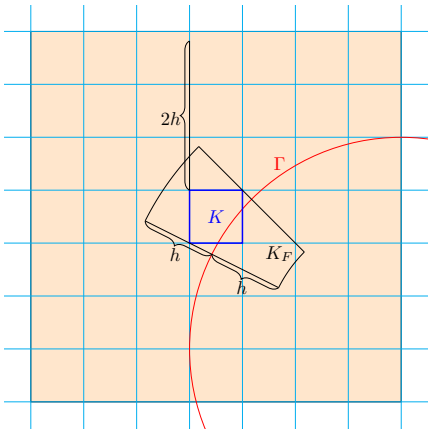

Figure 4.1: An illustration interface element K (blue) and its fictitious element K_F (black). Note the fictitious element is contained in the 7^2 elements highlighted in orange.

□

4.2 Approximation Capabilities

In this section, we prove the optimal approximate capabilities of the Frenet IFE space. First, we consider a function $\hat{u} \in \mathcal{H}_\beta^{m+1}(\hat{K}_F)$, and we show that its L^2 projection $\hat{\Pi}\hat{u} \in \hat{\mathcal{V}}_{\hat{\beta}}^m(\hat{K}_F)$ satisfies

$$\left|\hat{u} - \hat{\Pi}\hat{u}\right|_{i,\hat{K}_F} \lesssim_m h^{m+1-i} |\hat{u}|_{m+1,\hat{K}_F}, \qquad i = 0, 1, \ldots, m+1. \tag{4.9}$$

It is worth highlighting here that the hidden constants in the inequality (4.9) are independent of the diffusion coefficient β. This is yet another attractive property that the Frenet IFE space possesses.

The ideas in our analysis below are inspired in part by the analysis carried in [51]. More

precisely, we proceed by projecting $\hat{u}$ on $Q^m(\hat{K}_F^+)$ and on $Q^m(\hat{K}_F^-)$ separately. Then, we show that these two projections satisfy the interface conditions (3.25) approximately, which will be enough for us to prove (4.9). The proofs in this section are adapted from our paper [19] with minor modifications to the notation, and an additional theorem at the end covering the global projection error.

In the remainder of this section, we assume, without loss of generality, that $\hat{K}_F^+ = [0, h] \times [\xi_0, \xi_1]$ and $\hat{K}_F^- = [-h, 0] \times [\xi_0, \xi_1]$ to avoid any confusion, and we use $\hat{u}^\pm$ to denote $\hat{u}|_{\hat{K}_F^\pm}$ as usual.

Now, Let $s \in \{+, -\}$ and let $\hat{\Pi}^s : H^{m+1}(\hat{K}_F^s) \to Q^m(\hat{K}_F^s)$ be the L^2 projection, that is, for $u^s \in H^{m+1}(\hat{K}_F^s)$, $\hat{\Pi}^s u^s \in Q^m(\hat{K}_F^s)$ is the unique solution to

$$\left(\hat{\Pi}^s u^s, v_h\right)_{\hat{K}_F^s} = (u^s, v_h)_{\hat{K}_F^s}, \qquad \forall v_h \in Q^m(\hat{K}_F^s).$$

It is well known [37] that the L^2 projection converges optimally as stated in the following lemma.

Lemma 4.3. *Let $s \in \{+, -\}$ and let $\hat{u}^s \in H^{m+1}(\hat{K}_F^s)$, then*

$$\left|\hat{\Pi}^s \hat{u}^s - \hat{u}^s\right|_{i, \hat{K}_F^s} \lesssim_m h^{m+1-i} |\hat{u}^s|_{m+1, \hat{K}_F^s}. \tag{4.10}$$

For all integers $0 \le i \le m+1$.

Now, since the dimensions of $\hat{K}_F^\pm$ are comparable to h as shown in Lemma 4.1, the classical trace inequality holds on $H^1(\hat{K}_F^s)$ as expressed in the following lemma.

Lemma 4.4. *Let $s \in \{+, -\}$ and let $\hat{u}^s \in H^1(\hat{K}_F^s)$, then*

$$\|\hat{u}^s\|_{0, \hat{\Gamma}_{K_F}} \lesssim_m h^{-1/2} \|\hat{u}^s\|_{\hat{K}_F^s} + h^{1/2} |\hat{u}^s|_{1, \hat{K}_F^s}. \tag{4.11}$$

Next, we combine Lemma 4.3 and Lemma 4.4 to obtain an estimate on the projection error on $\hat{\Gamma}_{K_F}$.

Corollary 4.1. *Let $s \in \{+,-\}$ and let $\hat{u}^s \in H^{m+1}(\hat{K}_F^s)$, then*

$$\left|\hat{\Pi}^s\hat{u}^s - \hat{u}^s\right|_{i,\hat{\Gamma}_{K_F}} \lesssim_m h^{m+\frac{1}{2}-i}|\hat{u}^s|_{m+1,\hat{K}_F^s}, \tag{4.12}$$

for all integers $i = 0,\dots,m$.

Proof. Using (4.11), we have

$$\left|\hat{\Pi}^s\hat{u}^s - \hat{u}^s\right|_{i,\hat{\Gamma}_{K_F}} \lesssim_m h^{-1/2}\left|\hat{\Pi}^s\hat{u}^s - \hat{u}^s\right|_{i,\hat{K}_F^s} + h^{1/2}\left|\hat{\Pi}^s\hat{u}^s - \hat{u}^s\right|_{i+1,\hat{K}_F^s},$$

which is combined with (4.10) to obtain (4.12). □

Next, we will use Corollary 4.1 to obtain some estimates on the Laplacian of the residual $\hat{\Pi}^s\hat{u}^s - \hat{u}^s$ on $\hat{\Gamma}_{K_F}$.

Lemma 4.5. *Let $s \in \{+,-\}$ and let $\hat{u}^s \in H^{m+1}(\hat{K}_F^s)$, then*

$$\left\|\frac{\partial^j}{\partial\eta^j}\mathscr{L}(\hat{\Pi}^s\hat{u}^s - \hat{u}^s)\right\|_{0,\hat{\Gamma}_{K_F}} \lesssim_m h^{m+\frac{1}{2}-2-j}|\hat{u}^s|_{m+1,\hat{K}_F^s}, \tag{4.13}$$

for all integers $j = 0,1,\dots,m-2$.

Proof. Recall that from our assumptions (4.6), we have $\|\mathbf{g}'\| \simeq 1$ and $\|\mathbf{g}'\|, \|\mathbf{g}''\|, |\kappa|, |\kappa'| \lesssim 1$. Therefore, it follows immediately from (3.22) that

$$\left|\frac{\partial^l\rho_i}{\partial\eta^l}(0,\xi)\right| \lesssim_m 1, \qquad \forall\xi \in \hat{\Gamma}_{K_F}, \quad 0 \le l \le m-2, \quad 0 \le i \le 2. \tag{4.14}$$

Now, we use (3.28) and Corollary 4.1 to obtain

$$\left\|\frac{\partial^j}{\partial\eta^j}\mathscr{L}(\hat{\Pi}^s\hat{u}^s-\hat{u}^s)\right\|_{0,\hat{\Gamma}_{K_F}}\underset{m}{\lesssim}\left\|\hat{\Pi}^s\hat{u}^s-\hat{u}^s\right\|_{j+2,\hat{\Gamma}_{K_F}}\underset{m}{\lesssim}h^{m+1/2-2-j}|\hat{u}^s|_{m+1,\hat{K}_F^s}. \qquad \square$$

We now consider a function $\hat{u}$ that satisfies the interface conditions (3.24), and we estimate the discontinuities across the Frenet fictitious interface $\hat{\Gamma}_{K_F}$ for its projection $\hat{\Pi}^{\pm}\hat{u}^{\pm}$ in the following lemma.

Lemma 4.6. *Let $\hat{u}\in\mathcal{H}_\beta^{m+1}(\hat{K}_F)$ be a function that satisfies (3.24) and let $\hat{\Pi}^s\hat{u}^s$ be the L^2 projections of $\hat{u}^s$ onto $Q^m(\hat{K}_F^s)$ for $s\in\{+,-\}$. Then*

$$\left\|\hat{\Pi}^+\hat{u}^+-\hat{\Pi}^-\hat{u}^-\right\|_{0,\hat{\Gamma}_{K_F}}\underset{m}{\lesssim}h^{m+\frac{1}{2}}|\hat{u}^+|_{m+1,\hat{K}_F}, \tag{4.15a}$$

$$\left\|\beta^+(\hat{\Pi}^+\hat{u}^+)_\eta-\beta^-(\hat{\Pi}^-\hat{u}^-)_\eta\right\|_{0,\hat{\Gamma}_{K_F}}\underset{m}{\lesssim}(\beta^++\beta^-)h^{m-\frac{1}{2}}|\hat{u}^+|_{m+1,\hat{K}_F}, \tag{4.15b}$$

$$\left\|\beta^+\frac{\partial^j}{\partial\eta^j}\mathscr{L}(\hat{\Pi}^+\hat{u}^+)-\beta^-\frac{\partial^j}{\partial\eta^j}\mathscr{L}(\hat{\Pi}^-\hat{u}^-)\right\|_{0,\hat{\Gamma}_{K_F}}\underset{m}{\lesssim}(\beta^++\beta^-)h^{m-\frac{3}{2}-j}|\hat{u}^+|_{m+1,\hat{K}_F}, \tag{4.15c}$$

for $j=0,1,\dots m-2$.

Proof. The first estimate follows from applying the triangle inequality to Corollary 4.1:

$$\begin{aligned}\left\|\hat{\Pi}^+\hat{u}^+-\hat{\Pi}^-\hat{u}^-\right\|_{0,\hat{\Gamma}_{K_F}}&\le\left\|\hat{\Pi}^+\hat{u}^+-\hat{u}^+\right\|_{0,\hat{\Gamma}_{K_F}}+\left\|\hat{\Pi}^-\hat{u}^--\hat{u}^-\right\|_{0,\hat{\Gamma}_{K_F}}+\underbrace{\left\|\hat{u}^+-\hat{u}^-\right\|_{0,\hat{\Gamma}_{K_F}}}_{=0}\\&\underset{m}{\lesssim}h^{m+\frac{1}{2}}|\hat{u}^+|_{m+1,\hat{K}_F^+}+h^{m+\frac{1}{2}}|\hat{u}^-|_{m+1,\hat{K}_F^-},\end{aligned}$$

where we used $\hat{u}^+ = \hat{u}^-$ on $\hat{\Gamma}_{K_F}$. We can prove the second estimate similarly:

$$\begin{aligned}\left\|\beta^+(\hat{\Pi}^+\hat{u}^+)_\eta - \beta^-(\hat{\Pi}^-\hat{u}^-)_\eta\right\|_{0,\hat{\Gamma}_{K_F}} &\le \beta^+\left\|(\hat{\Pi}^+\hat{u}^+ - \hat{u}^+)_\eta\right\|_{0,\hat{\Gamma}_{K_F}} + \beta^-\left\|(\hat{\Pi}^-\hat{u}^+ - \hat{u}^-)_\eta\right\|_{0,\hat{\Gamma}_{K_F}} \\ &\quad + \underbrace{\left\|\beta^+\hat{u}^+_\eta - \beta^-\hat{u}^-_\eta\right\|_{0,\hat{\Gamma}_{K_F}}}_{=0} \\ &\lesssim_m \beta^+ h^{m-\frac{1}{2}}|\hat{u}^+|_{m+1,\hat{K}_F^+} + \beta^- h^{m-\frac{1}{2}}|\hat{u}^-|_{m+1,\hat{K}_F^-}.\end{aligned}$$

The proof of the last estimate is similar and uses Lemma 4.5. □

We have shown in Lemma 3.8 that for $s \in \{+,-\}$ and a polynomial $q^s \in Q^m(\hat{K}_F^s)$, there is a unique polynomial $q^{s'} \in Q^m(\hat{K}_F^{s'})$, where s' is the dual of s, such that $q = q^+\chi_{\hat{K}_F^+} + q^-\chi_{\hat{K}_F^-} \in \hat{\mathcal{V}}^m_{\hat{\beta}}(\hat{K}_F)$, where χ is the indicator function. For simplicity, we will use (q^-, q^+) to denote $q \in \hat{\mathcal{V}}^m_{\hat{\beta}}(\hat{K}_F)$. Next, we define $\mathcal{E}^s : Q^m(\hat{K}_F^{s'}) \to Q^m(\hat{K}_F^s)$ to be the unique mappings such that

$$(q^-, \mathcal{E}^+(q^-)) \in \hat{\mathcal{V}}^m_{\hat{\beta}}(\hat{K}_F), \quad (\mathcal{E}^-(q^+), q^+) \in \hat{\mathcal{V}}^m_{\hat{\beta}}(\hat{K}_F), \quad \forall q^- \in Q^m(\hat{K}_F^-) \text{ and } \forall q^+ \in Q^m(\hat{K}_F^+).$$

According to Lemma 3.8, the mappings $\mathcal{E}^s$ for $s \in \{+,-\}$ are well-defined. Furthermore, they are linear. The next lemma shows that $\hat{\Pi}^s\hat{u}^s$ and $\mathcal{E}^s(\hat{\Pi}^{s'}\hat{u}^{s'})$ are close to each other on $\hat{\Gamma}_{K_F}$.

Lemma 4.7. *Let $\hat{u} \in \mathcal{H}^{m+1}_\beta(\hat{K}_F)$ be a function that satisfies (3.24), then*

$$\left\|\frac{\partial^j}{\partial\eta^j}\left(\hat{\Pi}^s\hat{u}^s - \mathcal{E}^s(\hat{\Pi}^{s'}\hat{u}^{s'})\right)\right\|_{0,\hat{\Gamma}_{K_F}} \lesssim_m \left(1 + \frac{\beta^{s'}}{\beta^s}\right) h^{m+\frac{1}{2}-j}|\hat{u}|_{m+1,\hat{K}_F}, \tag{4.16}$$

for all $j = 0, 2, \ldots, m$ and $s \in \{+,-\}$.

Proof. Without loss of generality, we will only consider the case $s = +$. To prove (4.16) for

$j=0$, we recall that $\mathcal{E}^+(\hat{\Pi}^-\hat{u}^-)=\hat{\Pi}^-\hat{u}^-$ on $\hat{\Gamma}_{K_F}$, Therefore, by (4.15a), we have

$$\left\|\hat{\Pi}^+\hat{u}^+-\mathcal{E}^+(\hat{\Pi}^-\hat{u}^-)\right\|_{0,\hat{\Gamma}_{K_F}}=\left\|\hat{\Pi}^+\hat{u}^+-\hat{\Pi}^-\hat{u}^-\right\|_{0,\hat{\Gamma}_{K_F}}\lesssim_m h^{m+\frac{1}{2}}|\hat{u}|_{m+1,\hat{K}_F}.$$

Similarly, we have $\beta^+\frac{\partial}{\partial\eta}\mathcal{E}^+(\hat{\Pi}^-\hat{u}^-)=\beta^-\frac{\partial}{\partial\eta}(\hat{\Pi}^-\hat{u}^-)$ on $\hat{\Gamma}_{K_F}$. Hence, we can use (4.15b) to obtain

$$\begin{aligned}\left\|\frac{\partial}{\partial\eta}\left(\beta^+\hat{\Pi}^+\hat{u}^+-\beta^+\mathcal{E}^+(\hat{\Pi}^-\hat{u}^-)\right)\right\|_{0,\hat{\Gamma}_{K_F}}&=\left\|\frac{\partial}{\partial\eta}\left(\beta^+\hat{\Pi}^+\hat{u}^+-\beta^-\hat{\Pi}^-\hat{u}^-\right)\right\|_{0,\hat{\Gamma}_{K_F}}\\&\lesssim_m(\beta^++\beta^-)h^{m+\frac{1}{2}-1}|\hat{u}|_{m+1,\hat{K}_F},\end{aligned}\tag{4.17}$$

which implies (4.16) for $j=1$. Next, we prove (4.16) for $2\le j\le m$ using strong induction. We assume that (4.16) holds for $j=0,1,\dots,i_0$, where $1\le i_0\le m$, then we prove it for $j=i_0+1$.

To avoid lengthy expressions, we will use w to denote $\hat{\Pi}^+\hat{u}^+-\mathcal{E}^+(\hat{\Pi}^-\hat{u}^-)$. Hence, our induction hypothesis can be written as

$$\left\|\frac{\partial^j}{\partial\eta^j}w\right\|_{0,\hat{\Gamma}_{K_F}}\lesssim_m\left(1+\frac{\beta^-}{\beta^+}\right)h^{m+\frac{1}{2}-j}|\hat{u}|_{m+1,\hat{K}_F},\qquad j=0,1,\dots,i_0.\tag{4.18}$$

Since $w|_{\hat{\Gamma}_{K_F}}\in\mathcal{P}^m(\hat{\Gamma}_{K_F})$, we can use the classical 1D inverse inequality on polynomials [37] to obtain

$$\left\|\frac{\partial^{i+j}}{\partial\xi^i\partial\eta^j}w\right\|_{0,\hat{\Gamma}_{K_F}}\lesssim_m\left(1+\frac{\beta^-}{\beta^+}\right)h^{m+\frac{1}{2}-j-i}|\hat{u}|_{m+1,\hat{K}_F},\qquad j=0,1,\dots,i_0,\quad 1\le i\le m.\tag{4.19}$$

Now, we recall that (3.25b) with $j=i_0-1$ yields

$$\int_{\hat{\Gamma}_{K_F}}\beta^+\frac{\partial^{i_0-1}}{\partial\eta^{i_0-1}}\mathscr{L}(\mathcal{E}^+(\hat{\Pi}^-\hat{u}^-))v=\int_{\hat{\Gamma}_{K_F}}\beta^-\frac{\partial^{i_0-1}}{\partial\eta^{i_0-1}}\mathscr{L}(\hat{\Pi}^-\hat{u}^-)v,\qquad\forall v\in\mathcal{P}^m(\hat{\Gamma}_{K_F}).$$

Therefore, for any $v \in \mathcal{P}^m(\hat{\Gamma}_{K_F})$, we have

$$\begin{aligned}\int_{\hat{\Gamma}_{K_F}} \beta^+ \frac{\partial^{i_0-1}}{\partial \eta^{i_0-1}} \mathscr{L}(w) v &= \int_{\hat{\Gamma}_{K_F}} \beta^+ \frac{\partial^{i_0-1}}{\partial \eta^{i_0-1}} \mathscr{L}(\hat{\Pi}^+ \hat{u}^+) v - \beta^+ \frac{\partial^{i_0-1}}{\partial \eta^{i_0-1}} \mathscr{L}(\mathcal{E}^+(\hat{\Pi}^- \hat{u}^-)) v \\ &= \int_{\hat{\Gamma}_{K_F}} \left(\beta^+ \frac{\partial^{i_0-1}}{\partial \eta^{i_0-1}} \mathscr{L}(\hat{\Pi}^+ \hat{u}^+) - \beta^- \frac{\partial^{i_0-1}}{\partial \eta^{i_0-1}} \mathscr{L}(\hat{\Pi}^- \hat{u}^-) \right) v\end{aligned}$$

We apply Cauchy-Schwarz inequality and use (4.15c) to obtain

$$\begin{aligned}\left| \int_{\hat{\Gamma}_{K_F}} \beta^+ \frac{\partial^{i_0-1}}{\partial \eta^{i_0-1}} \mathscr{L}(w) v \right| &\leq \|v\|_{0,\hat{\Gamma}_{K_F}} \left\| \beta^+ \frac{\partial^{i_0-1}}{\partial \eta^{i_0-1}} \mathscr{L}(\hat{\Pi}^+ \hat{u}^+) - \frac{\partial^{i_0-1}}{\partial \eta^{i_0-1}} \beta^- \mathscr{L}(\hat{\Pi}^- \hat{u}^-) \right\|_{0,\hat{\Gamma}_{K_F}} \\ &\underset{m}{\lesssim} \|v\|_{0,\hat{\Gamma}_{K_F}} (\beta^+ + \beta^-) h^{m+1/2-i_0-1} |\hat{u}|_{m+1,\hat{K}_F}, \end{aligned} \tag{4.20}$$

Next, we combine (4.14), (3.28) and the triangle inequality to obtain

$$\left\| \frac{\partial^{i_0-1}}{\partial \eta^{i_0-1}} \mathscr{L}(w) - \frac{\partial^{i_0+1}}{\partial \eta^{i_0+1}} w \right\|_{0,\hat{\Gamma}_{K_F}} \underset{m}{\lesssim} \sum_{j=0}^{i_0} \sum_{i=0}^{i_0-j+1} \left\| \frac{\partial^{j+i}}{\partial \xi^i \partial \eta^j} w \right\|_{0,\hat{\Gamma}_{K_F}} \underset{m}{\lesssim} \left(1 + \frac{\beta^-}{\beta^+} \right) h^{m+\frac{1}{2}-i_0-1} |\hat{u}|_{m+1,\hat{K}_F}, \tag{4.21}$$

where the last inequality follows from (4.19). Then, by (4.20), (4.21) and Cauchy Schwarz inequality

$$\begin{aligned}\left| \int_{\hat{\Gamma}_{K_F}} \frac{\partial^{i_0+1} w}{\partial \eta^{i_0+1}} v \right| &\leq \left| \int_{\hat{\Gamma}_{K_F}} \left(\frac{\partial^{i_0-1}}{\partial \eta^{i_0-1}} \mathscr{L}(w) - \frac{\partial^{i_0+1}}{\partial \eta^{i_0+1}} w \right) v \right| + \left| \int_{\hat{\Gamma}_{K_F}} \frac{\partial^{i_0-1}}{\partial \eta^{i_0-1}} \mathscr{L}(w) v \right|, \\ &\underset{m}{\lesssim} \|v\|_{0,\hat{\Gamma}_{K_F}} \left(1 + \frac{\beta^-}{\beta^+} \right) h^{m+1/2-i_0-1} |\hat{u}|_{m+1,\hat{K}_F}.\end{aligned}$$

Finally, we replace v with $\frac{\partial^{i_0+1} w}{\partial \eta^{i_0+1}}(0,\cdot)$, to get

$$\left\| \frac{\partial^{i_0+1} w}{\partial \eta^{i_0+1}} \right\|_{0,\hat{\Gamma}_{K_F}} \lesssim_m \left(1+\frac{\beta^-}{\beta^+}\right) h^{m+1/2-i_0-1} |\hat{u}|_{m+1,\hat{K}_F},$$

which proves (4.16) for $j = i_0 + 1$. □

Lemma 4.8. *Let $\hat{u} \in \mathcal{H}^{m+1}_\beta(\hat{K}_F)$ be a function that satisfies (3.24) and let $s \in \{+,-\}$, then*

$$\left| \hat{\Pi}^s \hat{u}^s - \mathcal{E}^s(\hat{\Pi}^{s'} \hat{u}^{s'}) \right|_{i,\hat{K}_F^s} \lesssim_m \left(1+\frac{\beta^{s'}}{\beta^s}\right) h^{m+1-i} |\hat{u}|_{m+1,\hat{K}_F}, \tag{4.22}$$

for $i = 0, 1, \ldots, m+1$.

Proof. As before, we will restrict our proof to the case $s = +$,and we let $w = \hat{\Pi}^+ \hat{u}^+ - \mathcal{E}^+(\hat{\Pi}^- \hat{u}^-)$. Since $w \in Q^m(\hat{K}_F^+)$, we have for any $(\eta, \xi) \in \hat{K}_F^+$

$$w(\eta,\xi) = \sum_{j=0}^{m} \frac{\eta^j}{j!} \frac{\partial^j w}{\partial \eta^j}(0,\xi).$$

By taking the (k,l) derivative of w, we obtain

$$\frac{\partial^{k+l} w}{\partial \eta^k \partial \xi^l}(\eta,\xi) = \sum_{j=k}^{m} \frac{\eta^{j-k}}{(j-k)!} \frac{\partial^{j+l} w}{\partial \eta^j \partial \xi^l}(0,\xi).$$

Then, we take the norm and use the triangle inequality on the right-hand side

$$\begin{aligned}
\left\| \frac{\partial^{k+l} w}{\partial \eta^k \partial \xi^l} \right\|_{0,\hat{K}_F^+} &\lesssim_m \sum_{j=0}^{m} \left(\int_0^h \eta^{2(j-k)} d\eta \right)^{1/2} \left\| \frac{\partial^{j+l} w}{\partial \eta^j \partial \xi^l} \right\|_{0,\hat{\Gamma}_{K_F}} \\
&\lesssim_m \sum_{j=0}^{m} h^{j-k+1/2} \left\| \frac{\partial^{j+l} w}{\partial \eta^j \partial \xi^l} \right\|_{0,\hat{\Gamma}_{K_F}} \lesssim_m \sum_{j=0}^{m} h^{j-k-l+1/2} \left\| \frac{\partial^j w}{\partial \eta^j} \right\|_{0,\hat{\Gamma}_{K_F}},
\end{aligned}$$

where the last inequality follows from the one-dimensional inverse inequality for polynomials [37]. Now, we apply Lemma 4.7 to the right-hand side

$$\left\| \frac{\partial^{k+l} w}{\partial \eta^k \partial \xi^l} \right\|_{0,\hat{K}_F^+} \underset{m}{\lesssim} \sum_{j=k}^{m} h^{j-k-l+1/2} . h^{m+1/2-j} \left(1 + \frac{\beta^-}{\beta^+}\right) |\hat{u}|_{m+1,\hat{K}_F} = \left(1 + \frac{\beta^-}{\beta^+}\right) h^{m+1-l-k} |\hat{u}|_{m+1,\hat{K}_F}.$$

Finally, (4.16) follows from the sum of the estimate above over all non-negative integers $k + l = i$. □

At this point, we are ready to state our first result on the approximation capabilities of the proposed IFE space. For simplicity, we will use $\hat{\Pi}\hat{u}$ to denote the L^2 projection of a function $\hat{u} \in L^2(\hat{K}_F)$ onto $\hat{\mathcal{V}}_{\hat{\beta}}^m(\hat{K}_F)$.

Theorem 4.1. *Let $\hat{u} \in \mathcal{H}_{\beta}^{m+1}(\hat{K}_F)$ be a function that satisfies (3.24), then*

$$\left\| \hat{\Pi}\hat{u} - \hat{u} \right\|_{0,\hat{K}_F} \underset{m}{\lesssim} h^{m+1} |\hat{u}|_{m+1,\hat{K}_F}, \tag{4.23}$$

Proof. Without loss of generality, we assume that $\beta^+ \geq \beta^-$, then by (4.10) and (4.22), we have

$$\left\| \hat{u}^+ - \mathcal{E}^+(\hat{\Pi}^- \hat{u}^-) \right\|_{0,\hat{K}_F^+} \underset{m}{\lesssim} h^{m+1} |\hat{u}|_{m+1,\hat{K}_F}.$$

Therefore, by choosing $q = (\hat{\Pi}^- \hat{u}^-, \mathcal{E}^+(\hat{\Pi}^- \hat{u}^-))$ and using (4.10), we get

$$\|q - \hat{u}\|_{0,\hat{K}_F} \underset{m}{\lesssim} h^{m+1} |\hat{u}|_{m+1,\hat{K}_F}.$$

Since $\left\| \hat{\Pi}\hat{u} - \hat{u} \right\|_{0,\hat{K}_F} \leq \|q - \hat{u}\|_{0,\hat{K}_F}$, we obtain (4.23). □

So far, we have investigated the approximation capabilities of the IFE space on $\hat{K}_F$. In the

next step, we will use the mappings P and R to derive error bounds for the L^2 projection of a function u that satisfies the jump conditions (3.1c) and (3.1d). For that we essentially follow the ideas in [115], where an analysis of an isoparametric finite element method was discussed. Nevertheless, we will show the details for the sake of completeness. First, we define the projection operator $\Pi : L^2(K_F) \to \mathcal{V}_\beta^m(K_F)$ using $\hat{\Pi}$ in the following way

$$\Pi u = (\hat{\Pi}\hat{u}) \circ R, \qquad \hat{u} = u \circ P. \tag{4.24}$$

Theorem 4.2. *Let $u \in \mathcal{H}_{\Gamma,\beta}^{m+1}(K_F)$, then*

$$\|\Pi u - u\|_{0,K_F} \leq h^{m+1} \|u\|_{m+1,K_F}, \qquad 0 \leq i \leq m+1.$$

Proof. We recall that $\mathbf{g} \in C^{m+2}([\xi_s, \xi_e])$ and $h\kappa_\Gamma \leq \frac{1}{2}$. This implies that $P, R \in C^{m+1}([\xi_s, \xi_e])$ and

$$\max_{\hat{K}_F} \left\| \frac{\partial^{k+l} P}{\partial \eta^k \partial \xi^l} \right\| \lesssim_m 1, \qquad \max_{K_F} \left\| \frac{\partial^{k+l} R}{\partial x^k \partial y^l} \right\| \lesssim 1, \tag{4.25}$$

where $0 \leq k, l \leq m+1$. Now, we use (4.24) to obtain

$$\|\Pi u - u\|_{0,K_F} = \left\| \left(\hat{\Pi}\hat{u} - \hat{u} \right) \circ R \right\|_{0,K_F}.$$

The change of variables P, the inequality $|\hat{D}P| \lesssim 1$ and Theorem 4.1 leads to

$$\|\Pi u - u\|_{0,K_F} \lesssim_m \left\| \hat{\Pi}\hat{u} - \hat{u} \right\|_{0,\hat{K}_F} \lesssim_m h^{m+1} |\hat{u}|_{m+1,\hat{K}_F}. \tag{4.26}$$

Now, to relate the right-hand side to u, we recall that $\hat{u} = u \circ P$. Therefore, applying the

chain rule $m+1$ times yields

$$\left|\frac{\partial^{m+1}\hat{u}}{\partial\eta^j\partial\xi^{m+1-j}}(\eta,\xi)\right| \leq \left(\sum_{l,k=0}^{m+1}\max_{\hat{K}_F}\left\|\frac{\partial^{k+l}P}{\partial\eta^k\partial\xi^l}\right\|\right)\left(\sum_{k,l=0}^{m+1}\left|\frac{\partial^{k+l}u}{\partial x^k\partial y^l}\left(P(\eta,\xi)\right)\right|\right).$$

Finally, we take the L^2 norm of both sides and use the change of variables R

$$|\hat{u}|_{m+1,\hat{K}_F} \lesssim \|u\|_{m+1,K_F},$$

which, when substituted into (4.26), completes the proof. □

Unlike the traditional finite element approximation results, our estimate in Theorem 4.2 involves the $m+1$ norm, rather than the $m+1$ semi-norm. This is due to the non-linearity of the Frenet transformation. Hence, we should not expect the L^2 projection to be exact if u is a polynomial. Nevertheless, this is not an issue since interface problems have piecewise polynomial solutions only if the interface is an algebraic curve, the boundary data is a piecewise polynomial, and the source term is a piecewise polynomial as well, which is rarely the case. For example, see Example 5.2 where the interface and the boundary conditions are designed such that the solution is a piecewise polynomial function.

To finish this section, we consider Theorem 4.2 on all interface elements, and use Lemma 4.2 to obtain the following approximation result on the whole mesh $\mathcal{T}_h$.

Theorem 4.3. *Let $u \in \mathcal{H}^{m+1}_{\Gamma,\beta}(\mathcal{T}_h)$ and let $P_h u \in \mathcal{V}^m_\beta(\mathcal{T}_h)$ be its L^2 projection, then*

$$\|u - P_h u\|_{0,\Omega} \underset{m}{\lesssim} h^{m+1}\|u\|_{m+1,\Omega}. \tag{4.27}$$

Proof. For any non-interface element K, we have $u \in H^{m+1}(K)$. Hence, by [37],

$$\sum_{K\in\mathcal{T}_h^n} \|u - P_h u\|_{0,K} \lesssim_m h^{m+1} \sum_{K\in\mathcal{T}_h^n} |u|_{m+1,K}. \tag{4.28}$$

On the other hand, Theorem 4.2 combined with Lemma 4.2 us that

$$\begin{aligned}\sum_{K\in\mathcal{T}_h^i} \|u - P_h u\|_{0,K} &\lesssim_m \sum_{K\in\mathcal{T}_h^i} \|u - P_h u\|_{0,K_F} \\ &\lesssim_m h^{m+1} \sum_{K\in\mathcal{T}_h^i} \|u\|_{m+1,K_F} \\ &\lesssim_m h^{m+1} \sum_{K\in\mathcal{T}_h^i} \|u\|_{m+1,K}\,.\end{aligned} \tag{4.29}$$

Finally, we combine (4.28) and (4.29) to obtain (4.27). □

4.3 Numerical Examples

To illustrate the results of the previous section, we propose two numerical examples. In both examples, we present the L^2 projection errors for different degrees $m = 1, 2, 3, 4$, and for different contrast ratios $\beta^+/\beta^- = 10, 100, 1000$. Here, the mesh $\mathcal{T}_h$ is an $n \times n$ uniform mesh on the domain Ω. In both examples, we observe that our approximation result in Theorem 4.3 holds true.

Example 4.1. In this example, we set the domain $\Omega = (-1, 1)^2$ and the interface $\Gamma = \{\mathbf{x} \in \Omega \mid \|\mathbf{x}\| = r_0\}$. The interface splits the domain Ω into $\Omega^- = \{\mathbf{x} \in \Omega \mid \|\mathbf{x}\| < r_0\}$ and

$\Omega^+ = \{\mathbf{x} \in \Omega \mid \|\mathbf{x}\| > r_0\}$, where r_0 is set to $\frac{1}{\sqrt{3}}$, and we define u as

$$u(\mathbf{x}) = \begin{cases} \dfrac{1}{\beta^-} \cos\left(\pi \|\mathbf{x}\|^2\right), & \mathbf{x} \in \Omega^-, \\ \dfrac{1}{\beta^+} \cos\left(\pi \|\mathbf{x}\|^2\right) + \cos\left(\pi r_0^2\right) \left(\dfrac{1}{\beta^-} - \dfrac{1}{\beta^+}\right), & \mathbf{x} \in \Omega^+. \end{cases} \tag{4.30}$$

In this example, we fix β^- and record the approximation error $\|u - P_h u\|_{0,\Omega}$ for $\beta^+ = 10, 100, 1000$. We observe in Table 4.1 that $\|u - P_h u\|_{0,\Omega} \lesssim h^{m+1}$, as expected.

Example 4.2. In this example, we set the domain $\Omega = (-1, 1)^2$ and the interface

$$\Gamma = \{\mathbf{x} \in \Omega \mid h(\mathbf{x}) = 0\}, \tag{4.31}$$

where the function h is given by

$$h(\mathbf{x}) = h(x_1, x_2) = \left(\left(x_1 + \frac{\pi}{6}\right)^2 + \left(x_2 + \frac{\pi}{6}\right)^2\right)^2 - \left(\left(x_1 + \frac{\pi}{6}\right)^3 + \left(x_2 + \frac{\pi}{6}\right)^3\right). \tag{4.32}$$

This interface is illustrated in Figure 3.1b, and it is parametrized by

$$\mathbf{g}(\xi) = \left(\left(\cos^3(t) + \sin^3(t)\right)\cos(t) - \frac{\pi}{6}, \left(\cos^3(t) + \sin^3(t)\right)\sin(t) - \frac{\pi}{6}\right), \qquad \xi \in [0, \pi], \tag{4.33}$$

and we define u as

$$u(\mathbf{x}) = \begin{cases} \dfrac{1}{\beta^+} \sin(h(\mathbf{x})) & h(\mathbf{x}) > 0, \\ \dfrac{1}{\beta^-} \sin(h(\mathbf{x})) & h(\mathbf{x}) \leq 0, \end{cases} \tag{4.34}$$

We fix $\beta^- = 1$, and we vary $\beta^+ \in \{10, 100, 1000\}$ and compute the projection errors presented in Table 4.2. Again, we observe the optimal convergence of the L^2 projection.

$m = 1$						
	$\beta^+ = 10$		$\beta^+ = 100$		$\beta^+ = 1000$	
n	$\|u - P_h u\|_{0,\Omega}$	rate	$\|u - P_h u\|_{0,\Omega}$	rate	$\|u - P_h u\|_{0,\Omega}$	rate
20	3.4480e-03	NA	3.1139e-03	NA	3.1074e-03	NA
40	8.9495e-04	1.9459	8.1931e-04	1.9262	8.1818e-04	1.9252
60	4.0397e-04	1.9618	3.7171e-04	1.9492	3.7129e-04	1.9487
80	2.2852e-04	1.9805	2.1080e-04	1.9716	2.1058e-04	1.9712
100	1.4634e-04	1.9972	1.3510e-04	1.9939	1.3496e-04	1.9937
$m = 2$						
	$\beta^+ = 10$		$\beta^+ = 100$		$\beta^+ = 1000$	
n	$\|u - P_h u\|_{0,\Omega}$	rate	$\|u - P_h u\|_{0,\Omega}$	rate	$\|u - P_h u\|_{0,\Omega}$	rate
20	1.1304e-04	NA	8.7452e-05	NA	8.7157e-05	NA
40	1.4311e-05	2.9817	1.1150e-05	2.9714	1.1114e-05	2.9712
60	4.2550e-06	2.9914	3.3219e-06	2.9865	3.3112e-06	2.9864
80	1.7979e-06	2.9944	1.4050e-06	2.9912	1.4005e-06	2.9912
100	9.2124e-07	2.9966	7.2019e-07	2.9947	7.1790e-07	2.9947
$m = 3$						
	$\beta^+ = 10$		$\beta^+ = 100$		$\beta^+ = 1000$	
n	$\|u - P_h u\|_{0,\Omega}$	rate	$\|u - P_h u\|_{0,\Omega}$	rate	$\|u - P_h u\|_{0,\Omega}$	rate
20	4.9582e-06	NA	3.3572e-06	NA	3.3204e-06	NA
40	3.0703e-07	4.0133	2.2446e-07	3.9027	2.2294e-07	3.8966
60	6.0482e-08	4.0068	4.5508e-08	3.9357	4.5267e-08	3.9321
80	1.9128e-08	4.0016	1.4559e-08	3.9615	1.4488e-08	3.9602
100	7.8441e-09	3.9947	5.9999e-09	3.9728	5.9713e-09	3.9721
$m = 4$						
	$\beta^+ = 10$		$\beta^+ = 100$		$\beta^+ = 1000$	
n	$\|u - P_h u\|_{0,\Omega}$	rate	$\|u - P_h u\|_{0,\Omega}$	rate	$\|u - P_h u\|_{0,\Omega}$	rate
20	2.1740e-07	NA	1.6047e-07	NA	1.5879e-07	NA
40	6.6183e-09	5.0377	5.0443e-09	4.9915	5.0131e-09	4.9853
60	8.6876e-10	5.0079	6.7118e-10	4.9745	6.6811e-10	4.9705
80	2.0622e-10	4.9990	1.6059e-10	4.9713	1.5991e-10	4.9703
100	6.7909e-11	4.9779	5.3174e-11	4.9533	5.2954e-11	4.9527

Table 4.1: L^2 projection errors and convergence rates with degree 4 Frenet IFE spaces for Example 4.1.

$m=1$						
	$\beta^+=10$		$\beta^+=100$		$\beta^+=1000$	
n	$\|u-P_hu\|_{0,\Omega}$	rate	$\|u-P_hu\|_{0,\Omega}$	rate	$\|u-P_hu\|_{0,\Omega}$	rate
20	3.6641e-03	NA	9.9918e-04	NA	9.3392e-04	NA
40	9.4747e-04	1.9513	2.6308e-04	1.9252	2.4671e-04	1.9205
60	4.2385e-04	1.9839	1.1946e-04	1.9471	1.1229e-04	1.9413
80	2.3897e-04	1.9920	6.7783e-05	1.9698	6.3776e-05	1.9664
100	1.5312e-04	1.9947	4.3599e-05	1.9775	4.1046e-05	1.9749
$m=2$						
	$\beta^+=10$		$\beta^+=100$		$\beta^+=1000$	
n	$\|u-P_hu\|_{0,\Omega}$	rate	$\|u-P_hu\|_{0,\Omega}$	rate	$\|u-P_hu\|_{0,\Omega}$	rate
20	4.5734e-04	NA	5.4938e-05	NA	3.0913e-05	NA
40	5.8379e-05	2.9697	7.1032e-06	2.9513	4.1071e-06	2.9120
60	1.7382e-05	2.9880	2.1281e-06	2.9727	1.2459e-06	2.9420
80	7.3458e-06	2.9939	9.0112e-07	2.9871	5.2958e-07	2.9739
100	3.7641e-06	2.9963	4.6240e-07	2.9901	2.7248e-07	2.9781
$m=3$						
n	$\|u-P_hu\|_{0,\Omega}$	rate	$\|u-P_hu\|_{0,\Omega}$	rate	$\|u-P_hu\|_{0,\Omega}$	rate
20	4.5408e-05	NA	4.5840e-06	NA	7.7734e-07	NA
40	3.0069e-06	3.9166	3.0326e-07	3.9180	4.9742e-08	3.9660
60	5.9988e-07	3.9755	6.0502e-08	3.9755	9.9247e-09	3.9752
80	1.9045e-07	3.9882	1.9209e-08	3.9880	3.1555e-09	3.9832
100	7.8132e-08	3.9930	7.8806e-09	3.9929	1.2954e-09	3.9899
$m=4$						
n	$\|u-P_hu\|_{0,\Omega}$	rate	$\|u-P_hu\|_{0,\Omega}$	rate	$\|u-P_hu\|_{0,\Omega}$	rate
0520	4.5734e-06	NA	4.5746e-07	NA	4.6890e-08	NA
40	1.4774e-07	4.9521	1.4778e-08	4.9522	1.5147e-09	4.9521
60	1.9565e-08	4.9861	1.9571e-09	4.9859	2.0178e-10	4.9716
80	4.6524e-09	4.9929	4.6540e-10	4.9928	4.8124e-11	4.9826
100	1.5259e-09	4.9957	1.5265e-10	4.9957	1.5784e-11	4.9959

Table 4.2: L^2 projection errors and convergence rates for $m=1,2,3,4$ Frenet IFE spaces for Example 4.2.

Chapter 5

Application of the Frenet IFE Space to Interface Problems

In this chapter, we present a Frenet IFE based symmetric interior penalty discontinuous Galerkin (SIPDG) method to solve the elliptic interface problem (3.1) and the hyperbolic interface problem. In Section 5.1, we present an immersed SIPDG formulation for the elliptic interface problem with numerical examples showing the optimal convergence of the numerical solution. In Section 5.2, we re-use the SIPDG formulation to present a fully-discrete immersed SIPDG method for the hyperbolic interface problem.

The results in this chapter are reported partially in [19].

5.1 The immersed SIPDG Method for the Elliptic Interface Problem

We consider the elliptic interface problem (3.1), which we recall below

$$\begin{cases} -\nabla \cdot (\beta \nabla u) = f, \quad \text{in } \Omega^+ \cup \Omega^-, \\ u|_{\partial\Omega} = g, \\ [\![u]\!]_\Gamma = 0, \\ [\![\beta \nabla u \cdot \mathbf{n}]\!]_\Gamma = 0, \end{cases}, \tag{5.1}$$

where $\beta|_{\Omega^\pm} = \beta^\pm > 0$ is piecewise constant, and $\mathbf{n}$ is the unit normal vector on Γ.

From now on, we assume that the solution u to the problem (5.1) is in $\mathcal{H}^2_{\Gamma,\beta}(\mathcal{T}_h)$, defined in (4.3a). This allows us to characterize $u \in \mathcal{H}^2_{\Gamma,\beta}(\mathcal{T}_h)$ as the solution to

$$a_h(u, v) = L_h(v), \qquad \forall v \in \mathcal{H}^2_{\Gamma,\beta}(\mathcal{T}_h), \tag{5.2a}$$

where $a_h : \mathcal{H}^2_{\Gamma,\beta}(\mathcal{T}_h) \times \mathcal{H}^2_{\Gamma,\beta}(\mathcal{T}_h) \to \mathbb{R}$ is the following symmetric bilinear form

$$\begin{aligned} a_h(u, v) = &\sum_{K \in \mathcal{T}_h} (\beta \nabla u, \nabla v)_K \\ &- \sum_{e \in \mathcal{E}_h} \left(\langle [\![\beta \nabla u \cdot \mathbf{n}_e]\!]_e, \{\!\{v\}\!\}_e \rangle_e + \langle \{\!\{u\}\!\}_e, [\![\beta \nabla v \cdot \mathbf{n}_e]\!]_e \rangle_e - \frac{\sigma_e}{h} \langle [\![u]\!]_e, [\![v]\!]_e \rangle_e \right), \end{aligned} \tag{5.2b}$$

and $L_h : \mathcal{H}^2_{\Gamma,\beta}(\mathcal{T}_h) \to \mathbb{R}$ is the linear form defined as follows

$$L_h(v) = (f, v)_\Omega + \sum_{e \in \mathcal{E}_h^b} \left\langle -\beta \nabla v \cdot \mathbf{n}_e + \frac{\sigma_e}{h} v, g \right\rangle_e. \tag{5.2c}$$

Here, $\mathbf{n}_e$ is the unit normal vector on the edge e. On an interior edge $e \in \mathcal{E}_h^\circ$, $\{\!\{\cdot\}\!\}_e$ and $[\![\cdot]\!]_e$ denote the average of a function across an edge e. On a boundary edge $e \in \mathcal{E}_h^b$, we take $\{\!\{v\}\!\}_e$ and $[\![v]\!]_e$ to be traces of v on e [92].

Since our local Frenet IFE space is locally conforming, meaning $\mathcal{V}_\beta^m(K) \subset \mathcal{H}_{\Gamma,\beta}^2(K)$ for every interface element K, we use the weak formulation (5.2a) with no additional integrals on the interface Γ for our discrete weak formulation. This is in contrast to other high order IFE methods such as the one in [51], where penalties on the interface are needed. More specifically, our Frenet symmetric interior penalty discontinuous Galerkin (SIPDG) scheme is as follows

$$\text{Find } u_h \in \mathcal{V}_\beta^m(\mathcal{T}_h) \text{ such that } a_h(u_h, v_h) = L_h(v_h), \quad \forall v_h \in \mathcal{V}_\beta^m(\mathcal{T}_h). \tag{5.3}$$

As with the standard interior penalty method [92], the discrete formulation (5.3) leads to a sparse symmetric linear system $\mathbf{Sc} = \mathbf{b}$.

5.1.1 Numerical Examples

In this section, we demonstrate numerically that the proposed immersed SIPDG method converges optimally. Following the estimates of the penalty parameters for the classical symmetric interior penalty method in [42], we set $\sigma_e = m^2\sigma_0\beta^e$ where $\sigma_0 = 4$ and β^e is the maximum value of β on an edge e. In each example, we fix $\beta^- = 1$ and vary $\beta^+ \in \{10, 100, 1000\}$ and present the relative L^2 errors for different degrees $m = 1, 2, 3, 4$ in Example 5.1 and Example 5.2 and degrees $m = 1, 2, \ldots, 8$ in Example 5.3.

Example 5.1. We re-use the interface and solution u from example Example 4.1 here to study the accuracy of our proposed method. That is, we consider $\Omega = (-1, 1)^2$ split by the interface $\Gamma = \{\mathbf{x} \in \Omega \mid \|\mathbf{x}\| = r_0\}$, where $r_0 = \frac{1}{\sqrt{3}}$, and we set

$$u(\mathbf{x}) = \begin{cases} \frac{1}{\beta^-}\cos\left(\pi\left\|\mathbf{x}\right\|^2\right), & \mathbf{x}\in\Omega^-, \\ \frac{1}{\beta^+}\cos\left(\pi\left\|\mathbf{x}\right\|^2\right) + \cos\left(\pi r_0^2\right)\left(\frac{1}{\beta^-}-\frac{1}{\beta^+}\right), & \mathbf{x}\in\Omega^+. \end{cases} \tag{5.4}$$

Here, again, $\Omega^- = \{\mathbf{x}\in\Omega \mid \|\mathbf{x}\| < r_0\}$, $\Omega^+ = \{\mathbf{x}\in\Omega \mid \|\mathbf{x}\| > r_0\}$, and f and g are obtained from the solution u. We report the errors in the L^2 norm and the broken H^1 semi-norm in Table 5.1 and Table 5.2, where we observe that $\|u-u_h\|_{0,\Omega} \lesssim h^{m+1}$ and $|u-u_h|_{1,\Omega} \lesssim h^m$ as expected.

Example 5.2. In this example, we consider the problem discussed in [12], where $\Omega = (.6, 1.6)\times(.2, 1.2)$ and the interface is given by

$$\Gamma = \left\{\mathbf{x}\in\Omega \mid L(\mathbf{x}) := (x_1^2-x_2^2)^2 - 4x_1^2x_2^2 + \frac{1}{2} = 0\right\}, \tag{5.5}$$

with $\Omega^+ = \{\mathbf{x}\in\Omega \mid L(\mathbf{x}) > 0\}$ and let $\Omega^- = \{\mathbf{x}\in\Omega \mid L(\mathbf{x}) < 0\}$. Next, we define $\tilde{L}$ to be the harmonic conjugate of L given by $\tilde{L}(\mathbf{x}) = 4x_1x_2(x_1^2-x_2^2)$, and we choose f and g such that

$$u(\mathbf{x}) = \frac{1}{\beta(\mathbf{x})}L(\mathbf{x}) + \tilde{L}(\mathbf{x}) + \frac{1}{\beta(\mathbf{x})}\tilde{L}(\mathbf{x})L(\mathbf{x}).$$

Thus, u is a piecewise 7-th degree bi-variate polynomial and the parametrization is given by:

$$\mathbf{g}(\xi) = \frac{1}{2}\left(\sqrt[4]{2e^{2\xi}+1}, \sqrt{3\sqrt{2e^{2\xi}+1}-4e^{\xi}}\right).$$

This example showcases the ability of the proposed IFE space to handle solutions that have non-vanishing tangential derivatives on Γ as well as interfaces with non-linear curvature such as (5.5). We report the errors in the L^2 norm and the broken H^1 semi-norm in Table 5.3 and Table 5.4, where we observe that the numerical solution converges optimally under mesh refinement, that is $\|u-u_h\|_{0,\Omega} \lesssim h^{m+1}$ and $|u-u_h|_{1,\Omega} \lesssim h^m$.

$m = 1$						
	$\beta^+ = 10$		$\beta^+ = 100$		$\beta^+ = 1000$	
n	$\|u - u_h\|_{0,\Omega}$	rate	$\|u - u_h\|_{0,\Omega}$	rate	$\|u - u_h\|_{0,\Omega}$	rate
20	6.7734e-03	NA	6.2547e-03	NA	6.5613e-03	NA
40	1.7573e-03	1.9465	1.5923e-03	1.9739	1.6034e-03	2.0328
60	7.9840e-04	1.9457	7.1937e-04	1.9596	7.2024e-04	1.9738
80	4.5381e-04	1.9637	4.1415e-04	1.9193	4.0868e-04	1.9697
100	2.9197e-04	1.9765	2.6263e-04	2.0413	2.6220e-04	1.9890
$m = 2$						
	$\beta^+ = 10$		$\beta^+ = 100$		$\beta^+ = 1000$	
n	$\|u - u_h\|_{0,\Omega}$	rate	$\|u - u_h\|_{0,\Omega}$	rate	$\|u - u_h\|_{0,\Omega}$	rate
20	1.6129e-04	NA	1.2745e-04	NA	1.2724e-04	NA
40	2.0316e-05	2.9890	1.5978e-05	2.9958	1.5930e-05	2.9977
60	6.0461e-06	2.9892	4.7502e-06	2.9916	4.7357e-06	2.9918
80	2.5568e-06	2.9917	2.0076e-06	2.9937	2.0014e-06	2.9938
100	1.3108e-06	2.9941	1.0287e-06	2.9964	1.0255e-06	2.9964
$m = 3$						
	$\beta^+ = 10$		$\beta^+ = 100$		$\beta^+ = 1000$	
n	$\|u - u_h\|_{0,\Omega}$	rate	$\|u - u_h\|_{0,\Omega}$	rate	$\|u - u_h\|_{0,\Omega}$	rate
20	8.4093e-06	NA	5.9235e-06	NA	5.9654e-06	NA
40	5.1370e-07	4.0330	3.8131e-07	3.9574	3.7887e-07	3.9769
60	1.0050e-07	4.0238	7.6051e-08	3.9762	7.5548e-08	3.9767
80	3.1712e-08	4.0094	2.4186e-08	3.9822	2.3928e-08	3.9965
100	1.3027e-08	3.9870	9.9948e-09	3.9603	9.8832e-09	3.9625
$m = 4$						
	$\beta^+ = 10$		$\beta^+ = 100$		$\beta^+ = 1000$	
n	$\|u - u_h\|_{0,\Omega}$	rate	$\|u - u_h\|_{0,\Omega}$	rate	$\|u - u_h\|_{0,\Omega}$	rate
20	3.3540e-07	NA	2.5952e-07	NA	2.6142e-07	NA
40	9.8860e-09	5.0843	7.7100e-09	5.0730	7.6502e-09	5.0948
60	1.2857e-09	5.0308	9.9784e-10	5.0428	9.9014e-10	5.0427
80	3.0349e-10	5.0184	2.3595e-10	5.0123	2.3408e-10	5.0131
100	9.9876e-11	4.9808	7.8036e-11	4.9585	7.7484e-11	4.9546

Table 5.1: The L^2 errors and convergence rates for the immersed SIPDG method applied to Example 5.1.

$m=1$						
	$\beta^+=10$		$\beta^+=100$		$\beta^+=1000$	
n	$\lvert u-u_h\rvert_{1,\Omega}$	rate	$\lvert u-u_h\rvert_{1,\Omega}$	rate	$\lvert u-u_h\rvert_{1,\Omega}$	rate
20	2.7328e-01	NA	2.4921e-01	NA	2.5429e-01	NA
40	1.3937e-01	0.9714	1.2807e-01	0.9604	1.2878e-01	0.9816
60	9.3961e-02	0.9724	8.6694e-02	0.9623	8.6895e-02	0.9702
80	7.0793e-02	0.9841	6.7027e-02	0.8944	6.7142e-02	0.8964
100	5.6661e-02	0.9979	5.2404e-02	1.1030	5.2507e-02	1.1018
$m=2$						
	$\beta^+=10$		$\beta^+=100$		$\beta^+=1000$	
n	$\lvert u-u_h\rvert_{1,\Omega}$	rate	$\lvert u-u_h\rvert_{1,\Omega}$	rate	$\lvert u-u_h\rvert_{1,\Omega}$	rate
20	1.3623e-02	NA	1.0497e-02	NA	1.0470e-02	NA
40	3.4355e-03	1.9875	2.6701e-03	1.9750	2.6619e-03	1.9757
60	1.5304e-03	1.9944	1.1927e-03	1.9876	1.1889e-03	1.9879
80	8.6171e-04	1.9964	6.7249e-04	1.9917	6.7036e-04	1.9917
100	5.5172e-04	1.9982	4.3086e-04	1.9951	4.2949e-04	1.9952
$m=3$						
	$\beta^+=10$		$\beta^+=100$		$\beta^+=1000$	
n	$\lvert u-u_h\rvert_{1,\Omega}$	rate	$\lvert u-u_h\rvert_{1,\Omega}$	rate	$\lvert u-u_h\rvert_{1,\Omega}$	rate
20	8.5365e-04	NA	5.7410e-04	NA	5.6758e-04	NA
40	1.0124e-04	3.0758	7.3574e-05	2.9640	7.2904e-05	2.9608
60	2.9395e-05	3.0500	2.2048e-05	2.9720	2.1919e-05	2.9639
80	1.2290e-05	3.0313	9.3552e-06	2.9801	9.2541e-06	2.9974
100	6.2763e-06	3.0115	4.8023e-06	2.9883	4.7407e-06	2.9976
$m=4$						
	$\beta^+=10$		$\beta^+=100$		$\beta^+=1000$	
n	$\lvert u-u_h\rvert_{1,\Omega}$	rate	$\lvert u-u_h\rvert_{1,\Omega}$	rate	$\lvert u-u_h\rvert_{1,\Omega}$	rate
20	4.5412e-05	NA	3.4274e-05	NA	3.3311e-05	NA
40	2.7136e-06	4.0648	2.0852e-06	4.0389	2.0542e-06	4.0193
60	5.3105e-07	4.0229	4.0987e-07	4.0121	4.0562e-07	4.0010
80	1.6726e-07	4.0159	1.2980e-07	3.9970	1.2863e-07	3.9920
100	6.8591e-08	3.9947	5.3462e-08	3.9751	5.3030e-08	3.9710

Table 5.2: The errors and convergence rates for the immersed SIPDG method applied to Example 5.1 in the broken H^1 semi-norm.

$m=1$						
	$\beta^+ = 10$		$\beta^+ = 100$		$\beta^+ = 1000$	
n	$\|u-u_h\|_{0,\Omega}$	rate	$\|u-u_h\|_{0,\Omega}$	rate	$\|u-u_h\|_{0,\Omega}$	rate
20	3.8004e-02	NA	3.7935e-02	NA	3.8109e-02	NA
40	9.9012e-03	1.9405	9.8826e-03	1.9406	9.8929e-03	1.9457
60	4.4961e-03	1.9470	4.4897e-03	1.9459	4.5113e-03	1.9366
80	2.5605e-03	1.9570	2.5574e-03	1.9563	2.5605e-03	1.9688
100	1.6518e-03	1.9645	1.6494e-03	1.9653	1.6543e-03	1.9575
$m=2$						
	$\beta^+ = 10$		$\beta^+ = 100$		$\beta^+ = 1000$	
n	$\|u-u_h\|_{0,\Omega}$	rate	$\|u-u_h\|_{0,\Omega}$	rate	$\|u-u_h\|_{0,\Omega}$	rate
20	7.0794e-04	NA	7.0927e-04	NA	7.2730e-04	NA
40	8.9823e-05	2.9785	8.9832e-05	2.9810	9.1198e-05	2.9955
60	2.6746e-05	2.9878	2.6760e-05	2.9868	2.7065e-05	2.9960
80	1.1315e-05	2.9902	1.1325e-05	2.9890	1.1432e-05	2.9959
100	5.8013e-06	2.9940	5.7983e-06	3.0001	5.8313e-06	3.0166
$m=3$						
	$\beta^+ = 10$		$\beta^+ = 100$		$\beta^+ = 1000$	
n	$\|u-u_h\|_{0,\Omega}$	rate	$\|u-u_h\|_{0,\Omega}$	rate	$\|u-u_h\|_{0,\Omega}$	rate
20	6.8882e-06	NA	6.9920e-06	NA	8.2335e-06	NA
40	4.4534e-07	3.9512	4.4696e-07	3.9675	4.9744e-07	4.0489
60	8.9038e-08	3.9702	8.9204e-08	3.9745	9.7205e-08	4.0266
80	2.8327e-08	3.9810	2.8388e-08	3.9799	3.0417e-08	4.0386
100	1.1639e-08	3.9861	1.1656e-08	3.9890	1.2243e-08	4.0784
$m=4$						
	$\beta^+ = 10$		$\beta^+ = 100$		$\beta^+ = 1000$	
n	$\|u-u_h\|_{0,\Omega}$	rate	$\|u-u_h\|_{0,\Omega}$	rate	$\|u-u_h\|_{0,\Omega}$	rate
20	4.2601e-08	NA	5.6492e-08	NA	1.3885e-07	NA
40	1.3268e-09	5.0048	1.4842e-09	5.2503	2.9392e-09	5.5619
60	1.7473e-10	4.9999	1.8696e-10	5.1096	3.4886e-10	5.2563
80	4.3318e-11	4.8479	4.4602e-11	4.9816	8.8922e-11	4.7514
100	1.4993e-11	4.7549	1.6095e-11	4.5676	2.9143e-11	4.9991

Table 5.3: The L^2 errors and convergence rates for the immersed SIPDG method applied to Example 5.2.

$m=1$						
	$\beta^+ = 10$		$\beta^+ = 100$		$\beta^+ = 1000$	
n	$\lvert u-u_h\rvert_{1,\Omega}$	rate	$\lvert u-u_h\rvert_{1,\Omega}$	rate	$\lvert u-u_h\rvert_{1,\Omega}$	rate
20	$4.4156e+00$	NA	$4.4002e+00$	NA	$4.4020e+00$	NA
40	$2.1927e+00$	1.0099	$2.1847e+00$	1.0102	$2.1847e+00$	1.0107
60	$1.4581e+00$	1.0064	$1.4527e+00$	1.0063	$1.4532e+00$	1.0055
80	$1.0914e+00$	1.0068	$1.0874e+00$	1.0069	$1.0873e+00$	1.0083
100	8.7202e-01	1.0057	8.6890e-01	1.0052	8.7433e-01	0.9770
$m=2$						
	$\beta^+ = 10$		$\beta^+ = 100$		$\beta^+ = 1000$	
n	$\lvert u-u_h\rvert_{1,\Omega}$	rate	$\lvert u-u_h\rvert_{1,\Omega}$	rate	$\lvert u-u_h\rvert_{1,\Omega}$	rate
20	1.2294e-01	NA	1.2342e-01	NA	1.3280e-01	NA
40	3.0657e-02	2.0037	3.0688e-02	2.0079	3.2771e-02	2.0188
60	1.3615e-02	2.0019	1.3634e-02	2.0010	1.4123e-02	2.0760
80	7.6564e-03	2.0009	7.6659e-03	2.0014	7.9088e-03	2.0155
100	4.8984e-03	2.0016	4.8994e-03	2.0062	5.0382e-03	2.0208
$m=3$						
	$\beta^+ = 10$		$\beta^+ = 100$		$\beta^+ = 1000$	
n	$\lvert u-u_h\rvert_{1,\Omega}$	rate	$\lvert u-u_h\rvert_{1,\Omega}$	rate	$\lvert u-u_h\rvert_{1,\Omega}$	rate
20	1.3728e-03	NA	1.4043e-03	NA	1.9398e-03	NA
40	1.7314e-04	2.9871	1.7465e-04	3.0073	2.2325e-04	3.1192
60	5.1503e-05	2.9903	5.1812e-05	2.9970	6.3749e-05	3.0911
80	2.1760e-05	2.9949	2.1888e-05	2.9952	2.5790e-05	3.1457
100	1.1150e-05	2.9964	1.1198e-05	3.0034	1.2674e-05	3.1838
$m=4$						
	$\beta^+ = 10$		$\beta^+ = 100$		$\beta^+ = 1000$	
n	$\lvert u-u_h\rvert_{1,\Omega}$	rate	$\lvert u-u_h\rvert_{1,\Omega}$	rate	$\lvert u-u_h\rvert_{1,\Omega}$	rate
20	1.1894e-05	NA	1.6671e-05	NA	4.9726e-05	NA
40	7.3619e-07	4.0140	8.5376e-07	4.2874	2.0989e-06	4.5663
60	1.4495e-07	4.0080	1.5926e-07	4.1412	3.7476e-07	4.2491
80	4.5826e-08	4.0028	4.9747e-08	4.0447	1.3046e-07	3.6681
100	1.8757e-08	4.0033	2.0358e-08	4.0041	5.0928e-08	4.2153

Table 5.4: The errors and convergence rates for the immersed SIPDG method applied to Example 5.2 in the broken H^1 semi-norm.

Example 5.3. This example is for demonstrating the p-convergence of the proposed higher degree immersed SIPDG method, that is, the convergence of the numerical solution with respect to the degree m on a fixed mesh. Here, we refer to the problems in Example 5.1 and Example 5.2 as Problem 1 and Problem 2, respectively. For both problems, the immersed SIPDG solutions are produced on a mesh of size 5×5 on $\Omega = [-1, 1]^2$ for Problem 1 and on $\Omega = [0.6, 1.6] \times [.2, 1.2]^2$ for Problem 2 as shown in Figure 5.1.

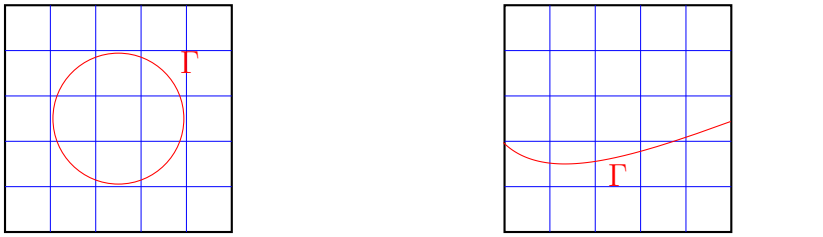

(a) A 5×5 mesh for Problem 1 (b) A 5×5 mesh for Problem 2

Figure 5.1: A 5×5 mesh for solving Problem 1 (left) and Problem 2 (right).

The errors of the immersed SIPDG method versus the total number of degrees of freedom shown in Figure 5.2 and Figure 5.3 in log-log scale demonstrate the exponential convergence of the immersed SIPDG method with increasing degree m in the L^2 norm and in the broken H^1 semi-norm. It is worth noting that the interface conditions (3.1c) are satisfied exactly by the proposed IFE functions, and, we believe, such a desirable and distinct feature makes it possible for this immersed SIPDG method to produce very accurate solutions on coarse meshes such as those in Figure 5.1.

In terms of efficiency, this p-convergence enables the proposed immersed SIPDG method to outperform other IFE methods by several orders of magnitude. For instance, when the meshes shown in Figure 5.1 are used with the IFE space $\mathcal{V}_\beta^8(\mathcal{T}_h)$, the total number of degrees of freedom of the proposed method is 2025. Nevertheless, the IFE solutions produced by the proposed method on such coarse meshes are more accurate than those produced by other IFE methods in the literature, such as [12], requiring more than $100,000$ degrees of freedom.

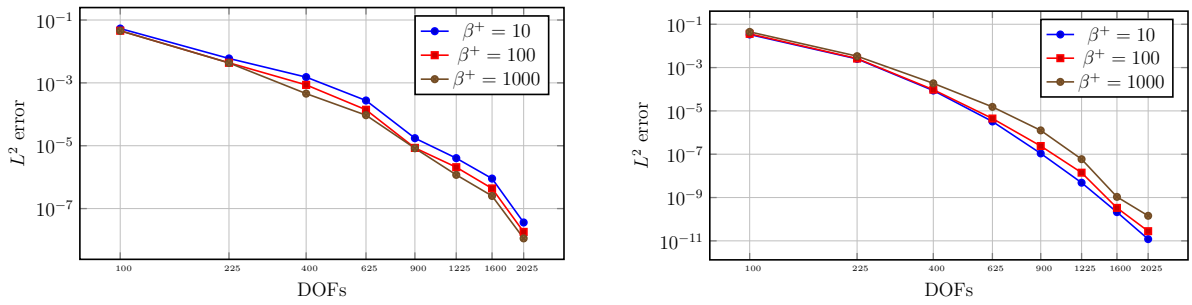

Figure 5.2: The relative errors (in log-log plot) of the immersed SIPDG method applied to Problem 1 (left), and Problem 2 (right) in the L^2 norm with a fixed mesh and varying degrees $1 \leq m \leq 8$, the x-axis represent the total number of degrees of freedom $DOF = 25(m+1)^2$.

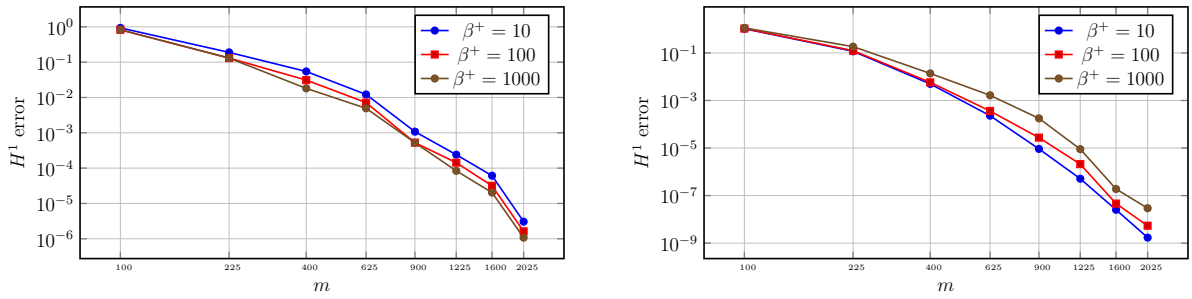

Figure 5.3: The relative errors (in log-log plot) of the immersed SIPDG method applied to Problem 1 (left), and Problem 2 (right) in the broken H^1 semi-norm with a fixed mesh and varying degrees $1 \leq m \leq 8$, the x-axis represent the total number of degrees of freedom $DOF = 25(m+1)^2$.

5.2 The Immersed SIPDG Method for the Hyperbolic Interface Problem

We consider the hyperbolic interface problem

$$\begin{cases} u_{tt} = \nabla \cdot (\beta \nabla u), & \text{in } \Omega^+ \cup \Omega^-, t > 0, \\ u|_{\partial\Omega} = g, & t \geq 0, \\ u(\cdot, 0) = u_0, & \text{in } \Omega, \\ u_t(\cdot, 0) = v_0, & \text{in } \Omega, \\ [\![u]\!]_\Gamma = 0, & t \geq 0 \\ [\![\beta \nabla u \cdot \mathbf{n}]\!]_\Gamma = 0, & t \geq 0. \end{cases} \tag{5.6}$$

Here $\beta = c^2$, where $c|_{\Omega^\pm} = c^\pm$ represents the speed of sound in the mediums Ω^+ and Ω^-, and u_0, v_0 represent the initial displacement and the initial velocity, respectively. Here, we restrict ourselves to the case where u is smooth enough around the interface such that

$$[\![\beta \Delta u]\!]_\Gamma = 0. \tag{5.7}$$

Hence, one can use bilinear and biquadratic Frenet IFE spaces to approximate the solution in space. Next, we re-use the bilinear form a_h from (5.2b) and the linear form L_h from (5.2c) with $f = 0$ to express u as the solution to

$$\begin{cases} (\partial_{tt} u, v)_\Omega + a_h(u, v) = L_h(v), \\ (u(\cdot, 0), v)_\Omega = (u_0, v)_\Omega, \\ (\partial_t u(\cdot, 0), v)_\Omega = (v_0, v)_\Omega, \end{cases} \qquad \forall v \in \mathcal{H}^2_{\Gamma,\beta}(\mathcal{T}_h), \tag{5.8}$$

which yields the following semi-discrete immersed SIPDG method

$$\begin{cases} (\partial_{tt} u_h, v_h)_\Omega + a_h(u_h, v_h) = L_h(v_h), \quad t > 0, \\ (u_h(\cdot, 0), v_h)_\Omega = (u_0, v_h)_\Omega, \qquad\qquad \forall v_h \in \mathcal{V}_\beta^m(\mathcal{T}_h). \\ (\partial_t u_h(\cdot, 0), v_h)_\Omega = (v_0, v_h)_\Omega, \end{cases} \tag{5.9}$$

However, this semi-discrete immersed SIPDG method leads to a stiff linear system of ordinary differential equations. To alleviate this issue, we propose using an implicit fully-discrete immersed SIPDG formulation based on [15, 73, 106].

More precisely, consider $\{t_i\}_{i=0}^N$ to be an equally spaced discretization of $[0, T]$ with a time-step $\Delta t = \frac{T}{N}$, and let $u_h^i = u_h(\cdot, t_i)$ be the numerical solution at time $t = t_i$. Similarly, we use g^i to denote $g(\cdot, t_i)$, and we use L_h^i to denote

$$L_h^i(v) = \sum_{e \in \mathcal{E}_h^b} \left\langle -\beta \nabla v \cdot \mathbf{n}_e + \frac{\sigma_e}{h} v, g^i \right\rangle_e . \tag{5.10}$$

Now, we are ready to state the fully-discrete weak problem: Find $\{u_h^i\}_{i=0}^N$ such that

$$\left(\frac{u_h^{i+1} - 2u_h^i + u_h^{i-1}}{(\Delta t)^2}, v_h \right)_\Omega + a_h \left(\frac{u_h^{i+1} + 2u_h^i + u_h^{i-1}}{4}, v_h \right) = \frac{1}{4} \left(L_h^{i+1}(v_h) + 2L_h^i(v_h) + L_h^{i-1}(v_h) \right) \tag{5.11}$$

For all $v_h \in \mathcal{V}_\beta^m(\mathcal{T}_h)$ and all $1 \leq i \leq N-1$. We take u_h^0 to be the L^2 projection of u_0, and

$$u_h^1 = u_h^0 + \Delta t v_0^h + \frac{(\Delta t)^2}{2} w_0^h,$$

where v_0^h is the L^2 projection of v_0 and w_0^h is an approximation of $u_{tt}(\cdot, 0)$ [15, 106, 113],

obtained by solving the system

$$(w_0^h, v_h)_\Omega = a_h(u_0, v_h), \qquad \forall v_h \in \mathcal{V}_\beta^m(\mathcal{T}_h).$$

5.2.1 Numerical Examples

In this section, we provide two numerical examples to demonstrate the convergence properties of the fully-discrete method (5.11). Since our time discretization is second order accurate, that is, the time discretization error is of the order $O(\Delta t^2)$, we restrict our numerical experiments to first and second order Frenet IFE spaces.

In the first example, we show that the numerical solution u_h converges optimally to the true solution u in the L^2 norm. In the second example, we are unable to obtain reliable error estimates since the solution is prohibitively expensive. However, we can observe from the plots that the true solution and the numerical solution are in agreement.

Example 5.4. We consider the same domain and interface as in Example 5.1. That is $\Omega = (-1, 1)^2$ and Γ is the circle centered at the origin with radius $r_0 = \frac{1}{\sqrt{3}}$. Again, $\Omega^+ = \{\mathbf{x} \in \Omega | \, \|x\| > r_0\}$ and $\Omega^- = \{\mathbf{x} \in \Omega | \, \|x\| < r_0\}$.

To construct an exact solution for (5.6), we let $\beta = c^2$, and we follow the techniques described in [100]. First, we use $u^\pm$ to denote the restrictions of u to $\Omega^\pm$. We decompose u^+ as the sum of an incident wave u^i and a reflected wave u^r, and we set the incident wave to be

$$u^i(r, \theta, t) = e^{i\omega t - \gamma^+ ir\cos(\theta)}, \qquad \gamma^+ = \frac{\omega}{c^+}. \tag{5.12}$$

That is, u^i is traveling in the x direction with speed c^+. Here, ω is a user-chosen constant representing the frequency. Next, we expand u^i in terms of Bessel functions of the first kind

using the Jacobi-Anger formula

$$u^i(r,\theta,t) = e^{i\omega t}\sum_{k=0}^{\infty}\varepsilon_k(-i)^k J_k(\gamma^+ r)\cos(k\theta), \tag{5.13a}$$

where $\varepsilon_0 = 1$ and $\varepsilon_k = 2$ for $k \geq 1$. Additionally, since the reflected wave propagates outside the domain, we express it as series of Hankel functions of the second kind

$$u^r(r,\theta,t) = e^{i\omega t}\sum_{k=0}^{\infty}A_k H_k^{(2)}(\gamma^+ r)\cos(k\theta), \tag{5.13b}$$

where A_k will be discussed shortly. In the subdomain Ω^-, the transmitted wave u^- is then given by the following series

$$u^-(r,\theta,t) = e^{i\omega t}\sum_{k=0}^{\infty}B_k J_k(\gamma^- r)\cos(k\theta), \qquad \gamma^- = \frac{\omega}{c^-}. \tag{5.13c}$$

Now, we enforce the interface conditions $[\![u]\!]_\Gamma = [\![\beta\nabla u\cdot\mathbf{n}]\!]_\Gamma = 0$ to obtain a 2×2 linear system of A_k and B_k, namely

$$\begin{cases} \varepsilon_k(-i)^n J_k(\gamma^+ r_0) + A_k H_k^{(2)}(\gamma^+ r_0) = B_k J_k(\gamma^- r_0), \\ c^+\left(\varepsilon_k(-i)^k J_k'(\gamma^+ r_0) + A_k H_k^{'(2)}(\gamma^+ r_0)\right) = c^- B_k J_k'(\gamma^- r_0). \end{cases} \tag{5.13d}$$

Next, we truncate the series (5.13) when the coefficient A_k and B_k are smaller than the machine epsilon. In our experiments, we set $\omega = 10$, and we truncate the series into a sum from 0 to 80 to obtain the exact solution

$$u(x,y,t) = \begin{cases} u^i(x,y,t) + u^r(x,y,t), & (x,y)\in\Omega^+, \\ u^t(x,y,t), & (x,y)\in\Omega^-, \end{cases} \tag{5.14}$$

which is illustrated in Figure 5.4. As for the initial and boundary conditions, we use $u_0 = u(\cdot,\cdot,t)$, $v_0 = \partial_t u(\cdot,\cdot,t)$ and $g = u|_{\partial\Omega}$.

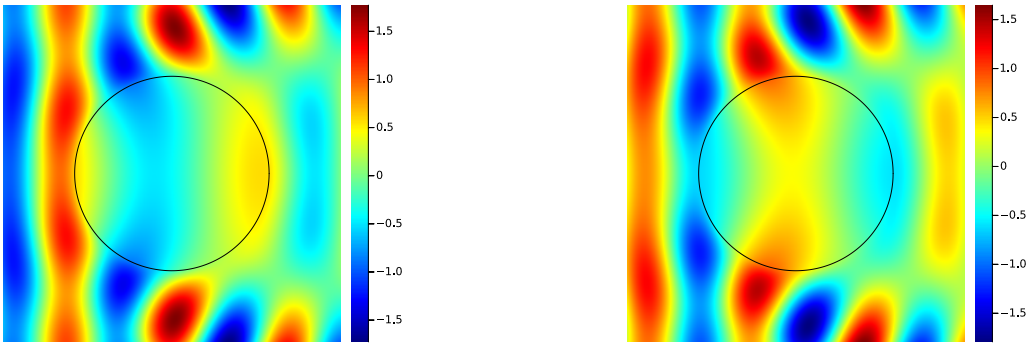

(a) $t = 0$ (b) $t = 1$

Figure 5.4: Particular solutions to the hyperbolic interface problem (5.6) at $t = 0$ (left) and $t = 1$ (right), with $(c^-, c^+) = (2, 1)$.

Now, we solve (5.6) using the fully-discrete weak formulation (5.11) on the time interval $[0, 1]$ with 6000 time-steps, and with degree $m = 1$ and degree $m = 2$ Frenet IFE spaces. In both examples, we set $(c^-, c^+) = (2, 1)$. We observe that the numerical solution converges to the true solution optimally in the L^2 norm and in the broken H^1 semi-norm, as shown in Table 5.5. Additionally, we report the relative error in the L^2 norm and in the broken H^1 semi-norm in Table 5.6.

	$m = 1$				$m = 2$			
n	$\|u - u_h\|_{0,\Omega}$	rate	$\|u - u_h\|_{1,\Omega}$	rate	$\|u - u_h\|_{0,\Omega}$	rate	$\|u - u_h\|_{1,\Omega}$	rate
20	2.7667e-1	NA	4.2045e-0	NA	5.6851e-3	NA	3.9273e-1	NA
40	7.9085e-2	1.8067	1.8022e-0	1.2221	6.6324e-4	3.0995	9.8582e-2	1.9942
60	3.6201e-2	1.9272	1.1285e-0	1.1545	1.9034e-4	3.0787	4.3691e-2	2.0069
80	2.0614e-2	1.9572	8.2335e-1	1.0959	7.9785e-5	3.0223	2.4348e-2	2.0324
100	1.3277e-2	1.9716	6.5298e-1	1.0389	4.0273e-5	3.0636	1.5396e-2	2.0539

Table 5.5: The errors and convergence rates of the immersed SIPDG method for the hyperbolic interface problem at $t = 1$ in the L^2 norm and in the broken H^1 semi-norm.

	$m=1$				$m=2$			
n	$\frac{\|u-u_h\|_{0,\Omega}}{\|u\|_{0,\Omega}}$	rate	$\frac{\|u-u_h\|_{1,\Omega}}{\|u\|_{1,\Omega}}$	rate	$\frac{\|u-u_h\|_{0,\Omega}}{\|u\|_{0,\Omega}}$	rate	$\frac{\|u-u_h\|_{1,\Omega}}{\|u\|_{1,\Omega}}$	rate
20	2.2312e-1	NA	3.6560e-1	NA	4.5847e-3	NA	3.4150e-2	NA
40	6.3778e-2	1.8067	1.5671e-1	1.2221	5.3487e-4	3.0995	8.5723e-3	1.9942
60	2.9194e-2	1.9272	9.8130e-2	1.1545	1.5350e-4	3.0787	3.7992e-3	2.0069
80	1.6624e-2	1.9572	7.1595e-2	1.0959	6.4342e-5	3.0223	2.1172e-3	2.0324
100	1.0707e-2	1.9716	5.6780e-2	1.0389	3.2478e-5	3.0636	1.3387e-3	2.0539

Table 5.6: The relative errors and convergence rates of the immersed SIPDG method for the hyperbolic interface problem at $t = 1$ in the L^2 norm and in the broken H^1 semi-norm.

Example 5.5. In this example, we set $\Omega = (-1, 1)^2$ and Γ is the circle centered at the origin with radius $r_0 = \frac{\pi}{10}$. As before, $\Omega^- = \{\mathbf{x} \in \Omega \mid \|\mathbf{x}\| < r_0\}$, $\Omega^+ = \{\mathbf{x} \in \Omega \mid \|\mathbf{x}\| > r_0\}$, and $\beta = c^2$. For simplicity, we will set $c^+ = 1$ in this example.

Consider the case where the incident wave is of the form $u^i(x, y, t) = f(t - x)$. First, we expand f as a Fourier series

$$f(x) = \sum_{l\in\mathbb{Z}} c_l e^{i\omega_l x}, \qquad \omega_l = l\pi, \quad c_l = \frac{1}{2}\int_{-1}^{1} f(x)e^{-i\omega_l x}\, dx. \tag{5.15}$$

Now, the incident wave in polar coordinates becomes

$$u^i(r, \theta, t) = \sum_{l\in\mathbb{Z}} c_l e^{i\omega_l t} e^{-i\omega_l r\cos(\theta)},$$

which, by the Jacobi-Anger formulas, can be written as a double sum

$$u^i(r, \theta, t) = \sum_{l\in\mathbb{Z}} c_l e^{i\omega_l t} \sum_{k=0}^{\infty} \varepsilon_k (-i)^k J_k(\omega_l r)\cos(k\theta). \tag{5.16a}$$

Note here that this is an infinite sum of functions in the form (5.13a). Hence, the reflected

and the transmitted waves are given by

$$u^r(r,\theta,t) = \sum_{l\in\mathbb{Z}} c_l e^{i\omega_l t} \sum_{k=0}^{\infty} A_k^{(l)} H_k^{(2)}(\omega_l r)\cos(k\theta), \tag{5.16b}$$

$$u^t(r,\theta,t) = \sum_{l\in\mathbb{Z}} c_l e^{i\omega_l t} \sum_{k=0}^{\infty} B_k^{(l)} J_k\left(\frac{\omega_l}{c^-} r\right)\cos(k\theta), \tag{5.16c}$$

where $A_k^{(l)}$ and $B_k^{(l)}$ are the solutions to

$$\begin{cases} \varepsilon_k(-i)^k J_k(\omega_l r_0) + A_k^{(l)} H_k^{(2)}(\omega_l r_0) = B_k^{(l)} J_k\left(\frac{\omega_l}{c^-} r_0\right), \\ c^+\left(\varepsilon_k(-i)^k J_k'(\omega_l r_0) + A_k^{(l)} H_k'^{(2)}(\omega_l r_0)\right) = c^- B_k^{(l)} J_k'\left(\frac{\omega_l}{c^-} r_0\right). \end{cases} \tag{5.17}$$

Then, the series (5.16) are truncated both in l and k to produce an approximation of the solution.

In this example, we choose f such that $u(x,y,0) = (x+.7)e^{-(15(x+.7))^2}$, we reduce the sum over $l \in \mathbb{Z}$ to the sum over $-200 \le l \le 200$, we reduce the sum over $k \ge 0$ to the sum over $0 \le k \le 100$, and we set $c^- = 2$. Then, we take the real part of u. Thus, we obtain an approximation u_{GFS} of u as shown in the left half of Figure 5.5. As for the immersed SIPDG solution, we solve the fully-discrete formulation (5.11) on a 120×120 mesh with degree 2 Frenet IFE space as our spatial discretization and a time-step $\Delta t = \frac{0.9}{9000}$ to obtain the numerical solution showed in the right half of Figure 5.5 at $t = 0.7$ and $t = 0.9$. At both times, we observe that our numerical scheme preserves the behavior of the solution, and that the two solutions are almost indistinguishable.

Remark 5.1. Unlike the previous example where the error tables are provided, it is extremely expensive to compute the exact solution u accurately in this example. Hence, we only included the plots of the truncated generalized Fourier series of the solution and the immersed SIPDG solution.

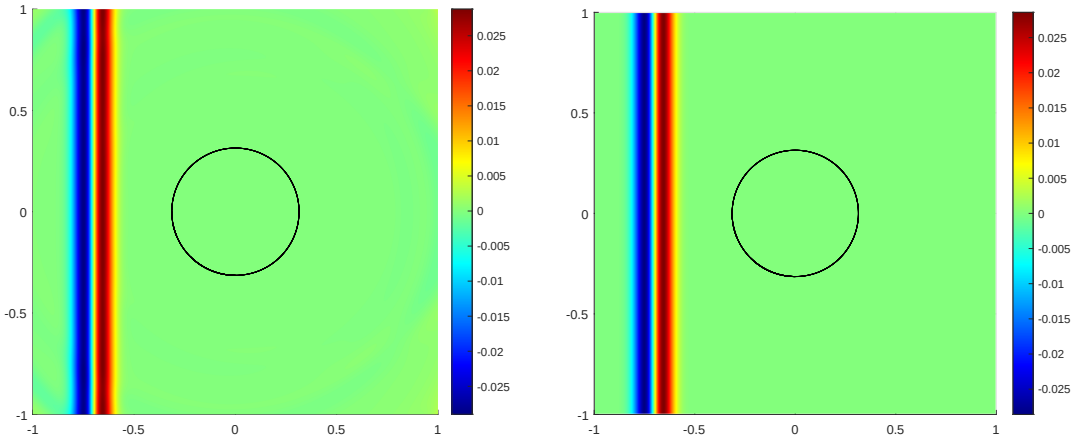

(a) u_{GFS} at $t = 0$

(b) u_h at $t = 0$

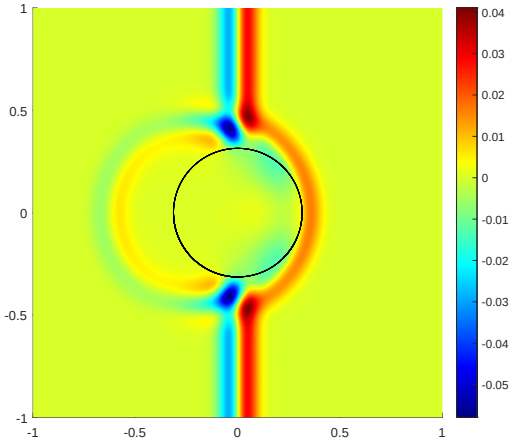

(c) u_{GFS} at $t = 0.7$

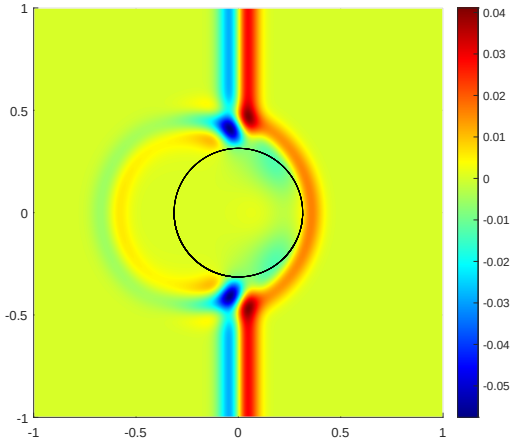

(d) u_h at $t = 0.7$

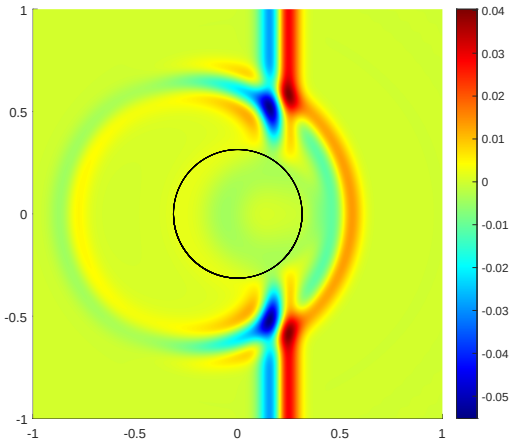

(e) u_{GFS} at $t = 0.9$

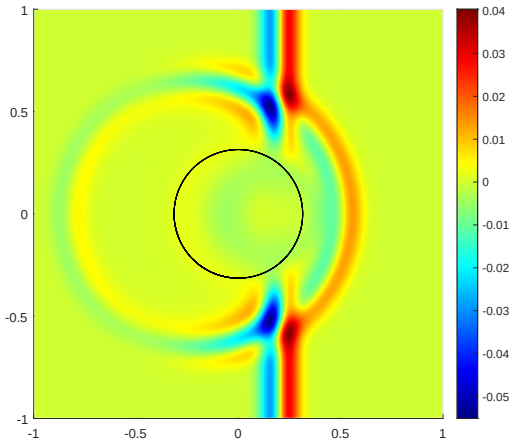

(f) u_h at $t = 0.9$

Figure 5.5: The generalized Fourier series approximation u_{GFS} (left) and the immersed SIPDG solution u_h (right) at $t = 0$ (top), $t = 0.7$ (middle) and $t = 0.9$ (bottom).

Chapter 6

Conclusions and Future Research

6.1 Contributions

In this dissertation, we presented a unified framework to analyze various immersed finite element methods of arbitrary polynomial degree in one spatial dimension, and we presented a new approach to construct higher order IFE spaces in two spatial dimensions using the differential geometry properties of the interface.

In one spatial dimension, we have extended the classical scaling argument techniques [29, 37] to IFE methods, which allowed us to provide optimal error estimates for several immersed FE and immersed dG methods, such as the elliptic interface problem [7], the parabolic interface problem [70], the Euler-Bernoulli interface problem [78, 81], the transport interface problem, and the acoustic interface problem [8]. Our main contribution in this chapter lies in the construction and study of a general IFE space which encompasses the IFE spaces for various interface problems, alongside with a series of theorems and properties allowing us to utilize the already existing techniques to derive optimal error estimates.

In two spatial dimensions, we introduced a Frenet transformation to construct an m-th degree Frenet IFE space for the elliptic interface problem with optimal approximation capability. In the construction, we utilized several differential geometry features of the interface, such as the curvature and the tubular neighborhood, to obtain an IFE space that is locally conforming

to the weak formulation of the problem. Furthermore, the majority of the basis functions of the Frenet IFE space can be constructed explicitly. Thus reducing the computational cost of the construction of the IFE basis greatly. Additionally, we have shown that the Frenet IFE space has optimal approximation capabilities in the L^2 norm. When applied to the elliptic interface problem, the Frenet IFE method exhibited an optimal convergence under mesh refinement, and an exponential convergence under degree refinement. Furthermore, the Frenet IFE space was applied to solve the hyperbolic interface problem successfully, which showcases the versatility of this approach and its applicability to various interface problems.

6.2 Future Work

In the future, we plan to continue and expand the work presented in this dissertation. Below, we list a few possible research directions involving the Frenet IFE space that we plan to pursue.

6.2.1 Analysis of the Frenet SIPDG method

Through numerous numerical examples, we observed that the Frenet SIPDG method discussed in Section 5.1 provides an optimally convergent numerical approximation, that is $\|u - u_h\|_{0,\Omega} = O(h^{m+1})$, where m is the degree, and u_h is the numerical solution. In the future, we plan to present a rigorous mathematical proof of this observation.

Since we proved the optimal approximation capabilities of the Frenet IFE space, it remains to derive an inverse inequality for the Frenet IFE functions. More precisely, we are interested

in proving the following inequality

$$\|\beta\nabla\varphi\|_{0,\partial K} \leq Ch^{-1/2}\left\|\sqrt{\beta}\nabla\varphi\right\|_{0,K}, \qquad \forall\varphi\in\mathcal{V}_\beta^m(K), \tag{6.1}$$

where C is a constant independent of h. The inequality (6.1) will then be used to prove the coercivity of the bilinear form a_h (5.2b) for sufficiently large penalty parameter σ, and to obtain an optimal error estimate.

6.2.2 Frenet IFE Spaces in Three Dimensions

Many applications in science and engineering require solving interface problems in three spatial dimensions. Recently, extensive research is being conducted on unfitted methods [52, 58, 74] for three-dimensional interface problems. In three dimensions, a surface is parametrized by two variables $(\xi,\zeta)\mapsto\mathbf{g}(\xi,\zeta)$, and the partial derivatives $\mathbf{g}_\xi$ and $\mathbf{g}_\zeta$ provide tangent lines on the interface, which are linearly independent if the parametrization is regular [41]. The normal line is then given by the normalized cross product

$$\mathbf{n}(\xi,\zeta)=\frac{\mathbf{g}_\xi(\xi,\zeta)\times\mathbf{g}_\zeta(\xi,\zeta)}{\|\mathbf{g}_\xi(\xi,\zeta)\times\mathbf{g}_\zeta(\xi,\zeta)\|}.$$

Now, the Frenet transformation becomes

$$P(\eta,\xi,\zeta)=\mathbf{g}(\xi,\zeta)+\eta\mathbf{n}(\xi,\zeta).$$

Then, the inverse Frenet transformation $R=P^{-1}$ maps the interface locally to a subset of the plane $\eta=0$. In the future, we plan to employ this idea to construct Frenet IFE spaces for various interface problems in three dimensions following similar techniques to the ones discussed in Section 3.5.

6.2.3 Vector Interface Problems and Multi-physics Problems

In the future, we plan to extend the Frenet Framework to vector interface problems, such as the acoustic interface problem [9, 86], the Stokes interface problem [11, 60] and the elasticity interface problem [53, 79, 83] amongst others. Typically, vector PDEs are more challenging than scalar PDEs since they require more degrees of freedom on the same mesh. Hence, higher order unfitted methods are highly desirable. Furthermore, the interface conditions for such problems often involve the normal and the tangent vectors on the interface, which appear naturally in the Frenet framework.

After that, we plan to construct Frenet IFE spaces for a multitude of multi-physics models, where the partial differential equations on Ω^- and Ω^+ are different in nature. For a start, we intend to study the acoustic-elastic interface problem [17, 86, 102], and the Stokes-Darcy interface problem [44, 72].

Bibliography

[1] Marco Abate and Francesca Tovena. *Curves and Surfaces*. Springer-Verlag, Italy, 2012.

[2] Wassim Abdel Nour, Joseph Jabbour, Damien Serret, Philippe Meliga, and Elie Hachem. A stabilized finite element framework for anisotropic adaptive topology optimization of incompressible fluid flows. *Fluids*, 8(8), 2023.

[3] Milton Abramowitz and Irene A. Stegun. *Handbook of Mathematical Functions*. Dover, New York, 1965.

[4] Robert A. Adams. *Sobolev Spaces*, volume 65 of *Pure and Applied Mathematics*. Academic Press, 1975.

[5] Slimane Adjerid. A study of high-order immersed finite element spaces by pointwise interface conditions on curved interfaces. *Computers and Mathematics with Applications*, 128:331–353, 2022.

[6] Slimane Adjerid and Mahboub Baccouch. Asymptotically exact a posteriori error estimates for a one-dimensional linear hyperbolic problem. *Applied Numerical Mathematics*, 60(9):903–914, 2010.

[7] Slimane Adjerid and Tao Lin. A p-th degree immersed finite element for boundary value problems with discontinuous coefficients. *Applied Numerical Mathematics*, 59: 1303–1321, 2009.

[8] Slimane Adjerid and Kihyo Moon. A higher order immersed discontinuous Galerkin finite element method for the acoustic interface problem. In *Advances in Applied Mathematics*, pages 57–69. Springer International Publishing, 2014.

[9] Slimane Adjerid and Kihyo Moon. An immersed discontinuous Galerkin method for acoustic wave propagation in inhomogeneous media. *SIAM Journal on Scientific Computing*, 41(1):A139–A162, 2019.

[10] Slimane Adjerid, Mohammed Ben-Romdhane, and Tao Lin. Higher degree immersed finite element methods for second-order elliptic interface problems. *International Journal of Numerical Analysis and Modeling*, 11(3):541–566, 2014.

[11] Slimane Adjerid, Nabil Chaabane, and Tao Lin. An immersed discontinuous finite element method for Stokes interface problems. *Computer Methods in Applied Mechanics and Engineering*, 293:170–190, 2015.

[12] Slimane Adjerid, Ruchi Guo, and Tao Lin. High degree immersed finite element spaces by a least squares method. *International Journal of Numerical Analysis And Modeling*, 14(4-5):604–625, 2017.

[13] Slimane Adjerid, Mohamed Ben-Romdhane, and Tao Lin. Higher degree immersed finite element spaces constructed according to the actual interface. *Computers and Mathematics with Applications*, 75(6):1868–1881, 2018.

[14] Slimane Adjerid, Nabil Chaabane, Tao Lin, and Pengtao Yue. An immersed discontinuous finite element method for the Stokes problem with a moving interface. *Journal of Computational and Applied Mathematic*, 362, 2019.

[15] Slimane Adjerid, Tao Lin, and Qiao Zhuang. Error estimates for an immersed finite element method for second order hyperbolic equations in inhomogeneous media. *Journal of Scientific Computing*, 84(35), 2020.

[16] Slimane Adjerid, Ivo Babuška, Ruchi Guo, and Tao Lin. An enriched immersed fi-

nite element method for interface problems with nonhomogeneous jump conditions. *Computer Methods in Applied Mechanics and Engineering*, 404:115770, 2023.

[17] Slimane Adjerid, Tao Lin, and Haroun Meghaichi. An immersed discontinuous Galerkin method for wave propagation in acoustic elastic media. *Journal of Computational Physics*, 472:111651, 2023.

[18] Slimane Adjerid, Tao Lin, and Haroun Meghaichi. A unified immersed finite element error analysis for one-dimensional interface problems. *BIT Numerical Mathematics*, 64 (13), 2023.

[19] Slimane Adjerid, Tao Lin, and Haroun Meghaichi. A high order geometry conforming immersed finite element for elliptic interface problems. *Computer Methods in Applied Mechanics and Engineering*, 420:116703, 2024.

[20] I. Babuška and J. E. Osborn. Can a finite element method perform arbitrarily badly? *Mathematics of Computation*, 69(230):443–462, 2000.

[21] Ivo Babuška. The finite element method for elliptic equations with discontinuous coefficients. *Computing*, 5:207–213, 1970.

[22] Viorel Barbu. *Differential Equations*. Springer Cham, 2016.

[23] Jonathan Barzilai and Jonathan. M. Borwein. Two-point step size gradient methods. *IMA Journal of Numerical Analysis*, 8(1):141–148, 1988.

[24] R. Becker, E. Burman, and P. Hansbo. A Nitsche extended finite element method for incompressible elasticity with discontinuous modulus of elasticity. *Computer Methods in Applied Mechanics and Engineering*, 198:3352–3360, 2009.

[25] Mohamed Ben Romdhane. *Higher-Degree Immersed Finite Elements for Second-Order Elliptic Interface Problems*. PhD thesis, Virginia Tech, 2011.

[26] Dietrich Braess. *Finite Elements*. Cambridge University Press, second edition, 2001.

[27] James H. Bramble and Stephen R. Hilbert. Estimation of linear functionals on sobolev spaces with application to Fourier transforms and spline interpolation. *SIAM Journal on Numerical Analysis*, 7(1):112–124, 1970.

[28] James H. Bramble and J. Thomas King. A finite element method for interface problems in domains with smooth boundaries and interfaces. *Advances in Computational Mathematics*, 6(1):109–138, 1996.

[29] Susanne .C. Brenner and L. Ridgway Scott. *The Mathematical Theory of Finite Element Methods*. Springer-Verlag, New York, third edition, 2007.

[30] Erik Burman, Susanne Claus, Peter Hansbo, Mats G. Larson, and André Massing. Cutfem: Discretizing geometry and partial differential equations. *International Journal for Numerical Methods in Engineering*, 104(7):472–501, 2015.

[31] Thomas Carraro and Sven Wetterauer. On the implementation of the eXtended finite element method (XFEM) for interface problems. *Archive of Numerical Software*, 4(2): 1–23, 2016.

[32] Jean Céa. Approximation variationnelle des problèmes aux limites. *Annales de l'Institut Fourier*, 14(2), 1964.

[33] Nabil Chaabane. *Immersed and Discontinuous Finite Element Methods*. PhD thesis, Virginia Tech, 2015.

[34] Long Chen, Ruchi Guo, and Jun Zou. A family of immersed finite element spaces and applications to three-dimensional H(curl) interface problems. *SIAM Journal on Scientific Computing*, 45(6):A3121–A3149, 2023.

[35] Yuan Chen and Xu Zhang. A P2-P1 partially penalized immersed finite element method for Stokes interface problem. *International Journal of Numerical Analysis and Modeling*, 18(1), 2021.

[36] Yuan Chen, Songming Hou, and Xu Zhang. An immersed finite element method for elliptic interface problems with multi-domain and triple junction points. *Advances in Applied Mathematics and Mechanics*, 11(5):1005–1021, 2019.

[37] Phillipe G. Ciarlet. *The Finite Element Method for Elliptic Problems*. North-Holland, Amsterdam, 1978.

[38] Susanne Claus, Erik Burman, and Andre Massing. CutFEM: a stabilised Nitsche XFEM method for multi-physics problems. In *ACME 2015 Conference Proceedings*, 2015.

[39] R.W. Clough and J.L. Tocher. Finite element stiffness matrices for analysis of plates in bending. In *Matrix Methods in Structural Mechanics*, pages 515–545, 1966.

[40] Bernardo Cockburn. *An Introduction to the Discontinuous Galerkin Method for Convection-Dominated Problems*, pages 150–268. Springer Berlin Heidelberg, Berlin, Heidelberg, 1998.

[41] Manfredo Do Carmo. *Differential Geometry of Curves and Surfaces*. Prentice-Hall, first edition, 1976.

[42] Yekaterina Epshteyn and Béatrice Rivière. Estimation of penalty parameters for symmetric interior penalty Galerkin methods. *Journal of Computational and Applied Mathematics*, 206(2):843–872, 2007.

[43] Alexandre Ern and Jean-Luc Guermond. *Finite Elements I: Approximation and Interpolation*, volume 72 of *Texts in Applied Mathematics*. Springer Cham, 2021.

[44] Vivette Girault and Béatrice Rivière. DG approximation of coupled Navier–Stokes and Darcy equations by Beaver–Joseph–Saffman interface condition. *SIAM Journal on Numerical Analysis*, 47(3):2052–2089, 2009.

[45] Yan Gong, Bo Li, and Zhilin Li. Immersed-interface finite-element methods for elliptic interface problems with nonhomogeneous jump conditions. *SIAM Journal on Numerical Analysis*, 46(1):472–495, 2008.

[46] Christian Grossmann, Hans-G. Roos, and Martin Stynes. *Numerical Treatment of Partial Differential Equations*. Universitext. Springer-Verlag, Berlin Heidelberg, 2007.

[47] Antonio José Guirao, Vicente Montesinos, and Václav Zizler. *Renormings in Banach Spaces*. Monografie Matematyczne, Birkhäuser, 2022.

[48] Ruchi Guo. *Design, Analysis, and Application of Immersed Finite Element Methods*. PhD thesis, Virginia Tech, 2019.

[49] Ruchi Guo. Solving parabolic moving interface problems with dynamical immersed spaces on unfitted meshes: Fully discrete analysis. *SIAM Journal on Numerical Analysis*, 59(2):797–828, 2021.

[50] Ruchi Guo and Tao Lin. A group of immersed finite element spaces for elliptic interface problems. *IMA Journal of Numerical Analysis*, 39(1):482–511, 2019.

[51] Ruchi Guo and Tao Lin. A higher degree immersed finite element method based on a Cauchy extension. *SIAM Journal On Numerical Analysis*, 57(4):1545–1573, 2019.

[52] Ruchi Guo and Tao Lin. An immersed finite element method for elliptic interface problems in three dimensions. *Journal of Computational Physics*, 414:109478, 2020.

[53] Ruchi Guo, Tao Lin, and Yanping Lin. Approximation capabilities of immersed finite element spaces for elasticity interface problems. *Numerical Methods for Partial Differential Equations*, 35(3):1243–1268, 2019.

[54] Ruchi Guo, Tao Lin, and Yanping Lin. A fixed mesh method with immersed finite elements for solving interface inverse problems. *Journal of Scientific Computing*, 79 (1):148–175, April 2019.

[55] Ruchi Guo, Tao Lin, and Qiao Zhuang. Improved error estimation for the partially penalized immersed finite element methods for elliptic interface problems. *International Journal of numerical analysis and modeling*, 16(4), 2019.

[56] Ruchi Guo, Tao Lin, and Yanping Lin. Recovering elastic inclusions by shape optimization methods with immersed finite elements. *Journal of Computational Physics*, 404:109123, 2020.

[57] Guo, Ruchi, Lin, Tao, and Lin, Yanping. Error estimates for a partially penalized immersed finite element method for elasticity interface problems. *Mathematical Modelling and Numerical Analysis*, 54(1):1–24, 2020.

[58] Daoru Han, Pu Wang, Xiaoming He, Tao Lin, and Joseph Wang. A 3d immersed finite element method with non-homogeneous interface flux jump for applications in particle-in-cell simulations of plasma-lunar surface interactions. *Journal of Computational Physics*, 321:965–980, 2016.

[59] Anita Hansbo and Peter Hansbo. An unfitted finite element method, based on Nitsche's method, for elliptic interface problems. *Computer Methods in Applied Mechanics and Engineering*, 191, 2002.

[60] Peter Hansbo, Mats G. Larson, and Sara Zahedi. A cut finite element method for a stokes interface problem. *Applied Numerical Mathematics*, 85:90–114, 2014.

[61] Xiaoming He. *Bilinear Immersed Finite Elements For Interface Problems*. PhD thesis, Virginia Tech, 2009.

[62] Xiaoming He, Tao Lin, and Yanping Lin. Approximation capability of a bilinear immersed finite element space. *Numerical Methods for Partial Differential Equations*, 24(5):1265–1300, 2008.

[63] Xiaoming He, Tao Lin, and Yanping Lin. Immersed finite element methods for elliptic interface problems with non-homogeneous jump conditions. *International Journal of Numerical Analysis and Modeling*, 8(2), 2011.

[64] Xiaoming He, Tao Lin, Yanping Lin, and Xu Zhang. Immersed finite element methods for parabolic equations with moving interface. *Numerical Methods for Partial Differential Equations*, 29(2):619–646, 2013.

[65] Jan S. Hesthaven and Tim Warburton. *Nodal Discontinuous Galerkin Methods*. Texts in Applied Mathematics. Springer, 2008.

[66] Morris W. Hirsch. *Differential Topology*. Springer New York, New York, NY, 1976.

[67] J. Guzmán, M. A. Sánchez, and M. Sarkis. Higher-order finite element methods for elliptic problems with interfaces. *ESAIM: Mathematical Modelling and Numerical Analysis*, 50(5):1561–1583, 2016.

[68] Seungmin Jeong, Sunghoon Lim, and Seungjae Min. Level-set-based topology optimization using remeshing techniques for magnetic actuator design. *IEEE Transactions on Magnetics*, 52(3):1–4, 2016.

[69] Claes Johnson. *Numerical Solutions of Partial Differential Equations by the Finite Element Method*. Cambridge University Press, 1987.

[70] Derrick Jones and Xu Zhang. A high order immersed finite element method for parabolic interface problems. In *International Conference on Computational Methods and Applications in Engineering*, 2019.

[71] Raed Kafafy, Tao Lin, Yanping Lin, and Joseph Wang. Three-dimensional immersed finite element methods for electric field simulation in composite materials. *International Journal for Numerical Methods in Engineering*, 64:904–972, 2005.

[72] G. Kanschat and B. Rivière. A strongly conservative finite element method for the coupling of Stokes and Darcy flow. *Journal of Computational Physics*, 229(17):5933–5943, 2010.

[73] Stig Larsson and Vidar Thomée. *The Finite Element Method for Hyperbolic Equations*, pages 201–216. Springer Berlin Heidelberg, Berlin, Heidelberg, 2003.

[74] Christoph Lehrenfeld. High order unfitted finite element methods on level set domains using isoparametric mappings. *Computer Methods in Applied Mechanics and Engineering*, 300:716–733, 2016.

[75] Randall J. Leveque and Zhilin Li. The immersed interface method for elliptic equations with discontinuous coefficients and singular sources. *SIAM Journal on Numerical Analysis*, 31(4):1019–1044, 1994.

[76] Zhilin Li. The immersed interface method using a finite element formulation. *Applied Numerical Mathematics*, 27(3):253–267, 1998.

[77] Zhilin Li, Tao Lin, Yanping Lin, and Robert C. Rogers. An immersed finite element

space and its approximation capability. *Numerical Methods for Partial Differential Equations*, 20(3):338–367, 2004.

[78] Min Lin, Tao Lin, and Huili Zhang. Error analysis of an immersed finite element method for Euler-Bernoulli beam interface problems. *International Journal of Numerical Analysis And Modeling*, 14(6):822–841, 2017.

[79] Tao Lin and Xu Zhang. Linear and bilinear immersed finite elements for planar elasticity interface problems. *Journal of Computational and Applied Mathematics*, 236(18): 4681–4699, 2012.

[80] Tao Lin and Qiao Zhuang. Optimal error bounds for partially penalized immersed finite element methods for parabolic interface problems. *Journal of Computational and Applied Mathematics*, 366:112401, 2020.

[81] Tao Lin, Yanping Lin, Weiwei Sun, and Zhu Wang. Immersed finite element methods for 4th order differential equations. *Journal of Computational and Applied Mathematics*, 235(13):3953–3964, 2011.

[82] Tao Lin, Yanping Lin, and Xu Zhang. A method of lines based on immersed finite elements for parabolic moving interface problems. *Advances in Applied Mathematics and Mechanics*, 5(4):548–568, 2013.

[83] Tao Lin, Dongwoo Sheen, and Xu Zhang. A locking-free immersed finite element method for planar elasticity interface problems. *Journal of Computational Physics*, 247:228–247, 2013.

[84] Tao Lin, Yanping Lin, and Xu Zhang. Partially penalized immersed finite element methods for elliptic interface problems. *SIAM Journal on Numerical Analysis*, 53(2): 1121–1144, 2015.

[85] Tao Lin, Qing Yang, and Xu Zhang. Partially penalized immersed finite element methods for parabolic interface problems. *Numerical Methods for Partial Differential Equations*, 31(6):1925–1947, 2015.

[86] Bruno Lombard and Joël Piraux. Numerical treatment of two-dimensional interfaces for acoustic and elastic waves. *Journal of Computational Physics*, 195(1):90–116, 2004.

[87] Xiong Meng, Chi-Wang Shu, and Boying Wu. Optimal error estimates for discontinuous galerkin methods based on upwind-biased fluxes for linear hyperbolic equations. *Mathematics of Computation*, 85(299):1225–1261, 2016.

[88] Kihyo Moon. *Immersed Discontinuous Galerkin Methods for Acoustic Wave Propagation in Inhomogeneous Media*. PhD thesis, Virginia Tech, 2016.

[89] Ajit Panesar, David Brackett, Ian Ashcroft, Ricky Wildman, and Richard Hague. Hierarchical remeshing strategies with mesh mapping for topology optimisation. *International Journal for Numerical Methods in Engineering*, 111(7):676–700, 2017.

[90] Joël Piraux and Bruno Lombard. A new interface method for hyperbolic problems with discontinuous coefficients: One-dimensional acoustic example. *Journal of Computational Physics*, 168(1):227–248, 2001.

[91] Edoardo Provenzi. *From Euclidean to Hilbert Spaces: Introduction to Functional Analysis and its Applications*. John Wiley and Sons, Ltd, 2021.

[92] Beatrice Rivière. *Discontinuous Galerkin Methods for Solving Elliptic and Parabolic Equations*, volume FR35 of *Frontiers in Applied Mathematics*. SIAM, Philadelphia, 2008.

[93] Prihambodo H. Saksono, Wulf G. Dettmer, and Djordje Perić. An adaptive remeshing

strategy for flows with moving boundaries and fluid-structure interaction. *International Journal for Numerical Methods in Engineering*, 71(9):1009–1050, 2007.

[94] Robert I. Saye. High-order quadrature methods for implicitly defined surfaces and volumes in hyperrectangles. *SIAM Journal on Scientific Computing*, 37(2):993–1019, 2015.

[95] Zheng Sun and Yulong Xing. On generalized Gauss-Radau projections and optimal error estimates of upwind-biased DG methods for the linear advection equation on special simplex meshes. *Journal of Scientific Computing*, 95(3), 2023.

[96] Tayfun E. Tezduyar, Mark A. Behr, Sanjay Mittal, and Jun Liou. A new strategy for finite element computations involving moving boundaries and interfaces—the deforming-spatial-domain/space-time procedure: II. Computation of free-surface flows, two-liquid flows, and flows with drifting cylinders. *Computer Methods in Applied Mechanics and Engineering*, 94(3):353–371, 1992. ISSN 0045-7825.

[97] Vidar Thomée. *Galerkin Finite Element Methods for Parabolic Problems*. Springer Series in Computational Mathematics. Springer Berlin, Heidelberg, 2006.

[98] Victor A. Toponogov. *Differential Geometry of Curves and Surfaces : A Concise Guide*. Birkhäuser, Boston, 2006.

[99] Sylvain Vallaghé and Théodore Papadopoulo. A trilinear immersed finite element method for solving the electroencephalography forward problem. *SIAM Journal on Scientific Computing*, 32(4), 201-.

[100] Kristoffer Virta and Daniel Appelo. Formulae and software for particular solutions to the elastic wave equation in curved geometries, 2015. URL https://github.com/appelo/pewe.

[101] Tzin S. Wang. *A Hermite cubic immersed finite element space for beam design problems.* PhD thesis, Virginia Tech, 2005.

[102] Lucas C. Wilcox, Georg Stadler, Carsten Burstedde, and Omar Ghattas. A high-order discontinuous Galerkin method for wave propagation through coupled elastic–acoustic media. *Journal of Computational Physics*, 229(24):9373–9396, 2010.

[103] Yuanming Xiao, Jinchao Xu, and Fei Wang. High-order extended finite element methods for solving interface problems. *Computer Methods in Applied Mechanics and Engineering*, 364:112964, 2020.

[104] Yanan Xing, Lina Song, Xiaoming He, and Changxin Qiu. A generalized finite difference method for solving elliptic interface problems. *Mathematics and Computers in Simulation*, 178:109–124, 2020.

[105] Jinchao Xu. Estimate of the convergence rate of finite element solutions to elliptic equations of second order with discontinuous coefficients. *Natural Science Journal of Xiangtan University*, 1, 1982.

[106] Qing Yang. Numerical analysis of partially penalized immersed finite element methods for hyperbolic interface problems. *Numerical Mathematics: Theory, Methods and Applications*, 11(2):272–298, 2018.

[107] Yang Yang and Chi-Wang Shu. Analysis of optimal superconvergence of discontinuous Galerkin method for linear hyperbolic equations. *SIAM Journal on Numerical Analysis*, 50(6):3110–3133, 2012.

[108] Yang Yang and Chi-Wang Shu. Analysis of optimal superconvergence of discontinuous Galerkin method for linear hyperbolic equations. *SIAM Journal on Numerical Analysis*, 50(6):3110–3133, 2012.

[109] Qinghui Zhang and Ivo Babuška. A stable generalized finite element method (SGFEM) of degree two for interface problems. *Computer Methods in Applied Mechanics and Engineering*, 363:112889, 2020.

[110] Qinghui Zhang, Uday Banerjee, and Ivo Babuška. Strongly stable generalized finite element method (SSGFEM) for a non-smooth interface problem. *Computer Methods in Applied Mechanics and Engineering*, 344:538–568, February 2019.

[111] Xu Zhang. *Nonconforming Immersed Finite Element Methods for Interface Problems*. PhD thesis, Virginia Tech, 2013.

[112] Zhilin, Tao Lin, and Xiaohui Wu. New cartesian grid methods for interface problems using the finite element formulation. *Numerische Mathematik*, 96:61–93, 2003.

[113] Qiao Zhuang. *Immersed Finite Elements for a Second Order Elliptic Operator and Their Applications*. PhD thesis, Virginia Tech, 2020.

[114] Qiao Zhuang and Ruchi Guo. High degree discontinuous Petrov–Galerkin immersed finite element methods using fictitious elements for elliptic interface problems. *Journal of Computational and Applied Mathematics*, 362:560–573, 2019.

[115] Miloš Zlámal. Curved elements in the finite element method. I. *SIAM Journal on Numerical Analysis*, 10(1):229–240, 1973.